UNIVERSITÀ DEGLI STUDI DI SALERNO

Dipartimento di Ingegneria Civile

Dottorato di Ricerca

in

Rischio e sostenibilità nei sistemi dell'ingegneria civile, edile ed ambientale

XXXI Ciclo (2015-2018) Anno 2017/2018

Tesi di dottorato in:

Innovative probabilistic methodologies to assess seismic vulnerability of simple supported girder bridges

Angelo Mammone

I Tutor
Prof. Luigi Petti

Il Coordinatore
Prof. Fernando Farternali

Prof. Vincenzo Piluso

Il Dottorando
Ing. Angelo Mammone

To infinity and beyond!

Acknowledgment

At the end of this PhD project, I feel the duty and the pleasure of thanking everybody that supported me. I want to express my most sincere gratefulness to the Prof. Ing. Luigi Petti who gave me the opportunity to undertake this course of research, in particular on multiple issues of structural engineering, and he was a guide and a point of reference for me. I also thank Prof. Ing. Vincenzo Piluso for his scientific support.
A special thanks to Doctor Francesco Sicignano for his assistance and essential suggestions, Ing. Antonio Ansalone for his welcome opinion and his support, Ing. Domenico Greco and Dott. Carmine Di Muro which gave me a support a in performing my tasks.
I would also like to thank the Department of Steel and Composite Structures of the University of Kassel and all the staff, for the valuable support of research activities for the thesis during my study period abroad.

Index

1. Introduction

Seismic events are natural disasters that affect populations and anthropic systems, often with catastrophic consequences. Scientific research, with several studies in the various branches (geophysics, geotechnics, engineering structures, etc.), has tried to mitigate the destruction and damages caused by earthquakes. In this context, for several years, methodologies have been introduced for the evaluation of seismic risk on buildings to define the expected damage following a seismic shock on a given urban reality and to identify all the elements at high risk. In these risk assessments, an essential component has often been neglected or at least left in the background: the transport system.

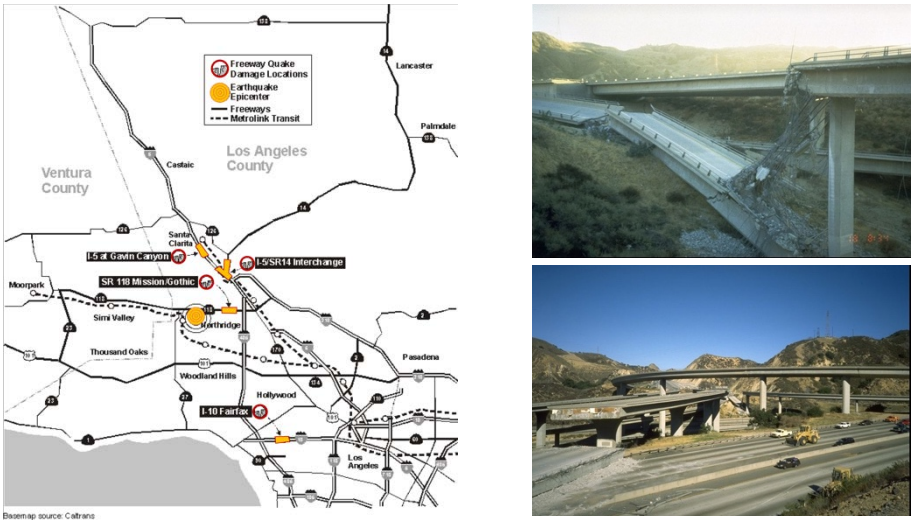

Figure 1.1: Damage distribution on the transportation line Northridge (left), Intersection Interstate 5 to State Route 14 damage (right) USGS Response to an Urban Earthquake: Northridge '94.

The Californian earthquakes of Loma Prieta (1989) and Northridge (1994) (Figure 1.1) and the Japanese earthquake of Kobe (1995) have dramatically highlighted the importance of the transport network and the need for it to remain usable even after an earthquake. If this is the case, the rescue teams will have the possibility to quickly

and easily reach the affected areas, avoiding or limiting further hazards (such as fires) that could cause damage of magnitude comparable to those induced by the earthquake. Another aspect of fundamental importance in the global assessment of the seismic risk is the exposure of the user population to the transport networks, in addition to the "classical" one of the resident populations. Highways, roads, railways, stations, etc. they are widely used infrastructure where the number of people present is comparable to that found in buildings. In this regard, it is recalled that in the Californian earthquake of 1989 (Loma Prieta) the collapse of the viaducts that formed the elevated part of the busy Cypress Street caused most of the victims.

1.1 Seismic vulnerability and the damages

The seismic vulnerability is defined as the propensity of people, artefacts, activities or goods to suffer damage or modification caused by the earthquake (Dolce 1997). Considering a single element or to the whole system, vulnerability is a measure of the loss or the reduction of capacity to perform a normal function. Since the concept of seismic vulnerability is extremely complex and differently structured according to the object to which it is applied, it is useful to distinguish the following components: direct, induced and deferred.

The direct vulnerability is defined as the propensity of a single element, simple or complex, to be damaged or collapsed following a seismic shock. For example, one can talk about the direct vulnerability of a building or a viaduct. With the term vulnerability induced, it is referred, instead, to the effects of the crisis of the organisation of the territory caused by the collapse of one or more elements that constitute it (for example the crisis of the mobility system induced by the impracticability of a road). Deferred vulnerability refers to all the effects that occur in the subsequent phases of the earthquake, such as to modify, if not distort, the habits and behaviour of the settled populations. For example, consider the discomfort produced by the temporary use of emergency housing (tent cities, containers, schools, etc.) or the reduction of the employment base due to the collapse of industrial plants.

A very delicate passage on which it is undoubtedly appropriate to make some reflections is the extension of the concept of vulnerability from the single element to a group. In the past, an attempt was made to make the global vulnerability coincide with the sum of the vulnerabilities of the single constituent elements. It immediately becomes clear that such a definition is insufficient to describe the real conditions of the global vulnerability of the system. For example, consider an urban aggregate:

with a methodology of this type, some fundamental aspects would not be taken into account, such as the interrelations that occur between the buildings for the induced damage that some may cause to others.

In other cases, it may be essential to give a hierarchical classification of the elements: for example, think of a system organised with a tree structure. In this case it immediately becomes clear that the global vulnerability of the system cannot be expressed as a simple sum of the elements: a failure on one of the main branches would, in fact, put a good part of the network out, while a failure on a secondary or quasi-terminal branch would cause minimal damage.

Therefore, for a correct assessment of the global vulnerability, it is necessary to assign different "weights" to the individual elements, depending on the hierarchical role they play within the network. In general, it is possible to affirm that the global vulnerability of a system depends both on the direct vulnerability of the individual elements that are part of it, and on the interrelation between them and its structural organisation.

The concept of vulnerability so far discussed was intended as purely "physical", that is, "structural". However, it has been recently shown that the damage caused by an earthquake is vitally linked to the quality and quantity of the functions and activities that took place before the earthquake. By evaluating, in the long term, the effects of deferred seismic vulnerability, it is essential to keep in mind that, as a result of the earthquake, the conditions for carrying out the complex functions assigned to the various elements of the system or a part of the system of it could not subsist.

The lack of functionality of some elements or the interruption of the performance of certain activities could cause significant damages to the territorial system affected by the earthquake: this is why the concept of functional vulnerability has been introduced alongside the already treated physical (or structural) vulnerability (ASCE 1995).

Many studies have also highlighted the extreme importance of some economic and social factors for the assessment of the global vulnerability of an area (ASCE 1990, ASCE 1991). Indeed, experience has shown that, beyond the purely "physical" damage suffered by a building due to an earthquake, economic, social and political conditions are those that more than others have had greater weight on resilience and reconstruction capabilities of the area. Damages, even if not very extensive, are difficult to heal in weak contexts from an economic and social point of view. On the

contrary, in the presence of flourishing economic conditions and stable social context, autonomous resilience capacities increase considerably. The concept of socio-economic vulnerability has been introduced to give an evaluation of these last aspects (ASCE 1992; ASCE 1996).

1.2 The social economic contest

The study of the anthropised territories represents a complicated and extremely complex operation to be managed for different reasons. The first difficulty to be faced derives very often from the considerable size of the area to be analysed, especially when compared to the level of detail required by some types of study. Secondly, considering the extreme variability and the vast number of anthropic activities distributed throughout the urbanized areas, starting an exhaustive analysis that does not neglect any aspect, appears almost an impossible task if not supported by an appropriate methodological approach.

What is briefly described above applies even more in a multidisciplinary procedure such as the seismic risk assessment. This assessment is based on territorial analysis that requires the acquisition of a large number of data, from different origins and of different nature, which will subsequently be assembled and processed according to appropriate and efficient criteria, to obtain realistic, reliable results and significance. It is, therefore, necessary to refer to a precise and rigorous application methodology, but that needs to be very flexible to be adapted to the different anthropic realities distributed on the studied territory. One of the most used methodologies for seismic risk assessment is the territorial analysis with a systemic approach. A group of objects is defined, indicating with an element each of the objects that compose it. A set able to pursue a goal or to perform a function through the interrelation between its components takes the name of system. It is, therefore, possible to imagine the territory as a complex system, that is composed of a series of related subsystems, each of which plays a particular role in the overall functioning of the system.

The morphological configuration, the function performed, and the typology of the elements make it possible to subdivide the territorial subsystems into two broad categories: space systems and network systems. Spatial systems have a precise localisation within the territory and perform different functions: residential, productive, commercial, administrative, etc. According to the various possible scales of analysis, space systems can identify themselves, in a context territorial area, with an urban settlement or, in a less extensive area of study, with parts of it (for example, the commercial district or the industrial sector) until reaching the individual building

(for example a business centre) for extremely localized studies. The scale of study most commonly used to develop territorial applications for seismic risk assessment is regional or sub-regional. Network systems are sets of linear entities (branches) that converge and diverge from various points called nodes, constituting real networks on the territory. Each network has the function of guaranteeing a specific type of relationship between the multiple space systems: connections, distribution of goods and resources (energy, raw materials, information). It is crucial to bear in mind the distinction between these two types of territorial anthropic systems because it involves considerable differences regarding definitions, approach and application of any methodological procedure. For example, in a seismic risk assessment study, in the definition of exposure of the population reference should be made to the residing persons in the case of a spatial system with residential functionality, to the traffic flows present in the various hours of the day in the case of a network system aimed at road communications. Therefore, the same object (the population exposed to seismic risk) should be studied as a static entity in the case of a spatial system or as a dynamic entity in the case of a network system. For this reason, in the following paragraphs will be developed and deepened the issues related to the infrastructures with a typical type of network systems lifelines.

1.3 The lifelines system

Modern society is dependent on a sophisticated and complex network of infrastructures of vital importance for the existence of current human settlements distributed throughout the territory. These systems of infrastructures, called lifelines, are entrusted with numerous services and functions that are indispensable for regular use of the current urban realities as well as for the performance of any human activity. The lifelines, in essence, are network systems that appear on the territory, on the surface, in elevation or the subsoil. The lifelines connect the various space systems, guaranteeing them a multitude of essential and indispensable services for the survival of the current society: the transport, distribution of energy resources (gas, electricity), the functioning of the toilets and health (aqueducts, sewers), telecommunications, etc.

The lifelines represent the set of network systems (always composed of linear elements) that are used to guarantee all those services indispensable for the survival of the local anthropic settlements. Synthetically we can define lifelines the set of equipment, facilities and services that are part of all those human infrastructures essential to ensure the vital functions of these systems. The lifelines can be divided into the different areas of interest listed below:

- transport;
- electric energy;
- gas and liquid fuels;
- aqueducts and drainage system;
- telecommunications.

Each of these systems has its own functional and technical construction characteristics, so it may seem risky to bring them together under the same definition. However, they have a common feature: they are all networked systems that provide vital functionality for any settlement. In anticipation or case of an emergency, therefore, even if from a technical-operational point of view it is difficult and often impossible to implement common interventions or constructive devices that reduce the vulnerability, from a regional planning point of view the approach and the treatment criteria for these systems are similar.

For these reasons today we speak, in research environments, of real seismic engineering of lifelines (Lifeline Earthquake Engineering). This term indicates all the knowledge and methodologies to design these systems according to a plan that minimises exposure and to build following technologies that, for each type of infrastructure, reduce vulnerability. It is important to underline that lifeline engineering must not only refer to seismic events but, in general, to any type of emergency arising from a generic natural or anthropic disaster: meteorological or hydrogeological catastrophes, floods, fires, etc. Therefore, designing according to these criteria the lifeline systems means having greater guarantees of reliability and efficiency in an emergency condition. These aspects of the design and management of infrastructures, long neglected in the past, have been taken into consideration and deepened only for some years now. Recent experiences have shown the extreme importance of the proper functioning of the lifelines in the emergency conditions that follow any catastrophic event.

Some lifelines must be able to function immediately after an earthquake (sometimes even during) to allow rapid and effective implementation of the assistance and rescue procedures and support all emergency services. An interruption in the transport network, for example, makes access to the affected areas impossible to rescue vehicles: this aspect, which may seem negligible, assumes a decisive weight in reality. The speed and promptness in providing operations valid and useful help have proved to be an essential element for the health (or even survival) of the affected populations. On the other hand, any rescue operation needs, to be practical, an organisation based on the coordination of several bodies, each with its skills and

human and economic resources. It is evident that the collapse of telecommunications lifelines would negatively affect the organisation of relief efforts, causing difficulties and slowness in managing contacts and, consequently, poor exploitation of (usually) scarce resources available. Likewise, the non-functioning of the electricity or water distribution networks would make useless or at least poorly efficient many elements considered "strategic" for public health, especially in emergency conditions: hospitals, civil protection structures, military barracks and fire brigades, etc. It is also essential that the whole set of lifelines, possibly damaged, can be repaired rather quickly to provide for the improvement of the movements and services required for the sustenance of the population and to start the post-earthquake reconstruction process as soon as possible. What has been said so far highlights the importance and usefulness of taking advantage of efficient lifelines in the phases immediately following the seismic event.

However, it should not be forgotten that the proper design of the lifelines can also be advantageous to prevent many of the damaging effects of the earthquake. Consider, for example, fires caused by the breaking of urban gas pipes or broken electricity lines. In a zone whose accessibility has been compromised as a result of the shock, the fire can have catastrophic effects comparable to those of the earthquake itself. The Japanese city of Kobe, for example, hit in 1995 by a violent earthquake, was devastated by both the fires caused by the earthquake and the earthquake itself. Damage due to fire was aggravated by the interruption of the access routes that made the rescue operations difficult for many hours. The systems of the lifelines, therefore, represent, as already mentioned, an essential element that must undoubtedly be taken into consideration in all the anthropised areas that present a specific seismic hazard. It is important that, in these areas, they are designed according to appropriate criteria that always refer to two fundamental rules: the determination of the best territorial location, avoiding, as far as possible, the places with the highest danger; the application of construction technologies aimed at the vulnerability reduction.

Therefore, it is essential that in any modern seismic risk assessment process the study of lifeline networks, to be integrated with the more traditional building analysis, is taken into due consideration. The present work will be dedicated to a type of lifeline: the transport network for road infrastructures.

1.4 Road infrastructures of the transport system

Most of the transport system consists of infrastructures that are fully included in the lifeline category. Suffice it to think of the road and rail networks that serve the territory and urban settlements, or to the typical urban mobility systems such as subways or tramways: they are all network systems that connect different locations in order to meet transport needs — both passengers and goods. It is therefore entirely correct, according to the definitions given, to include these types of transport infrastructures within the lifelines.

The main characteristic that distinguishes transport infrastructures from all other types of lifelines is the direct use by humans to meet their mobility needs. All the other lifeline systems, even though close to humans, are never directly used by them. Although most of these systems, due to the transported elements (for example gas), indirectly exposes man to considerable risk in case of the seismic event, with consequences often severe (fires, etc..) it is always however indirect risks that fall on the population.

In the case of transport systems, there is direct exposure to the seismic risk of the users. Therefore, if a road infrastructure were exposed to seismic risk, with it would be exposed directly all the users. This singular characteristic, which is not found in any other type of lifeline, is significant for a complete evaluation of the seismic risk of an area because the principal object of the exposure analysis is constituted by the population that could be directly affected following a seismic event. For reasons of simplicity of design and economic convenience of construction and management, it is now customary that many wiring or pipe installation systems take place within the road body. The methane pipelines, water pipes, electric cables and telecommunications are often passed through road sections with the following advantages: it is possible to use an existing territorial tracing. The installation is generally very simplified as it takes place in parts of the road section specially designed and leased to various entities by the road management company. Moreover, during installation, management and maintenance will always be guaranteed great accessibility to each part of the network.

However, these numerous advantages come with numerous problems linked to the risk of natural disasters such as an earthquake. With such an integration of the lifelines, it becomes indeed complicated, if not impossible, to evaluate the effects of an earthquake only on one lifeline, neglecting the others. The interactions between the various networks are so tight that it is possible to evaluate just a global effect

(presumably of considerable entity) as a consequence of the mutually induced effects between the various systems. If the seismic shocks damaged a road infrastructure built in this way, the effects induced by the possible damage of the integrated lifelines could have repercussions on the road itself, regardless of the damage directly suffered. These induced phenomena would further exacerbate the damage to the road.

The reasons for which transport infrastructures play a decisive role, in an area hit by an earthquake, both in the phases immediately following the earthquake and at longer expiry will be highlighted. For the same reasons it is essential that, in any seismic risk assessment procedure in an area, the transport system is taken into great consideration, which must be examined in all its components according to exposure and vulnerability.

1.5 Objectives and scope of research

Bridges undoubtedly represent the components that most strongly affect the risk of a network system such as road infrastructure. Many are the elements that determine this vulnerability and among these the morphology and the structural characteristics of the same play a fundamental role. Furthermore, the configuration of bridges involves general structures throughout the territory and, therefore, too high risks for different hazards. The damage or collapse of a network bridge can determine, the loss of functionality of the entire branch to which it belongs would inevitably lack the link between two nodes.

The loss of functionality of the bridges is at the centre of the studies of many international organisations in the field of transport such as CALTRANS, AASTHO, FHWA, JRPA, EUROCODE; these associations have long paid attention to aspects related to the fragility of these structures. In the design phase of bridges in seismic zones, the concept of expected performance or performance has been introduced over the last decades. A new design philosophy called Performance-Based Seismic Design was introduced.

The primary objective of the work is the study of an innovative method for the evaluation of the seismic vulnerability of existing reinforced concrete bridges in a probabilistic way, by using fragility curves. Fragility curves, as can be seen in the scientific literature, have highlighted the complexity of the bridge system, making it difficult to use in daily practice. This difficulty depends on being able to consider the bridge in its entirety, the use of a new combination between the engineering

parameters would give the possibility both to understand the behaviour of the single structural element that of the entire bridge.

In particular, the research study wants to investigate the problems of simple supported girder bridges through the study of a sample bridge defined by geometrical and mechanical characteristics typical of Italian bridges of the 60s.

The methodology for assessing the seismic vulnerability, in a probabilistic way, of existing bridges and viaducts, consists in the construction of the so-called "fragility curves", i.e. the relationships that represent the probability of exceeding a predefined level of damage for a given value of seismic intensity (Padgett 2007). The degree of safety has been evaluated in a probabilistic way, that is through the calculation of the probability of failure of the individual bridges, whose capacity has a duly characterised uncertainty when faced with a specific seismic scenario, also defined statistically. Various analytical procedures have therefore been developed to determine a correlation between the possible seismic event and its likely consequences concerning damage status (Padgett 2007). The study of each of the aspects mentioned was systematically done using parametric studies, in which the results were subjected to statistical treatment, to allow the coverage of a large number of different structural configurations and earthquakes and to achieve generalised results.

A portfolio of bridges, together with a relatively large number of seismic events, has been used for this research. These analyses make it possible to define the seismic efficiency of the bridges, thus allowing to suppose what level of damage should be expected for a given seismic event and which are the most subject to damage with equal seismic intensity.

The levels of damage depend directly on the choice of the Engineering Demand Parameters (EDP). This choice often influences the results especially for complex structures such as the bridges, to make the fragility curves immediately readable, it is herein proposed an innovative combined use of the EDPs to understand both the behaviour of the single bridge elements and global behaviour. All this has the purpose of defining and planning which are the structural interventions of pre-earthquake adjustment to be done and how these improve the resistance capacity of the manufactured articles. This information is significant for the managing bodies of infrastructural networks that nowadays have more to deal with than the construction of new road networks, but with the management and maintenance of the built heritage.

2. Damage of bridges during recent earthquakes

2.1 Recent earthquakes

The strong earthquakes that affected both the most developed and the least developed countries have consequences that have always been significant and, sometimes, devastating for the populations. In the last fifty years, the exponential increase in the number of bridges and viaducts has made visible the effect of earthquakes on these structures, attracting the attention of the international scientific community. Bridges are complex structures composed of different structural elements that work together. Sometimes during the earthquakes, their behaviour is unpredictable, making their study significant to improve our understanding of these structures further.

In fact, in the last years, many studies have described the seismic behaviour of bridges describing the most relevant seismic events of the twentieth century, recalling the relevance of the study of seismic actions. In the twentieth century, there were hundreds of high magnitude earthquakes all over the world. However, for structural engineering, those that have occurred in regions with a high density of buildings, are more interesting, as they have involved a greater quantity of construction, bridges and viaducts designed with more advanced anti-seismic criteria. The analysis of the damages caused by the most representative earthquakes is very important for their contribution at the development of the anti-seismic design criteria. The goal of this chapter is to explain the damages caused by the earthquakes, for the bridge structures, of the most critical seismic events, occurred in the last years.

2.1.1 Loma Prieta earthquake

The earthquake of Loma Prieta, which shook the San Francisco Bay area in California in 1989, is a classic example of a natural disaster that has mostly affected a high population density area with an extensive network of motorway transport. Causing a total of 63 victims and nearly 4,000 injured, one particular aspect of this earthquake was that 42 of the victims were due to the collapse of the two levels of the Cypress Street viaduct of Interstate 880 in West Oakland, (Figure 2.1).

Nevertheless, less than 5% of the bridges exposed to ground shaking have been damaged.

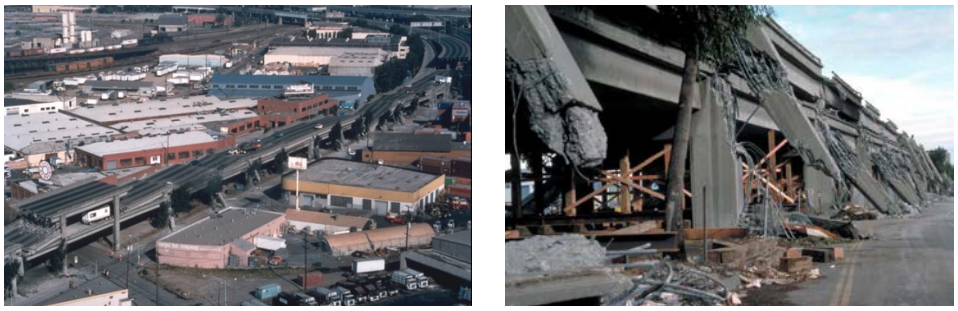

Figure 2.1: Cypress viaduct collapse left – aerial view; right – piers failure detailed view. (Nakata et al. 1999)

The main factors that led to the collapse of the viaduct built in the late 50s, in addition to resonance effects, are geotechnical problems and deficiencies in the design of reinforced concrete structures. Two-column bents connected the upper and lower levels composing the structure in a combination of cast concrete and four pins (shear key) connections. The upper part in some sections was not firmly connected to the lower floor and, while the bridge vibrated during the earthquake, even the nodes that linked the levels began to vibrate, that led to the failing of the concrete that surrounded the nodes. There is no transversal reinforcement for the nodes between the piers and the deck.

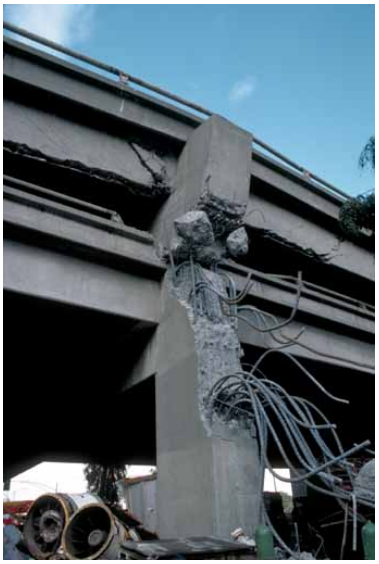

Figure 2.2: Cypress viaduct: lack of proper reinforcement in pier-deck connections. (Nakata et al. 1999)

The connections of structural elements are often subject to a higher demand than the single parts, but in this case, ductile connections have not been used in the design or retrofitting phase. As for the geotechnical part, the viaduct was built on soft mud, weak soil, that is susceptible to liquefaction during an earthquake with large ground motion. Without the presence of the foundation under the piers, those elements slid sideways under the weight of the upper deck that led to the collapse of a large portion of the upper deck (Yashinsky, 1998a).

Therefore, some aspects of the design and construction of the structure contributed to the bridge collapse: inadequate transverse reinforcement in the columns, ineffective bent cap and pin connection design (Moehle, 1999) and inadequate compensation for weak soil conditions (Yashinsky, 1998a).

Figure 2.3: Oakland Bay Bridge: a collapsed portion of the upper deck. (Nakata et al. 1999).

The Oakland Bay Bridge has reported minor damages (Figure 2.3) a span of the upper road has collapsed on the lower deck, indirectly causing the death of some people. The satisfactory behaviour of this bridge can be attributed to the steel structure, a material with greater ductility than concrete, less vulnerable to seismic events. The need to pay attention to reinforced concrete bridges is therefore clear.

2.1.2 Northridge earthquake

The Northridge earthquake, named after a district in the city of Los Angeles, California, occurred in 1994, for about 45 seconds. With one of the highest ground accelerations measured in urban North America, around the 1.0g range, it has become one of the most expensive natural disasters in US history, causing 70 deaths

and over 9,000 injuries. After the 1989 Loma Prieta earthquake, a modernisation program began on Californian bridges and was yet to end when the Northridge earthquake took place. In the epicentre area, there were about 2000 bridges, ten of which were damaged, with four of them that had to be demolished and rebuilt. The damage reported following the earthquake involved a large part of the vast motorway network, with particular attention to the Santa Monica Freeway, which is used daily by millions of commuters, and the Antelope Valley Freeway, (Figure 2.4)

Figure 2.4: Collapsed section in Santa Monica (left) and Antelope Valley Freeway (right). (Todd et al. 1994)

The collapse of the bridges was mainly due to the failure of the piers, designed and built before 1971, a critical moment, given that after the San Fernando earthquake the anti-seismic standards began to be considerably strengthened. The lack of adequate confinement of the reinforced concrete, with the consequent "bird cadging" effect of the steel reinforcement, or poor behaviour of flared pier tops are some typical examples of column failure, (Figure 2.5).

Figure 2.5: Failure of columns: insufficient confinement (left); shear failure (right). (Todd et al. 1994)

On the one hand, the retrofitted bridge did not report severe damage, according to (Yashinsky, 1998b) studies, only minor cracks to the slope paving. On the other hand, the damages on not retrofitted bridges, built in the same site, turned out to be high, (Figure 2.6) (Cooper et al., 1994).

Figure 2.6: Failure of the column due to the failure of circular confinement steel (left); good behaviour of column retrofitted (right). (Todd et al. 1994)

Other damages to bridges include spalling and cracking of concrete abutments, spalling of the concrete covering the columns, overturning or displacement of the steel and neoprene bearings. From these observations, it can be said that bridges designed and built before 1971 proved to be worse than those designed according to the latest standards, with the piers being the most damaged components (Basoz and Kiremidjian, 1998). However, the damage caused by the earthquake revealed that some structural specifications did not work as well as expected, as in the case of two bridges, both built shortly after the 1971 earthquake, on the Simi Valley-San Fernando Valley expressway. These bridges presented severe problems to the columns that caused the bridge to fail.

2.1.3 Kobe earthquake

The great earthquake of Hanshin occurred in January 1995 is often referred to as the Kobe earthquake because that was the most damaged city. The earthquake caused more than six thousand casualties, with 4600 from the city of Kobe. As it is easy to imagine, this was the worst earthquake in Japan since 1923. The comparison with the Northridge earthquake, which occurred only a year earlier, was inevitable. The city of Kobe was less fortunate since the damages caused by the earthquake was

much bigger than of those caused by the American earthquake. This difference mainly derives from the particular soil type in Kobe, as well as the not reinforced lightweight structures in masonry and wood. The damages observed at the bridges of the motorway network is the most familiar images of this seismic event:

- substructure failure, originating from simple shear failure in reinforced concrete columns;
- premature shear failure at terminations of longitudinal bars with insufficient development lengths;
- extensive failure of steel columns, the first in the world;
- soil liquefaction, leading to settlements and tilting of foundations and substructures and lateral spreading of ground associated.

One of the most important structural disasters was the collapse of the eighteen spans of the Fukae viaduct, serving Route 3, inside the elevated Hanshin Expressway, (Figure 2.7).

Figure 2.7: Collapsed Fukae Viaduct (left) and Premature Shear Failure of Reinforced Concrete Column, Fukae Viaduct (right) (Kawashima, 2007).

The viaduct was designed by using the 1964 Design Specification and was completed in 1969. Insufficient code provisions have led to significant problems in the design of the viaduct: the overestimated allowable shear effort, the insufficient development length of the longitudinal bars terminated at half height and the inadequate amount of tie bars. The combination of these aspects has led to the already mentioned failure of premature rupture.
In Figure 2.8, by Kawashima (Kawashima, 2007), is shown the possible mechanism of collapse of the viaduct that highlights the importance of the correct reinforcement of the piers, especially at the base, since the P-Δ effects were not considered.

The soil failure was equally frequent as many of the bridges had been built on sand-gravel terraces (alluvial deposits) that covered deposits of gravel and sand at depths

of less than ten meters, a condition that is believed to have led to the amplification of the site of the rocky substrate motions.

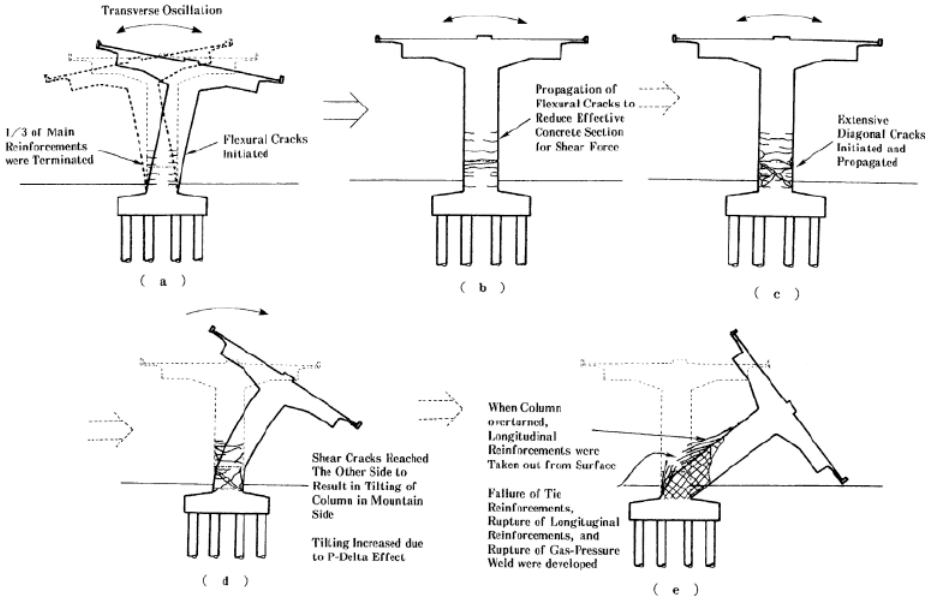

Figure 2.8: Collapse mechanism of Fukae Viaduct (Kawashima, 2007).

There were also several situations of liquefaction and lateral spreading, with consequent permanent deformations of the substructure and loss of superstructure support (Moehle and Eberhard, 1999). The collapse of the span of the Nishinomiya-ko bridge approach, (Figure 2.9), is an excellent case of how the site conditions have significantly increased vulnerability.

Figure 2.9: Nishinomiya-ko Bridge approach span collapse (Kobe Collection, EERC Library, University of California, Berkeley).

The further collapse of bridges is a result of the damage of the device to prevent the unseating of the span, over the forces transmitted through unseating prevention devices.

2.1.4 L'Aquila earthquake

The L'Aquila earthquake, in April 2009, happened in the Abruzzo region, in central of the Italy, with a magnitude of 6.3 on the Richter scale. The epicentre was near L'Aquila, the capital of Abruzzo, which suffered the most significant damages together with the closer villages. The earthquake was felt throughout central Italy, with 308 casualties, making it one of the deadliest earthquakes that have hit Italy since 1980. Even though it has occurred in a well-developed country, with relatively advanced seismic regulation, the resulting damages were significant. This was mainly due to the high number of medieval, historic buildings and buildings with unreinforced walls, known to be very susceptible to seismic action. But not only the ancient structures in L'Aquila have suffered damage.

Many modern buildings considered resistant to the earthquake were damaged, such as a local university dormitory and the new wing of L'Aquila Hospital. The former was constructed with nonductile concrete, an irregular planar layout that led to soft story collapse. The latter, opened in 2000 and was designed to withstand a strong earthquake in safety, suffered considerable damage and had to be closed. This thing was surprising, given that the event was moderate and within the code provisions. The failure was admitted mainly due to the lack of a consistent seismic design (Miyamoto et al., 2009). However, the structures of the transport network, in particular bridges, have behaved well, suffering few damages. Usually, more damages are expected to this type of structures for an earthquake of greater magnitude or a longer duration of strong ground shaking. The worst case was a short 35-meter-long, three-span reinforced concrete bridge, not far from the epicentre, which collapsed on the riverbed, (Figure 2.10).

Figure 2.10: Bridge collapsed on the Aterno river, near Fossa (M. Indirli, 2010).

The four piers of reinforced concrete with hexagonal sections were broken at the connections of the base of the pier, sliding sideways and penetrating in the bridge deck. A masonry arch bridge, which had previously collapsed and was repaired with limestone, collapsed again during the earthquake, due to the probable movement of the abutments, with the consequent loss of the arched effect. Finally, some of the viaducts inside the A24 motorway near L'Aquila have been hit by the earthquake, even though the same highway has not collapsed anywhere (Aydan et al., 2009). Once again, the critical point is that, given the moderate nature of the earthquake, seismically designed bridges should not have collapsed, which indicates the need for a code review and a careful assessment of the safety of existing structures.

2.1.5 Haiti earthquake

The earthquake in Haiti, one of the most recent earthquakes and probably one of the most catastrophic, occurred in February 2010, causing the death of over 230,000 people. The consequences have been devastating mainly due to the general lack of attention to seismic design principles and construction practices that have led to the poor quality of the majority of the existing construction. The historical model of the earthquakes in Haiti indicates that one seismic event could damage southern Haiti near Port-au-Prince at any time. According to reports following the earthquake, no type of damaged bridges was recognised due to the earthquake. Within Port-au-Prince, the most affected city, most of the river crossing bridges did not collapse, (Figure 2.11). In any case, these river crossings can be dangerous in the future, since a large amount of dirt accumulated upstream that can, combined with silt and debris, prevent water from passing through the underground canals (Eberhard et al., 2010).

Figure 2.11: Box culvert in Port-au-Prince (left); damage to the shear key at intermediate support of bridge (right) (Eberhard et al., 2010).

Most of the crossings on the National River and 2, are bridges precast girders resting on cast-in-place reinforced concrete piers and supporting a cast-in-place deck. Damage was observed on two of these bridges. The Momance river bridge had minor pounding damage to the shear key on one of the intermediate supports that had probably not been adequately and accurately reinforced. A similar bridge in the Carrefour section of Port-au-Prince suffered damage on the outside of the shear keys on both intermediate supports, apparently caused by the lack of anchorage of the hook at the end of the reinforcement of the upper beam.

The simple damage analysis of Haiti earthquake allowed to conclude that the ground motion was not significant enough to severely damage well-designed structures. The absence of seismographic stations that worked during the main earthquake doesn't allow for an accurate estimation of the intensity of the ground motions.

Several buildings and supporting structures survived the earthquake without severe damage. Similarly, bridges near the epicentre suffered only minor damages and could be immediately used after the seismic event. Unfortunately, this framework confirms the lack of attention to seismic design that persist throughout the world, with a significant incidence in developing countries.

2.1.6 Christchurch earthquake and Tōhoku earthquake

Both events described here, not only because they occurred in the same year but also because they both have happened in the so-called developed, prosperous, New Zealand and Japanese countries. The 2011 Christchurch earthquake was a 6.3 magnitude earthquake that struck the Canterbury region on the South Island of New Zealand on February 22, 2011, causing widespread damage and multiple deaths, although no collapse of bridges was reported. The earthquake of Canterbury of magnitude 7.3 in 2011, occurred almost six months later, causing significant damage to the region, but with no casualties. Analysts have estimated that the earthquake could cost insurers 12 billion dollars. Of the 3,000 buildings inspected in the city centre, around 45% could not be used for safety problems, and a thousand would have been demolished (about 25% of the total number of buildings). Many buildings of the cultural heritage have also received red stickers after the inspections but, in general, not many buildings have collapsed.

Examples include two six-story buildings: the Canterbury Television building and the PGC Building, (Figure 2.12), a reinforced concrete structure that was built in 1963-1964, which drew much attention to the high vulnerability of the buildings constructed before the '70. The seismic behaviour of these buildings includes the

failure of a column, column shear failure, beam-column joint failure, the onset of soft-storey failure, shear wall failure, etc. The 26-storey Grand Chancellor building, the tallest hotel in Christchurch, was on the verge of collapse and subsequently demolished in the following months. The most extensive damages occurred in older buildings, especially those with unreinforced masonry and those built before earthquake codes were introduced, the high rises constructed in the last twenty to thirty years have worked well (Kam, 2011).

Figure 2.12: The Pyne Gould Corporation (PGC) Building following the 2011 Christchurch earthquake (Kam 2011).

The Tōhoku earthquake on March 11, 2011, officially called the Great East Japan Earthquake, was a magnitude 9.0 earthquake. It is considered the most potent known earthquake in Japan, and one of the five most powerful earthquakes in the world since the beginning of the modern recording in 1900. The earthquake caused extremely destructive tsunami waves, causing numerous victims (around 14 616 deaths, 5278 injured and 11 111 missing persons), destruction of infrastructure and numerous nuclear accidents. The total cost exceeds $ 300 billion. Structurally, over 125,000 buildings have been damaged or destroyed, as well as roads, railways and bridges and a dam have collapsed.

Figure 2.13: Bridge collapse in 2011 Japan Earthquake and Tsunami. (TRDB 2011).

Apart from the obvious many structural failures, such as the failure of the bridge (Figure 2.13), the Japan earthquake of 2011 caused a severe nuclear accident, which has hit, over the present and future years, the natural resources of the planet. The devastating way in which the earthquake recently struck New Zealand and Japan is a sad but important reminder of how modern society is vulnerable to such events, even in relatively well-prepared countries.

2.1.7 Emilia Romagna earthquake

On 20 May 2012, an earthquake with a magnitude of ML = 5.9 hit the Emilia-Romagna Region and a small part of the Lombardy Region in the north of Italy. Subsequent earthquakes occurred on May 29, 2012 with ML = 5.8 and ML = 5.3. The earthquakes caused 27 deaths and 14,000 homeless people, including 13 on industrial buildings, 12,000 buildings were severely damaged. Also, serious damages have occurred to historical monuments, estimated at around 5-6 billion euros. In the reports of the post-earthquake observations, only minor damages to bridges and viaducts in RC are reported. The bridge in the outskirts of the city of Finale Emilia (Figure 2.14), the only visible damage is an insignificant cracking in an external section of the bridge at an expansion joint.

Instead, slight damage was observed in the masonry abutments of an old reinforced concrete arch bridge (Bomporto Bridge) built in 1914. No visible damage to the

reinforced concrete structure. However, the breakage of both masonry abutments (Figure 2.15), which in turn caused cracks in the road surface (Figure 2.15). This bridge had to be put on a regime of reduced traffic to lessen the load on the shoulders (Figure 2.15).

Figure 2.14: Precast concrete bridge outside Finale Emilia

Figure 2.15: Bomporto Bridge, damage report (EPICentre Report No. EPI-FO-290512).

2.1.8 Central Italy earthquake

On 24 August 2016, at 1.36 UTC, 3.36 local time, an earthquake with an epicentre located in the municipality of Accumoli, with a magnitude of MW 6.0, began the seismic sequence that affected Central Italy until 2017. The event of the 24 August was followed by countless aftershocks, the most important of which occurred on 26 October near Castelsantangelo sul Nera (MW 5.4 and MW 5.9), on 30 October near Norcia (MW 6.5) and on 18 January 2017 close to Capitignano, with four shocks with a magnitude of MW between 5.0 and 5.5. This seismic sequence caused considerable damage in a large area of central Italy, involving the four regions of Lazio, Umbria, Marche and Abruzzo, causing 298 deaths, 17,000 homeless.

Immediately after the seismic sequences of Central Italy, numerous inspections were done on several bridges with masonry structure, mixed masonry and RC and steel-concrete compounds. The RC bridges had a deck consisting of beams in RC prestressed. The beams are supported by elastomeric bearings, located above the piles, without the use of anchorage. It should be noted that these elastomeric bearings have been designed not as seismic isolation devices, but to resist vertical actions and to allow small displacements and relative rotations due to thermal variations. Moreover, due to the absence of anchorage or bolts, these devices allow the horizontal actions to be transferred between the deck and the transverse only as friction between the rubber and the concrete: for this reason, the deck tends to slide as soon as the lateral forces exceed the friction resistance. It is therefore evident that in this configuration the bridge deck is poorly constrained against horizontal displacements relative to the substructure (pier), although shear keys are sometimes made on the cross Girder and on the abutment, to prevent excessive lateral movements (Di Sarno et al. 2018).

Figure 2.16: Viaduct "Scandarello" SS4 Amatrice Italy.
(ANAS, Relazione Esecutiva, 2010).

Despite the weak connection between the deck and the substructure, the elastomeric bearing appeared in good condition in all the inspected viaducts, with no signs of sliding concerning their original position, (Figure 2.17). Although no loss of support for beams supporting the deck was documented, slight damage due to excessive longitudinal displacements was found. These displacements caused hammering phenomena between successive spans or between end spans and abutment, causing cracks and concrete detachments on the cross girder and the abutment, (Figure 2.18). In the inspected viaducts no, significant damage to the piers was detected.

Figure 2.17: Elastomeric Bearing (Totaro photos).

Figure 2.18: Relative displacement of the Abutment

2.2 State of the art of the Italian road

The Italian road infrastructural heritage is composed of the national network, road (20773 km) and highway (6668 km), from the regional and provincial networks

(151583 km) and a countless of municipal road networks (72081 km). In particular, it consists of a large number of bridges, viaducts and overpasses necessary for the orography of the territory and the high urban density.

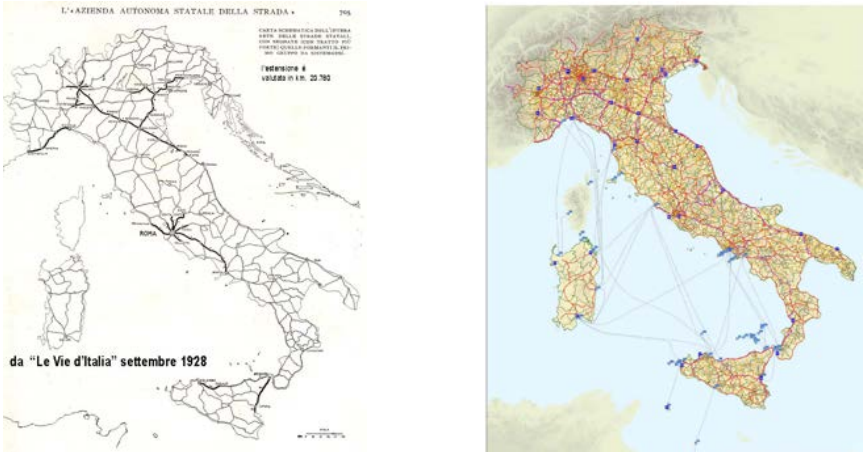

Figure 2.19: Evolution of the road infrastructures in Italy (ANAS).

Table 2.1: Evolution of the road infrastructures in Italy (Office of Statistics 2014).

Years	1930	1990	2000	2012
Road [km]	20780	161938	167725	180175

Figure 2.19 Shows the exponential increase of Italian road infrastructures from 1928 to today; in 1928 the road network was 21,000 km long that has grown, according to data provided by ANAS and the Ministry of Infrastructure and Transport in the annual report (Office of Statistics 2014), to 180175 km by the end of 2012. 14% (Autostrade per l'Italia SpA 2015) (Figure 2.20) of this network are viaducts or bridge structures. (Casarotti, 2004) proposed an adequate structural classification of simple multi-span bridges built in the '70s and' 90s.

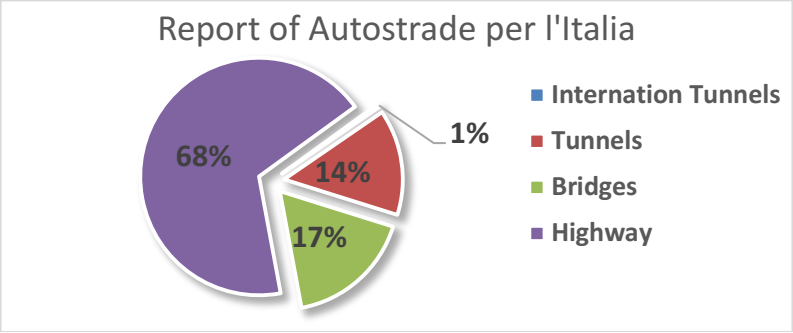

Figure 2.20: Report of Autostrade per l'Italia.

From this study, it was possible to understand that in about 61% are used neoprene bearing devices and that most of the cases analysed have some span exceeding five (Figure 2.21).

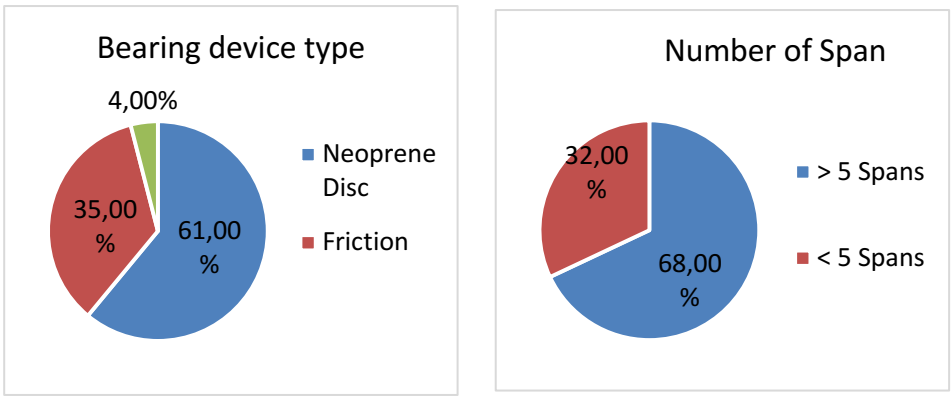

Figure 2.21: Bearing device (left) and a number of spans of Italian Bridge (right).

2.2.1 Recurring damage to Italian bridges

Road infrastructures are very vulnerable, as they are affected by design (structural and technological) deficiencies related mainly to the construction period, to the applied technologies and the materials used, together, especially in the last few years, to a lack of adequate maintenance. Most of the bridges and viaducts in Italy were built between the 50s and 60s when the economic boom generated unlimited confidence in the use of concrete as a durable material for eternity. Moreover, most of these structures of the Italian road network were realised through the technology of the pre-stressed reinforced concrete, hardly compatible, with the concrete concepts of reliability. The inadequacy of the old design philosophies has been observed in the last decades, given the high vulnerability of these structures to the various seismic events that occurred in different parts of the world, even if the infrastructures had been designed with anti-seismic criteria (Priestley 1996).

These structures are difficult to analyse for their very low ductility. This lack of ductility cannot be considered a design error. It would be more appropriate to underline that in the 60s two fundamental factors led to this situation:

- no awareness reinforced concrete could have such a short life and could suffer attacks and deterioration due to atmospheric agents and environmental;
- there were no automatic calculation tools, so, where possible, statically determined patterns were preferred, much more straightforward to calculate.

Therefore, it is, need to improve performance with the efficiency and level of simply supported multi-span bridges. The most frequent damage from the most recent earthquakes is that the common failure mechanisms are:

- Pier flexural failure;
- Pier shear failure;
- Unseating of the deck.

3. Seismic Probabilistic Risk Analysis: Performance-based Earthquake Engineering (PBEE)

The seismic methodology of probabilistic risk analysis (SPRA) (Kennedy et al., 1980; Wakefield et al., 2003) has, for decades, been the most commonly used approach to assess the seismic safety of nuclear structures. In the last few years, this methodology has also become popular to characterise the seismic behaviour of other civil structures (Hamburger et al., 2003, FEMA, 2012). It was developed by the Pacific Earthquake Engineering Research Center (PEER), with the name of Performance-Based Earthquake Engineering (PBEE). The PBEE methodology can be divided into four processes shown in Figure 3.1: hazard analysis, structural analysis, analysis of damage and loss analysis.

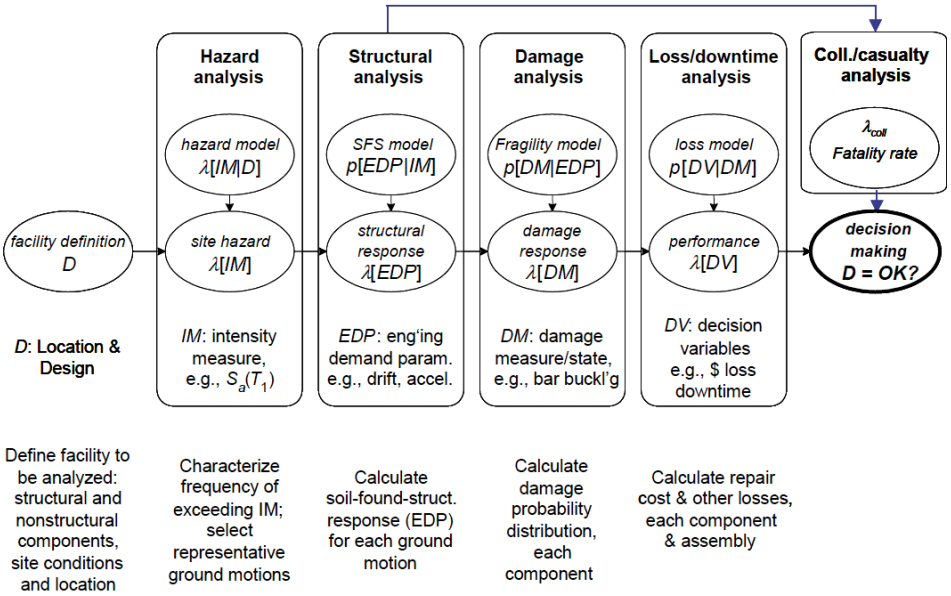

Figure 3.1: PEER-PBEE methodology. Reproduced from Krawinkler (2005).

In the hazard analysis, the seismic risk is evaluated for the structure site and for the ground-motion time histories, where intensity measurements (*IM*) correspond to different levels of hazard. In the step of the structural analysis, nonlinear time history

analyses are carried out to calculate the structure's response to ground motions of a given IM regarding drift, top displacement, floor response spectrum characteristics, or others Engineering application parameters (*EDP*).

During the damage analysis step, this *EDPs* are used together with the component fragility functions to determine the specific damage measures (*DMs*) for the components of the system. Finally, defined these *DMs*, it is possible to evaluate a series of variables, including operability, repair/duration costs and potential victims. These performance measures are referred to as decision variables (*DV*) as they serve to inform the stakeholders about performance for future decisions. The relationships between the fundamental variables in the PEER-PBEE framework Figure 3.2

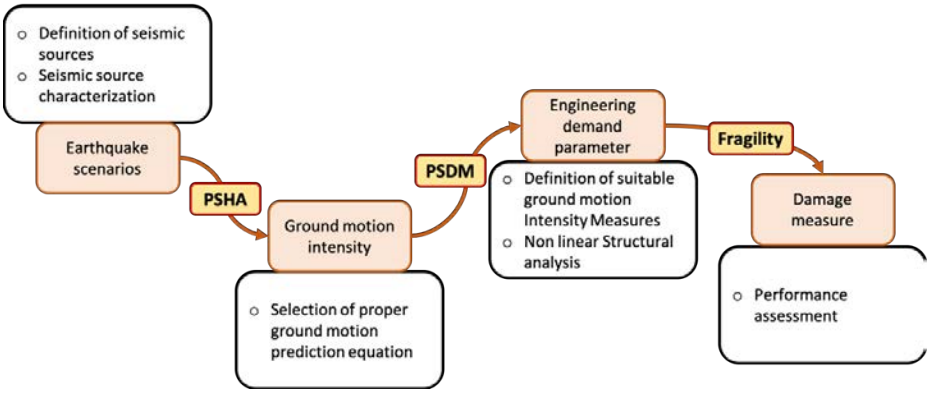

Figure 3.2: PEER performance-based earthquake engineering framework.

Studies carried out in the last decade (Luco, 2002; Baker and Cornell, 2004; Tothong and Cornell, 2006) have shown that the PBEE procedure can be made easier by separating the assessment of the design ground motion levels (probabilistic assessment of seismic risk, PSHA), and that of the structural response due to design ground motion (i.e. evaluation of the probabilistic seismic demand, PSDA). Details of the methodology of the PSDA.

Each step of the process, from design to IMs, IMs to EDPs, EDPs to DMs and DMs to DVs, includes uncertainties and is treated probabilistically. The probabilistic expressions of the components of the PBEE methodology can be combined using the total probability theorem (Benjamin and Cornell, 1970) and expressed as:

$$\lambda(DV) = \int_{DM}\int_{EDP}\int_{IM} p[DV|DM]p[DM|EDP]p[EDP|IM]\lambda(IM)dIM\ dEDP\ dDM \qquad 3\text{-}1$$

where:

$p[..|..]$ = Probability Density Function (PDF)

$\lambda(IM)$= Mean Annual Frequency of events with intensity IM

$\lambda(DV)$= Mean Annual Frequency of events with value DV of the decision variable

Each function are an element of the analysis methodology:

- $\lambda(IM)$ is the results of the hazard analysis;
- $p[EDP|IM]$ is the result of the structural analysis;
- $p[DM|EDP]$ symbolises the damage analysis;
- $p[DV|DM]$ give back the loss analysis.

The analysis of equation 3-1 shows that it is possible to divide the problem of evaluation into the four basic elements of risk analysis, structural analysis, damage analysis and loss estimation, by introducing three intermediate variables: *IM, EDP* and *DM*. Successively, can use the integration on all levels of the selected intermediate variables to re-pair the elements. This integration allows the evaluation of the conditional probabilities $p[EDP|IM]$, $p[DM|EDP]$ and $p[DV|DM]$ parametrically in a suitable range of *DM*, *EDP* and *IM* levels.

The hypothesis is that suitable variables are chosen (*IM*, *EDP* and *DM*) so that the conditioning information should not be "carried forward", for example, selected the *EDPs*, the *DM* is conditionally independent of *IM*, else, *IM* should appear after the *EDPs*. The right way to choose the *EDPs* is that should be selected so that the *DMs* and the *DVs* do not change even with the intensity, once the *EDP* has been specified. In the same way, it is possible to choose the Intensity Measure (IM) so that, once defined, the dynamic response (*EDP*) is not further influenced, for example, by the magnitude or distance from the source of the seismic event, which is already integrated into the determination of $\lambda(IM)$ (Krawinkler and Miranda, 2004).

3.1 Hazard Analysis

The PBEE analysis aims to guarantee that a structure can resist an assigned level of ground shaking while keeping a chosen level of performance. Because of the considerable uncertainty regarding the position, the size and the consequent intensity of the shaking of future earthquakes, it is difficult to define the parameters in a deterministic way. To quantify these uncertainties and match them to produce an

explicit description of the distribution of future earthquakes that could occur on a site, it is possible to use the Probabilistic Seismic Hazard Analysis (PSHA) (Cornell, 1968; Kramer, 1996; Baker, 2008).

The first part of the problem is the estimation of the annual rate exceeded of the IM. In other words, seismic risk analysis represents a link between seismic scenarios and the intensity of ground motion, shown in Figure 3.1. Traditionally, the probabilistic seismic risk analysis (PSHA) due to a point source is performed by evaluating the following equation (Cornell, 1968; McGuire, 2004):

$$v\,(IM > z) = N_{\min} \cdot \int_M \int_R f_M(M)\, f_R(M,R) P(IM > z|M,R) \times \mathrm{d}M \times \mathrm{d}R \qquad 3\text{-}2$$

where:
R is the distance from the source to the site;
M is the magnitude of the earthquake;
$N_{\min}$ is the annual rate of earthquakes with ma agnitude higher than or equivalent to the minimum magnitude;
$f_M(M)$and$f_R(M,R)$ are the probability density functions representing magnitude and distance;
$P(IM > z|M,R)$ is the probability of observing an IM higher than z for a specified magnitude and earthquake distance;
IM is the quantification of the characteristics of a ground movement that are important for the structural response.

The PSHA needs the definition of seismic sources close to the specific site and the characterisation of these seismic sources through proper probability density functions and recurrence models. After the definition of a series of earthquake scenarios, it is possible to evaluate the range of ground motion for every earthquake scenario, and the annual rate of each combination of seismic scenario and ground motion is calculated. The probability that IM exceeded z, $P(IM > z|M,R)$, is obtained from the prediction equation of soil movement (GMPEs) and includes an implicit integration on the variability of the ground motion. The probability that the IM exceeds z is given by:

$$P\,(IM > z|M,R) = \int_\varepsilon f_\varepsilon(\varepsilon) \times P(IM > z|M,R,\varepsilon) \times \mathrm{d}\varepsilon \qquad 3\text{-}3$$

where epsilon (ε) is the number of standard deviations around the median, $f_\varepsilon(\varepsilon)$ is the probability density function for epsilon, stated by the standard normal distribution, and $P(IM > z|M, R, \varepsilon)$ is 0 or 1. In this formulation, $P(IM > z|M, R, \varepsilon)$ identifies earthquake scenarios and combinations of ground motion that lead to *IM* greater than *z*. The hazard equation 3-2 can, therefore, be written as:

$$v\,(IM > z) = N_{\min} \cdot \int_M \int_R \int_\varepsilon f_M(M) f_R(M,R) f_\varepsilon(\varepsilon) P(IM > z|M,R,\varepsilon) \times \mathrm{d}M \times \mathrm{d}R \times \mathrm{d}\varepsilon \qquad 3\text{-}4$$

Although this form is more complexed than Equation 3-1, it has the benefit of clearly showing that the risk integral takes into account the random variability in three main parameters of the earthquake of the scenario: magnitude, distance and epsilon (Gülerce and Abrahamson, 2010). Using equation 3-4, the annual rate of exceedance of any measure of ground motion intensity can be calculated using seismic source models and GMPEs suitable for the region.

Furthermore, based on the recent approach developed by (Bommer and Acevedo, 2004; Katsanos et al., 2010) and to be consistent with the probabilistic analysis of seismic risk, the selected earth motions should in principle be compatible with the combination of magnitude and distance that dominates the danger for a particular value of *IM* (Sommerville and Porter, 2005). It is now clear the important role of *IMs* in current seismic risk probabilistic analysis methods: quantifying the seismic hazard at the structure site.

3.2 Structural Analysis

In the PBEE method, structural analysis is done to determine the response of a structure at various levels of the earthquake hazard in a probabilistic way. To this end, a structural computational model must be developed. The parameters uncertainties present in the structural model (for example mass, damping, stiffness and resistance) can be considered by changing the properties in the model itself. However, it is worth mentioning that (Lee and Mosalam, 2006), using PEER-PBEE methodology, have shown that the variability of soil movement is more significant than the uncertainty of structural parameters in influence the *EDPs*.

For each level of earthquake hazard, nonlinear time history analyses are performed to estimate the structural responses with the selected engineering demand parameters

(*EDP*), using the ground motions chosen for that level of intensity. The *EDPs*, for example, can be local parameters as element forces or deformations, or global parameters like plane acceleration and global displacement. The *PBEE* formulation requests a single value for each *EDP*. It is possible to use various *EDPs* for the different damaged elements of a structure: e.g., inter-story drift can be used for a building's structural system (Krawinkler, 2005), while using floor acceleration for office equipment or laboratory (Comerio, 2005) of the same building. The results of the structural analysis step are conditional probabilities, $p[EDP|IM]$, that can then be integrated with $\lambda(IM)$ to calculate the average annual frequency of exceeding each *EDP*. The most immediate way to make probabilistic evaluation of earthquake damage is to formulate it as a function of *M* and *R*, such as:

$$(EDP) = N_{\min} \cdot \int_R \int_M f_m(M) \times f_r(M,R) \times P(EDP > y|M,R) \times \mathrm{d}M \times \mathrm{d}R \qquad 3\text{-}5$$

where $P(EDP > y|M,R)$ is the probability of analysing an *EDP* higher than y for a given magnitude and earthquake distance. PSHA procedures can be used to directly assess earthquake damage using this form of the risk equation.

To develop a predictive model of the specific response of the structure, the structure should be analysed for a large number of ground movements. The results of the nonlinear dynamic analysis can be used to model the distribution of structural demand with amplitude and distance by regression analysis. The assumptions implicit in this method are (Baker and Cornell, 2003):

- the efficient form of the regression equation;
- the absence of dependency of the *EDP* on the characteristics of the source not contained in the vector of independent variables (e.s. duration of the break);
- the lack of dependency of the *EDP* on the geometry of the error with respect to the site.

The need for numerous dynamic analyses to obtain a reliable estimate for the specific prediction model of the structure and response and the complications involved in the modelling process required a simplified procedure that independently treats the risk of soil movement and the structural response. Cornell and colleagues proposed the probabilistic seismic demand model (PSDM) (Tothong and Cornell, 2006; Baker and Cornell, 2003) approach in which the results of nonlinear dynamic analyses for a specific structure are used to evaluate the behaviour of important *EDPs* regarding *IM* levels. The main idea of these studies was to develop PSDMs for a particular

facility and to provide the annual frequency of exceeding a certain measure of structural engineering demand and conditioning on *IM*, such as:

$$v\,(EDP > y|IM) = \int_{IM} f_{EDP}(EDP|IM) \times \mathrm{d}v(IM) \qquad 3\text{-}6$$

where $f_{EDP}(EDP|IM)$ is the probabilistic model of seismic demand for a specific *EDP* and *IM*. *PSDMs* represented the link between *IM* and *EDP* as shown in Figure 3.1 and give information on the probability of exceeding the predefined critical levels of EDP for a definite category of structures. These models can be used as risk-based design tools, as they show the variability of the parameters of the structural demand for certain ground motion intensity. Furthermore, when coupled with PSHA, PSDMs can be used to calculate structural demand risk curves (Mackie and Stojadinovic, 2003). PSDMs can be incorporated into the risk integral (Gülerce and Abrahamson, 2010) to directly estimate the annual probability of exceeding a given *EDP*. If the *EDP* is considered as dependent just on a scalar ground motion *IM*, the hazard integral for the *EDP* becomes:

$$v\,(EDP > y) = \left\{ \begin{matrix} N_{\min} \cdot \int_M \int_R \int_\varepsilon f_M(M) f_R(M,R) f_\varepsilon(\varepsilon) \\ P\left(EDP > y|\widehat{EDP}[IM(M,R,\varepsilon)], \sigma_{\ln EDP}\right) \mathrm{d}M\mathrm{d}R\mathrm{d}\varepsilon \end{matrix} \right\} \qquad 3\text{-}7$$

where $\widehat{EDP}[IM(M,R,\varepsilon)]$ is the median *EDP* and $\sigma_{\ln EDP}$ is the standard deviation of *ln(EDP)* for a given *IM* (the EDP is modelled as a lognormal variable). This approach combines the hazard of site-specific ground motion with the structural result of nonlinear dynamic analysis for a given structure. The end result of the risk integral indicated in Equation 3-7 is a structural demand risk curve that represents the annual probability of exceeding a specified *EDP* value.

3.3 Damage and Loss Analyses

Once the probabilities of the *EDPs* have been defined in the structural analysis step, these probabilities should be used to determine the probability of *DM* overruns. This is achieved through the analysis of the damage and the phases of the analysis of the loss.

The goal of the damage analysis is to evaluate the probabilities of physical damage of the structural components or system as a function of the structural response. The response provided by the numerical application models is not necessarily related to

the physical descriptions of damage, failure and collapse. So, the experimental or numerical values of the observed damage, are frequently integrated into the PBEE formulation by defining the damage induced at different levels of structural response. The instrument used to determine the probabilities is the fragility function.

The fragility function, In the framework of PBEE in the phase of damage analysis, represents the probability of exceeding a damage measure *(DM)* for various values of *EDP*. Examples of damage measurements for R/C structural components are cracking, transverse reinforcement fracture, spalling, failure and longitudinal reinforcement buckling. Furthermore, damage measures can be defined regarding damage levels according to the repair measures necessary to restore the initial conditions (Porter, 2003). Mitrani-Reiser et al., 2006, defined DM of low, moderate and severe structural elements corresponding to the repair with epoxy resin injections, repair with coating and replacement element, respectively. In particular, to assess the values of the damage suffered, the fragility functions must be defined for each damage states, providing the probability of exceeding a damage status for a stated *EDP* level (represented by the third arrow in Figure 3.1). With information on structural capacity (fragility curves), the results of the PSDA can be used to calculate the annual frequency of exceeding a specified damage state. During the years, the researchers have implemented many methodologies for generating the seismic fragility curves, some of which are empirical, elastic-spectral, non-linear static and non-linear dynamic approaches (Nielson and Des-Roches, 2007).

The development of these specific fragility functions for each component and region is a topic of current and future research. It is important to say that the damage level of a damaged component shows a variation, even for the same *EDP* value. This is mainly due to differences in the model and the history of the structural response. Actually, *EDPs* more used as peak quantities, still, the differences in the path of getting to the same peak value cause differences in the observed damage and these differences produce changing of the *DM* corresponding to an *EDP* (for example, the same maximum value of inter-story drift can be *transitory* or *permanent*, corresponding to different damage states). Loss analysis is the last phase of the PEER-PBEE methodology, and its objective is to estimate the frequency with which the various performance levels are exceeded. In this phase, the information on the damage achieved from the damage analysis is converted into the final decision variables (*DV*). Decision Variables can be identified as the total cost of the repair, the number of victims or the duration of the repair. These decision variables can be used to design or re-evaluate the design process with the possibility to include

information important to the stakeholders to make decisions regarding design or retrofit of the structures.

4. Fragility curves: Methodologies and procedures

4.1 Introduction

Probabilistic risk assessment methods have been the focus of much of the international scientific community for over 30 years. These methods are developed together with the understanding of the concepts of risk analysis. The evolution of these methods has made fragility curves essential components in probabilistic risk assessments.

The fragility curves are defined according to the load conditions to which a structure is subjected in its life and giving information on their reliability. The main objectives of this chapter are to describe the meaning of the fragility curves and to show the link between the fragility curves and the concept of reliability, represented for example by the reliability index and the deterministic safety factor.

The introduction of methods for assessing the reliability of structures has changed considerability the design approach. In particular, performance engineering-based design approaches and risk-based decision-making approaches necessitate failure probability estimates that can be evaluated in absolute terms (Ellingwood 2008). To provide such information Fragility curves are used. The conditional probability of the whole system failure in the entire load range to which such a system could be exposed is defined as a fragility curve. The reliability indexes allow estimating the probability of nominal failure; instead, the fragility curves offer a complete perspective on the reliability of the system as it is a continuous function and not points; therefore, it is possible to define the absolute probabilities rather than nominal probabilities. However, for the fragility curves to work, it is needed the knowledge of probability distributions of the parameters considered.

Fragility curves were first used for the seismic risk assessment of nuclear power plants in 1980 (Kennedy et al., 1980, Kaplan et al., 1983). The methods for the construction of fragility curves are continually evolving as can be seen in the scientific literature, which presents many examples of seismic risk assessment and mainly relates to buildings and bridges.

In the following paragraphs, the fragility curves will be studied, and the use in risk assessment will be described. The chapter describes the approaches that can be used to construct fragility curves by analysing the case studies in the literature with references to bridges. The approaches present in the literature are: judging, empirical, hybrid and analytical (Martin T. Schultz 2010). Every single approach foresees different methodologies to derive the fragility curves. The analytical approach is the most used method that can be found in the literature. Further classifications can be done in function of the way of defining the limit state explicit or implicit function and for the approaches to estimating the probability of failure.

4.2 Overview of key concepts

4.2.1 Uncertainty and risk

The lack of awareness of a quantity represents the uncertainty of the method that can be defined in an aleatory or epistemic way. The aleatory uncertainty is defined by variability in time and space or by intrinsic randomness. The epistemic uncertainty is instead related to a lack of knowledge.

The collapse probability of structural is a function of two variables: the uncertainty of capacity and the uncertainty of demand. The ability of a structure to bear a load depends on its geometry and its properties. Thus, the probability of failure and the capacity of a structure is fixed and potentially can be known, but it can be difficult to evaluate them. In the case in which the reliability of an existing structure is assessed, the uncertainty in the structural capacity can be defined as epistemic. However, there are some particular cases in which we can consider the uncertainties in the structural capacity as aleatory and epistemic, for example when we consider the stresses of materials that are a function of environmental variables such as temperature and humidity, intrinsically variable.

A risk is a possibility of suffering potential damage with a negative consequence of gravity is unknown. The definition includes the potential of the event as a result that does not necessarily have to occur. The result, however, could lead to a loss of some kind, this is called potential, so we must add that the consequences could be negative. Furthermore, the possibility term includes the severity, because it gives information on how significant the damage is. Risks are characterised by a probability distribution in the interval of all possible outcomes or levels of consequences. Although risks are entirely defined by probability distributions relative to levels accordingly, they are often summarised to the expected value. Risk assessment is the

procedure of obtaining a probability distribution for the potential results. This is typically achieved through some form of system-level modelling. In risk assessments, fragility curves are increasingly used to describe the way in which the probability of failure changes as the load on the structure increases. Even in the event of multiple faults or load types, fragility curves can be generated to describe the probability of collapse. Furthermore, as discussed above, fragility curves may also be related to other reliability concepts.

4.2.2 Design factor of safety

The ability of the structures to withstand loads is traditionally assessed using a safety factor. A structure is reliable if it can perform the intended function satisfactorily. The safety design factor, *FS*, is the ratio of resistance *R* (i.e. capacity), that is the maximum load that the system can bear and with which it can perform the intended function, and the stress, *S* (i.e. load or demand), set on a system below design conditions:

$$FS = \frac{R}{S} \tag{4-1}$$

If $FS > 1$, there is a safety margin. Structures are generally designed for a safety factor greater than one to provide a fringe of safety. Z, equation 4-2, represents the safety fringe and is the difference among resistance and load:

$$Z = R - S \tag{4-2}$$

This function is known as an equation of the limit state or performance function (Figure 4.1). If $Z > 0$, means that the capacity is bigger than the demand, so there is a residual capacity, hence the system is in a state of survival. If the demand overcame capacity, $Z < 0$, the system exhibits failure. The condition $Z = 0$ is the limit state. For brittle systems whose behaviours are known, capacity can be well known. In many cases, there is uncertainty about the ability of a system to bear a load. There may also be uncertainty about which load is set on the system below design conditions.

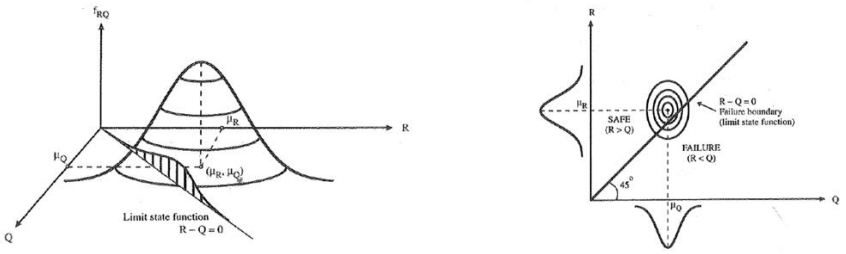

Figure 4.1: R-S domain.

When both uncertainties in capacity or demand, *R* and *S* became random variables, and it is possible to describe the uncertainty of these variables by the probability distributions: $F_R(r)$ and $F_S(s)$. In the presence of uncertainty in the evaluation of the behaviour of the system (failure or survival) there is the need to know the probabilities. Reliability, *r*, is the probability that the structure is in a state of survival:

$$r = 1 - p_f \tag{4-3}$$

p_f is the failure probability calculated by a combined probability density function for load and resistance:

$$p_f = p(Z \leq 0) = p(FS \leq 1) = \iint_{R \leq S} f_{RS}(r,s)drds \tag{4-4}$$

If we consider that R and S are independent, we can write that $f_{RS}(r,s) = f_R(r)f_S(s)$. Using the limit state equation it is possible to evaluate the safety margin *Z*. By deriving the probability distribution of the random variable, the probability density function is obtained: $f_R(r) = \frac{\partial F_R(r)}{\partial r}$ *and* $f_s(s) = \frac{\partial F_S(s)}{\partial s}$

4.2.3 Reliability index

The reliability index is used to measure reliability. If a normal distribution can be used to describe demand and capacity, the reliability index can be expressed as the ratio between the mean of the safety margin and the standard deviation:

$$\beta = \frac{\mu_Z}{\sigma_Z} = \frac{\mu_R - \mu_S}{\sqrt{\sigma_R^2 + \sigma_S^2 - 2\rho_{RS}\sigma_R\sigma_S}} \tag{4-5}$$

where μ_Z and σ_Z are respectively the mean and the standard deviation of the safety margin. Assuming that *R* and *S* are normally distributed, it is possible to derive these two moments of the safety margin from the first and second moments of *R* and *S*. If *R* and *S* are not correlated, it is possible to simplify the denominator to $\sqrt{\sigma_R^2 + \sigma_S^2}$. By using the standard normal distribution function (ϕ), from the reliability index the probability of failure can be calculated::

$$p_f = 1 - \phi(\beta) = \phi(-\beta) \qquad 4\text{-}6$$

This reliability assesses method is noted as the first-order second-moment method (FOSM) because the safety margin is a linear function (first-order) of the demand and capacity variables, and only the first and second random variables are used in estimating the reliability index. If the conditions of normality are satisfied, the probability of failure can be defined in absolute terms. Figure 4.2a illustrates the uncertainty regarding capacity, demand and distribution resulting in the safety margin. In this figure, the probability distributions that characterise the uncertainty in capacity and demand are used to obtain a probability distribution that describes the uncertainty in the safety margin, as shown in Figure 4.2b. The distribution for the safety margin has an average μ_Z and standard deviation σ_Z. The reliability index, β, is the ratio between μ_Z and σ_Z.

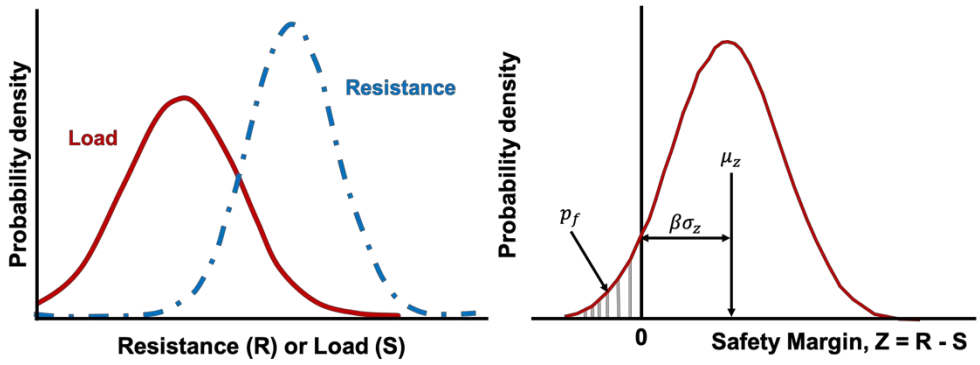

Figure 4.2: Reliability index. Probability distribution in capacity and demand (left) probability distributio of the safety margin (rigth).

The failure probability, p_f, is the area under the curve on the left of the y-axis. If the random variables of capacity and demand follow a lognormal distribution, then "first-order second-moment" can be reused to calculate the reliability index and a probability of failure:

$$\beta = \frac{\ln(m_R / m_S)}{\sqrt{\ln(1+V_R^2) + \ln(1+V_S^2) - 2\rho_{RS}\sqrt{\ln(1+V_R^2)\ln(1+V_S^2)}}} \quad 4\text{-}7$$

The variables m_R and m_S are respectively the medians of capacity and demand, and V is the coefficient of variation: $V = \sigma / \mu$. Again, if it is assumed that R and S like unrelated, the denominator is simplified to $\sqrt{\ln(1+V_R^2)\ln(1+V_S^2)}$. Because it becomes a lognormal random variable normally distributed when submitted to a natural log transformation, to calculate a probability of error using the standard normal density function, it is possible to use the standard normal function. When the distribution of demand and capacity is not normal or lognormal or their distributions are unidentified, the reliability index β can be assessed using the following equation:

$$\beta = \frac{\ln(\mu_R / \mu_S)}{\sqrt{V_R^2 + V_S^2}} \quad 4\text{-}8$$

while, the assessed failure probability could be only evaluated in nominal or relative terms. The precision of this method is affected on how closely the underlying distributions of capacity and the demand proceed a normal distribution, but this approach is frequently used in the absence of enough information to assess this condition. If the requirement is not satisfied, β acts as a nominal or relative reliability index because it varies monotonically with p_f. However, the probability estimate does not have a useful meaning in absolute terms (Melchers, 1999). The reliability index is the standard deviations, σ_Z, among the mean of estimated safety margin and the failure point. About the evaluation of the probability of structural failure, the FOSM method is limiting because it needs to hypothesise the distribution of uncertainty in the system variables. When these requirements do not exist, it is not difficult to use this method, as the probability of failure based on FOSM should only be assessed in relative terms. The use of analytical methods and numerical solutions could solve the FOSM limitations.

These methods, widely discussed in the scientific literature, often require greater efforts than the methods described above. For this reason, it should only be used when the relative or nominal estimates are not considered sufficient in the decision-making process. Fragility curves are very often used to express conditional probabilities in absolute terms.

In EN 1990 and ISO 2394, the standard recommendation about a required reliability level is frequently formulated regarding the reliability index β related to a certain design working life. The reliability index β, formally defined as a negative value of a standardised normal variable corresponding to the probability of failure p_f. Thus, the following relationship may be considered as a definition:

$$\beta = -\phi_u^{-1}\left(p_f\right) \qquad 4\text{-}9$$

where $\phi_u^{-1}\left(p_f\right)$ is the inverse standardised normal distribution function. Currently the, reliability index β defined by equation 4-9 is a frequently used measure of structural reliability in several international document (EN1990; ISO2394). It should be highlighted that the failure probability p_f and the reliability index β signify fully equivalent reliability measures with one to one mutual correspondence given by equation 4-9 and numerically illustrated in Table 4.1.

Table 4.1: Ratio between the failure probability $\boldsymbol{p_f}$ and the reliability index **β**.

$\boldsymbol{p_f}$	10^{-1}	10^{-2}	10^{-3}	10^{-4}	10^{-5}	10^{-6}	10^{-7}
β	1.3	2.3	3.1	3.7	4.2	4.7	5.2

4.2.4 Fragility curve

The fragility curves are functions explaining the probability of failure as a function of the possible load combinations to which a system is subjected. Although the fragility curves are strictly connected to the relative reliability index, they are different in several aspects. In detail:

- the fragility curves are functions not estimated point;
- the loads are considered in a deterministic way, so the fragility curves represent a probability of failure conditioned to the load instead than a total probability of failure;
- the probabilities are generally expressed in absolute terms.

Fragility curves can provide a complete perspective on the reliability of the system concerning the probability of failure, based on the traditional reliability index because they provide more information on the overall system reliability. The shape of a fragility curve describes the uncertainty in the system's ability to withstand a load or the uncertainty of which load will cause the failure of the system. If the uncertainty is low in capacity or demand, the fragility curve will get the shape of a step function, shown in Figure 4.3a. A step function has a $p_f = 0$ under the critical load and $p_f = 1$ above the critical load. The step function transmits absolute

certainty that the system will fail at the critical load and is appropriate for fragile and well-understood systems. For elastic systems, poorly understood or complex, there is no certainty about the system's ability to resist a load. In these cases, the fragility curve assumes the form of an S-shaped function, as shown in Figure 4.3b. The S-shaped function implies that, in a specific request interval, the state of the system can only be evaluated with a certain probability. The S-shaped fragility curve shows that there is uncertainty in the capacity of the system to resist a load.

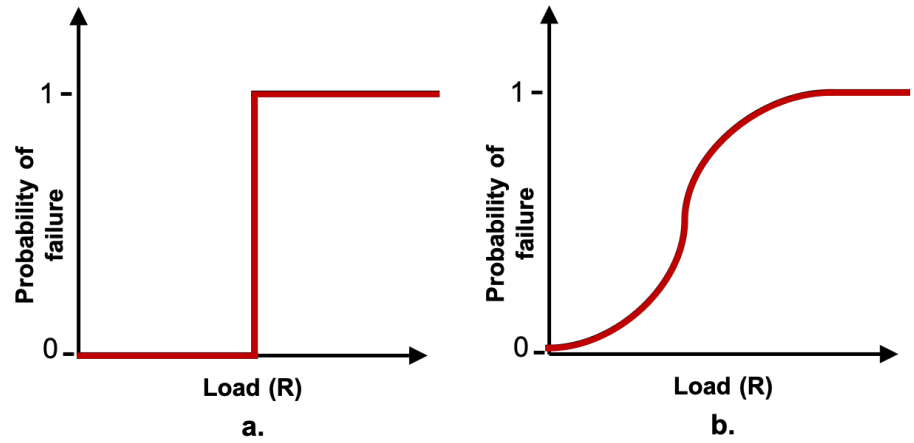

Figure 4.3: Example of fragility curve form. Step function (a). S-form function (b)

Fragility curves can be derived, using the reliability index, if all uncertainty is assumed to be within the capacity and the demand changes parametrically. In Figure 4.4 some fragility curves are represented considering a lognormal distribution of the uncertainty of the capacity. Thus, the fragility curve will also have a lognormal distribution, as proposed by many recent studies (Ellingwood et al., 2007). Whit the equation 4-10 it is possible to derive the conditional probability of failure:

$$p[Z \leq 0|S = s] = F_R(s) = \phi(-\beta) = \phi(\ln(s/m_R)/\sigma_{\ln R}) \qquad 4\text{-}10$$

$F_R(s)$ represent the cumulative distribution function through which it is possible to define the probability of conditional failure to the demand of the system, $p[Z \leq 0|S = s]$. The m_R variable is the median of a probability distribution that describes the uncertainty in capacity and $\sigma_{\ln R} = \sqrt{1 + V_R^2}$.

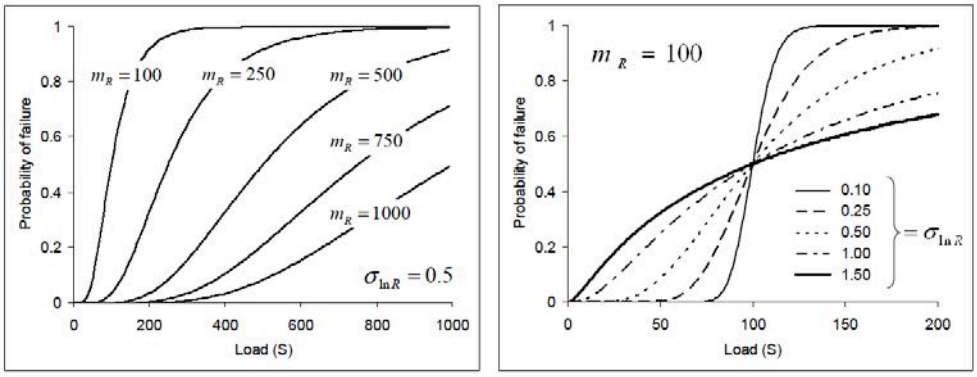

Figure 4.4: Fragility curves originated from the reliability index (Martin T. Schultz 2010).

In Figure 4.4a, m_R assumes values that range from 100 to 1000, though $\sigma_{\ln R}$ is maintained unvaried at 0.5. This graph illustrates that the probability of failure is related to the ratio between capacity and demand. If the demand grows compared to capacity, the probability of failure tend to one. When $m_R = s$, $\beta = 0$ and $p_f = 0.5$, represent that the system has a 50% probability to be in a failure state (Martin T. Schultz 2010).

As m_R increases, the median load that causes system failure tends to decrease the conditional probability of the system. When modifying the value $\sigma_{\ln R}$ in the range between 0.1 to 1.5 shows an increase in uncertainty in the system capacity. As $\sigma_{\ln R}$ rises, $p[Z \leq 0|S = s]$ increases before the value m_R but decrease for loads greater than m_R. It is noted that in any case $F_R(s) = 0.5$. This concept is shown in Figure 4.4b, where is illustrated some fragility curves for various values of $\sigma_{\ln R}$ meanwhile m_R is kept constant. Growing the variance of the capacity term (i.e., raise the uncertainty of the capacity) it is possible to decrease the conditional probability of failure for the elevated loads. The term failure indicates that the structure has exceeded its capacity for a given level of service. This does not necessarily imply the collapse of the structure (for example some elements of the structure have collapsed), but it represents that the performance of the structure is less than a predefined critical limit state. Fragility curves for seismic risk assessment have been developed to consider multiple levels of performance. In practice, it is indicated when the structure fails or when it does not satisfy a limit state condition (for example Ellingwood 2008). After exposure to a seismic event it is possible to define levels of damage status to mutually exclusive structures: fully functional, repairable, but altered, non-repairable and collapsed.

What has been described so far shows that there is a close connection between the safety factor, the reliability index and the fragility curves. The fragility curve can better characterise the reliability of the system concerning the safety factor or to the reliability index. Since very often the safety factor is used in a deterministic way considering the capacity of the structure. While the reliability index presents the uncertainty both in demand and in the capacity, also evaluating the reliability relative to a single design point. On the other hand, with the fragility curve, it is possible to characterise the reliability of the entire system and the whole range of loads to which a system could be exposed. Therefore, it provides more information than the reliability index.

However, by confirming the restrictive hypothesis in which both the demand and the capacity are not correlated and that are distributed as random variables, it is possible to use the reliability index to construct the fragility curves. If the demand and capacity distributions are not distributed as random variables or are not known, other types of methods may be used.

4.2.5 The risk assessment by use the fragility curves

The US federal emergency management software HAZUS-MH used to estimate potential flood losses, hurricanes and earthquakes, to assess risk uses fragility curves. The objective of the risk assessment is to define the probability that the losses do not exceed a pre-set potential level because potential losses, L, are not known a priori.

The total probability that losses surpass a level *l*, $p[L \geq 1]$, could be computed as follows:

$$p[L \geq 1] = \sum_{s} p[L \geq 1|S = s]\, p[Z \leq 0|S = s]\, p[S = s] \qquad 4\text{-}11$$

$p[S = s]$ represents the probability of occurring of a dangerous event, *S*, of severity, *s*. Instead $p[Z \leq 0|S = s]$ is the conditional probability of overcoming the system capacity when a hazard event of severity *s* happened. The fragility curve represents this probability. The probability of failure of the entire system is $p_f = p[Z \leq 0|S = s]\, p[S = s]$. Moreover, $p[L \geq 1|S = s]$ represent the probability that losses overcame a defined quantity, l, for a certain severity of the event. Not considering the use of the fragility curves, that describe the probability between 0 and 1, in the risk assessment could lead to a consequent overestimation of the probability of overcoming the loss$[L \geq 1]$. Because without using the fragility curves, the risk model can give only two kinds of results that are when the structure

never fails $(p_f = 0)$ when the structures always fail$(p_f = 1)$. I For this reason, the fragility curves are really important to allow for an accurate description of a risk analysis.

4.3 Seismic fragility analysis focused on the bridge

Motorway bridges are a significant part of a country's national economy and serve as a foundation for infrastructure development. They play an essential role in building fluid and fast communication system between cities and states. The damages caused by earthquakes in recent years have demonstrated that bridges are one of the most sensitive components of the transport system. For this reason, many researchers that have studied the damages reported by the road infrastructures in areas with high seismicity have focused their research on these issues (ATC, 1985, 1991, King et al., 1997; Werner et al. 1997; Shinozuka et al., 1997; Veneziano, et al. 2002) in order to examine in depth the problem and propose methodologies that would allow the assessment of the seismic risk for highway transportation systems. The fragility curves are used for seismic risk assessment for the first time in the 1975 when Whitman et al. (1975) described the seismic risk assessment procedure. Later, the Federal Emergency Management Agency (FEMA) and the Applied Technology Council (ATC) cooperated significantly to the evolution of the studies of fragility functions and seismic vulnerability assessment methodologies. For the first time, the notion of continuous fragility function was introduced in the ATC report 25 (ATC, 1991) that presented the continuous damage functions. The fragility curves or damage function were derived by using regression analysis of the different damage probability matrices. In 1997, FEMA introduced in the software, Hazard United States (HAZUS, 1997) based on geographic information system (GIS), the risk assessment. During the year HAZUS has undergone significant development, and the latest version HAZUS-MH 2.1 (HAZUS, 2012) can evaluate potential risks and losses from earthquakes, hurricanes and floods. In the last two decades, the fragility curves have emerged as a useful tool for critical decision making for the safety of facilities and infrastructures. Figure 4.5 shows the statistics of research publications related to the assessment of seismic brittle fragility in recent decades. Many relevant papers have been obtained from several reference journals (A.H.M. Muntasir Billah et al. 2015).

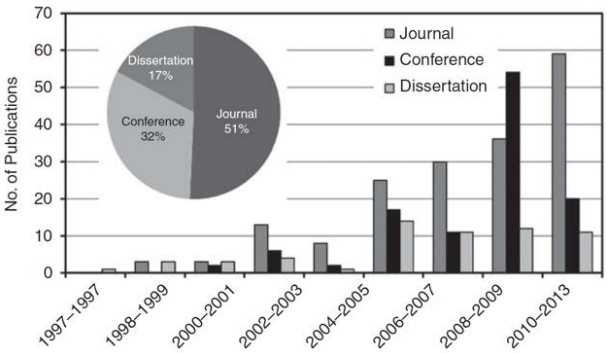

Figure 4.5: Statistic of papers on seismic fragility analysis of bridge since 1990 (A.H.M. Muntasir Billah et al. 2015).

This figure shows a growing trend of publications indicating the increase in research interest in this field. Since 1990 a total of 350 documents including dissertations, papers, and conference proceedings have been published, of which a significant part published on the scientific journals (51%). A considerable increase in the number of publications was found in 2006-2007 when the number of publications increased by almost 400% compared to the period 2004-2005. In the period 2010-2011 the number of publications was 102, and in 2012-2013 it is 90, which is expected to increase in the coming months.

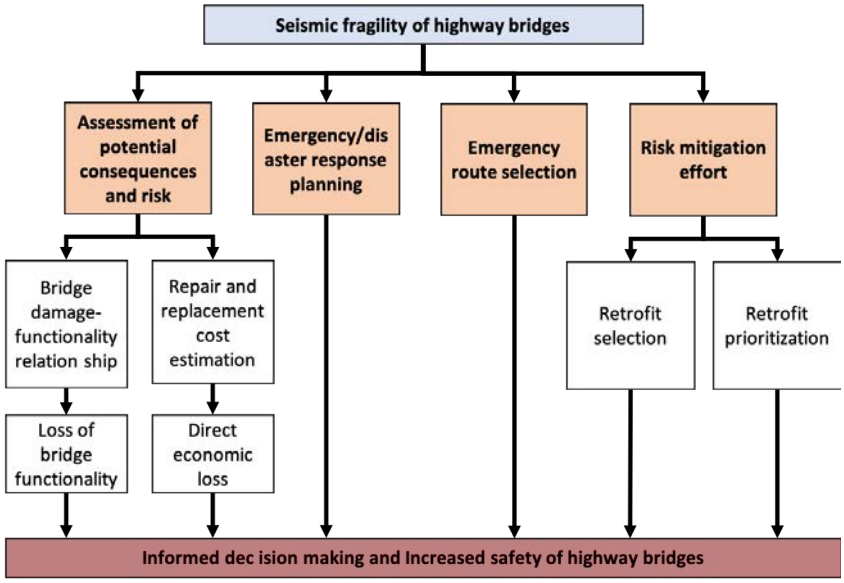

Figure 4.6: Various application of seismic fragility curves.

This increment in publications confirms the worldwide interest of the scientific community and the industry for the analysis of the seismic fragility of existing

bridges. Fragility curves can be used to make decisions both in disaster management before and after the earthquake, to make informed decisions about the allocation of resources for retrofit, the design and the best redundancy of a motorway network (Mackie & Stojadinovic, 2005). Figure 4.6 illustrates different applications of bridging curves for bridges.

4.4 Methods to develop Fragility Curves

Many researchers have developed different methods and approaches for the development of fragility curves such as judgmental, field observations, advanced analysis using analytical models and hybrid methods. Furthermore, various methodologies have been developed and used to evaluate the seismic fragility of bridges. Figure 4.7 shows the methods commonly used in the generation of the different types of fragility curves and Table 4.2 (Billah, Abu Hena MD Muntasir, 2015) shows the comparative evaluation of different methodologies.

Table 4.2: Comparison of different methods for the development of fragility curves.

Method	Advantages	Disadvantages
Expert-based/judgmental	Simple method. All factor can be incorporated	Extremely subjective. Depends on panel expertise. Often biased and lack reliability
Empirical	Represent a realistic picture. Shows the actual vulnerability.	Lack of adequate data. Region and structure-specific. The discrepancy in damage observation.
Experimental	Provides actual damage condition	Lack of adequate data. Subjective definition of DSs. Weak correlation between geometry and structural properties.
Analytical	Increased reliability. Consideration of all types of uncertainty. Less biased.	Computational cost. Time-consuming. Selection of analysis technique. Definition of DSs. Selection of probability distribution function.
Hybrid	Combination of experimental and analytical observation. Involves damage data from the post-earthquake survey. Reduced computational effort.	The requirement of multiple data sources. Extrapolation of damage data. Large dispersion in the demand model

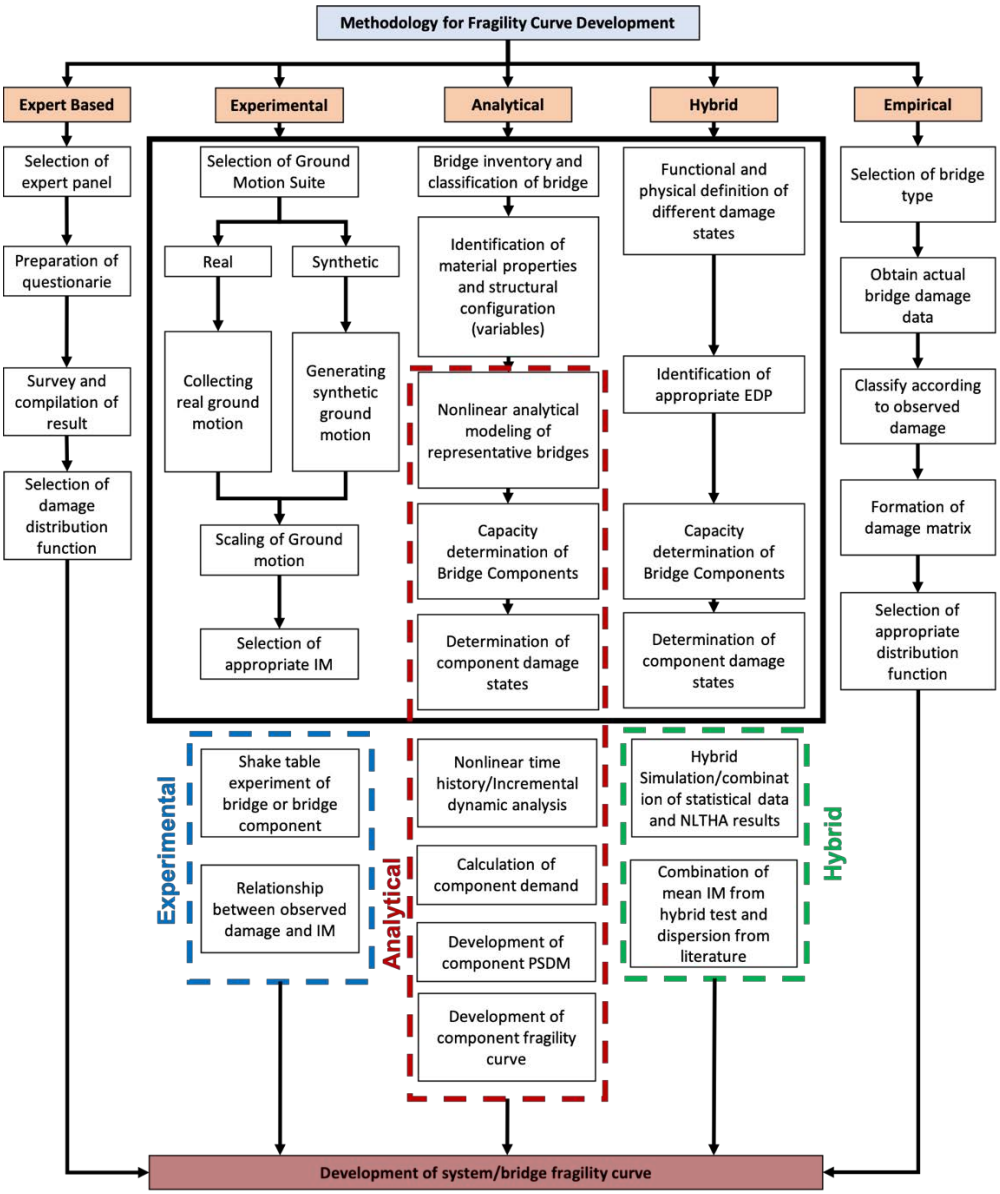

Figure 4.7: Methodology for developing seismic fragility curves.

4.4.1 Expert-based/Judgmental approaches

One of the simplest and oldest methods to derive fragility functions are fragility curves based on expert opinion or judgment. As a first step, this method involves the assessment by a group of experts, with experience in the field of seismic engineering, of the various essential components of a typical motorway bridge and subsequently the estimate on the likely distribution of damage when they are subjected to different

intensity earthquakes (Rossetto & Elnashai, 2003). Through the use of specific questionnaires, a survey was conducted among the experts. The probability distribution functions are updated, based on the expert opinion, to represent a particular level of damage at different levels of ground motion intensity. Since experts give their opinion on the exceeding of each DS damage state, fragility curves can be developed for each DS over a broad range of ground motion intensities. One example of the judgmental fragility curve is described in the report ATC-13 (ATC, 1985). This report documented the damages and associated risk matrices of the typical Californian infrastructure based on the opinion of a group of 42 experts. However, only 4 of the 42 experts had experience with the seismic performance of the highway bridges. Based on their responses, a probability matrix of the damages based on the Modified-Mercalli Intensity value was developed and included in the ATC-13 report.

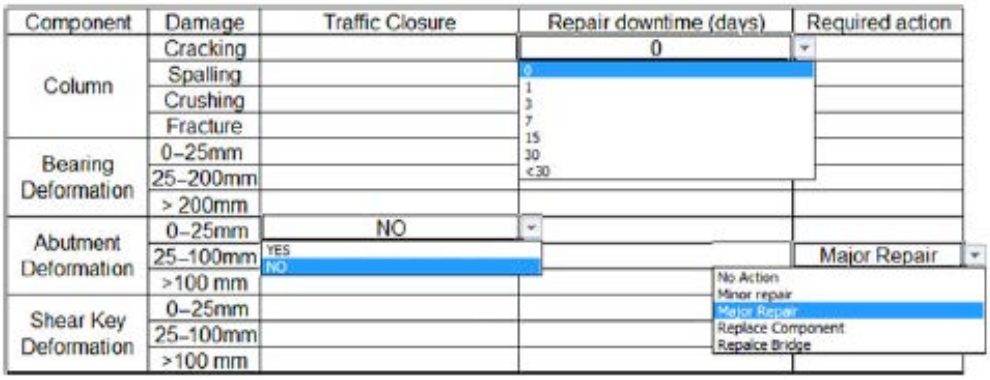

Figure 4.8: Technique to develop an expert-based fragility curve.

Figure 4.8 shows a typical survey technique that can be used to obtain expert advice. From the figure, it can be seen that, based on their experience and observation of the previous earthquakes, the experts can select different options. Based on the expert group's response, a damaged matrix including IM scenario and damage can be developed. Using the damaged matrix and an appropriate distribution function, fragility curves can be generated.

As expert advice is the only source of data for the development of this type of fragility curve, this method largely depends on the type of questionnaire used, the experience of the Expert Group and the number of experts consulted (Nielson, 2005). Very often these judgments are biased and involve some uncertainties that are not explicitly quantified in the vulnerability functions. Furthermore, these types of curves are often developed for defined structural types, assigned configurations,

details and materials. All these factors make the reliability of the judgment-based fragility curves questionable.

4.4.2 Empirical approaches

Data collected from post-earthquake field observations or damage reports can be used to develop empirical fragility curves. The concept of the empirical curve was developed, for the first time, from Basoz and Kiremidjian (1997) and Yamazaki Hamada, Motoyama and Yamauchi (1999), respectively for the earthquakes of Northridge of 1994 and of Kobe of 1995, since it had been possible to collect a large amount of damage data on different structures. Subsequently, other researchers (Der Kiureghian, 2002; Elnashai, Borzi, & Vlachos, 2004; Shinozuka, Feng, Kim, & Kim, 2000; Shinozuka, Feng, Kim, Uzawa, and Ueda, 2001) using data and observations on post-earthquake damage, have developed other types of approaches for the derivation of empirical fragility curves.

Basoz and Kiremidjian (1997), developed a damage frequency matrix using data from the damage data of the Northridge earthquake, developing empirical fragility curves through a logistic regression analysis. Instead, Shinozuka et al. (2001), based on observation of the Kobe earthquake data, applied the Maximum Likelihood criterion to evaluate the parameters of a lognormal probability distribution to derive the fragility curves, while Der Kiureghian (2002) used a Bayesian approach to develop fragility curves.

Despite the fact that the empirical fragility curves manage to describe a more realistic picture, they cannot be generalised for more cases and very often they are associated with a large degree of uncertainty. The uncertainties due to variability in the definition of the DS and also to the different methods of observing the damage of the various inspection groups reduce in a significant way the usefulness and reliability of the empirical vulnerability curves.

An example of the reliability of this typology of curves can be understood by A.H.M. Muntasir Billah & M. Shahria Alam (2015) who compared empirical fragility curves obtained from Yamazaki et al. (2000) and Shinozuka et al. (2001) for damage on the Hanshin highway during the Kobe earthquake of 1995.

From Figure 4.9 it is possible to observe that their empirical fragility curves, obtained using the same damage data, are significantly different from one anotherThe differences between the fragility curves can depend on the number of failure bridges considered, to their structural layout and the definition of DS. Using the damage

statistics, these errors are difficult to avoid. Also, they lead to a dispersion of large data even when considering a single event and a limited area of investigation (Rossetto & Elnashai, 2003).

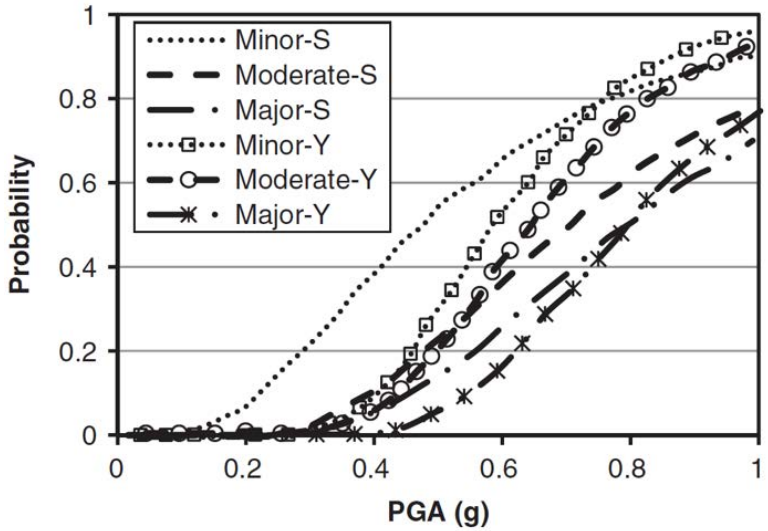

Figure 4.9: Comparison of empirical fragility curves developed by Shinozuka et al. (2001) [S] and Yamazaki et al. (2000) [Y] using damage data from the Kobe earthquake (A.H.M. Muntasir Billah & M. Shahria Alam (2015).

4.4.3 Experimental fragility curves

The bridges, given their size, do not lend themselves to full-scale experiments as they would have high costs, so even the data of tests on the shaking table to derive fragility curves are rare. Therefore, it is not common to derive fragility curves for bridges using experimental results. Even if the results of the experimental analyses are useful for the definition of the damage measures for the analytical fragility curves, their direct application for the derivation of the fragility curves is still very limited.

Despite the high costs for the construction of fragility curves, some researchers Vosooghi and Saiidi (2012) developed experimental fragility curves based on experimental results obtained from a vibrating table and cyclic loading tests on bridge pylons. In this study, they developed a probabilistic relationship that links experimental damage data to seismic response parameters and permits to derive the fragility curves. Instead, Banerjee and Chi (2013), using an almost full-scale bridge model, developed fragility curves for bridges using data on the damage obtained from vibration table tests. However, the absence of adequate data at all levels of DS

and a poor correlation between structural and geometry properties restricts the application of experimental fragility curves.

4.4.4 Analytical approaches

When the damage data is not available, fragility functions can be calculated using the analytical method. Analytical fragility curves can be developed using a variety of methods such as elastic spectral analysis (Hwang, Jernigan and Lin, 2000), the probabilistic seismic demand model (PSDM) using a Bayesian approach (Gardoni, et al., 2002; Gardoni et al. , 2003), nonlinear static analysis (Mander & Basoz, 1999; Moschonas et al., 2009; Shinozuka et al., 2000) or linear/nonlinear chronological analysis (NLTHA) (Bhuiyan & Alam, 2012; Choi, DesRoches, & Nielson, 2004; Kwon & Elnashai, 2010; Nielson & DesRoches, 2007a, 2007b; Pan, Agrawal, Ghosn, & Alampalli, 2010a; Ramanathan, DesRoches, & Padgett, 2012; Tavares, Padgett, & Paultre, 2012) and incremental dynamic analysis (IDA) (Alam et al., 2012; Billah, Alam, & Bhuiyan, 2013; Mackie & Stojadinovic 2005; Zhang & Huo 2009). The following paragraphs show a description of the different analytical approaches used in the scientific literature to generate fragility curves.

4.4.4.1 Elastic spectral analysis

The derivation of fragility curves for the bridges through the elastic spectral analysis is one of the simplest and fastest methods (Hwang et al., 2000; Yu et al., 1991). The method foresees that the capacity and the demand of the different components are calculated and through the relationship, it is possible to evaluate their potential seismic damage. Precisely because of its simplicity, the elastic spectral demand analysis method is often used to verify the performance during the design phase of particularly critical structural elements such as the piers of the bridge. Hwang et al. (2000) and Jernigan and Hwang (2002) have adopted this method to construct fragility curves for the bridges of Memphis.

The resistant capacities of the single components of the bridge are determined using linear elastic models considering the properties of effective stiffness, while the demand for the individual components is calculated using the elastic spectral analysis. After calculating the capacity/demand ratios for the different structural elements, these must be compared with particular DS for the various levels of IM. Thus, a damage frequency matrix of the bridge is generated that is used to develop fragility curves. Although this technique is simple, it has several limitations, since this method is functional when one wants to investigate the linear behaviour of bridges. On the other hand, if the bridge is subject to non-linearity, with this method,

it is difficult to predict the demand accurately, thus making the reliability of the derived fragility function questionable.

4.4.4.2 Nonlinear static analysis

This method gives the possibility to use non-linear static analysis, overcoming the limit of the spectral analysis as it offers the advantage of considering non-linearity directly in the computational model and also requires less time. Many researchers (Banerjee & Shinozuka, 2007; Dutta & Mander, 1998; Mander, 1999; Mander & Basoz, 1999; Shinozuka et al., 2000) have used this method to derive fragility curves for bridges. The nonlinear static analysis method calculates the structural capacity using non-linear pushover static analysis while the demand is estimated from a reduced response spectrum. By identifying the intersection point between the capacity curve obtained from the analyses and the demand spectra in the same graph, it is defined the maximum response of the structure under the specific ground motion (in the deterministic analysis).

Whenever the uncertainty of capacity and demand is taken into account, it is represented by tracing the distributions on capacity and demand curves. The intersection between the capacity curve and the curve of demand distribution (Figure 4.10), allows the estimation of the probability of failure for a particular level of intensity. By increasing the IM level and the various DSs, fragility curves can be generated for the bridge.

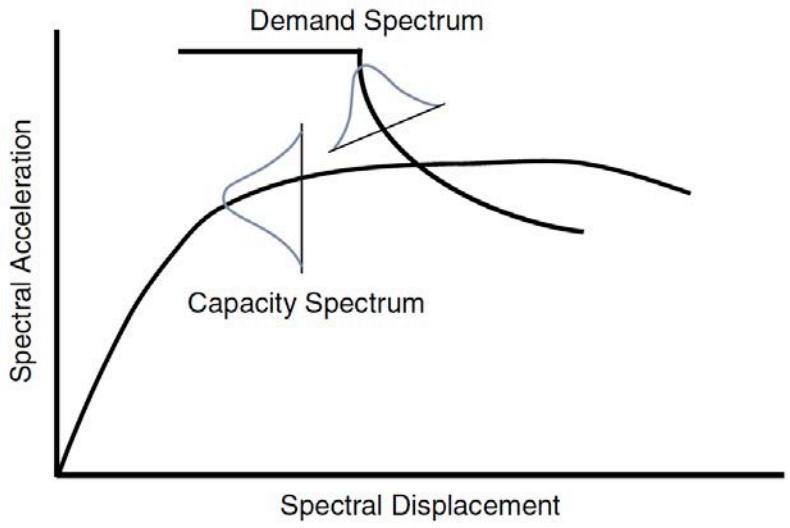

Figure 4.10: Representation of capacity and demand spectra in a probabilistic way (Mander & Basoz, 1999).

Although this method was developed based on the recommendations of the ATC 40 (ATC, 1996), a method developed for buildings, it has some limitations. The non-linear static analysis method does not provide the definition of the bridge type as well as the estimation of the effective hysteretic damping, which is always of primary importance in the evaluation of seismic performance.

4.4.4.3 Nonlinear time history analysis

The NLTHA method, even if it requires a high computational burden, is always the most reliable method to derive the fragility curves (Shinozuka et al., 2000). From the studies of many researchers (Billah & Alam, 2013; Choi et al., 2004; Karim & Yamazaki 2003; Kwon & Elnashai 2010; Nielson & DesRoches, 2007a, 2007b; Padgett, 2007; Pan et al ., 2010a; Ramanathan et al., 2012; Tavares et al., 2012) who have used this method for the derivation of the fragility curves, it is evident that it can provide a reliable estimate of the seismic vulnerability of the bridges. Increased reliability derives from the possibility to consider the geometric nonlinearity and the inelasticity of the material, that allows an accurate prediction of the large displacement behaviour and the collapse load of the bridges under dynamic load. All applications follow the steps shown in Figure 4.11.

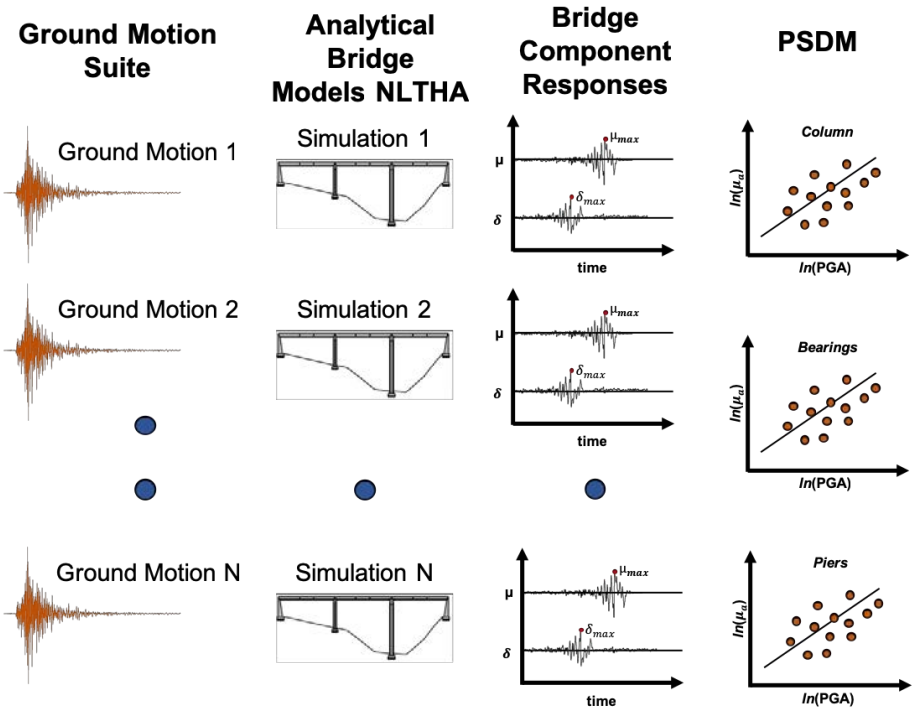

Figure 4.11: Schematic representation of the NLTHA procedure used to develop PSDMs.

The reliability and accuracy of the fragility curves produced by this method strongly depend on the number of ground motion used for dynamic analyses, although the number of ground movements needed to build reliable fragility curves is still at the heart of many researchers studies.

The first step to derive the fragility curves is the selection of an appropriate set of ground movements that represent the seismicity of the bridge location and captures the associated uncertainties (for example, epicentral distance, magnitude). Once the ground movements have been selected, the geometries of the sample bridges are designed considering the variability of the geometrical, structural and material properties. Using appropriate probability distributions for different random variables, the FEM bridge models of the 3D/2D type are developed. Subsequently, these bridge models are randomly matched with different ground movements, and NLTHA is performed for each ground motion sample. The requests for maximum components considered critical for the vulnerability of the bridge are extrapolated from each sample. Using the peak component response and the appropriate IM, it is possible to generate a PSDM using regression analysis or the maximum likelihood method. The calculation of the limit states of the capacity of the different components can be made by expert opinion, experimental investigation or an analytical approach. By transforming the capacity model with PSDM, fragility curves can be developed for bridges for different DSs. The negative aspects of this method are the a priori hypothesis on the probabilistic distribution of the seismic demand and a large number of earthquakes that make it computationally difficult.

4.4.4.4 Incremental dynamic analysis

The study of the researchers has tried to reduce the significant number of ground motion necessary using the NLTHA methods, by defined a new method called Incremental Dynamic Analysis IDA. The IDA is a particular type of NLTHA in which the ground motions are scaled incrementally, and then analyses are performed at different levels of intensity. It is necessary to choose intensity levels to cover the entire range of structural response, from the elastic phase to the yielding to dynamic instability (or until a limit state occurs). This methodology was implemented by Luco and Cornell (1998) and is analysed in detail by Vamvatsikos and Cornell (2002) and Yun, Hamburger, Cornell and Foutch (2012). Several researchers (Billah et al., 2013; Bhuiyan & Alam, 2012; Zhang & Huo, 2009; Mackie & Stojadinovic, 2005) preferred this technique to NLTHA to develop fragility curves.

Regardless, this incremental scaling of a large number of earthquakes may in some cases lead to a higher computational burden than required in the NLTHA method.

Although this method requires a significant computational effort, the previous assumptions regarding the probabilistic distribution of the seismic demand are not necessary for the derivation of the fragility functions (Zhang & Huo, 2009). This technique is like to the NLTHA approach; though, peak component responses must be calculated for each scale factor. IDA results allow the generation of fragility curves deriving the relationship of occurrence for each damage state and for each level of ground motion or evaluating the density function of the Intensity Measure for the ground motion in which the thresholds of the damage state are overcome (Bhuiyan & Alam, 2012). The Incremental Dynamic Analysis method is mainly used for assessing the fragility of structures. Even this method, like the others, has few drawbacks. As stated by (Baker, 2013), the selection of earthquakes, the number of ground movements required and the scaling of ground movements, could lead to over or underestimate the vulnerability of the structures.

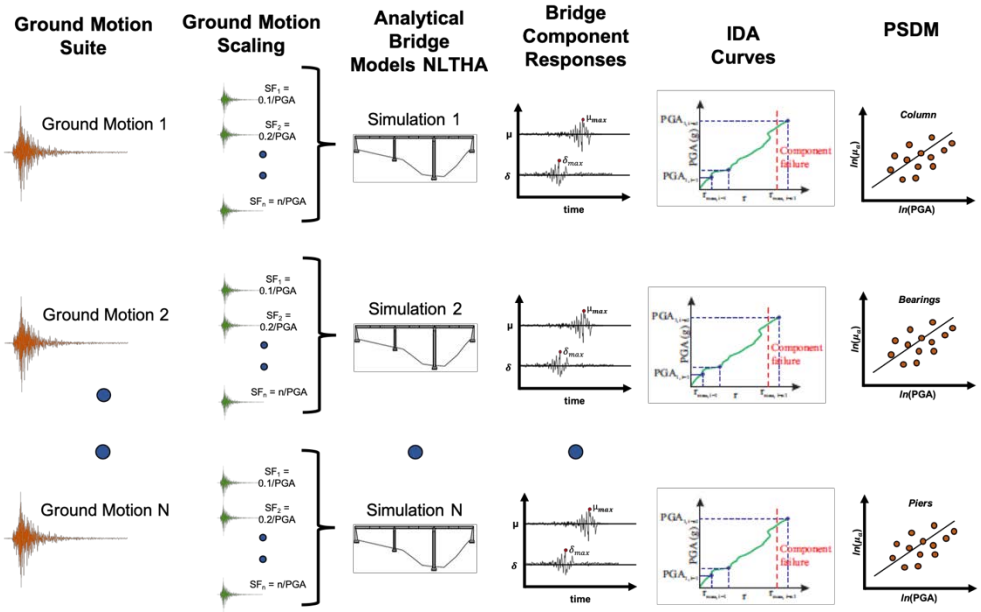

Figure 4.12: Schematic representation of the IDA procedure used to develop PSDMs.

4.4.4.5 Fragility assessment using Bayesian approach

Using the damage index of Park and Ang (1985), Singhal and Kiremidjian (1996) fragility curves were developed by the Bayesian analysis of the observed damage data of structural systems. Many researchers have used the Bayesian technique for the development of fragility curves (Gardoni et al., 2002, 2003; Der Kiureghian, 2002; Koutsourelakis, 2010; Singhal & Kiremidjian, 1996) through the convolution

of demand and capacity models. While Der Kiureghian (2002) used the maximum likelihood method together with the Bayesian approach, while Koutsourelakis (2010) used Markov Chain-Monte Carlo techniques to develop surfaces of fragility multidimensional according to the multiple characteristics of the ground motion. Gardoni et al. (2002) for the generation of fragility curves for reinforced concrete bridges (RC), revisited the traditional deterministic forecasts of capacity and demand models and introduced reliability. This study developed fragility curves for typical two-column RC highway bridges in California. Successively, Zhong, Gardoni, Rosowsky and Haukaas (2008) developed PSDM using the Bayesian approach to the reinforced concrete bridges with two columns that considered uncertainty and models errors. Huang, Gardoni and Hurlebaus (2010) have developed an update of the Bayesian method based on virtual experiment demand data, proposing a new approach of the PSDM type for the generation of fragility curves for the bending of single-column RC bridges. In this study, model errors, different types of uncertainties, the variation of soil characteristics and ground motion were considered. The new Bayesian method update procedure allows the formulation of confidence limits expressing the epistemic uncertainty close to the median fragility curves. This is one of the primary advantages of the Bayesian technique.

4.4.5 Hybrid approaches

All methods of deriving fragility curves have advantages and disadvantages, in order to compensate for the defects between the various methods, such as, for example, inadequate damage data obtained from the damages observation of the earthquake, the subjectivity of judgmental data, the uncertainties and the lacks of modelling associated with analytical procedures, the scientific community has been developed hybrid method for the derivation of fragility curves. The hybrid approach tries to reduce the computational burden of analytical modelling and compensates for the personal prejudice of the expert judgment method (Kappos, Panagopoulos, Panagiotopoulos, & Penelis, 2006).

The hybrid method was first used by Penelis, Sarigiannis, Stavrakakis and Stylianidis (1989) for the development of fragility curves that combined inelastic dynamic analysis and the 1978 Thessaloniki earthquake database. Also, Kappos, Stylianidis and Pitilakis (1998), Kappos et al. (2006) and Kappos and Panagopoulos (2010) developed and used hybrid fragility curves for the assessment of the vulnerability of RC and unreinforced masonry buildings in Greece. This method includes the available damage data of similar areas and structural typologies, examined and matched with the analytical damage statistics achieved using nonlinear analysis of typical structures (Kappos et al., 2006).

Furthermore, the hybrid method also allows the use of large-scale experimental test results that more accurately describe the structural response. Lately, the Network for Earthquake Engineering Simulation has developed a hybrid method for generating fragility curves based on hybrid simulation results with the calibrated analytical response (Lin, Li9, Elnashai and Spencer, 2012). This study implemented an analytical model of 2D frames in ZEUS-NL and executed a small-scale test of the column in a hybrid test facility. Using the average peak ground acceleration (PGA) derived from hybrid tests and dispersions obtained from scientific literature sources, they developed hybrid fragility curves assuming the lognormal distribution. Hybrid fragility curves may be considered another option for the development of reliable fragility curves, although the method has some negative aspects such as extrapolation of data on the damage and the relationship between the intensity of the earthquake and the level of structural damage (Kappos, 1997).

Also, this method implies great uncertainty and epistemic uncertainty which turns into a significant dispersion in the probabilistic model. While the method to derive the fragility curves is at the centre of scientific research; the applications are limited to buildings yet. Frankie (2013) developed hybrid fragility curves for a four-span curved bridge using hybrid and NLTHA simulation. The limit states for the bridge pier were generated by the experimental results obtained from the piers response under load combination: axial, bending, shear and torsional load. By merging these experimental results with the analytical structural response, fragility curves were developed for different DSs.

4.5 Intensity Measure for Fragility Analysis

The Hazard Analysis starts with the selection of one (or more) ground motion Intensity Measure (IM) that should capture the significant characteristics of earthquake ground motion influencing the response of the structures. Choosing the right parameter of intensity (IM) is an important step in developing fragility curves because they characterize the probability that the seismic demand of the structure exceeds a defined performance state according to the chosen intensity (IM) measurement. The choice of an appropriate IM to evaluate the fragility of a structure has been discussed in the scientific community for many years. In the ATC-13 (ATC 1985) the modified Mercalli scale was used as the IM instead the FEMA P695 (FEMA 2009) preferred as IM the spectral acceleration in the first period, S_a (T_1) (or simply S_a). Luco and Cornell (2007) recommended three criteria for the choice of an suitable IM, i.e. the efficiency, sufficiency and computability of the risk. The most used IM is the spectral acceleration in the first period, S_a (T_1) (or simply S_a).

Likewise, PGA, Peak Ground Velocity (PGV), Arias Intensity (A_I) and other types can be used as alternative IM as proposed and developed by numerous researchers, Giovenale (2003) and Mackie and Stojadinovic (2007). Mackie and Stojadinovic (2005), wanting to identify an ideal IM, have investigated the use of 65 IMs divided into three classes. An excellent IM must be practical, efficient, sufficient and robust. The studies conducted led to defining the S_a and the spectral displacement (S_d) relating to the fundamental period as ideal IMs because they are used to reduce the uncertainty in the demand models. Furthermore, the peak ground acceleration (PGA) has also been identified by Padgett and DesRoches (2008) as an optimal IM because it is representative of the severity of soil movement.

The PGA can be defined as an efficient, practical and useful IM for the calculation of seismic risk, but, if it is compared to other intensity measurements, it is not always representative of structural damage. It is possible to use other spectral characteristics (Avsar et al., 2011) such as ground velocity (PGV), peak ground displacement (PGD), the duration of the strong movement (T_d), the intensity of the spectrum (S_I). Other researchers have proposed measures of intensity of the vector type for the definition of the probabilistic model of the demand (Shome and Cornell 1999, Bazzurro and Cornell 2002, Baker and Cornell 2005). Shafieezadeh et al. (2012) suggested the use of a fractional order for the PSDM intensity of motorway bridges. The proposed fractional method IM predicted the use of a single degree of freedom (SDF) system with the fractional response and fractional damping and matched the peak ground response with the spectral accelerations at 0.2 and 1.0 s, respectively. These studies have shown that the proposed fractional order IM has superior performance compared to the usual IM. However, this intensity measure, at the moment, cannot be used for risk analysis because there are no regional risk curves for this type of measure. It is useful to classify the Intensity Measures into three main classes (Table 4.3):

- *Peak based IMs*: measures of maximum in absolute terms of the values of ground motions;
- *Duration-based IMs*: integration of a ground motion time histories characteristic of the signal;
- *Frequency-response based IMs*: constructed on the elastic response of oscillator to the ground motion time history.

Table 4.3: IMs, from literature (De Biasio M., 2014).

Type	IM	Notes
Frequency Response Based	$S_{pa}(T_1)$	S_{pa} = pseudo-spectral acceleration fundamental period
	$I_H = \int_{0.1}^{2.5} S_V(T,\xi)\ dT$	S_V = spectral velocity ξ = damping ratio
	$EPA = \frac{1}{2.5}\int_{0.1}^{2.5} S_{pa}(T,\xi)\ dT$	S_{pa} = pseudo-spectral acceleration ξ = damping ratio
	$ASI = \frac{1}{2.5}\int_{0.1}^{0.5} S_{pa}(T,\xi)\ dT$	S_{pa} = pseudo-spectral acceleration ξ = damping ratio
	$S^* = S_{pa}(T_1)\left(\frac{S_{pa}(T_2)}{S_{pa}(T_1)}\right)^{0.5}$	S_{pa} = pseudo-spectral acceleration T_1 = fundamental period $T_2 = 2 \cdot T_1$
	$I_{NF} = S_{pa}(T_1)\left(\frac{S_{paAV}(T_1,\ldots\ldots,T_2)}{S_{pa}(T_1)}\right)^{0.4}$	S_{paAV} = Averaged pseudo-spectral acceleration between T_1 and T_2 T_1 = fundamental period $T_2 = 2 \cdot T_1$
Peak Based	$PGA = max\ \lvert a(t)\rvert$	$a(t)$ = acceleration time history
	$PGV = max\ \lvert v(t)\rvert$	$v(t)$ = velocity time history
Duration Based	$I_A = \frac{\pi}{2g}\int_0^{t_f} a(t)^2\ dt$	$a(t)$= acceleration time history $t(f)$= total duration of the record
	$CAV = \int_0^{t_f} \lvert a(t)\rvert\ dt$	$a(t)$= acceleration time history $t(f)$= total duration of the record
	$SCAV = CAV_i + \int_{i-1}^{t_i} \lvert a(t)\rvert\ dt$	$a(t)$= acceleration values in one-second interval where at least one value exceeds 0.0025 g i = 1…, n whit n equal to the record length in seconds
	$a_{RMS} = \sqrt{\frac{1}{T_d}[a(t)]^2 dt}$	$a(t)$= acceleration time history T_d = the time elapsed between the first and last excursions of the acceleration above 0.05g
	$I_c = a_{RMS}^{1.5} T_d^{0.5}$	T_d = the time elapsed between the first and last excursions of the acceleration above 0.05g

4.6 Damage state for Fragility Analysis

The fragility curves represent the probability of reaching a certain damage status defined as an IM of ground movement. In particular, each defined damage states (DS) for bridges is associated with a defined functional level, and each state of damage indicates a specified level of performance. The DS of the bridge components

is determined through the use of damage indices. Park and Ang (1985) developed a damage index based on the ability to dissipate energy and on demand for ductility, while Hwang et al. (2000) used as the relationship between capacity/demand of the bridge columns to generate the fragility curves. HAZUS (FEMA 2003) defines four states of damage: minor, moderate, extended and collapsed. These parameters are widely used for the evaluation of the seismic vulnerability of engineering structures. Instead, Dutta and Mander (1998) defined five different damage states based on the maximum displacement limits of the bridge pier. Mackie and Stojadinovic (2005) classified the EDPs as a parameter of local demand (material effort), intermediate (maximum moment) and global (drift ratio). In order to assess the fragility of motorway bridges, the researchers used different demand parameters, such as ductility of displacement (Zhang and Huo 2009, Bhuiyan and Alam 2012, Billah and others 2013), residual drift (Mackie and Stojadinovic 2004, Lee and Billington 2011, Billah and Alam 2012, Billah and Alam 2014c) the flexibility of the curvature of the columns (Nielson and DesRoches 2007a, Padgett and DesRoches 2008), drift ratio (Shinozuka et al., 2002, Tavares et al., 2012), cutting effort in isolation (Zhang and Huo 2009, Bhuiyan and Alam 2012), abutment deformation (Padgett and DesRoches 2008, Ramanathan et al., 2012, Tavares et al., 2012, Billah and Alam 2013), with displacement (Zhang and Huo 2009, Ramanathan et al., 2012 Billah and Alam 2013), Table 4.4 shows a summary of the various demand parameters and the threshold values used by the various researchers for the evaluation of the fragility of different components of the bridges.

Table 4.4: Summary of Threshold Value (Billah, Abu Hena MD Muntasi, 2015)

Component	Demand Parameter	Threshold Value				Reference
		Slight	Moderate	Extensive	Collapse	
Column	Curvature Ductility	1.29	2.1	3.52	5.24	Nielson 2005
		1	1.58	3.22	4.18	Ramanathan et al. 2012
		1	5.11	7.5	9	Ramanathan et al. 2012
		4.89	9.15	12.46	13.08	Ramanathan et al. 2010
		1.44	2.7	6.92	4.18	Ramanathan et al. 2010
		1	2	4	7	Vhoi et al 2004
		1	2.73	4.54	6.5	Jara et al. 2013
	Displacement Ductility	1	1.2	1.76	4.76	Alam et al. 2012, Hwang et al. 2000
		1	2	4	7	Alipour et al. 2013
		2.25	2.9	4.6	5	Banerjee and Prasad, 2013
		1	1.22	1.78	4.8	Billah and Alam 2014c
	Drift	5	7	11	30	Tavares et al 2012

		0.7	1.5	2.5	5	Akbari 2012
		1.45	2.6	4.3	6.9	Li et al. 2012
		0.7	1.5	2.5	5	Kim and Shinozuka 2004
	Rotational Ductility	3.14	3.14-5.9	5.9-9.42	>9.42	Banerjee and Chi 2013
		1.58	3.33	6.24	9.16	Banerjee and Shinozuka 2012
	Residual Drift (%)	0.25	0.25-0.75	0.75-1	>1	Billah and Alam 2014c
Elastomeric Bearing	Shear Strain (%)	100	150	200	250	Ala et al. 2012; Zhang and Huo 2009; Hwang et al. 2001
	Drif Ratio	0.007	0.015	0.025	0.05	Yi et al. 2007
	Displacement (mm)	0	50	100	150	Choi et al. 2004
		28.9	104.2	136.1	186.6	Ramanathan et al. 2010, Nielson 2005
		30	100	150	225	Ramanathan et al.2012
		30	60	150	300	Tavares et al. 2012
Fixed Bearing	Displacement (mm)	6	20	40	186.6	Ramanathan et al. 2010, Nielson 2005
		6	20	40	225	Ramanathan et al.2012
Abutment	Displacement (mm)	7	15	30	60	Tavares et al. 2012, Billah and Alam 2013
		9.8	37.9	77.2	N/A	Ramanathan et al. 2010, Nielson 2005
Pile Foundation	Displacement (mm)	28	42	86	115	Aygun et al. 2011

4.7 Estimating fragility function parameters

This section describes the statistical procedures for estimating parameters of fragility functions using structural analysis results. Analysing the problem from the mathematical point of view, the seismic fragility analysis of the structure can be described as the probability of overcoming a structural limit threshold:

$$F_R(X) = \phi\left[\frac{ln(x/m_r)}{\beta_r}\right] \qquad 4\text{-}12$$

where, $\phi[\ ]$ is the standard normal cumulative distribution function (CDF), m_r is the median demand expressed in terms of seismic intensity and β_r is the logarithmic standard deviation or dispersion of the demand parameters conditioned on IM.

The scientific literature proposes different methodologies to evaluate the parameter values for a fragility function that are consistent with observed data, that can be used depending on the chosen procedure used to obtain structural analysis data.

4.7.1 Fragility by the method of moments

In the method of moments, the parameters of lognormal fragility are obtained in such a way that the moments (e.g., mean and deviation) of the resulting distribution coincide with the moments of the observed data (Vamvatsikos, D., Cornell, C.A. 2002; Porter, K., Kennedy, R., Bachman, R. 2007; Lallemant, D., Kiremidjian, A., Burton, H, 2015). The estimation of fragility by this method is mainly associated with dynamic incremental analysis (IDA) (Vamvatsikos, D., Cornell, C.A. 2002), in which a selected set of the ground motion is scaled at different levels of IM and NLTHA are performed until a limit state of the threshold for all ground motion. With the available response data of IDA, the logarithmic moments of the distribution of IM in a particular limit state are obtained and the fragility curve for that specific limit state is estimated from the lognormal CDF to two parameters such as,

$$F_R(X) = \phi\left[\frac{ln(x/m_a)}{\beta_a}\right] \quad 4\text{-}13$$

where, $F_R(X)$ is the fragility for $IM = x$, m_a is the median acceleration capacity and β_a is the log-normal SD. The estimates of sample the mean, and SD in 4-13 is obtained as $\widehat{m_a} = E[\ln(IM_{LS})]$ and $\widehat{\beta_a} = \sqrt{var\left(ln(IM_{LS})\right)}$ where, IM_{LS} is the *IM* level corresponding to the considered limit state.

4.7.2 Fragility by least squares regression

In the analysis of fragility based on least squares regression, the parameters of fragility are estimated by minimising the sum of the quadratic error between the expected demand and the demand values obtained from the structural analysis. The question is represented as a function of IM that adopts a regression approach:

$$m_R = a(IM)^b \quad 4\text{-}14$$

where *a* and *b* are regression parameters. Least squares regression can be performed through the demand data obtained from NLTHA using a set of non-scaled ground motions, for example from the Cloud Analysis (CA) or by scaling the ground motion (IDA approach) to different intensity levels for an estimate m_R and β_R. In the Cloud Analysis (Jalayer, F., 2003) approach, the cloud response is obtained by applying a

series of ground motions (not scaled) to the considered structure. The choice of earthquakes should preferably correspond to the damage level of the considered position. For ground motions with arbitrary intensity $\{IM_i, i = 1, 2, \dots, N\}$ the structural responses $\{D_i, i = 1, 2, \dots, N\}$ are obtained and $\widehat{m_r}$ as a continuous function of IM from the regression parameters (*a, b*) minimizing the total quadratic error of the log linear regression in equation 4-14 and $\widehat{\beta_r}$ are calculated accordingly (Jalayer, F., 2003; Padgett, J.E., Nielson, B.G., DesRoches, R., 2008; Ghosh, S., Chakraborty, S., 2017). Finally, fragility is obtained for different levels of IM using Eq. 4 with the knowledge of the parameters $\left(\widehat{m_r}, \widehat{\beta_r}\right)$.

In the IDA-based method (Cimellaro, G.P., Reinhorn, A.M., D'Ambrisi, A., De Stefano, M. 2009; Baker, J.W., 2015), each ground motions from the suite are scaled to multiple IM levels and the response medians is adapted, and the median of the answers obtained from the structural responses. The parameter estimation procedure $\left(\widehat{m_r}, \widehat{\beta_r}\right)$ remains similar to the CA method. It can be seen that the considerable computation time required for the IDA-based method of a new intensity level can be drastically reduced in the CA-based method but compromising the level of accuracy (Mandal, T.K., Ghosh, S., Pujari, N.N., 2016).

4.7.3 Estimates fragility by maximum likelihood

The maximum likelihood method gives an estimate of fragility parameters associated with the highest probability of observing failure data obtained from structural analysis corresponding to a particular limit state (Shinozuka, M., Feng, M.Q., Lee, J., Naganuma, T., 2000). For any IM level $IM = x_i$, the likelihood function can be described as,

$$L(\theta|p_i) \propto f(p_i|\theta) = \prod_{i=1}^{N} f(p_i|\theta) \qquad 4\text{-}15$$

where, $f(\ \ )$ is the conditional pdf, p_i is the probability of failure at intensity level $IM = x_i$, *N* is the total number of ground motions considered for analysis and 'θ' is the parameters of the fragility function. Assuming two parameters log-normal distributed, the fragility function is expressed as shown in equation 4-13. For intensity level, $IM = x_i$ if the structure goes beyond the limit state for 'k' number of ground motions out of total *N* numbers, and if there are total *M* numbers of IM level considered, then for each IM level $IM = x_i$, the likelihood function can be expressed as,

$$L = \prod_{i=1}^{M} [F_R(x_i)]^{k_i} \, [1 - F_R(x_i)]^{N-k_i} \qquad 4\text{-}16$$

where, k_i is the observed numbers of failure at ith IM level. The maximum likelihood estimates, $(\widehat{m_a}, \widehat{\beta_a})$ of the fragility parameters (m_a, β_a) can be obtained by maximizing the likelihood function in equation 4-16. The binomial coefficient C_k^N is dropped in the above equation as it is not dependent on $F_R(x\ )$ and thus has no contribution in the maximization. It is computationally easier to maximize the logarithm of the likelihood function (Lallemant, D. et al. 2015) and hence the parameters $\widehat{m_a}$ and $\widehat{\beta_a}$ are obtained by maximizing the log-likelihood as,

$$(\widehat{m_a}, \widehat{\beta_a}) = \arg\max_{m_a, \beta_a} \sum_{i=1}^{M} \left[k_i \, ln\left(F_R(x_i)\right) + (N - k_i) \ln\left(1 - F_R(x_i)\right)\right] \qquad 4\text{-}17$$

The parameters, $\widehat{m_a}$ and $\widehat{\beta_a}$ that maximizes the above equation can be obtained by applying any suitable optimization algorithm.

4.7.4 Fragility by truncated IDA method

In the IDA-based method, the ground motions must be scaled to multiple levels of IM up to the observed failure (i.e. collapse). Furthermore, some studies question the reliability of the method because the low or moderate intensity earthquakes scaled to a higher intensity level may not be representative of the agitation caused by a recorded ground motion of the same intensity (Baker, J.W., Allin, C., 2005). Fragility values at higher levels of intensity are of lower interest than the lowest probability values associated with the tail of fragility curves for lower intensities (Baker, J.W., 2015). To circumvent them, the IDA is executed up to a certain IM_{max} intensity level and defined as the truncated IDA method. If in the analysis there are earth movements "N", then the "k" numbers of soil movements will cause the structure to collapse to levels of IM lower than IM_{max}. This type of truncated data is not suitable for the assessment of fragility by equation 4-13. However, the parameters $(\widehat{m_a}, \widehat{\beta_a})$ can be obtained from maximum likelihood estimates. The probability that a ground motions of the IM_i intensity causing collapse, given the fragility function can be defined as,

$$Likelihood = \phi\left(\frac{ln(IM_i/m_a)}{\beta_a}\right) \qquad 4\text{-}18$$

The likelihood of a scaled ground motion to IM_{max} not causing collapse is defined as the probability that $IM_i > IM_{max}$i.e.

$$Likelihood = 1 - \phi\left(\frac{ln(IM_{max}/m_a)}{\beta_a}\right) \quad 4\text{-}19$$

On the assumption of statistical independence of observed IM values, the likelihood of observing the entire data set can then be obtained from the product of the individual likelihoods as:

$$Likelihood = \left\{\prod_{i=1}^{k} \phi\left(\frac{ln(IM_i/m_a)}{\beta_a}\right)\right\}\left\{1 - \phi\left(\frac{ln(IM_{max}/m_a)}{\beta_a}\right)\right\}^{N-k} \quad 4\text{-}20$$

The MLE of the parameters $(\widehat{m_a}, \widehat{\beta_a})$ can be obtained by maximizing the logarithm of the likelihood function.

4.7.5 Fragility by multiple stripes analysis

The multiple strip analysis (MSA) approach is used when ground motions are selected for a given site with an assigned risk level as a target (Baker, J.W., 2015). The structural analysis is performed on several strips of IM levels, each with different groups of ground motions. As the target properties of ground motion differ at different IM levels, different ground motions are used at different levels. In the MSA approach, the number of ground movements that exceed the limit state cannot be estimated, as different ground movements are used.

To properly fit the data it is necessary to use the method of maximum likelihood, as has been noted by some researchers (Shinozuka et al. 2000; Baker and Cornell 2005b; Straub and Der Kiureghian 2008).

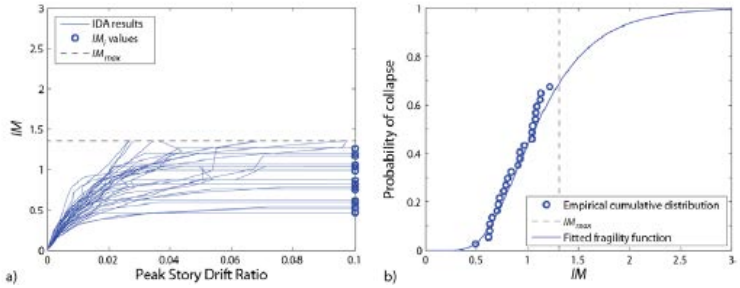

Figure 4.13: Example truncated IDA analysis results (left). Observed fraction of collapse as a function of IM, and a fragility function estimated (right) Baker, J. W. (2015).

In particular, for each level of seismic intensity IM_j considered, the probability $P(z_j)$ of exceeding the limit state is given by the binomial distribution equation 4-21:

$$P(z_j) = \binom{n_j}{z_j} p_j^{z_j} (1 - p_j)^{n_j - z_j} \quad 4\text{-}21$$

where n_j describes the number of seismic events considered, z_j the number of events for which the state limit is not fulfilled and pj the probability that it has an intensity IM_j. By using the maximum likelihood approach, then, the function of fragility is derived, which represents the function which corresponds to the highest probability of correlation with the results obtained from all the analyses done by varying the seismic intensity. To this end, assuming a log-normal law probability distribution to describe the state limit checks, the parameters average (θ) and variance (β) can be estimated as equation 4-22:

$$\{\hat{\vartheta}, \hat{\beta}\} = \arg\max_{\vartheta,\beta} \sum_{j=1}^{m} \left\{ \ln \binom{n_j}{z_j} + z_j ln\Phi\left(\frac{\ln\left(\frac{x_j}{\vartheta}\right)}{\beta}\right) + (n_j - z_j) \ln\left(1 - \Phi\left(\frac{ln\left(\frac{x_j}{\vartheta}\right)}{\beta}\right)\right)\right\} \quad 4\text{-}22$$

4.8 Overview of the literature

Most of the methodologies existing in the scientific literature for the derivation of fragility curves are analytical because the available earthquake damage data available to derive empirical bridge fragility curves is few. A great number of analytical methodologies is available in the literature (Table 4.5), and can be classified by considering multiple components (Avşar et al. 2011; Banerjee & Shinozuka 2007; Cardone, Perrone, & Dolce 2007; Cardone 2013; Choi et al. 2004; Crowley et al. 2011; Tsionis and Fardis 2012; De Felice & Giannini 2010), or only the most critical one (piers) in fragility analysis. In particular, regarding component capacity, either local (Crowley et al. 2011; Tsionis & Fardis 2012; De Felice & Giannini 2010; Dukes 2013), or global (Elnashai et al. 2004; Ghosh et al. 2013) engineering demand parameters are used, whereas quantification of damage, namely the limit state thresholds, is commonly based on experimental results (Hwang et al., 2001; Karim Yamazaki 2001,2003; Mackie & Stojadinović 2004). Regarding the calculation of seismic demand, different analysis methods have been put forward, namely inelastic static (pushover) analysis (e.g. Cardone, Perrone, & Dolce 2007; Cardone 2013; Choi et al. 2004), modal response spectrum method (e.g. Avşar et al.

2011; Mackie & Stojadinović 2004), and nonlinear response-history analysis (Mander & Basz 1999; Moschonas et al. 2008). The maximum likelihood method Nielson & DesRoches (2007a, b) or the probabilistic seismic demand model have been used for the calculation of fragility curves.

The variability in capacity and demand estimation in the frame of analytical methodologies for the derivation of fragility curves is depicted in Table 4.5. The main drawback of the existing methodologies is that capacity (limit state threshold) estimation is commonly based on experimental results ignoring the effect of structure-specific parameters like pier type, geometry, the material, and reinforcement properties on results, whereas advanced analysis tools are proposed for the estimation of seismic demand, increasing the computational cost when applied to large bridge inventories.

Table 4.5: Capacity and demand estimation in analytical methodologies for the derivation of fragility curves (Stefanidou, S. P. 2016).

	Capacity		**Seismic Demand**		
Research Group	**Engineering Demand Parameter**	**Limit State thresholds**	**Structural model**	**Seismic Input**	**Analysis Method**
Avşar *et al.* (2011)	Piers: φ Beams: φ, V_u Bearings: δ [3 LS]	*Piers:* Priestley *et al.*, (1996), Erduran & Yakut, (2004) *Bearings:* FHWA, (2006)	3D DM	25 accel. (no scaling)	NRHA
Banerjee & Shinozuka (2007)	Piers: μ_θ [5 LS]	Dutta, (1999)	3D DM	3 × 20 accel.	NRHA & CSM
Cardone, Perrone, & Dolce (2007), Cardone (2013)	Piers: δ Bearings: δ Abutments: δ [5 LS]	*Piers:* δ_y & δ_u *Bearings:* γ (%) Konstantinidis et al. (2008) *Abutments:* δ_{gap} & δ_u	MDOF→SDOF, Adaptive Pushover	Spec-trum	CSM (adap-tive)
Choi *et al.* (2004)	Piers: μ_φ Bearings: δ [5 LS]	*Piers:* Dutta, (1999) *Bearings:* Experiments	3D DM	100 synthetic accel.	NRHA
Crowley *et al.* (2011), Tsionis & Fardis (2012)	Piers: θ Bearings: δ [2 LS]	*Piers:* θ_y & θ_u Biskinis & Fardis, (2010a, b) *Bearings:* Bousias *et al.* 2007	SDOF*(Long)*, Beam with springs (*Trans*)	EC8 elastic spectrum	Equivalent Static
De Felice & Giannini (2010)	Piers: θ [2 LS]	θ_y & θ_u	Metamodels	2 ×4 accel.	NRHA - RSM
Dukes (2013)	Piers: μ_φ Bearings: δ Abutments: δ [4 LS]	*Piers:* Dutta, (1999) *Bearings - Abutments*: Caltrans (2010)	Metamodels	3 ×40 accel.	NRHA - RSM

Elnashai *et al.* (2004)	Piers: δ	δ_y & δ_u (Pushover Curve)	3D DM	7accel. (scaled)	NRHA
Ghosh *et al.* (2013)	Piers: μ_φ Bearings: δ Abutments: δ [4 LS]	Nielson & DesRoches (2007)	Metamodels	24 accel. (Wen& Wu)	NRHA - RSM
Hwang *et al*., (2001)	Piers: *C/D factors or* μ_δ [5 LS]	*Piers:* δ_y & δ_u	3D DM	100 acc. synthetic	NRHA
Karim & Yamazaki (2001,2003)	DI=(μ_δ+$\beta\mu_h$)/μ_u (Park-Ang) [5 LS]	*DI*=0.00~1.00	SDOF	250 accel.	Non-linear Static/NRHA
Mackie & Stojadinović (2004)	Drift (%)	Berry & Eberhard (2003)	3D DM	80 accel.	NRHA
Mander & Basöz (1999)	Piers: *δ/h (%)* Bearings: δ [5 LS]	Dutta, (1999)	SDOF	Elastic spectrum	CSM
Moschonas *et al.* (2008)	Bridge: δ [5 LS] [5 LS]	*Piers:* δ_y & δ_u (Pushover curve) *Bearings:* δ (γ %)	3D DM	Elastic spectrum	CSM
Nielson & DesRoches (2007a, b)	Piers: μ_φ Bearings: δ Abutments: δ [4 LS]	*Piers:* HAZUS (1997), FHWA (2006) *Bearings*, *Abutments*: Choi (2004)	3D DM	48 accel. (3 bins)	NRHA
Ramanathan, (2012)	Piers: μ_φ Bearings: δ Abutments: δ [4 LS]	*Piers:* Berry & Eberhard (2003), *Bearings*, *Abutments*: Caltrans (2010)	3D DM	320 accel. (4 bins)	NRHA
Shinozuka *et al.* (2000)	Piers: μ_δ [3 LS]	$1.0 \leq \mu_\delta \leq 2.0$	3D DM	80 accel.	NRHA
Tavares *et al.*, (2012)	Piers: μ_φ Bearings: δ Abutments: δ [4 LS]	HAZUS (1997)	3D DM	Synthetic Accel.	NRHA
Yi *et al.* (2007)	Piers: μ_φ Bearings: δ	Choi (2004)	2D Model	60 accel.	NRHA
Zhong *et al.* (2012)	Piers: Drift (%)	Probabilistic model (closed form relationship)	3D DM	Elastic spectrum	CSM

* ***3D DM:*** 3D Detailed Model, ***NRHA***: Nonlinear Response History Analysis ***CSM***: Capacity Spectrum Method

5. Specific design and retrofitting criteria for bridge

5.1 Criteria for bridge design in the international organisations

5.1.1 California USA (CALTRANS)

Caltrans has long been the international leader in bridges anti-seismic design and was the first state transportation department that used performance-based criteria. The anti-seismic design criterion of the Caltrans is based on the AASHTO SGS, in fact, there are many similarities between the two standards. The Caltrans method for anti-seismic bridge design is defined in the Memo to Designers 20-1 (Caltrans 2010b), where bridges are classified as important or ordinary according to the requirements of post-earthquake operability (i.e., if the bridge it is part of an access route to emergency facilities), if the prolonged closure causes economic damage and if the bridge is part of strategic routes in emergencies. Further classification can be made according to the structural geometry and layout, and geological conditions. Based on this classification of the bridges, the performance criteria have been defined as you can see in Table 5.1, together with the related definitions.

Table 5.1: Caltrans Seismic Performance Criteria.

Bridge Category	Seismic Hazard Evaluation level	Postearthquake Damage Level	Postearthquake Service Level
Important	Functional Safety	Minimal Repairable	Immediate Limited
Ordinary	Safety	Significant	No collapse

The ordinary design of standard bridges is set by the Seismic Design Criteria (Caltrans 2010a). The design earthquake is considered as a seismic event with a probability of 5% to happen in 50 years (return period of 975 years) and a deterministic ground motion characterised by the largest median response from the maximum failure of any failure within the vicinity of the bridge. Also, the minimum ground movement is imposed as the median spectrum generated by an earthquake of magnitude 6.5 on an impact glide fault at 12 km from the site.

The performances are considered acceptable when the structure subjected to the single design earthquake does not collapse. The deformation capacity is defined by the deformation limits of the material and the ductility requirements of the maximum displacements, defined according to the structural configuration of the bridge. Depending on the configuration of the bridge, an equivalent static analysis (linear elastic analysis based on force) or an equivalent dynamic analysis (linear elastic multimode analysis) can be used. The capacity to move the bridge is determined by static analysis (pushover).

Important and non-standard bridges are designed according to specific design criteria following the procedures described in the Memo to designers 20-11 (Caltrans 1999). This process includes peer review by Caltrans staff or an external review expert committee or both, based on the specific characteristic of the project and the expertise of the Caltrans staff.

5.1.2 Oregon USA (ODOT)

The Oregon Department of Transportation (ODOT) utilise the displacement-based seismic design procedures of the AASHTO SGS. A two-level approach is used in the seismic design, where the 1,000-year AASHTO return period (effective 975 years) is used to control the collapse prevention of a 500-year earthquake (effective 475 years), that can be used in turn to control of the service limit. Below is reported that controls based on ODOT displacement use different strain limits than those provided in the AASHTO SGS.

ODOT has developed the two-level design criteria listed above for new bridges to protect against the risk posed by the earthquake in Oregon. These criteria guarantee specific mitigation of the seismic risk for new buildings, especially for minor events and the CSZ. Also, the two-level criteria for retrofit evaluation, as outlined in the FHWA Retrofit Manual, have been improved to use a possibility of exceeding 500% or 15% of the earthquake in 75 years for the lower level event.

5.1.3 Japan road association

Succeeding the 1995 Hyogo-ken Nanbu (Kobe) earthquake, the Japan Road Association (JRA) revised its 1990 specifications, using the defined guidance for bridge repair and reconstruction after the Kobe event and research breakthroughs to write the new edition of seismic design specifications dated 1996 (JRA 1996). The new rules for seismic design included two models of seismic risks: Model 1 plate boundary type large-scale earthquakes and Model 2 inland direct strike type earthquakes. An example of model 1 can be the 1923 Great Kanto earthquake, and

recently the Great East of Japan (Tohoku) of 2011. While the case of model 2 can be the earthquakes similar to the Kobe event and magnitude of about 7. The new edition of specifications did not consider the data on the return period or the way to overcoming these ground motion.

Bridges in Japan are divided into two groups of importance depending on the bridge's function within the transportation system. Bridges of standard importance are classified Class A and bridges are of high importance are classified Class B. The new specifications also define the importance of the role of the bridge in regional disaster prevention plans, the volume of traffic carried by the bridge and whether alternative routes are feasible and if the cost and recovery time would be excessive. However, there is no quantitative methodology on how to make these decisions.

Table 5.2: Japan Road Association seismic motion and target seismic performance (National Academies of Sciences, Engineering, and Medicine. 2013).

Ground Motion to Be Taken into Account in Seismic Design		**Target Seismic Performance of Bridge**			**Seismic Calculation Method**
		Bridge standard importance (bridge of Class A)	**Bridge standard importance (bridge of Class B)**	**Static analysis method**	**Dynamic analysis**
Ground Motion highly probable to occur during the service period of bridge		No Damage		Seismic coefficient method	Time History Response
Ground Motion with high intensity, though less probable to occur during the service period of the bridge	Ground motion Type I	To prevent fatal damage	To limit Damage	Ductility design method	Time History Response
	Ground motion Type II				Response spectrum analysis

The seismic design provides two levels of performance. Bridges should not lose their integrity for small earthquakes. Table 5.2 describes the seismic risk and performance targets. In the specification, there is a force-based coefficient method to design the bridge for the smaller earthquakes. For the high-intensity earthquakes the Class A bridges do not have to sustain "fatal damage" (e.g. collapse), and for Class B bridges the damage is limited to local damages in the case of a major earthquake. These performances are required for both types of ground motion, models I and II.

The specifications require a ductile type of design and the design verifications are conducted only for upper-level of ground motion, as shown in Table 5.2. Design controls are based on displacement-based methodology. For many types of bridges, the admissible ductility requirements are provided based on the importance classification — this requirement guarantee that damage is proportional to the bridge class. Seismic isolation is also discussed in the JRA seismic specifications. Moreover, an additional check that is required as part of the JRA upper-level ground motion (Types I and II) is the residual displacement. The check is based on the calculated ductility demand of the pier. The residual displacement is a function of the ultimate strength of the pier, spectral acceleration coefficient, post-yield stiffness, the construction type—RC, steel, etc.—and the tributary seismic weight.

The JRA considers an allowable residual movement of up to 1% of the height of the pier unless specific studies are done to develop a specific value for the project. The arrangement of JRA residual drift is an unusual requirement that is not typically found in the design rules but is appreciable and reasonable. In the AASHTO specifications, there are not displacement limits other than the indirect controls necessary to meet the limits of the P-Delta effects or the limits of material deformation (in the case of the SGS), and these limits are not strictly connected to evaluate the post-earthquake function or the repair of a bridge.

5.1.4 Eurocode

The Eurocode 8 Part 2 - The bridge seismic design (EC8-2) (Eurocode 2008) defines the seismic design of bridges for the 22 national members of the European Committee for Standardization (CEN). The central philosophy of seismic design is represented by a ductile response, as for many of the national provisions on seismic design. The EC8-2 seismic design procedure for bridges is based on a force-based design approach, but displacement control is also required if irregularities are present. In this code, irregularity is defined when ductility requests are not kept relatively equal among the yielding components. If some components are predisposed by the configuration of the structure to have greater ductility requirements while others have lower requirements, the ratio is greater than a factor of 2, then a non-elastic displacement capacity check must be performed, which is similar to the procedure of the AASHTO SGS. Otherwise, a force-based approach alike to the AASHTO LRFD method is satisfactory. Capacity design and minimum detail are applied to all facilities

The EC8-2 uses a single level of seismic hazard in the seismic design procedure, which can be defined by the country follow the specification, although the seismic

risk is usually considered as a return period of 475 years or a 10% ground motion of the possibility of overcoming in 50 years. Performance goals are not collapse for the design event and the minimisation of damage in a smaller event. Usually, the design event is generally checked in the design step. As with AASTHO LRFD and SGS, the appropriate performance in the smallest event is deducted but not controlled. The bridge following the design earthquake should not report any damage that reduces its use as reported in the normative the "structure can support actions from emergency traffic and easily inspect". Furthermore, the EC8-2 goes on to state that "the non-collapse requirement for bridges under the seismic design event is more stringent than the relevant requirement for buildings, as it contains the continuation of emergency traffic." The EC8-2 admits two classes of structures - structures with ductile behaviour and structures with limited ductile behaviour - with the delimitation between the two factors of demand for system ductility of 1.5. The force reduction factor is based on the fact that a structure is ductile or ductile limited and the application of the factor is similar to the way R is treated in the method based on the AASHTO force. An important factor is also applied, which regulates the movement of the ground up or down by 1.30 or 0.85, similarly, depending on whether the bridge is above or below the average.

In general, the EC8-2 uses many concepts from the AASHTO seismic design procedures and is therefore comparable to the AASHTO methodologies on many aspects, even if the force and displacement-based methods are combined into a single specification. Although the choice of the design earthquake falls within the jurisdiction of the country, they are generally lower than the ASTHO, since a return period of 475 years is used more often.

5.2 Samples of retrofitting methods for R/C bridges

5.2.1 Introduction

Over the years, the scientific community has developed several techniques for the adaptation and seismic improvement of bridges useful for correcting design errors, which can be traced back to the lack of knowledge of the seismic phenomenon. The evolution of design techniques and at the same time of the regulations have made it necessary to retrofit the existing structures. In particular, a quick description of the most frequent damages that could be observed in the RC bridges following a seismic event will be described below for the piers, foundations, abutments, bearings. This damages are caused by underestimating the earthquake displacements and the seismic forces that generate breakages of the elements mentioned above.

In this chapter, which mainly incorporates the most extensive treatment in (fib, 007), the most common technical solutions for reinforcing the various parts of a bridge are presented, without providing the relative sizing procedures, for which reference are made to specialized documents (Priestley et al., 1996), (FHWA, 2006). In order to compensate for possible errors due to inadequate planning, it is possible to proceed with the seismic adaptation of existing bridges, which in general for bridges a girder in:

- Pipe extender;
- additional constraints made with bars and cables;
- longitudinal and transverse restraints;
- reinforcement of the piers;
- reinforcement of the cross girder;
- reinforcement of foundations;
- isolation and damping.

5.2.2 Bridge decks and girders

Following seismic events, the deficiencies commonly detected in the bridges, affecting the superstructure, concern the inadequacy of the seat and the seat lengths, factors that can easily lead to the loss of support and the consequent collapse of entire simply supported spans. The first reinforcement programs were developed in the United States following the earthquake in San Fernando, where they focused precisely on correcting these problems.

5.2.2.1 Seat Extender

The interventions for adapting the seat system are very varied and depend on the type of deck and the quality of the intervention to be done. The extension operation of the seat areas of the deck has the purpose of providing a larger seat length to the deck. To define the seat length, it needs to consider the maximum displacements of the decks in the case of asynchronous movements.

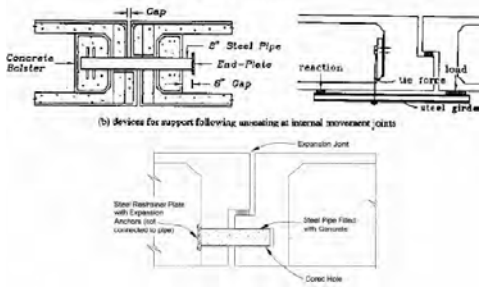

Figure 5.1: Example of an sttel pipe restrainers for the girder box bridge. (FHWA 2006)

Figure 5.2: Example of an intervent of seat extender. (Wright, T 2011)

5.2.2.2 Restrain

Restrainer failures drew attention to the need to design restrainer systems carefully. Restrainers must not only be stiff enough and strong enough to prevent joints from separating, but the remainder of the bridge must be able to resist the forces developed in restrainers (Selna and Malvar, 1987). Restraining devices may also transmit higher forces to other bridge components such as bearings and columns and may cause their failure if not properly designed.

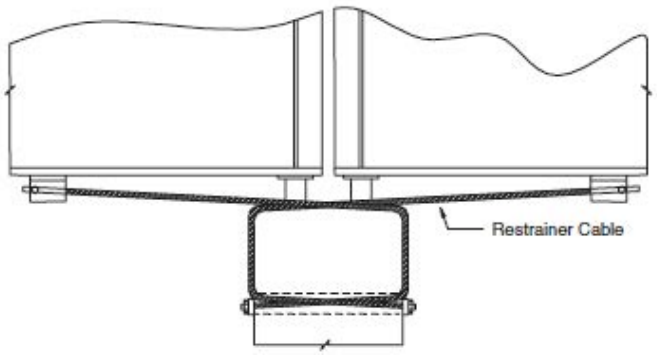

Figure 5.3: Restrainers at the pier with a positive tie to the pier. (FHWA 2006)

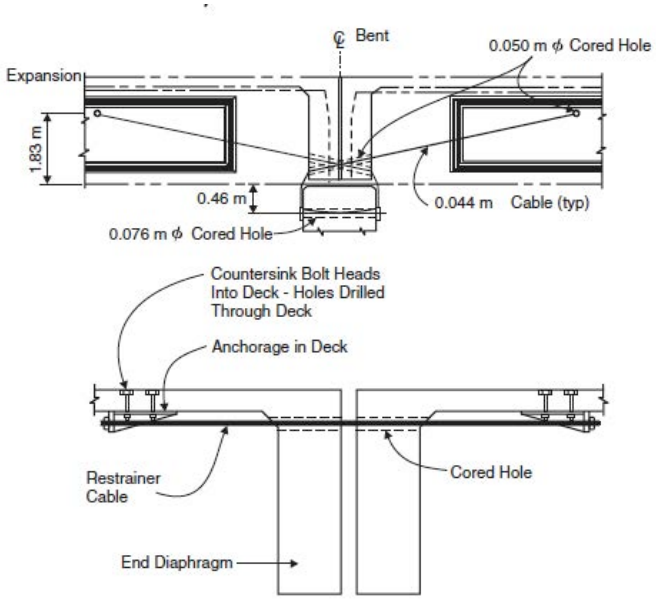

Figure 5.4: Restrainer anchorage schemes (FHWA 2006).

5.2.2.3 Bearings

A large part of the existing bridges, with the decking on the raised beams, have supports under each beam, in non-reinforced neoprene of small thickness, whose resistance to horizontal actions is negligible. An economical and effective intervention consists in replacing the existing supports with new supports of the same type and the realisation on top of the stack of a system of restraints that avoids the fall of the decks and limits relative displacements. This last type of intervention has the purpose of reducing the period of the structure, increasing the dissipative capacity and limiting the transmitted forces. The isolation and damping devices are used to reduce the forces transmitted to the substructure and to reduce displacements.

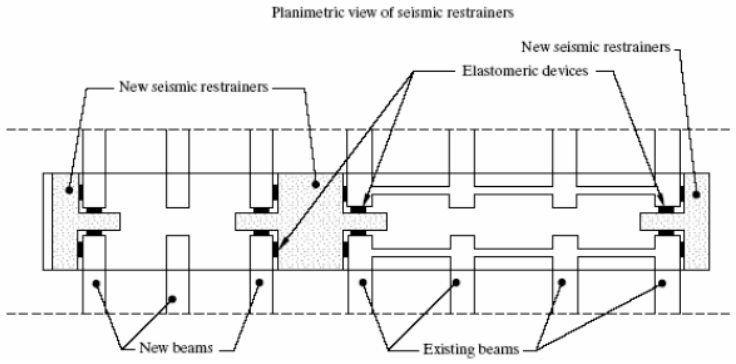

Figure 5.5: Example of seismic restrainer (Furlanetto ed al, 2008).

More effective measures can be by making the static scheme of the deck continuous. In this case, it is possible to avoid having supports under each beam by placing a small number of metal devices, fixed and mobile, or solvent devices on a single row. In the past, it has been frequently adopted a solution that provided for the "continuation" limited to the single slab, together with the arrangement of a number equal to the original one of rubber insulation devices.

5.2.2.4 Cap beam

The reinforcement of the cap beam has the purpose of increasing the shear strength, increasing the ductility and finally increasing the flexural strength. Approaches include metal plates, c.a. reinforcements and prestressing with high-strength cables.

Figure 5.6: Prestressed cable for the retrofitting of the cap beam. (Wright, T 2011)

5.2.3 Piers

The reinforced concrete piers designed by non-seismic criteria often have inadequate lengths of overlapping or anchoring of the longitudinal bars and reduced quantity of transversal reinforcement, however not anchored in the core: they result in a defect of shear strength and ductility (confinement of concrete and the longitudinal bars inadequate tablets, withdrawal of the stretcher bars). The reinforcement of the piers has the purpose of increasing the shear strength of the bearings, limiting displacements and increasing the ductility capacity of the piers itself. The possible interventions include metal plates, increase of the section with jackets in R/C, prestressing with cables or bars in high strength steel, reinforcements with composite materials.

Figure 5.7: Examples of the techniques to retrofitting piers. (Wright, T 2011)

5.2.4 Footings

The intervention on footings may be necessary in case the existing foundation is not suitable to transmit to the ground the forces coming from the superstructure, evaluated for a seismic verification action that is generally greater than that of the original project. In the case where the pier or abutment has been reinforced, it is necessary, by the principle of resistance hierarchy, to verify that the foundation can withstand the new increased forces that the elevation can transmit. Finally, the intervention is always necessary when the stack is widened to accommodate a larger deck.

6. Case study

6.1 Selected bridge geometrical configuration

The bridges and viaducts selected for the research are obtained starting from the structural characteristics of an existing viaduct, built in the 70s and located in the Campania Region (Figure 6.1).

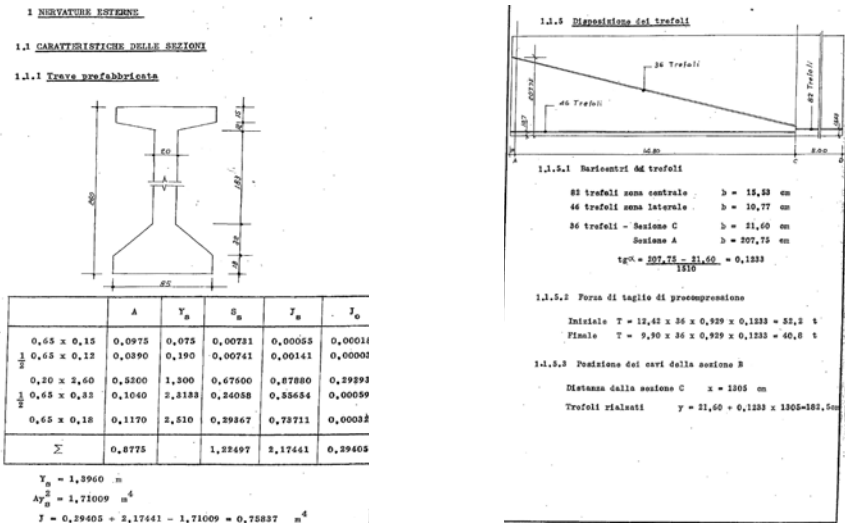
1 NERVATURE ESTERNE

1.1 CARATTERISTICHE DELLE SEZIONI

1.1.1 Trave prefabbricata

	A	Y_n	S_n	J_n	J_o
0,65 x 0,15	0,0975	0,075	0,00731	0,00055	0,0001
$\frac{1}{2}$ 0,65 x 0,12	0,0390	0,190	0,00741	0,00141	0,0000
0,20 x 2,60	0,5200	1,300	0,67600	0,87880	0,29293
$\frac{1}{2}$ 0,65 x 0,33	0,1040	2,3133	0,24058	0,55634	0,00059
0,65 x 0,18	0,1170	2,510	0,29367	0,73711	0,0003
Σ	0,8775		1,22497	2,17441	0,29405

$Y_n = 1,3960$ m

$Ay_n^2 = 1,71009$ m^4

$J = 0,29405 + 2,17441 - 1,71009 = 0,75837$ m^4

1.1.5 Disposizione dei trefoli

36 Trefoli

46 Trefoli

46 Trefoli

1.1.5.1 Baricentri dei trefoli

82 trefoli zona centrale b = 15,53 cm

46 trefoli zona laterale b = 10,77 cm

36 trefoli - Sezione C b = 21,60 cm

Sezione A b = 207,75 cm

$tg\alpha = \frac{207,75 - 21,60}{1510} = 0,1233$

1.1.5.2 Forza di taglio di precompressione

Iniziale T = 12,42 x 36 x 0,929 x 0,1233 = 52,2 t

Finale T = 9,90 x 36 x 0,929 x 0,1233 = 40,8 t

1.1.5.3 Posizione dei cavi della sezione B

Distanza dalla sezione C x = 1305 cm

Trefoli rialzati y = 21,60 + 0,1233 x 1305=182,5cm

Figure 6.1: Original drawing of the 1960 bridge design.

The bridge and viaduct, in reinforced concrete, develops on simply supported spans, each span equal to 41.00 meters (Figure 6.2). The piers can be classified into two different types, depending on the height and the geometric cross-section, both are box-type. The long piers, indicated with “L”, are circa 40 m tall and are characterised by a cross-section (Figure 6.6) larger than the short piers, indicated with “S”, that have half the height of L pier.

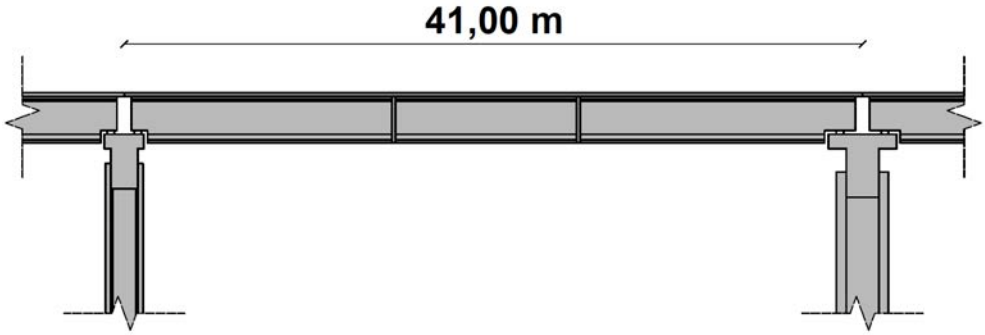

Figure 6.2: Span length selected bridge.

Different versions based on such geometrical configurations were considered by altering the number of spans and isolating/dissipating devices. In order to extend the study on more types of bridges and viaducts built in Italy between the 50s and 70s, four geometrical configurations have been selected with deck lengths varying from 120 to 360 meters and different piers arrangements (Figure 6.3)

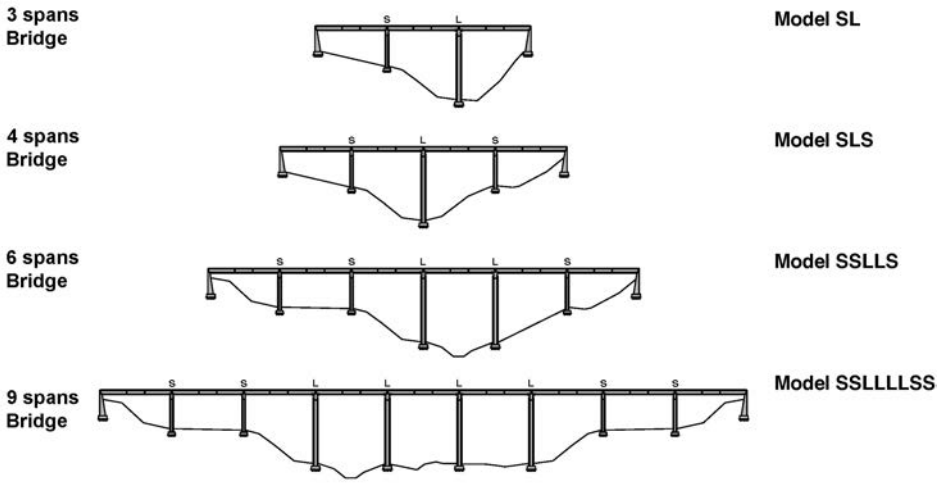

Figure 6.3: Considered bridge configuration.

6.1.1 Deck

The deck (Figure 6.4) consists of 8 longitudinal pre-stressed beams and deck slab of 20 cm. Transversely the beams are connected by cross girder. In correspondence of each of the eight beams, there is elastomeric support upon which the deck rests. The elastomeric support is located on the cap-beam and therefore on the stacks.

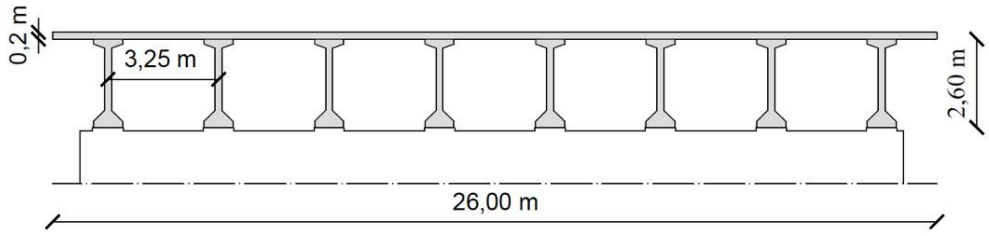

Figure 6.4: Deck configuration.

6.1.2 Bearings

In the selected bridge, between the deck and the cap beam, there are structural support devices in the reinforced elastomeric bearings (Figure 6.5), connected using mechanical anchors. They consist of an elastomer core in which steel layers are inserted to obtain adequate vertical stiffening. This type of support represents an intermediate constraint between the fixed and the mobile type devices, allowing deformations in the horizontal plane and, at the same time, generating elastic reactions of intensity proportional to the deformations themselves.

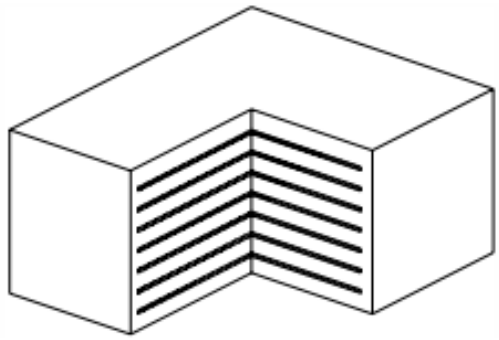

Figure 6.5: Elastomeric bearings (Priestley et al, 1996).

6.1.3 Piers

Two box-coupled piers are connected in the crosswise direction, thus forming a frame (Figure 6.6). The S pier is tall 21.99m, the L pier is tall 41.22m. The cross-section of the largest stack has a maximum longitudinal dimension in the plan (x-direction) equal to 2.8 m while transversely (y-direction) equal to 5.0 m.

Table 6.1: Geometric characteristic of the piers

Cross-Section Pier S		**Cross-Section Pier L**	
Area (m^2)	3,26	*Area* (m^2)	6,20
I_x (m^4)	2,59	I_x (m^4)	6,80
I_y (m^4)	5,10	I_y (m^4)	15,79

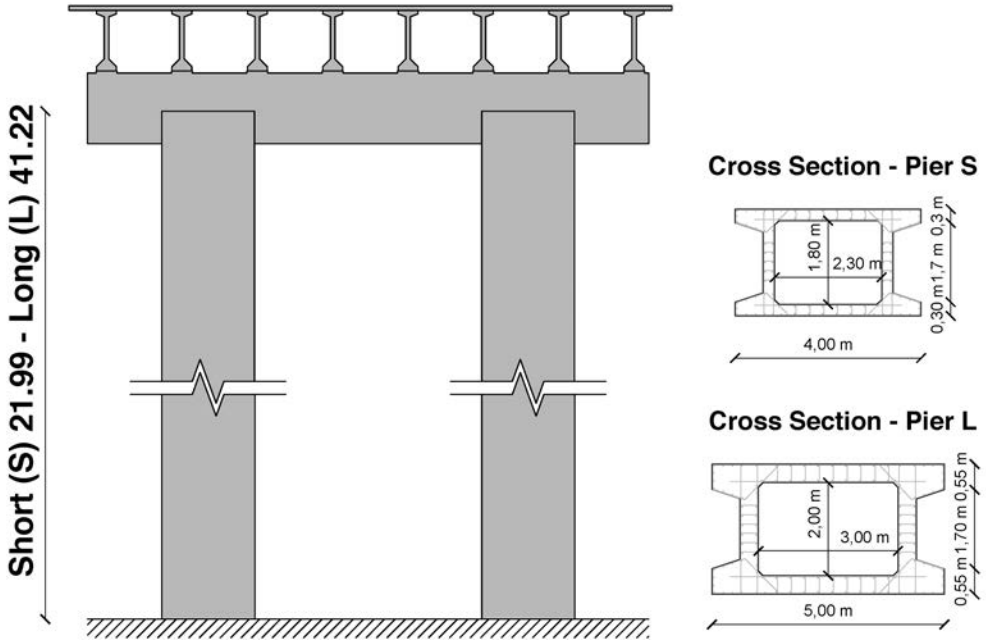

Figure 6.6: Piers configuration.

6.2 Retrofit Strategies

Considering a large number of existing bridges characterised by performances below the modern standards prescribed by the current codes, it is clear that the seismic upgrading cannot be done simultaneously and in the same way on the entire stock of bridges. The search for a method for the identification of existing bridges subject to higher risk is essential to understand which of them require priority adjustment measures, and which, even with the assumption of a small risk, can be adapted later. In particular, the problems of simply supported girder bridges will be investigated through the study of a sampling bridge defined by geometrical and mechanical characteristics typical of Italian bridges of the 60s. The proposed seismic protection strategies include the use of seismic isolation using sliding friction type isolators. The use of this device has been preferred to other types of isolators as it allows the decoupling of the horizontal movement of the superstructure and that of the substructure. This it is possible thanks to the sliding between a spherically shaped shell surface, made of steel, integral with an of the two parts of the isolated structure and a joint, bound to the opposite portion (Petti et al. 2013). The spherical surface is characterised by a certain radius of curvature R that represents the length of the

pendulum, and a coefficient of friction describes the sliding interface. Furthermore, the simplicity of installation and the low cost of the device have been preferred.

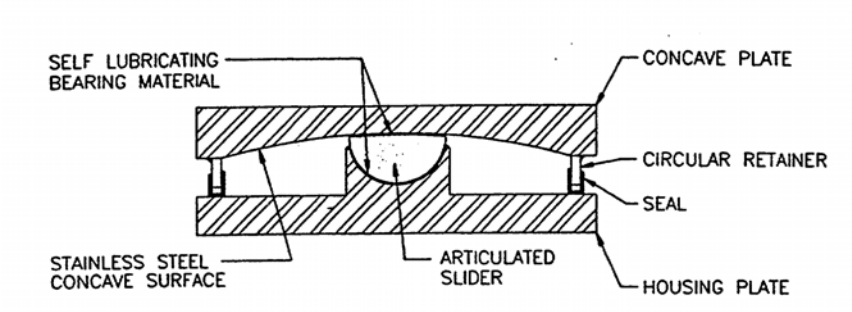

Figure 6.7: Bearing configuration (Priestley et al, 1996).

Different combinations of radius and friction coefficients for the insulation system were considered, in particular, R = 3.1m and R = 2.5m and coefficient of friction 2% and 5% were chosen (Petti et al. 2016). Herein, ten alternative schemes are adopted for rehabilitation of the case-study bridge infrastructure. The as-built configuration is characterised by neoprene bearings, the retrofitted one by Friction Pendulum System (FPS). Moreover, for both the support conditions, two different types of span configuration have been investigated: decks not longitudinally connected (as-built), and decks longitudinally connected by chain (retrofitted).

Table 6.2: Bridge Configurations

Retrofit Option	Description
ROD	The simply-supported decks are connected with longitudinal chains
R=2.5 2%	Friction Pendulum isolator with an effective radius of concave sliding surface equal to 2.5 m and Coulomb friction 2%
R=2.5 2% - ROD	Combination between R=2.5 2% and ROD
R=2.5 5%	Friction Pendulum isolator with an effective radius of concave sliding surface equal to 2.5 m and Coulomb friction 5%
R=2.5 5% - ROD	Combination between R=2.5 5% and ROD
R=3.1 2%	Friction Pendulum isolator with an effective radius of concave sliding surface equal to 3.1 m and Coulomb friction 2%
R=3.1 2% - ROD	Combination between R=3.1 2% and ROD
R=3.1 5%	Friction Pendulum isolator with an effective radius of concave sliding surface equal to 3.1 m and Coulomb friction 5%
R=3.1 5% - ROD	Combination between R=3.1 5% and ROD

6.3 Development of FEM Bridge Model

The model used is of the spine type with external constraints defined using joints. The different structural elements that compose it have been modelled taking into account the actual geometry and the mechanical and inertial characteristics derived from the design report and the available original drawings. In particular, the deck and the piers are schematised through frame elements arranged in correspondence with the barycentric axes of the real structural elements, providing for the deck a frame representative of the overall mechanical characteristics and the piers a single frame descriptive of the two box-coupled piers.

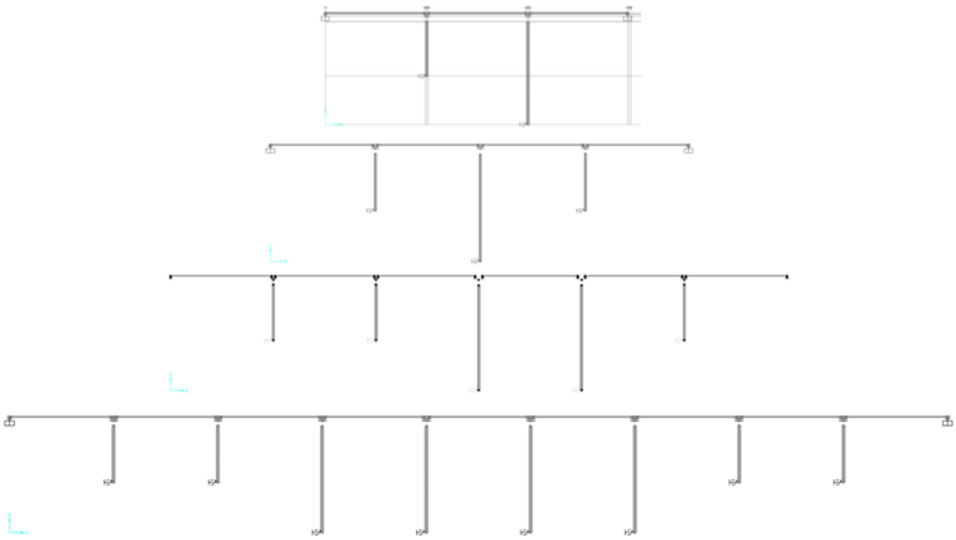

Figure 6.8: FEM Model of a bridges configuration.

The "X" axis represents the direction parallel to the longitudinal axis of the deck, the "Z" axis the vertical axis and, finally, the "Y" axis that orthogonal to the plane described by the "X" and "Y" axes. In order to take into account, the effects of cracking in the nonlinear field, the inertia of the sections of the cells have been reduced by 30%. The bridge was modelled with the software SAP2000 as a plane finite element numerical model (FEM).

6.3.1 Material Properties

The materials that have been defined in the model under examination are mainly two, the concrete for the deck and the piers, and the steel of the piers reinforcement (Aq60pile). The characteristics of these materials are reported Table 6.3.

Table 6.3: Concrete mechanical characteristic.

f_{cm}	$22\ MPa$
E_{cm}	$22000\ (f_{cm}/10)^{0.3} = 27871\ MPa$
ε_{cu}	3.5 ‰
ν	0.2
γ	$25\ kN/m^3$

The circular 617/2009 in paragraph C8A.6 suggests adopting a final deformation value of the appropriately determined concrete taking into account the effect of confinement. Since for the non-compact sections, such as the one under examination, the effectiveness of confinement is notoriously doubtful, it was decided to adopt the ultimate deformation value of the concrete equal to that which the NTC 2008 make assume in chapter 4 (3.5 ‰).

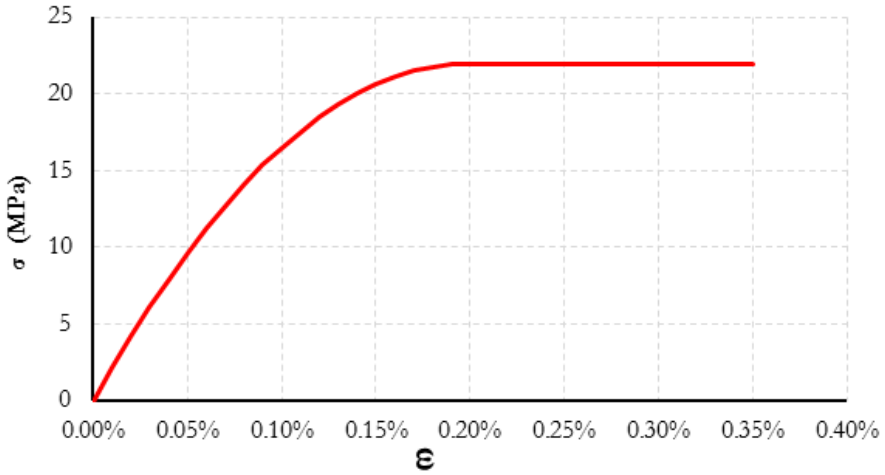

Figure 6.9: Concrete constitutive relationship

Again, concerning the same chapter of the NTC 2008, the parabolic-rectangle diagram in Figure 6.9 has been assumed for the constitutive bond of the concrete.

Table 6.4: Reinforcement steel mechanical characteristic.

f_{ym}	$370\ MPa$
E_{ym}	$210000\ MPa$
ε_{sm}	14 %
ν	0.3
γ	$78.5\ kN/m^3$

According to what is reported in the paper by Verderame et al., for steel Aq.60 the average breaking strain is equal to 22.5%, while the minimum and maximum values correspond respectively to 14% and 32% (Table 6.4).

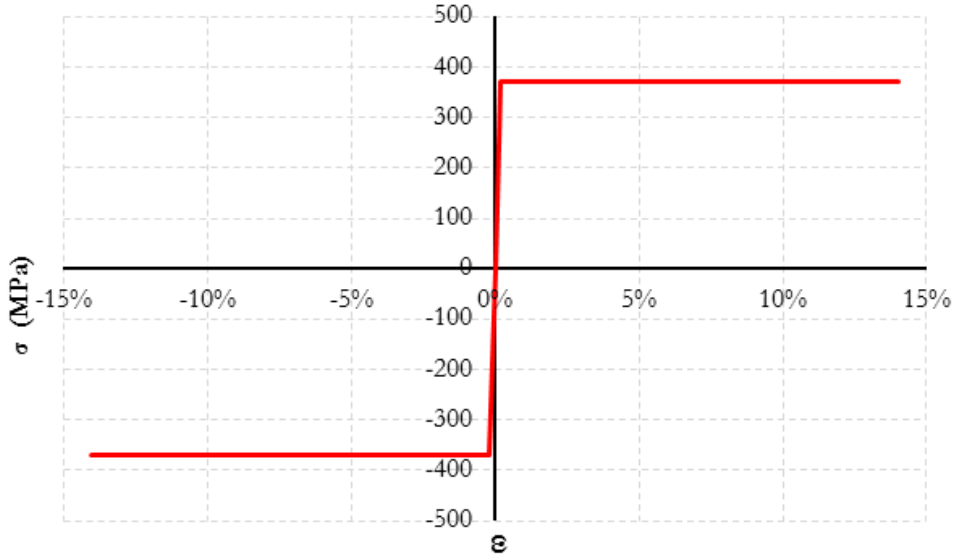

Figure 6.10: Reinforced steel constitutive relationship.

For the sake of safety, it is adopted as maximum deformation of the steel, the minimum value of 14%, this choice has no effect on the result given that the section's crisis always occurs due to excessive compression of the concrete. (Figure 6.10).

6.3.2 Modelling of Deck

The structural typology of the decks has suggested the adoption of a common discretisation scheme that foresees the use of finite elements of the beam type and masses concentrated in the nodes. The goal is to reduce as much as possible the numerical dimensions of the model, given its use in step-by-step analysis in the time domain. Therefore, the structural element is modelled with a "frame" element of the equivalent rectangular section regarding area and inertia, (Figure 6.11). Amplification factors of the moments of inertia have been defined in the X and Y directions of 1.18 and 51.08 respectively to ensure that equivalence is respected.

Table 6.5: Geometrical characteristic of the bridge deck.

Area (m^2)	I_x (m^4)	I_y (m^4)
12,22	*12,77*	*682,41*

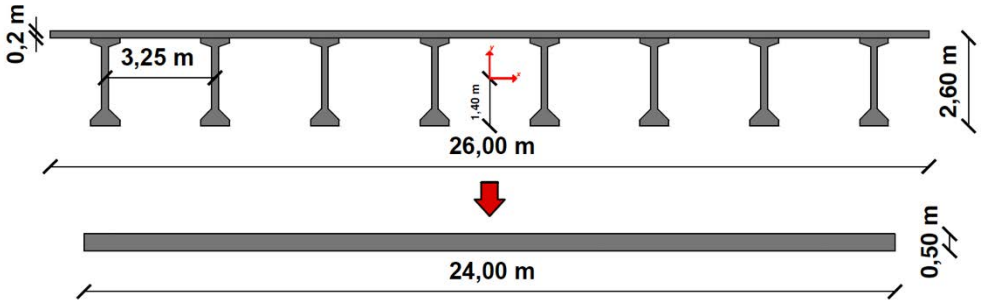

Figure 6.11: Equivalent section of the deck

6.3.3 Modelling of Cap-beam

The cap beam element was modelled with a node, corresponding to the centre of gravity of the cap beam itself, in which a mass is applied in the barycentric node. In particular, this mass has different values for the two types of piers, and is equal to 3123.20 kN for the Piles S, while it is equal to 4390.24 kN for the Piles L. This point is rigidly linked to the nodes representing the head of the piers and at the lower nodes of the springs which simulate the elastomeric bearings by means the "body" a type of internal constraint, (Figure 6.12).

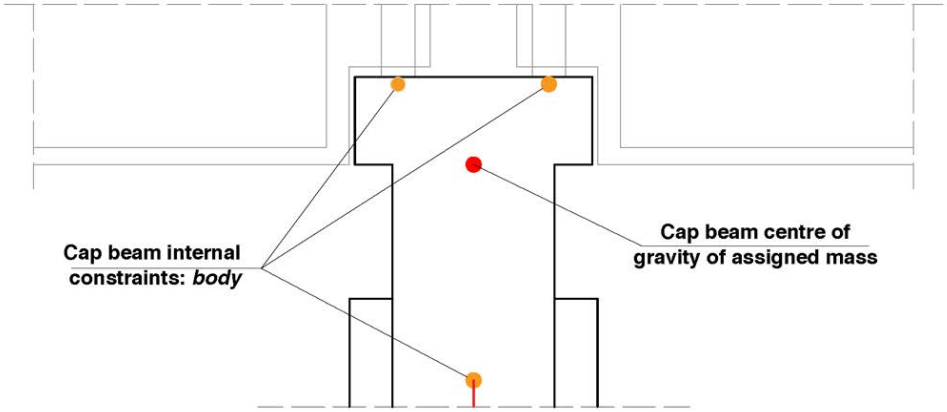

Figure 6.12: Modelling of Cap-Beam section.

6.3.4 Modelling of bearing

The bearings are described in the model with elastic links of the double-node Hook type (Figure 6.13). These springs are defined only in the three translational directions, assigning equal stiffness in the two horizontal directions and a much higher stiffness in the vertical direction (Table 6.6).

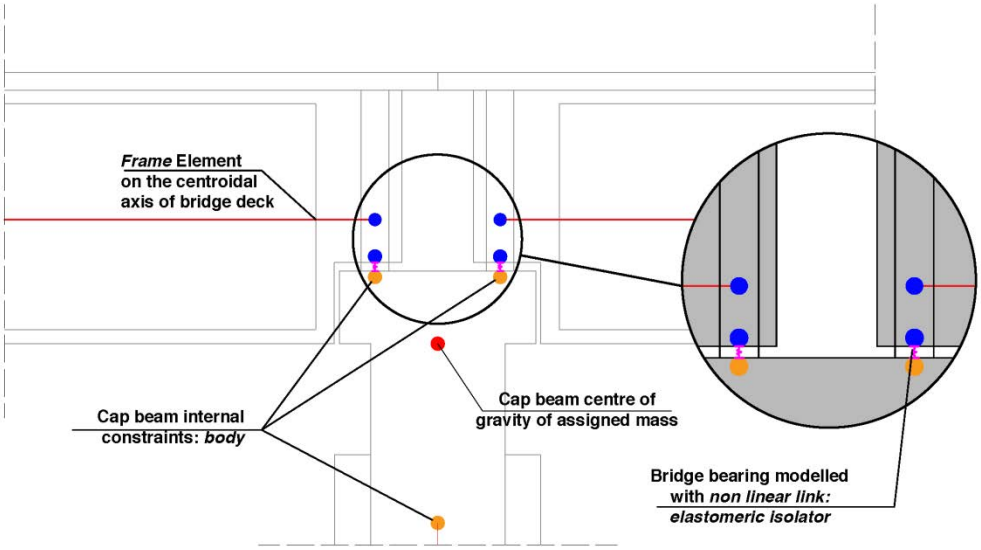

Figure 6.13: Geometrical modelling of the elastomeric bearings.

It should be noted that the stiffness values assigned to each of these springs in the model are equal to 8 times the values of Table 6.6 since in correspondence of each of the eight beams constituting the cross-section of the deck there is a support, but in the simplified model is given a single equivalent spring. The rotational stiffness R3 is zero: this allows to simulate the constraint condition of the deck which, as mentioned previously, is simply supported.

Table 6.6: Geometrical characteristic of the elastomeric bearing.

Axial stress (kN)	Axial stifness (kN/mm)	Effective stifness (kN/mm)
1250	3,43	1114

The upper link-element nodes are rigidly connected to the deck-beam nodes by rigid constraints. Moreover, there are nodes placed at the intrados of the beams and rigidly connected to the axis of the same (rigid constraints) to simulate the correct operation of the bearings.

6.3.5 Modelling of Piers

The piers of the sample viaduct were modelled as one Frame elements. The base constraint of the piers was modelled through a non-linear link-element, assuming therefore that, in the structure, in case of a seismic event, a significant amount of energy is dissipated in this area. In particular, "Multilinear Plastic Kinematic" type

have been defined (Figure 6.14), in which the behaviour of the element is defined with a moment-rotation diagram.

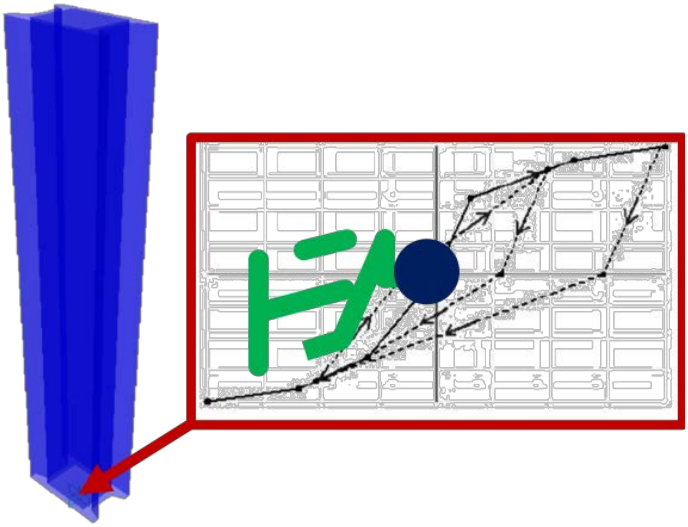

Figure 6.14: Modelling of Plastic Hinge by Multilinear Plastic Kinematic link.

Moreover, for their particular box-prismatic section and the size of the same, it may not be easy to model the viaduct piers correctly, to evaluate their non-linear behaviour. For this reason, a parametric analysis of the elastoplastic behaviour of the pier was developed, as described below. The characteristic parameters of this mechanical behaviour (moment-rotation diagram) were obtained using non-linear static analyses (push-over) done on the model of the single piers. The reference model is therefore done of the cantilever pier loaded with the weight of the cap beam and the deck weigh, at the base of which diffused plasticity hinge ("plastic hinge" with fibres) is inserted to localise the non-linearity of the element. The geometry of the concrete section and the reinforcements were modelled with the SAP2000 module *"Section designer",* realising the geometries illustrated in (Figure 6.15) and (Figure 6.16) respectively for the Pier L and the Pier S.

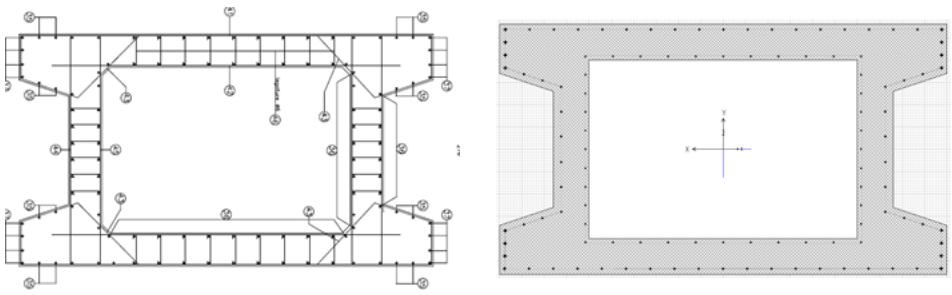

Figure 6.15: Cross section and FEM model Pier L.

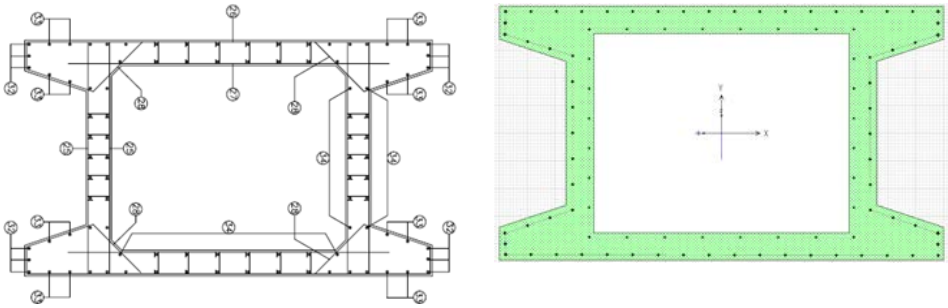

Figure 6.16: Cross section and FEM model Pier S.

This module allows the construction of the moment-curvature diagram of the section. The result is shown in Figure 6.18, where the values of the last moment and last curvature obtained in the crisis condition of the section are reported, both for the S and the L piers. The section failure has always been obtained for concrete breakage (ε_{cu} = 3.5‰) (NTC2018), while steel deformation is far from the final value defined. The reliability of the *"Section designer"* module was validated by constructing the moment-curvature diagram of the same section also with a consolidated program, called VcaSLU (Figure 6.17), and comparing the results (Figure 6.18).

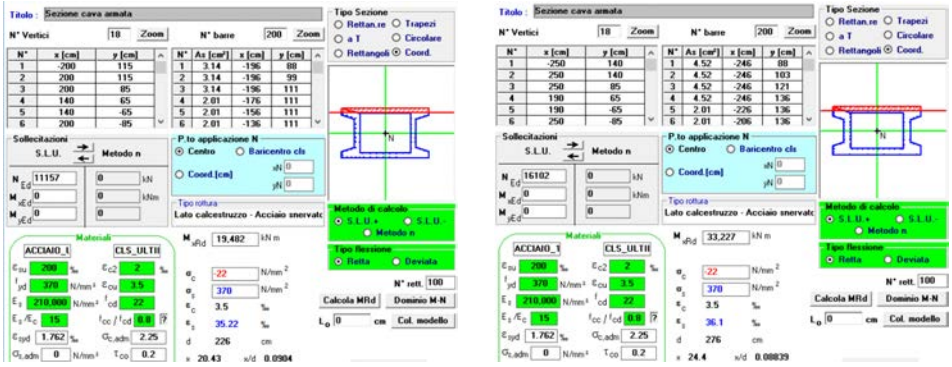

Figure 6.17: Modelling of the piers L and S with software VcaSLU.

It is observed (Figure 6.17) that the deformation of the steel, at the end of the last conditions of the two sections, is 3.5-3.6%, therefore widely contained, as anticipated, within the deformation limits of the steel in question.

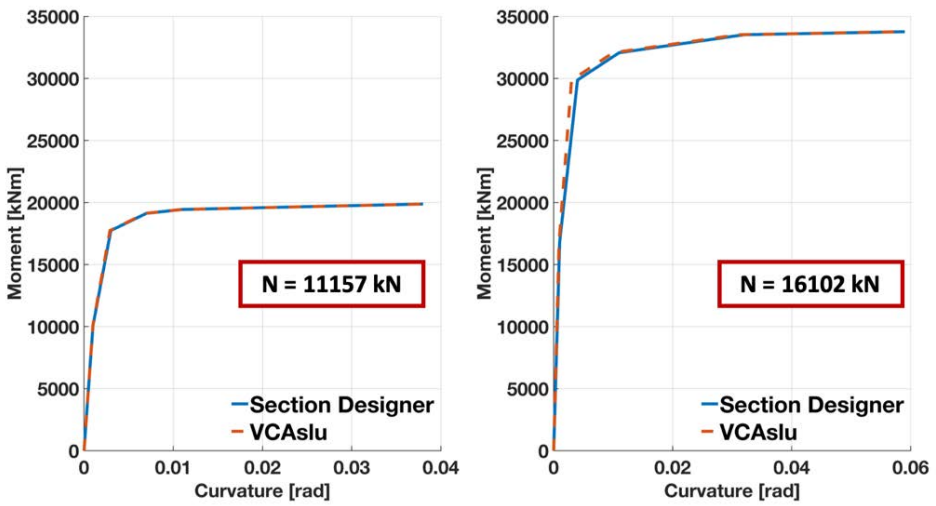

Figure 6.18: Comparison beetween the curve of Section Designer and VCAslu software.

Once the moment-curvature diagram of the section at the base of the pile was constructed, non-linear static analyses (push-over) on the stack were done by first applying only the vertical loads (phase 1, Figure 6.19), and subsequently, to starting from the results provided by this analysis, the horizontal loads (phase 2, Figure 6.19).

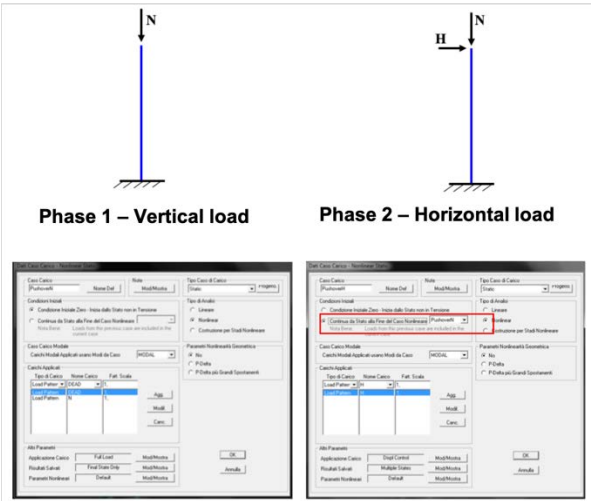

Figure 6.19: Pushover Analysis phases.

The plastic hinges at the base of the stacks have been defined by the "Fiber P-M2-M3 hinge" type of the SAP2000. The section modelled in "section designers" has been discretised into a large number of fibres. Each fibre is characterised by a well-defined geometric position, an area and a tension-strain bond: the axial stresses are

integrated by the software along the section to evaluate the normal stress P, and the bending moments M2 and M3. As the number of fibres in which the section is discretised increases, it improves, as is known, the accuracy of the result, to the detriment, however, of the computational burden (time and memory used). In the present case, the decision to divide the section of the pile S into 200x5 fibres and the section of the pile L into 300x5 fibres (Figure 6.20) was considered a satisfactory compromise (Figure 6.20).

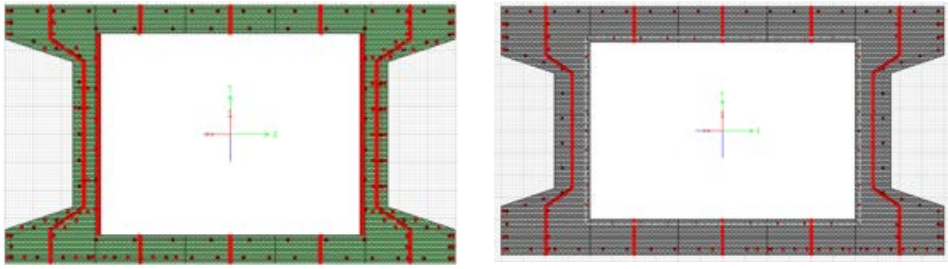

Figure 6.20: Fiber model of a plastic hinge of the Pier S (left) and Pier L (right).

The length of the plastic hinge was assumed to equal to 10% of the Ls shear capacity, following the suggestion of the circular (C8A.8.6.4) in the case of lack of more accurate analysis. In this case, as the shear capacity is precisely equal to the height of the cantilever-pier, a linear development equal to 10% of the height of the pier has been assumed for the plastic hinge. Figure 6.21 below shows the Moment-Rotation curves (at the middle section) as derived from non-linear static analyses conducted as described above.

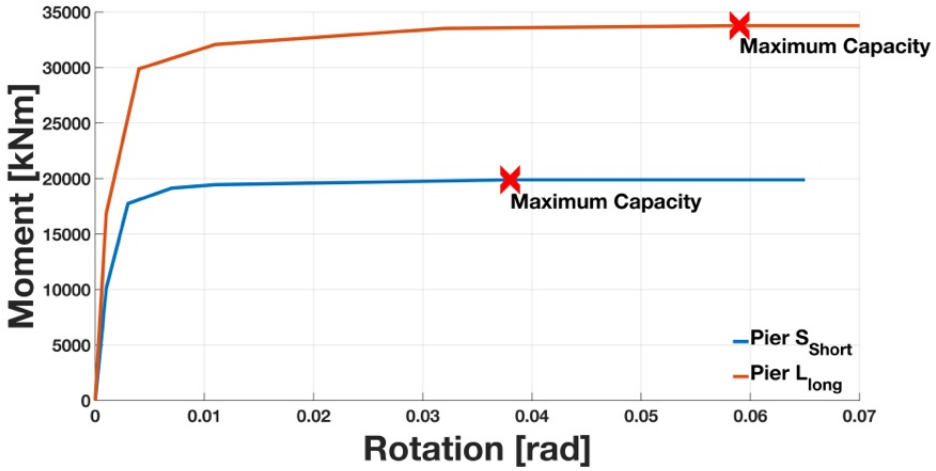

Figure 6.21: Moment – rotation relationship obtains from Push-over analysis.

The fibres discretisation of the plastic hinge in the P-M2-M3 model adopted for the push-over analysis allows showing, for each step of the analysis, the tension and strain demand for each fibre. Once the concrete fibre on the most compressed side was selected, it was possible to identify the step (Figure 6.22) that which corresponds to the drawing of the last condition of the section ($\varepsilon_c = \varepsilon_{cu} = 3.5$ ‰). Known the "last" step, on the moment-rotation curves of (Figure 6.24), the point corresponding to the press-flexion crisis of the section was identified. The same figure shows the values that assume the abscissas (last rotations) and the ordinates (last moments) of said points. The moment-rotation curves for the piers, truncated to the point corresponding to the last conditions, are shown in (Figure 6.24).

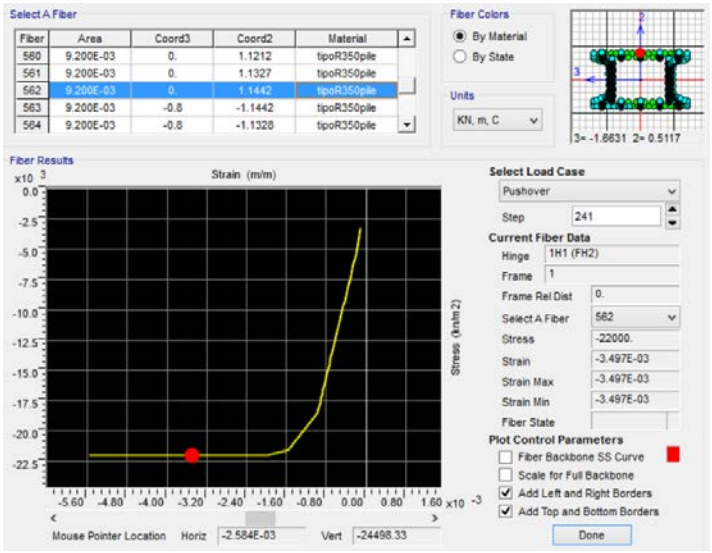

Figure 6.22: Identification of the failure point of the compressed top fiber of the concrete.

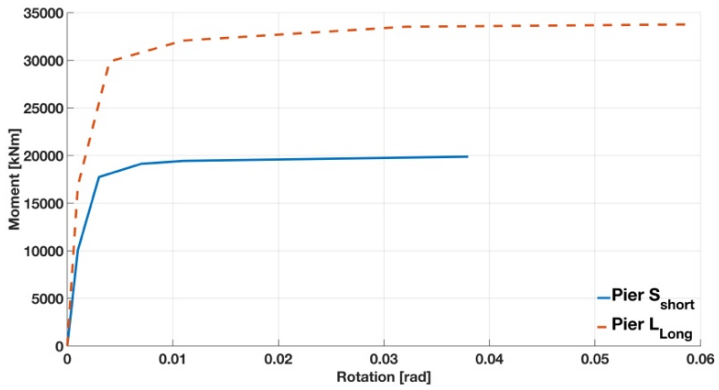

Figure 6.23: Moment-rotation curve blocked at the maximum capacity.

Finally, was determined the moment-rotation curves (Figure 6.24) The coordinates of these points are as follows (Table 6.7):

Table 6.7: Coordinates of the moment-rotation curve for the plastic hinge.

Pier S		Pier L	
R3 [rad]	**M3** [kNm]	**R3** [rad]	**M3** [kNm]
0.000	0	0.000	0
0.001	10063	0.001	16810
0.003	17744	0.004	29874
0.007	19132	0.011	32077
0.011	19440	0.032	33526
0.038	19881	0.059	33767

By assigning a ductility to the curvature bonds thus obtained, such as to achieve a curvature corresponding to the achievement of the ultimate deformation limit of the concrete or steel, the Multi-Linear Kinematic Plasticity, SAP2000 links have been characterised as shown below:

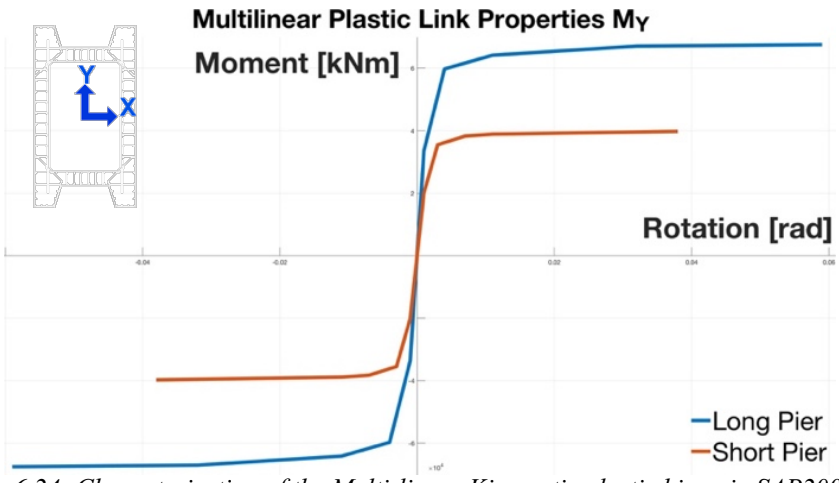

Figure 6.24: Characterization of the Multi-linear Kinematic plastic hinge in SAP2000.

The parameters of the links-element have been defined only for the rotation R3, the rotation around the axis three that in Figure 6.24 is equivalent to the axis in cyan. For other directions, the link-element prevents the corresponding degrees of freedom from being activated. For the R3 direction, the values of "effective stiffness" and "effective damping" were also defined (sufficiently high value to allow the simulation of a fixed constraint in the linear field - and 1%) to which the SAP2000 refers for linear analyses.

6.4 Modelling of the retrofit proposal

6.4.1 ROD

The model has the same configuration as the model presented in paragraph 6.4 except for the presence of an axially rigid element, called ROD-element in SAP2000, connecting the adjacent spans (Figure 6.25).

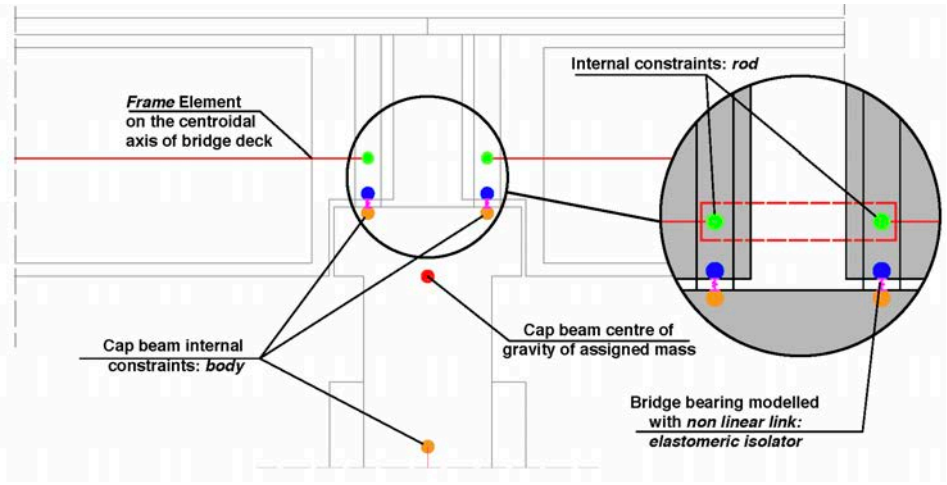

Figure 6.25: Modelling of the superstructure, span connected with longitudinal chains.

6.4.2 R=2,5 m and R=3,1 m

The model has the same configuration as the model presented in paragraph 6.4 except for the presence of supporting elements of the non-linear link type, which are representative of the friction isolator devices.

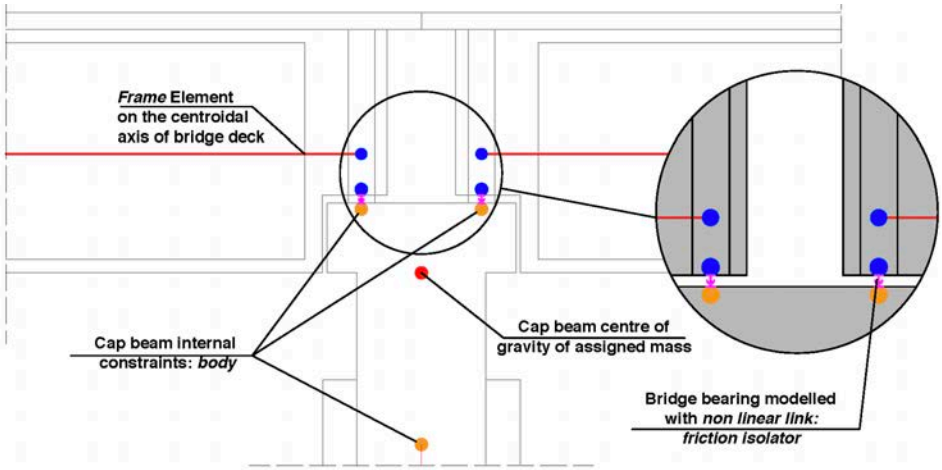

Figure 6.26: Modelling of the superstructure with FPS isolator device.

The model used to describe the behaviour of the bearings is the biaxial friction isolator, which allows to couple the friction properties for the two horizontal shear directions, characterised by post-slip stiffness in the shear directions due to the pendulum radius and gap behaviour in an axial direction. The first studies on sliding isolators were conducted by Zayas et al. 1987, which tested its performance. For the first time, Tsai et al. 1997 created a finite element model of the device, defining the friction force dependent on two parameters such as contact pressure and sliding speed. Recent studies conducted by Lomiento et al. 2011 considered the heating of the surface produced by the movement of the slider. Commercial finite element software, such as SAP2000, uses the contact pressure and the sliding velocity as characteristic parameters of the friction coefficient for the insulators to slip, leaving out the influence of the temperature variation. The study conducted by Lomieto et al. 2015 showed that the simplifications introduced by finite element software produce an underestimation of the peak displacements, of the peak forces and the peak base shear. This effect is more significant if the displacements of the slider are considered in the two directions and in the case in which earthquakes are considered in the two directions of the plane and vertical. In the study, considering that the objective is the analysis of the longitudinal behaviour of bridges consisting of simply supported decks, the errors that are committed to neglecting the effects of the increase in temperature on the sliding surface would be contained on average within a 5 %, except for particular seismic events characterized by a high energy content for high periods. Therefore, considering the objective of the thesis and the seismic demand considered for the study of fragility curves, this error is acceptable and allows the use of the SAP2000 software as finite element software for structural calculation, MATLAB and VISUAL BASIC as software for extrapolation from the data. For the analysis, two different values of the radius of curvature of 2.5 and 3.1 m were considered, as well as two different coefficients of friction of the sliding surface equal to 2% and 5%.

Table 6.8: Design State - Mechanical characteristics of FPS bearings with R=2,50m.

R (m)	K_{eff} (kN/mm)	K (kN/mm)	K_{axial} (kN/mm)
2.50	7189.35	3921.47	10105499

Table 6.9: Design State - Mechanical characteristics of FPS bearings with R=3,10m.

R (m)	K_{eff} (kN/mm)	K (kN/mm)	K_{axial} (kN/mm)
3.10	5123.21	3162.47	10105499

The FPS has been modelled with the Friction Isolator link (Computers and Structures Inc. 2016; Petti 2013) to better describe the characteristic of the device (radius of

curvature R, friction properties, axial stress F_{Rd}, axial stiffness K_{axial}, lateral stiffness K, effective stiffness K_{eff}). In Table 6.8 and in Table 6.9, are described the mechanical properties of the FPS isolator used in the model.

6.4.3 R ROD – Model

The model has the same configuration as the model presented in paragraph 6.4 with the exception of the presence of bearing elements of the non-linear link type friction isolator and the presence of an axially rigid element, called ROD-element in SAP2000, connecting the adjacent spans as shown in the figure.

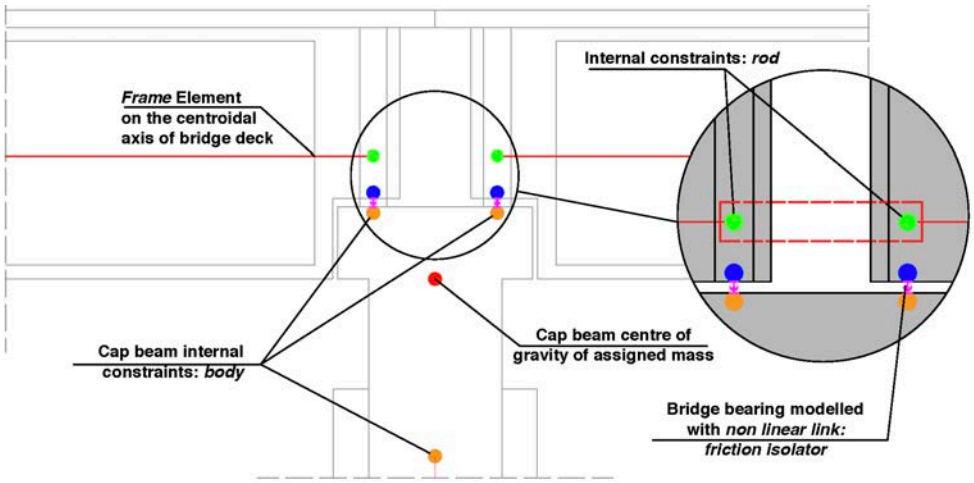

Figure 6.27: Modelling of the superstructure with FPS isolator device and span connected with longitudinal chains.

6.4.4 Modal Analysis

The bridge was modelled with the software SAP2000 as a plane finite element numerical model (FEM) for both the as-built and retrofitted configurations. In order to investigate the effectiveness of seismic isolation techniques chosen as retrofitting and previously illustrated, forty finite element models have been defined. The modal properties of bridges are a useful way to classify their general characteristics. Table 6.10, Table 6.11, Table 6.12 and Table 6.13 present the modal properties including period and frequency for all geometrical configurations (Figure 6.3) and in particular, for the not retrofitted model and for the retrofit option model R= 2.5m 2%, calculated for maximum displacements of 40 cm.

The SL model consists of three spans of 41.00 m length and two piers, one Pier L and the other Pier S (Figure 6.3). The table below shows the first three modal shapes for the not retrofitted model and the model with FPS isolators.

Table 6.10: Modal Periods and Frequencies Model SL.

Model	Modal Shape	Period	Frequency
Not Retrofitted	1	1.77	0.56
	2	1.23	0.80
	3	1.09	0.91
R=2,5 2%	1	3.04	0.33
	2	2.79	0.36
	3	2.71	0.37

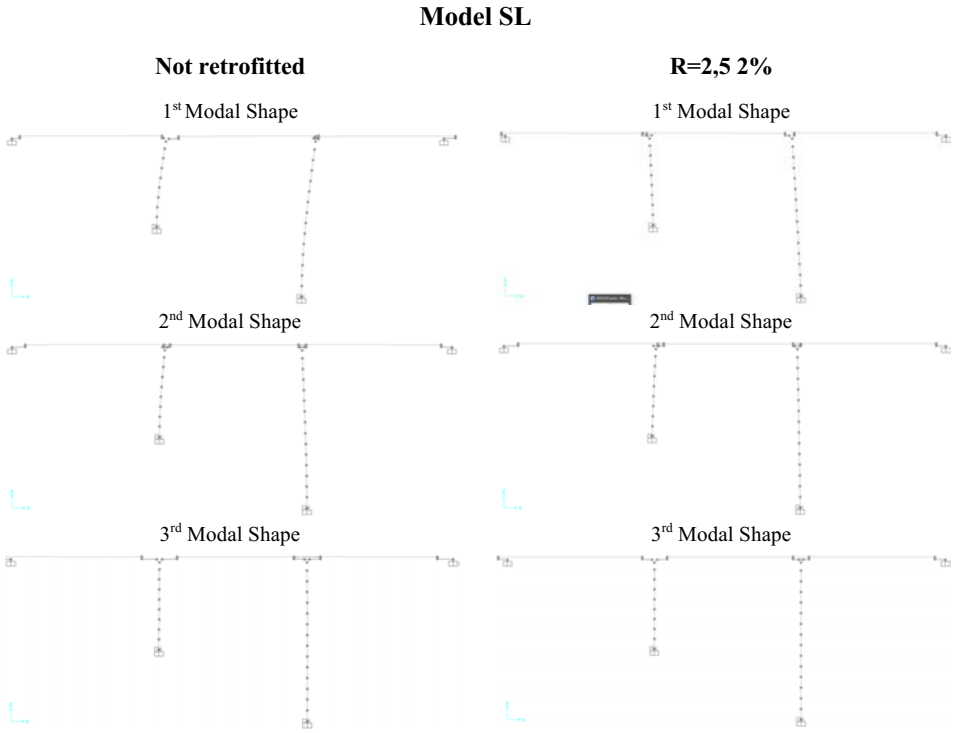

Figure 6.28: Modal Periods and Frequencies Model SL.

The SLS model consists of four spans of 41.00 m length and three piers, one Pier L and the other Piers S (Figure 6.3). The table below shows the first three modal shapes for the not retrofitted model and the model with FPS isolators.

Table 6.11: Modal Periods and Frequencies Model SLS.

Model	Modal Shape	Period	Frequency
Not Retrofitted	1	1.96	0.51
	2	1.37	0.73
	3	1.17	0.85
R=2,5 2%	1	2.87	0.35

	2	2.77	0.36
	3	2.74	0.36

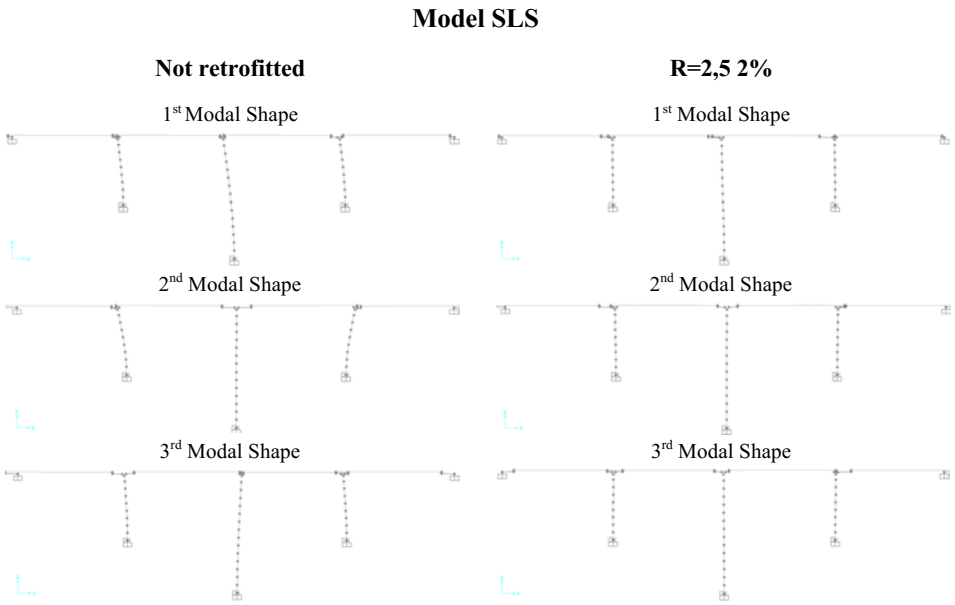

Figure 6.29: Modal Periods and Frequencies Model SLS

The SSLLS model consists of four spans of 41.00 m length and five piers, two Piers L and the others Pier S (Figure 6.3). The table below shows the first three modal shapes for the not retrofitted model and the model with FPS isolators.

Table 6.12: Modal Periods and Frequencies Model SSLLS.

Model	Modal Shape	Period	Frequency
Not Retrofitted	1	2.48	0.40
	2	1.72	0.57
	3	1.44	0.69
R=2,5 2%	1	2.87	0.35
	2	2.77	0.36
	3	2.74	0.36

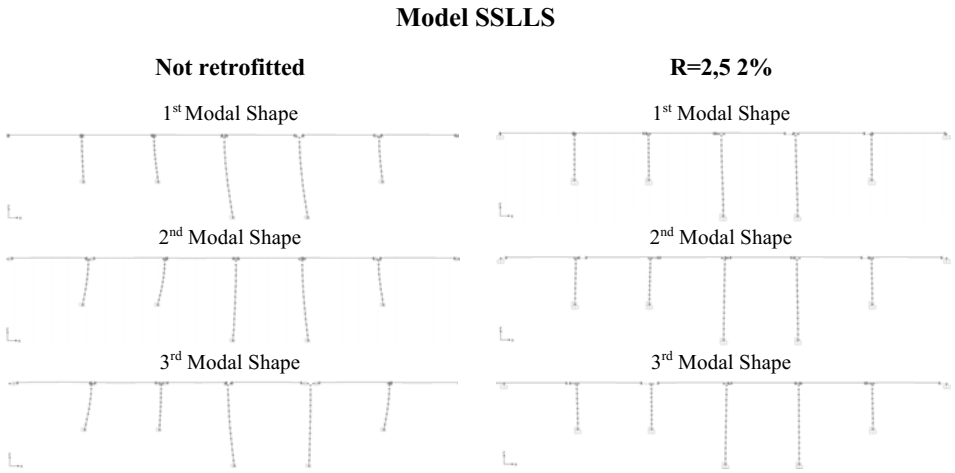

Figure 6.30: Modal Periods and Frequencies Model SSLLS

The SSLLLLSS model consists of four spans of 41.00 m length and eight piers, four Piers L and the other Piers S (Figure 6.3). The table below shows the first three modal shapes for the not retrofitted model and the model with FPS isolators.

Table 6.13: Modal Periods and Frequencies Model SSLLLLSS.

Model	Modal Shape	Period	Frequency
Not Retrofitted	1	2.57	0.39
	2	2.02	0.50
	3	1.69	0.59
R=2,5 2%	1	5.40	0.19
	2	4.55	0.22
	3	3.90	0.26

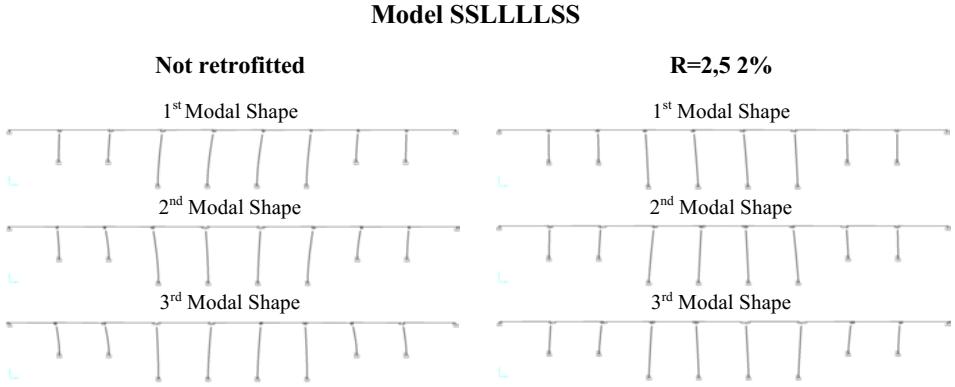

Figure 6.31: Modal Periods and Frequencies Model SSLLLLSS

6.5 Analytical Fragility Curves

The analytical fragility curves derive from the "observed" damage distribution and a large number of numerical simulations. Even if damage data are insufficient, the fragility curves can be generated using this technique. The analytical method is the most popular for developing seismic vulnerability curves because this approach has less bias. In this approach, we consider a suite of earthquakes representing a specific area, and through the help of the REXEL software (Iervolino et al. 2010), a group of spectra compatible accelerograms has been generated. Successively, the analysis of the non-linear response time history of all the samples is performed, and the maximum responses are recorded to construct models of probabilistic seismic demand (PSDM). The chosen approach is to develop the probabilistic analysis of the seismic demand of all components *EDP* by conducting a regression analysis of the maximum responses concerning intensity measure. The next step is the derivation, for each *EDP*, of the fragility curve corresponding to each damage state, and finally, the derivation of multi-damage state fragility curves, whit the MSA Method, previously described in the chapter 4.

The use of the multi-damage state approach allows a probabilistic characterisation of seismic risk for bridges. In this thesis it was decided to use this approach as the structural models to be used are not real but constructed in order to simulate bridges and viaducts built in Italy from the 60s onwards.

6.5.1 Description of bridge capacity

In the scientific literature, as illustrated in section 4.8, different methodologies are available for the quantification of the damage of the structural components of the different EDP global or local parameters, while the limit values are based, in most cases, on experimental results. The analytical estimate of the limit state thresholds is rarely proposed, while the component-specific analysis is necessary in this case, making the methodology dependent on the situation and simultaneously increasing the computational cost.

The analysis of the damage reported by the bridges during the recent earthquakes, discussed in chapter two, highlights the presence of structural deficiencies due to old design techniques. The main damages that are identified are the failure of the piers for shear and ductility mechanisms for the substructure, while the span pounding for the superstructures. Most studies on fragility analysis of bridges use column ductility as the primary damage measure. Park and Ang 1985 suggested a damage index based on energy dissipation, and Hwang et al. 2000, used the capacity/demand ratio of the

bridge piers to develop fragility curves. In this study, damage states are defined for piers ductility demand, piers shear demand and span pounding.

The discrete conditions of damage were defined based on the response of the structures obtained from the performed nonlinear static analyses. Nonlinear static analyses were conducted bridge piers, paragraph 6.4.5. Based on the obtained results, the comparison between the maximum (δ_{max}) and ultimate (δ_u) deformation or stress were used to define the model of damage.

$$DI = \delta_{max} \geq \delta_u \qquad 6\text{-}1$$

Recent studies on bridge infrastructures in Italy (Cardone et al. 2011, Borzi et al. 2014), consider two limit damage state (DS) or performance levels: Limit State Damage (LSG) and Limit State Collapse (LSC). The damage state LSG defines the condition of limited structural damages in which it would be careful to implement structural repairs. The damage state LSC describes the condition in which the bridge is severely damaged, and it is near to collapse. This implies that significant degradation has occurred in the stiffness and strength of the piers, and large displacements occur which might cause span pounding. Given that the objective of the study is to evaluate the seismic vulnerability of the entire bridge system, it will be considered only the LSC damage index.

Table 6.14: Definition of Limit States.

Damage State	Failure mechanism	Description	
Collapse (LSC)	Pier flexural capacity	Pier chord rotation exceeds pier chord rotation at collapse	$\theta \geq \theta_u$
	Pier shear capacity	Pier shear force exceeds pier shear resistance	$V \geq V_r(\theta)$
	Span pounding	Impact between adjacent spans	$\delta \geq \delta_u$
	Unseating of the deck	Deck displacement in the longitudinal direction is greater than the seat length	

6.5.2 Assessment of the Limit States thresholds

The capacity model is needed to measure the damage of structural components and the entire system, and it is described here concerning damage index (DI) as a function of the EDP. Damage models are formulated by experimental analyses where the observed damage and measured capacity are related to the applied demand level. Damage states (DS) are identified by the associated limit values (LS) of the DI

adopted for the various damage stages. Note that some uncertainties could be introduced into the capacity model and contribute to the overall structural fragility.

The values of resistant shear shown in Table 6.15 have been derived by using the Priestley formulation (Priestley 1996). The rotations Table 6.16 show the limit has been set by using the criteria set out in section 8 of the Italian NTC 2008 (Ministero delle Infrastutture e dei Trasporti 2008).

Table 6.15: Resisting shear V_R according to the Priestley formulation.

V_R [kN]									
	SLC			SLV			SLD		
Piers	**Not retrofitted**	**R=2.5 m**	**R=3.1 m**	**Not retrofitted**	**R=2.5 m**	**R=3.1 m**	**Not retrofitted**	**R=2.5 m**	**R=3.1 m**
S	1256	1270	1271	1289	1299	1308	1364	1364	1364
L	1397	1419	1421	1449	1465	1479	1568	1568	1568

Table 6.16: Base Plastic hinge limit rotations according to NTC 2008.

Piers	**ϑSLD (rad)**	**ϑSLV (rad)**	**ϑSLC (rad)**
S (short)	0.0068	0.0053	0.0071
L (long)	0.0148	0.0159	0.0212

For the geometry of the reference bridge used for the analyses and the retrofit techniques proposed, the span pounding is a dominant phenomenon of collapse compared to the unseating of the deck. From the original drawings, it has been found that the length between the two spans is equal to about 60 cm, it is considered the maximum allowable displacement before hammering for each span is equal to 30cm.

These types of damage were chosen because they represent the most common types of collapse observed on bridges following seismic events as described previously in chapters 2.

6.5.3 Seismic Demand

The MSA approach is used in combination with the Conditional Spectrum to select earthquakes that represent a specific site and IM level (Bradley 2010, Iervolino et al. 2010, Lin et al. 2013). According to the Italian Technical Regulations for Construction (Ministero delle Infrastutture e dei Trasporti 2008), the seismic actions that have to be considered for design purposes are defined from the "seismic hazard" of the construction site. The seismic actions are used to evaluate the structural performance compared to the considered limit states Figure 6.33.

The construction site chosen for the analysis is located in Campania Region (Italy) and situated at the following geographical coordinates: Longitude 14.975 - Latitude 41.0264 (Figure 6.32).

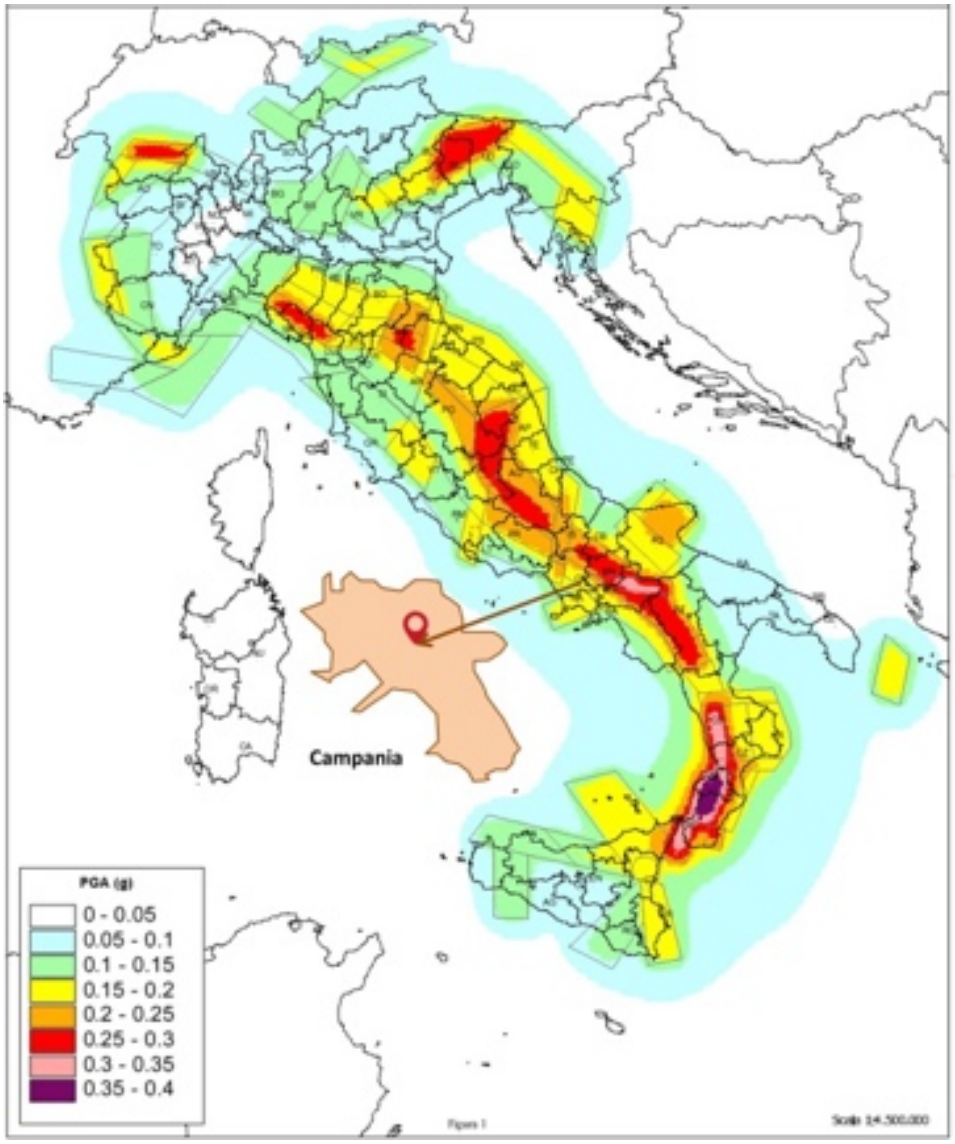

Figure 6.32: Positioning of the bridge.

T_r	$A_g\ (g)$	F_a	T_c^*
30	*0.060*	*2.355*	*0.279*
50	*0.080*	*2.307*	*0.296*
72	*0.096*	*2.297*	*0.317*
101	*0.114*	*2.312*	*0.327*
140	*0.133*	*2.319*	*0.335*
201	*0.158*	*2.327*	*0.345*
475	*0.228*	*2.421*	*0.366*
975	*0.302*	*2.503*	*0.383*
2475	*0.146*	*2.503*	*0.417*

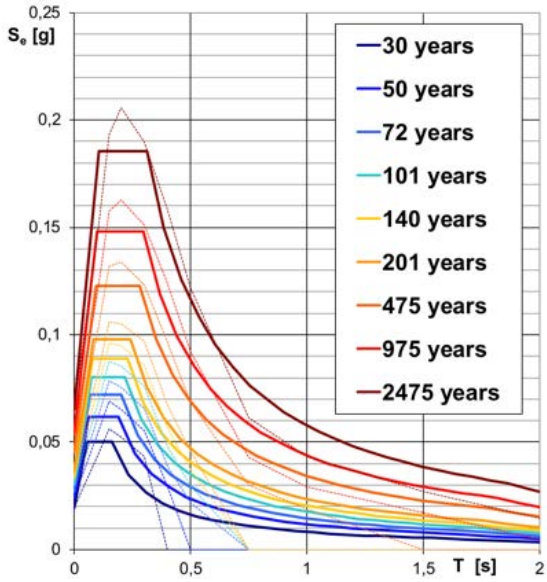

Figure 6.33: Basic seismic hazard parameters (Left) and elastic response spectra for different reference return period and location (Right).

In particular, 21 earthquakes have been selected through the software REXEL (Iervolino et al. 2009), which allowed to obtain combinations of accelerograms compatible with the design spectrum given by the Italian regulation in the appropriate interval of vibration periods. Figure 6.34, Figure 6.36 and Figure 6.38 describes a summary of the number of the considered earthquake records and the Elastic Demand Spectra for the Damage Limit State SLD, for the Life-saving Limit State SLV and the Collapse Limit State SLC. Moreover, the considered seismic events were scaled by changing the PGA in the range 0.0-1.0g with a step of 0.1g to implement the MSA analysis.

Table 6.17: Numbers of events for Limit States for a bridge of class III and V_n=50 years

Nominal Life V_n (years)	**50**
Use Class	III
SLC (events)	7
SLD (events)	7
SLV (events)	7

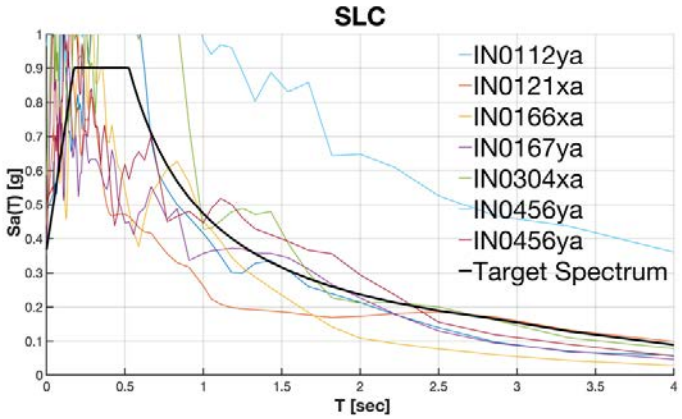

Figure 6.34: Elastic demand spectra for SLC, for a bridge of class III and Vn=50 years.

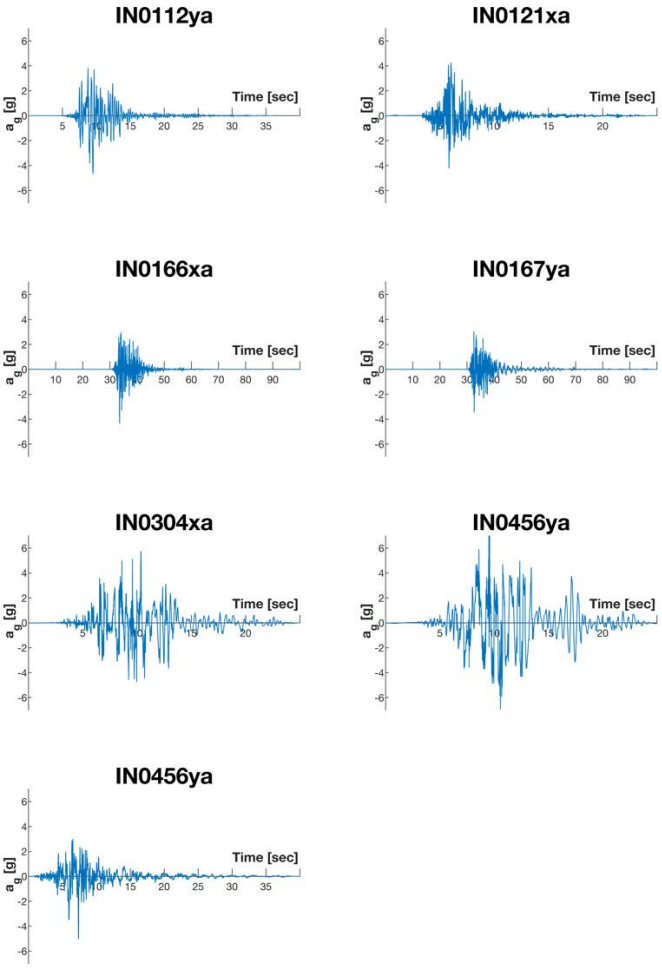

Figure 6.35: Accelerogram of the seismic events SLC.

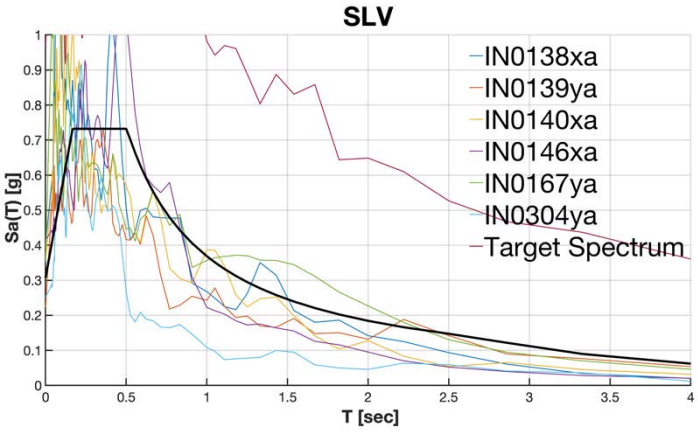

Figure 6.36: Elastic demand spectra for SLV, for a bridge of class III and Vn=50 years.

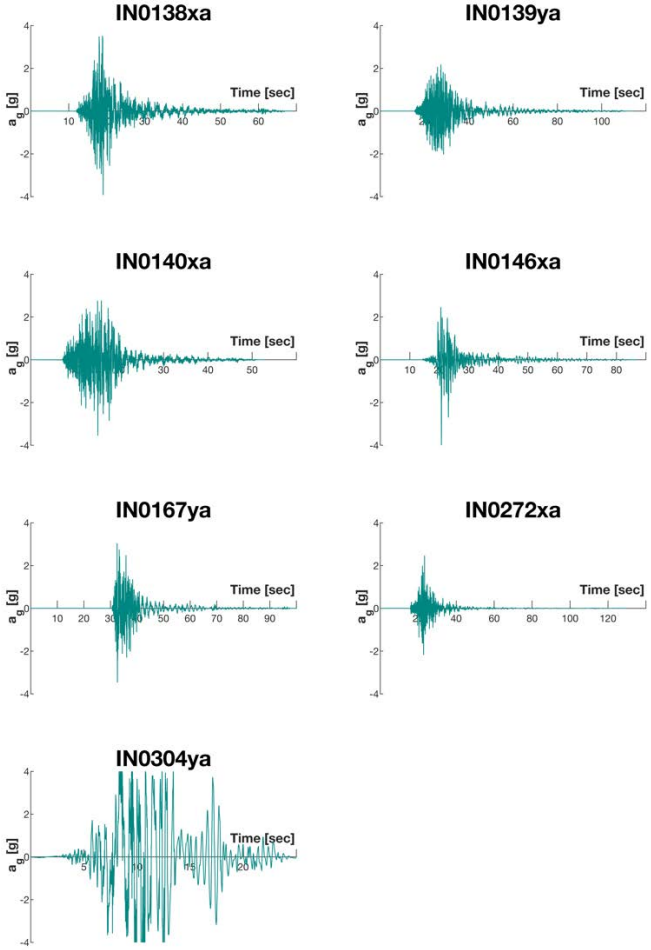

Figure 6.37: Accelerogram of the seismic events SLV.

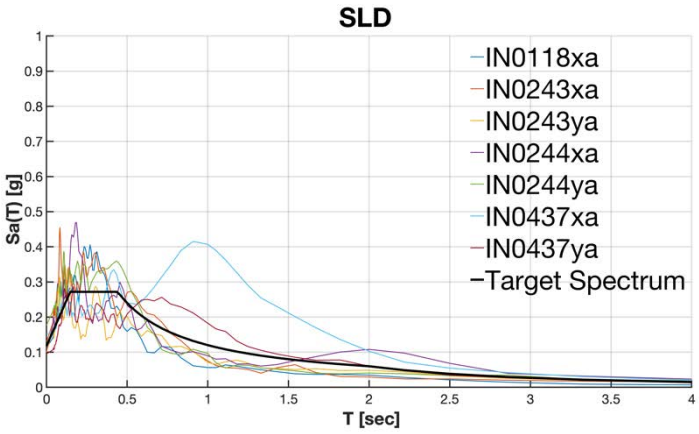

Figure 6.38: Elastic demand spectra for SLD, for a bridge of class III and Vn=50 years.

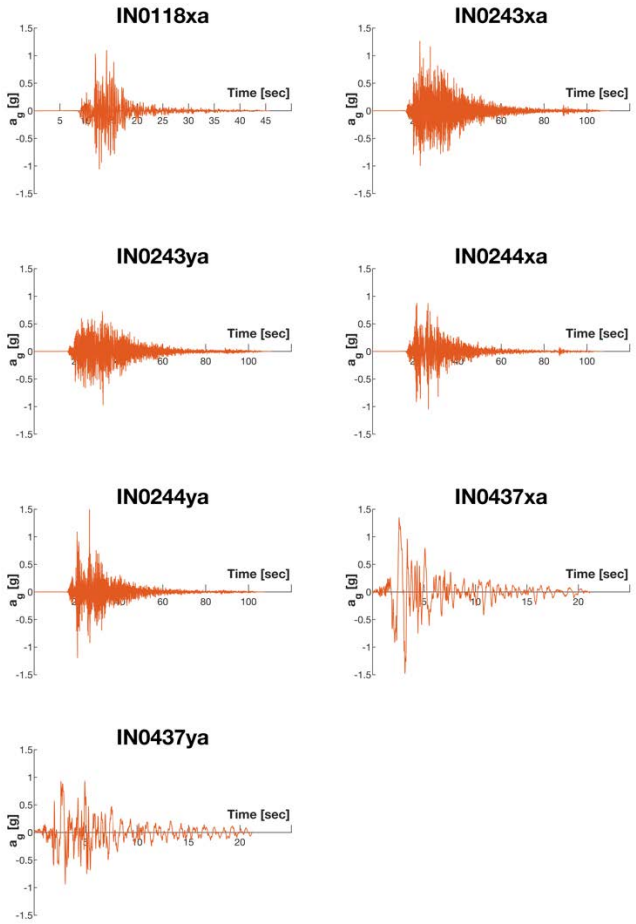

Figure 6.39: Accelerogram of the seismic events SLD.

6.5.4 Non-linear time history analysis

A set of incremental time history analyses has been performed by applying the accelerograms defined in paragraphs 6.6.3 to the FEM structural model. In order to take into account both the variability due to different ground motions (70 scaled accelerograms) and the variability of mechanical parameters in the structural model, it is necessary a very large number of analyses. Moreover, the considered seismic events were scaled by changing the PGA in the range 0.0-1.0g with a step of 0.1g. To reduce the calculation costs, calculation codes (Appendix A) have been implemented that have allowed more software to be linked to each other to export the almost 20000 results of the FEM analyses.

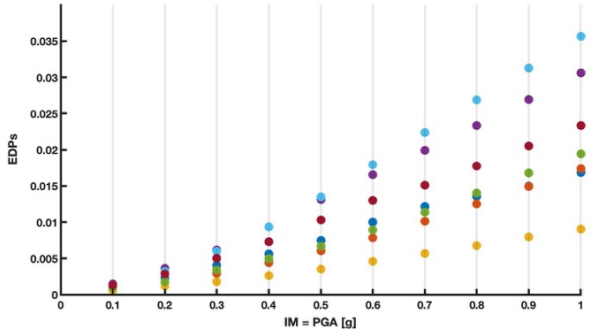

Figure 6.40: Example of the graphic correlation between the EDP and IM.

Furthermore, some of the results of the nonlinear dynamic analyse done for the SSLLS configuration for the not retrofitted (Shear stress for the piers Figure 6.41, Max displacement of the cap beam Figure 6.42, Hysteretic cycle of the Plastic Hinge at the base of the piers Figure 6.43 and Hysteretic cycle of the Elastomeric Bearings Figure 6.44) and the retrofit option R = 2.5 2% (Shear stress for the piers Figure 6.45, Max displacement of the cap beam Figure 6.46, Hysteretic cycle of the Plastic Hinge at the base of the piers Figure 6.47 and Hysteretic cycle of FPS isolator Figure 6.48) models are reported.

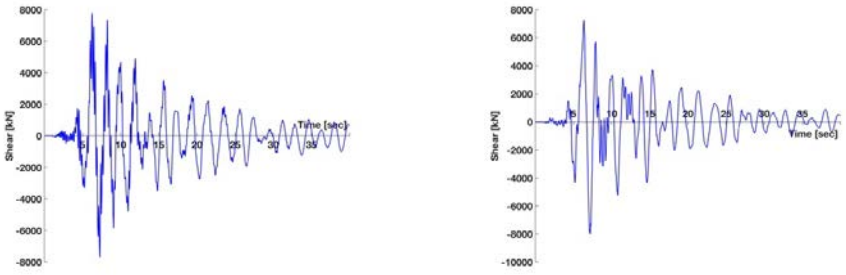

Figure 6.41: Time history of the shear Pier L (Left) and Pier S (Rigth).

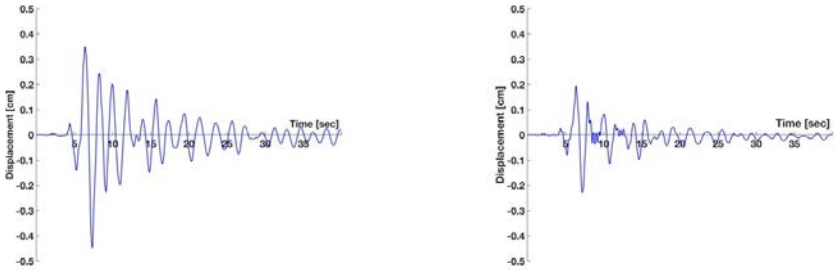

Figure 6.42: Time history of the displacement for the cap beam of the Pier L (Left) and Pier S (Rigth).

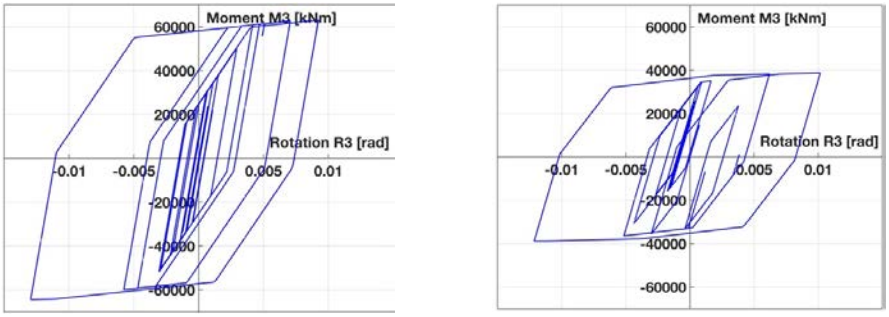

Figure 6.43: Plastic Hinge of the Pier L (Left) and Pier S (Rigth).

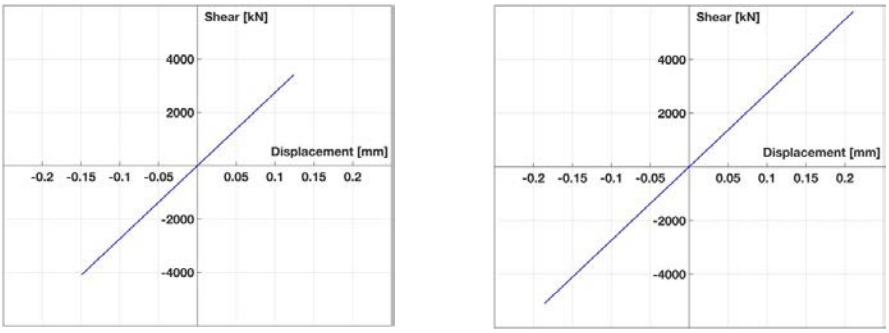

Figure 6.44: Hysteretic cycle of the Elastomeric bearings of the Pier L(Left) and Pier S(Rigth).

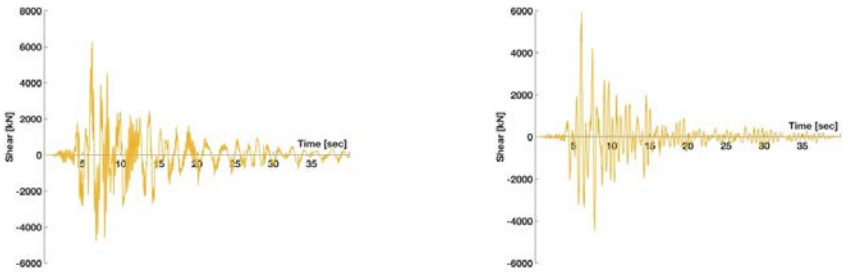

Figure 6.45: Time history of the shear Pier L (Left) and Pier S (Rigth).

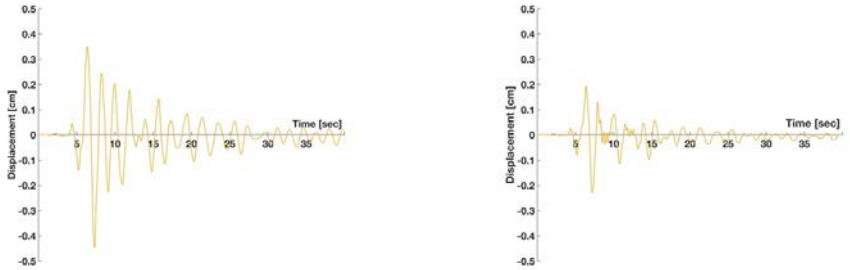

Figure 6.46: Time history of the displacement for the cap beam of the Pier L (Left) and Pier S (Rigth).

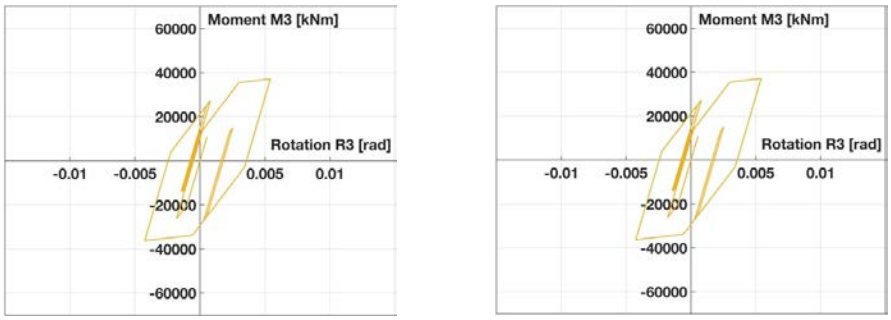

Figure 6.47: Plastic Hinge of the Pier L (Left) and Pier S (Rigth).

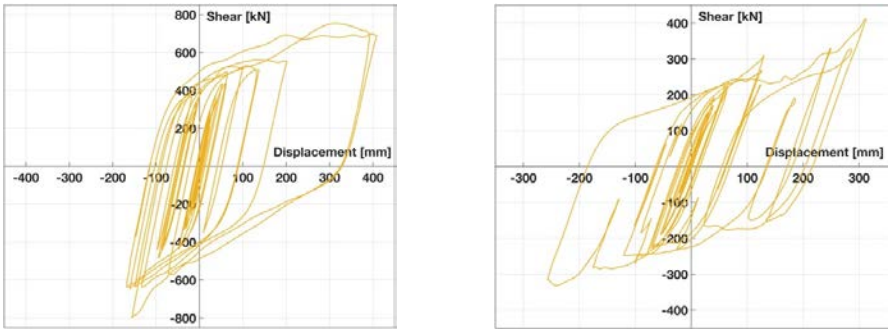

Figure 6.48: Hysteretic cycle of the FPS Isolator of the Pier L(Left) and Pier S(Rigth).

6.5.5 Component fragility curves

The figures below show the fragility curves for the various structural components, shear and rotation at the base of the piers and the span pounding EPDs, divided by the different geometric configurations.

6.5.5.1 Piers rotation

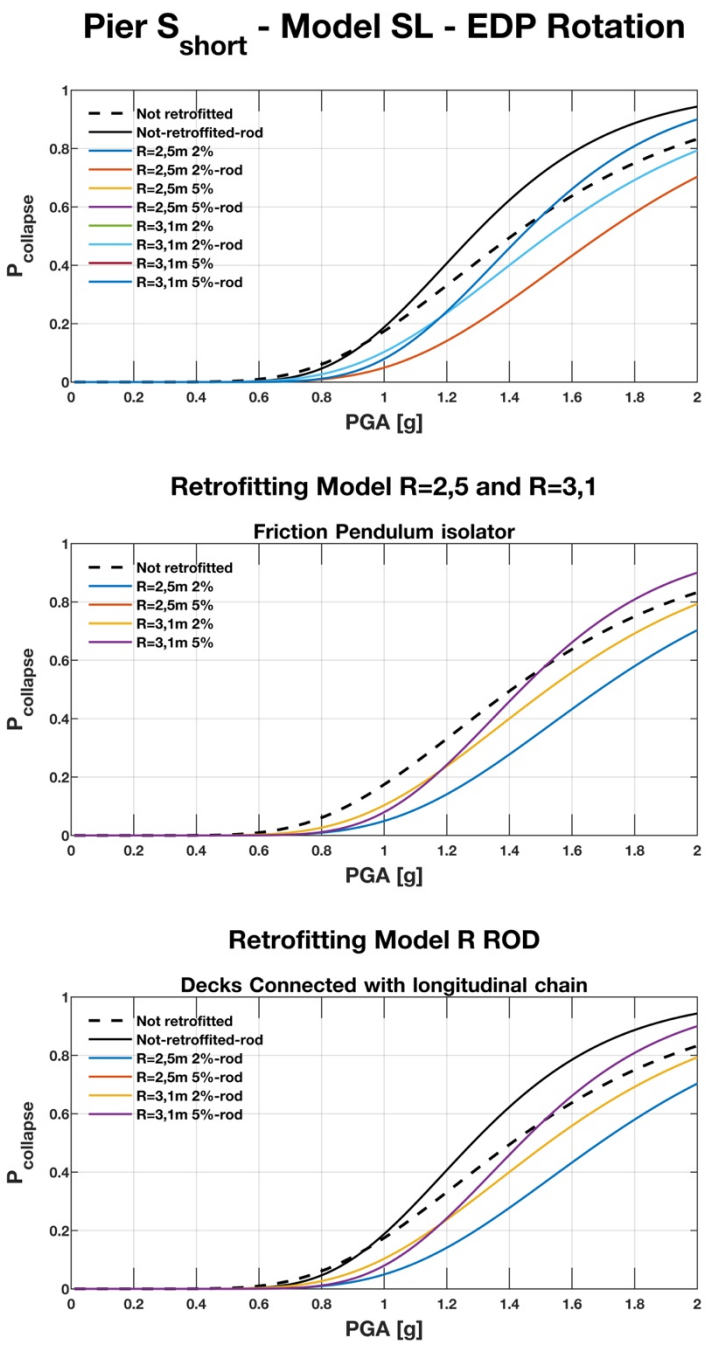

Figure 6.49: Fragility Curves Short Pier – Model SL – EDP Rotation.

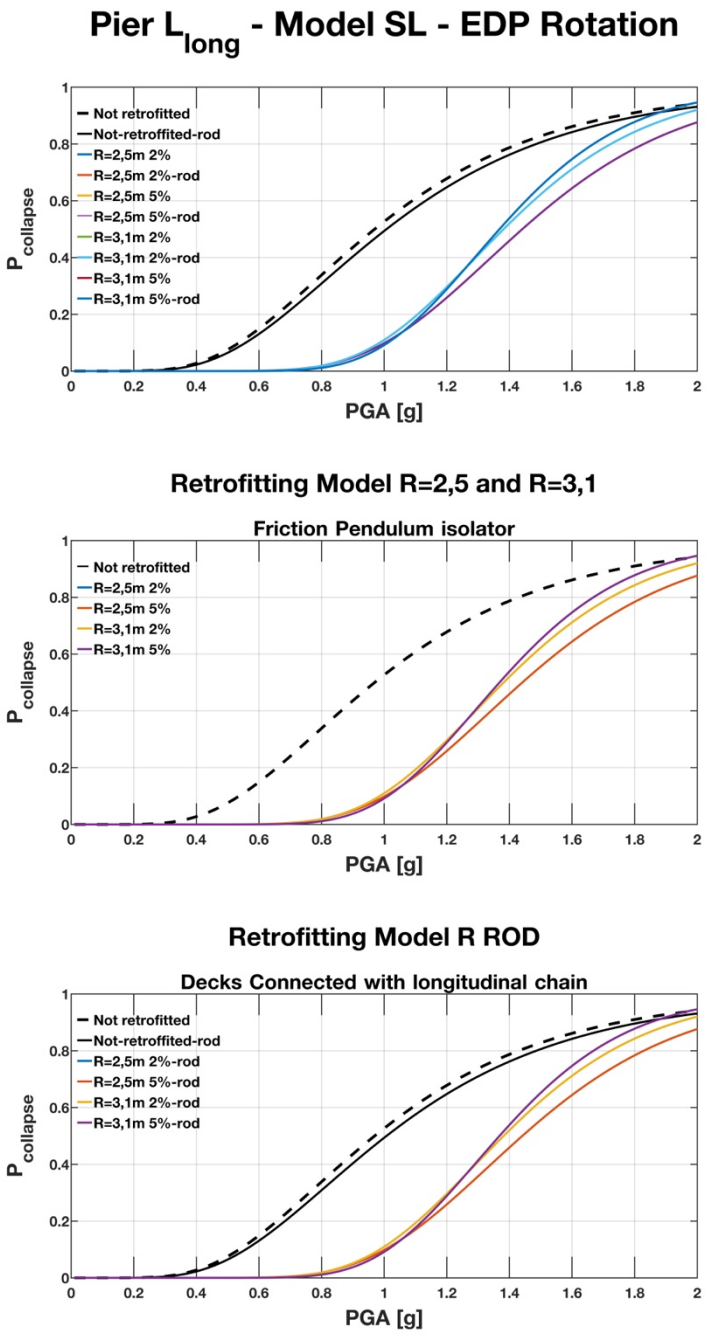

Figure 6.50: Fragility Curves Long Pier – Model SL – EDP Rotation.

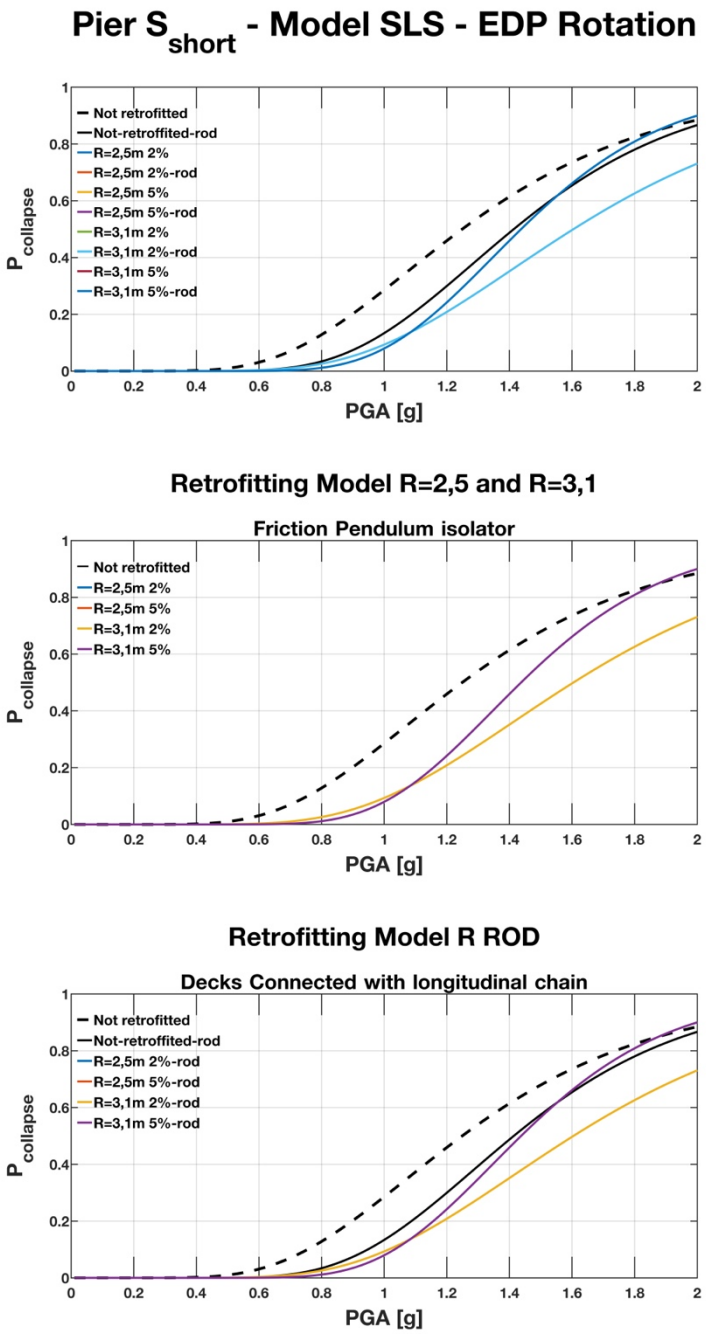

Figure 6.51: Fragility Curves Short Pier – Model SLS – EDP Rotation.

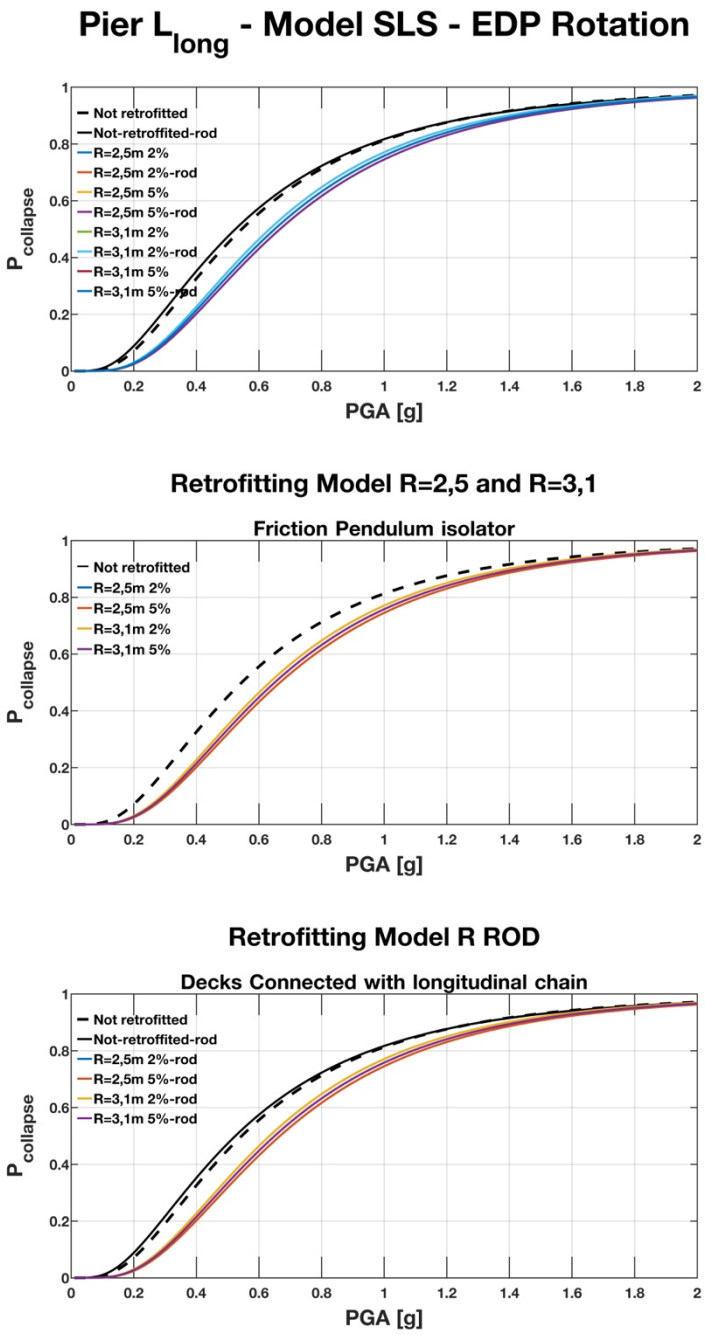

Figure 6.52: Fragility Curves Long Pier – Model SLS – EDP Rotation.

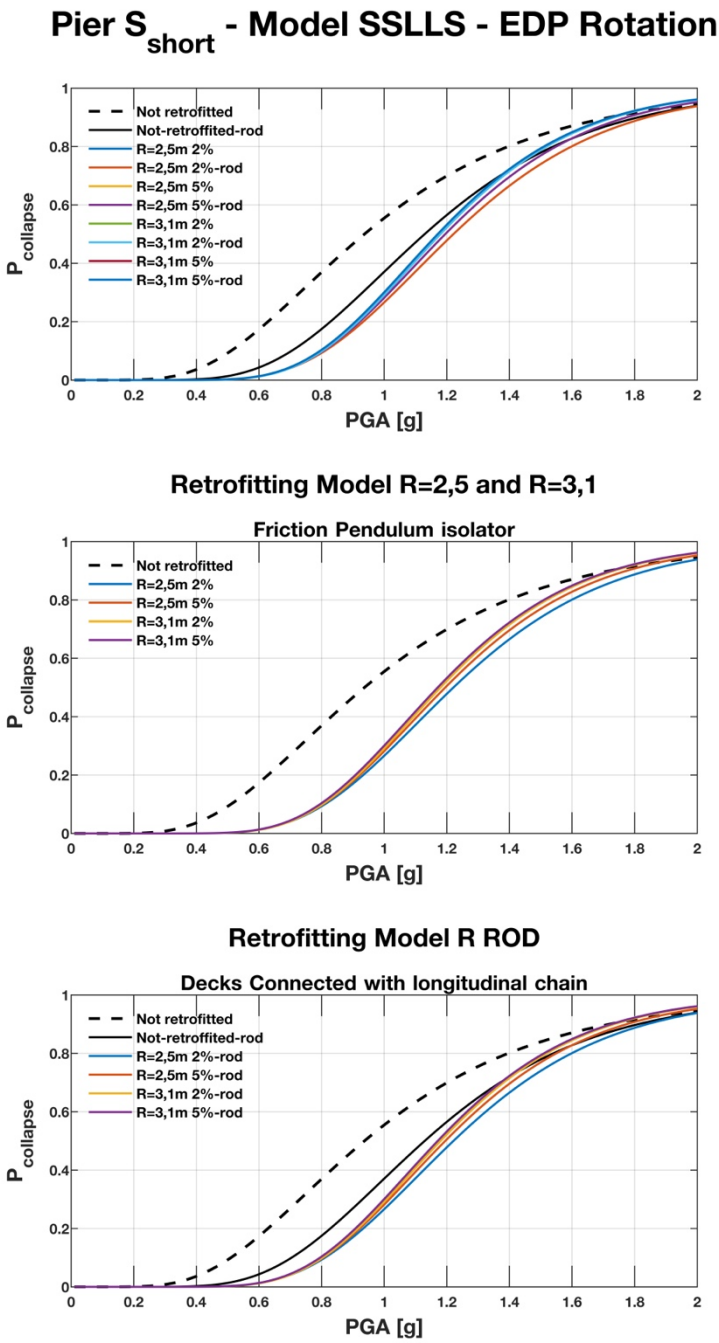

Figure 6.53: Fragility Curves Short Pier – Model SSLLS – EDP Rotation.

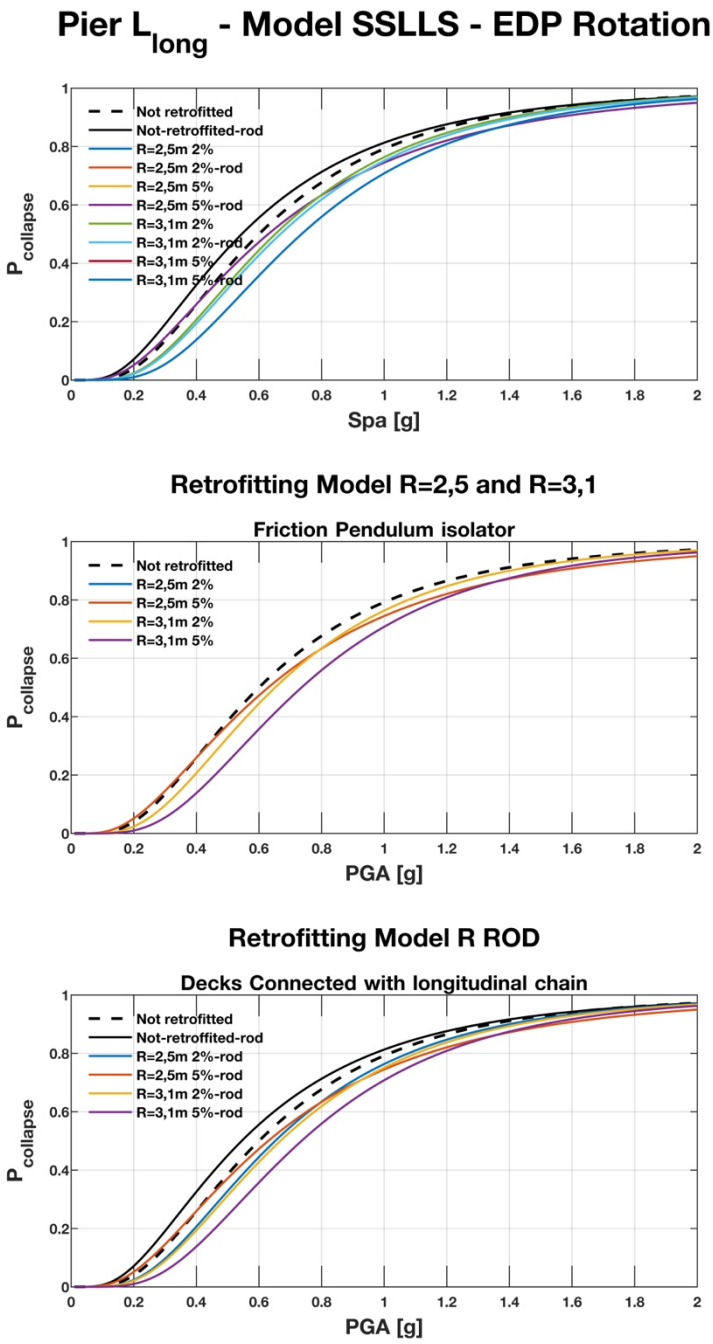

Figure 6.54: Fragility Curves Long Pier – Model SSLLS – EDP Rotation.

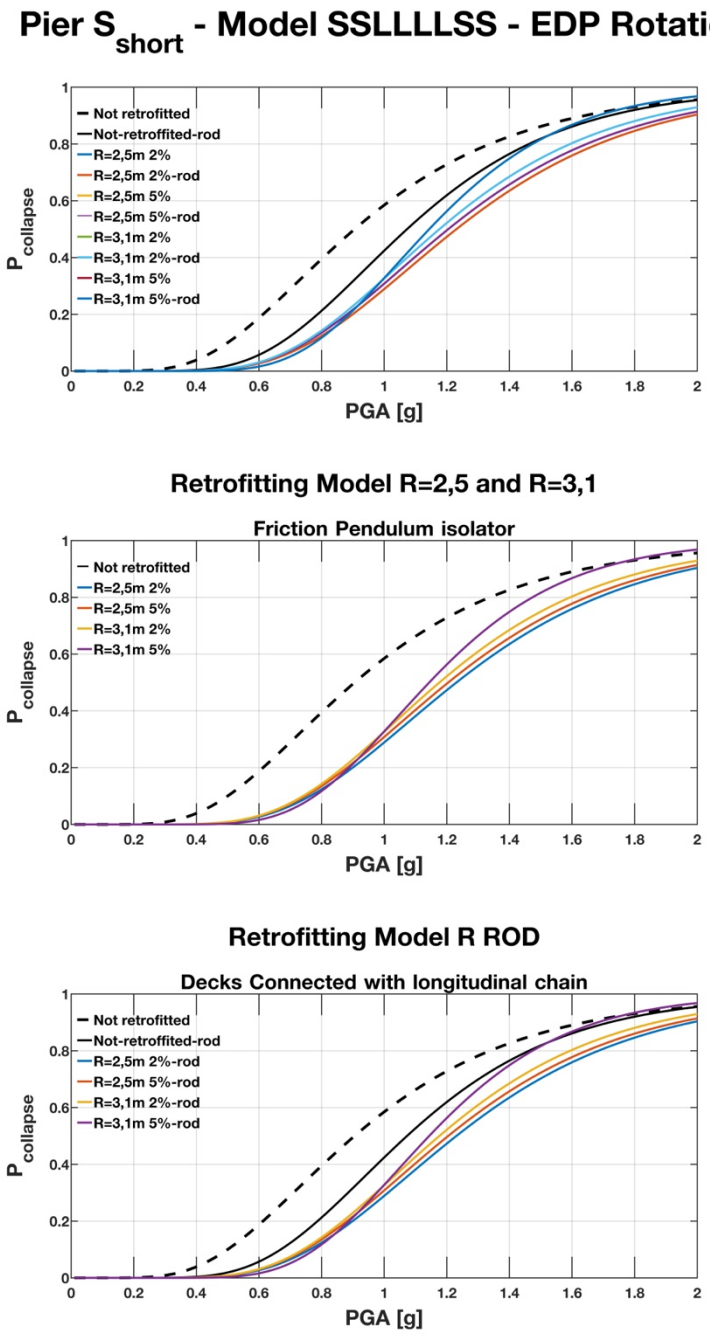

Figure 6.55: Fragility Curves Short Pier – Model SSLLLLSS – EDP Rotation.

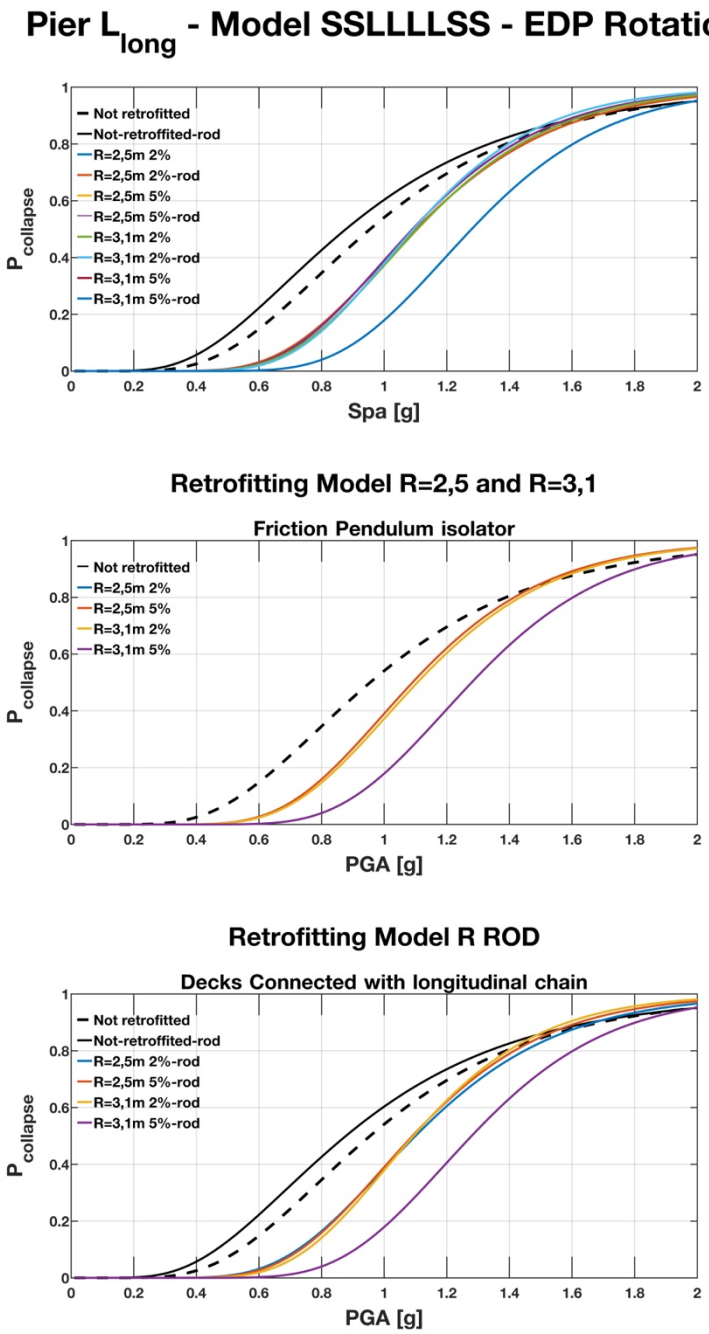

Figure 6.56: Fragility Curves Long Pier – Model SSLLLLSS – EDP Rotation.

6.5.5.2 Piers shear

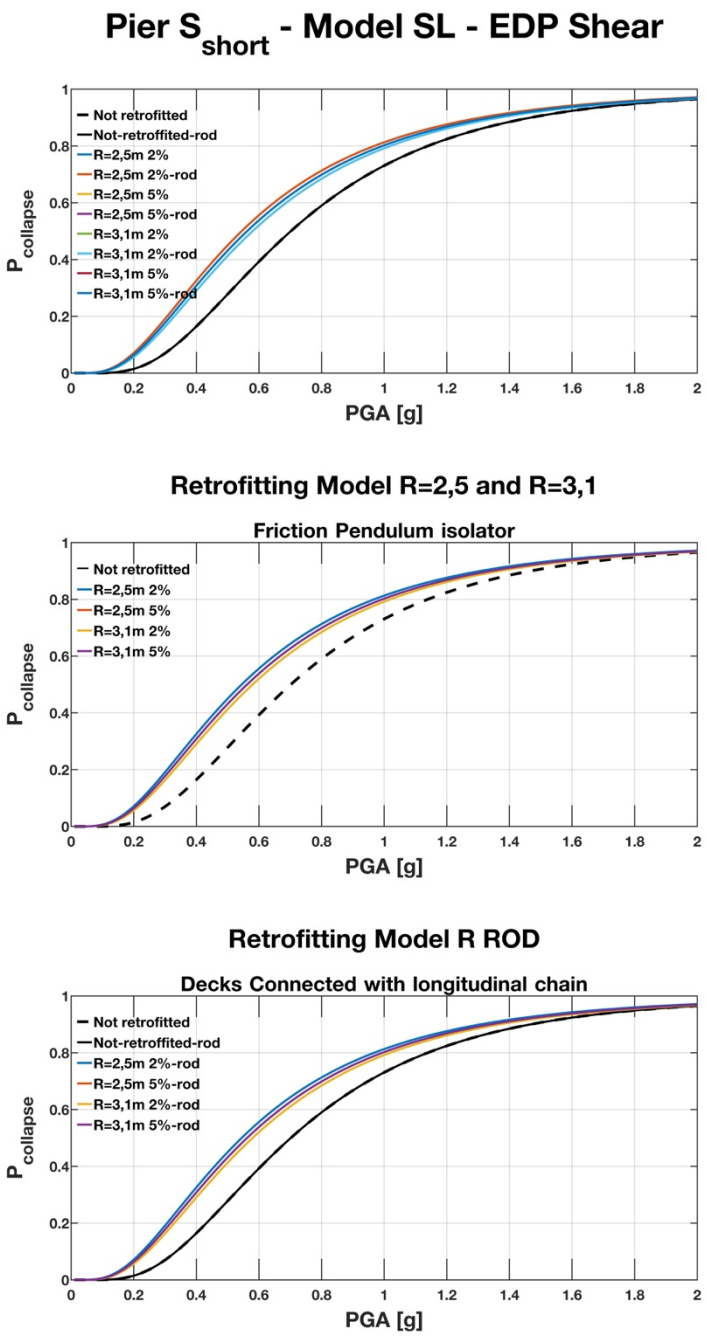

Figure 6.57: Fragility Curves Short Pier – Model SL – EDP Shear.

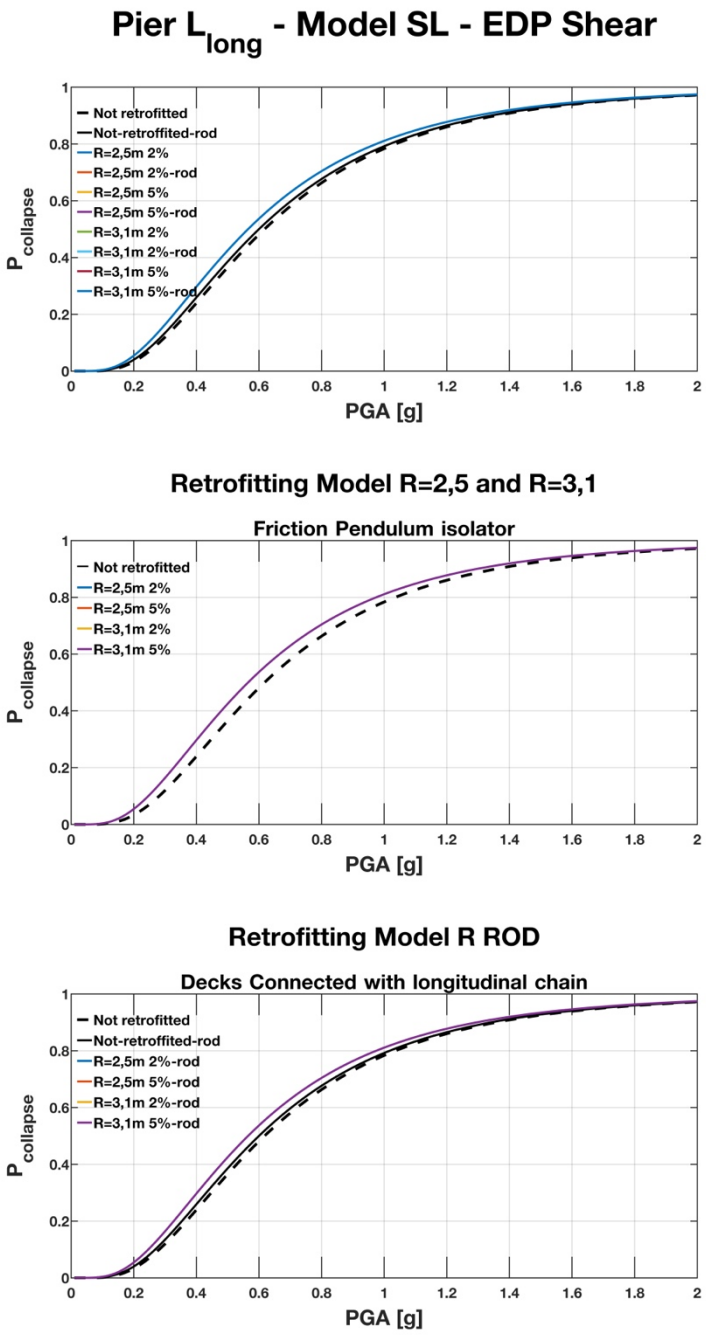

Figure 6.58: Fragility Curves Long Pier – Model SL – EDP Shear.

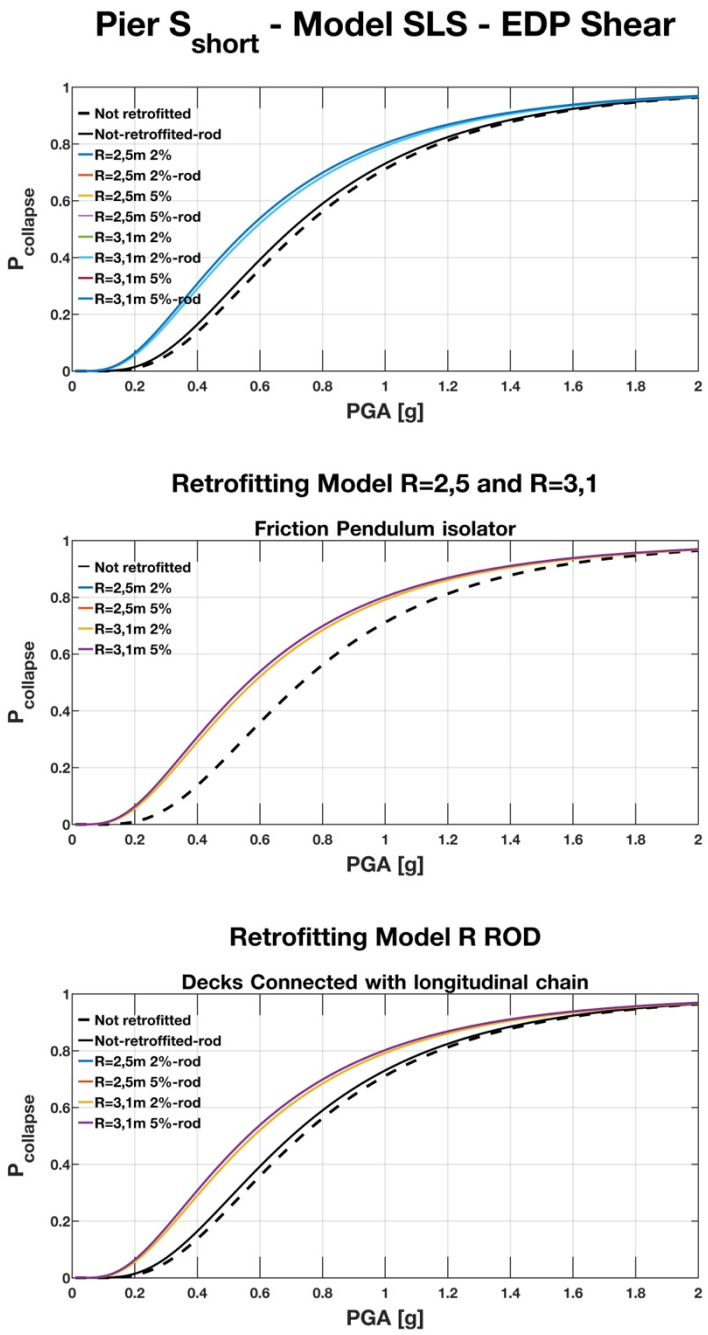

Figure 6.59: Fragility Curves Short Pier – Model SLS – EDP Shear.

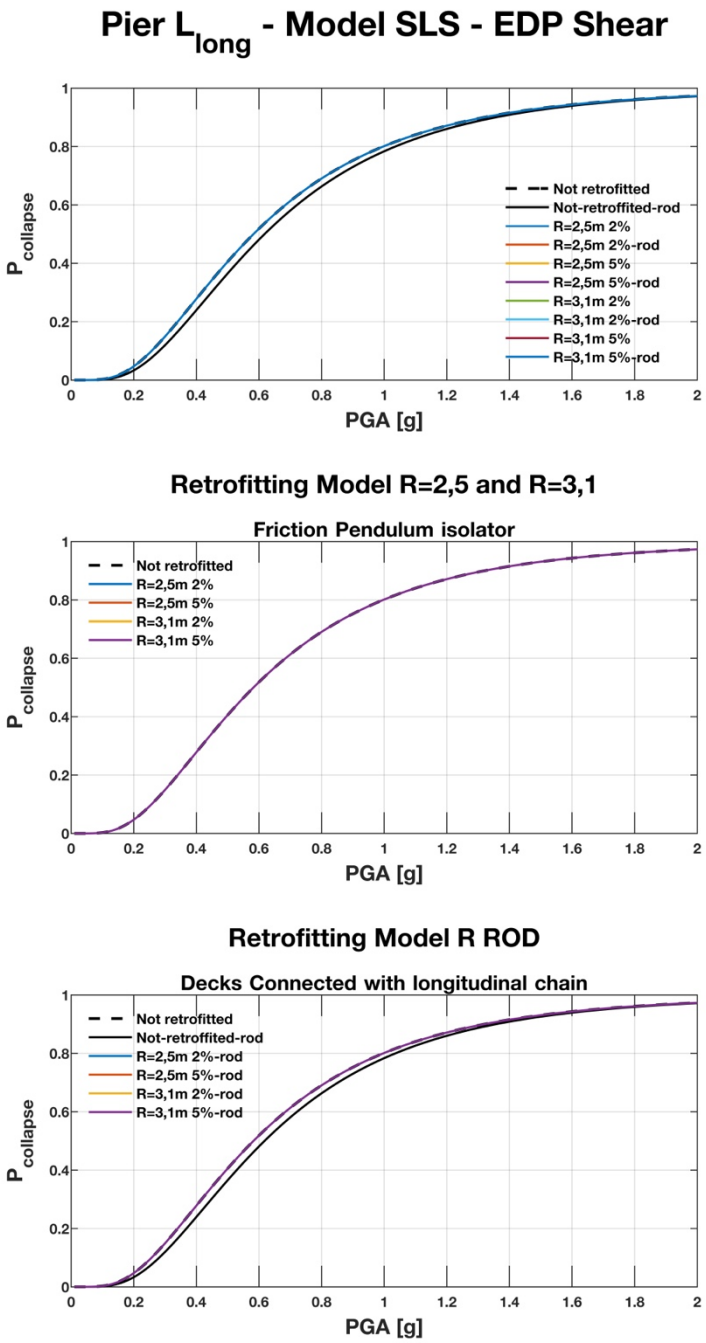

Figure 6.60: Fragility Curves Long Pier – Model SLS – EDP Shear.

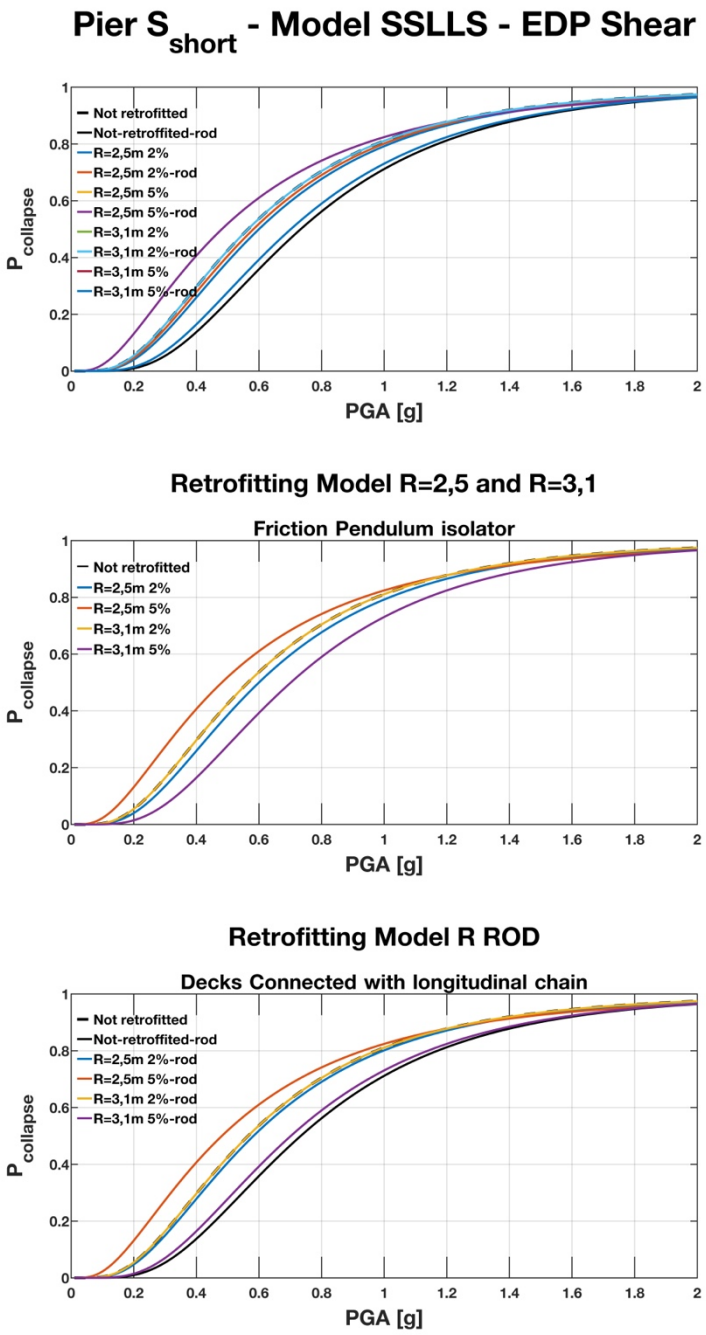

Figure 6.61: Fragility Curves Short Pier – Model SSLLS – EDP Shear.

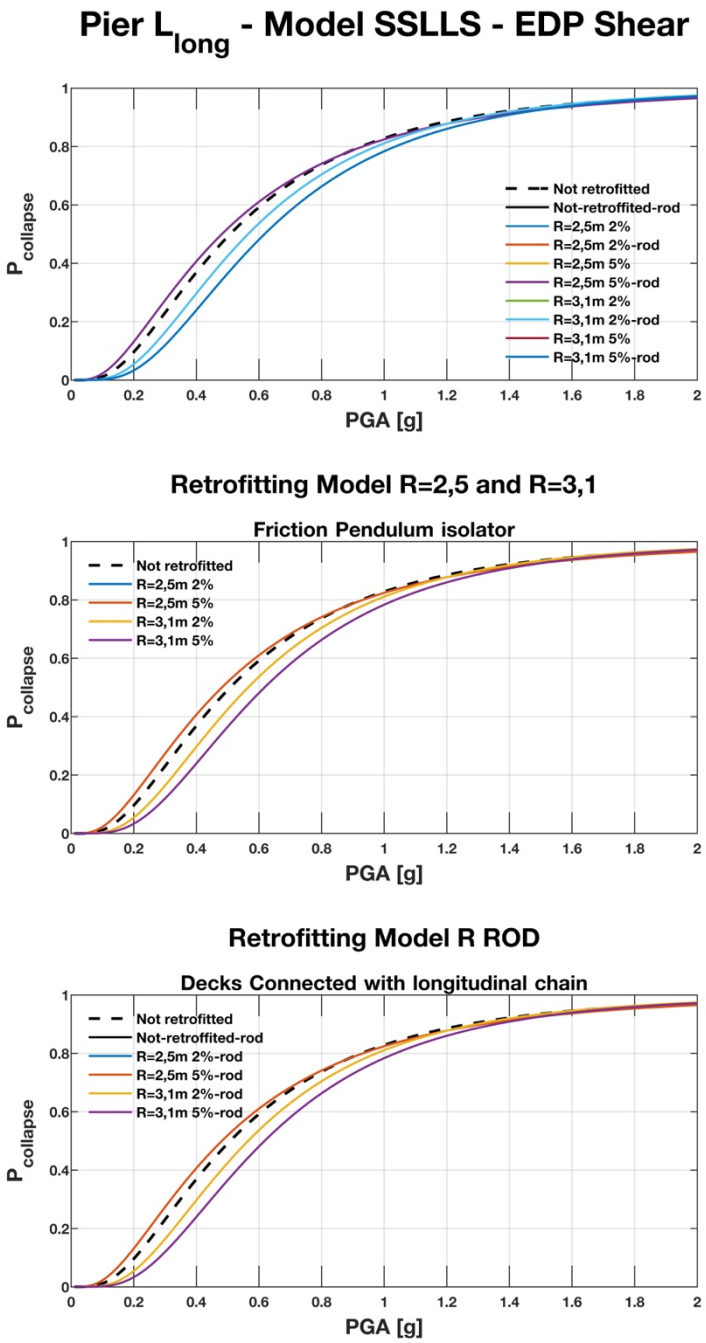

Figure 6.62: Fragility Curves Long Pier – Model SSLLS – EDP Shear.

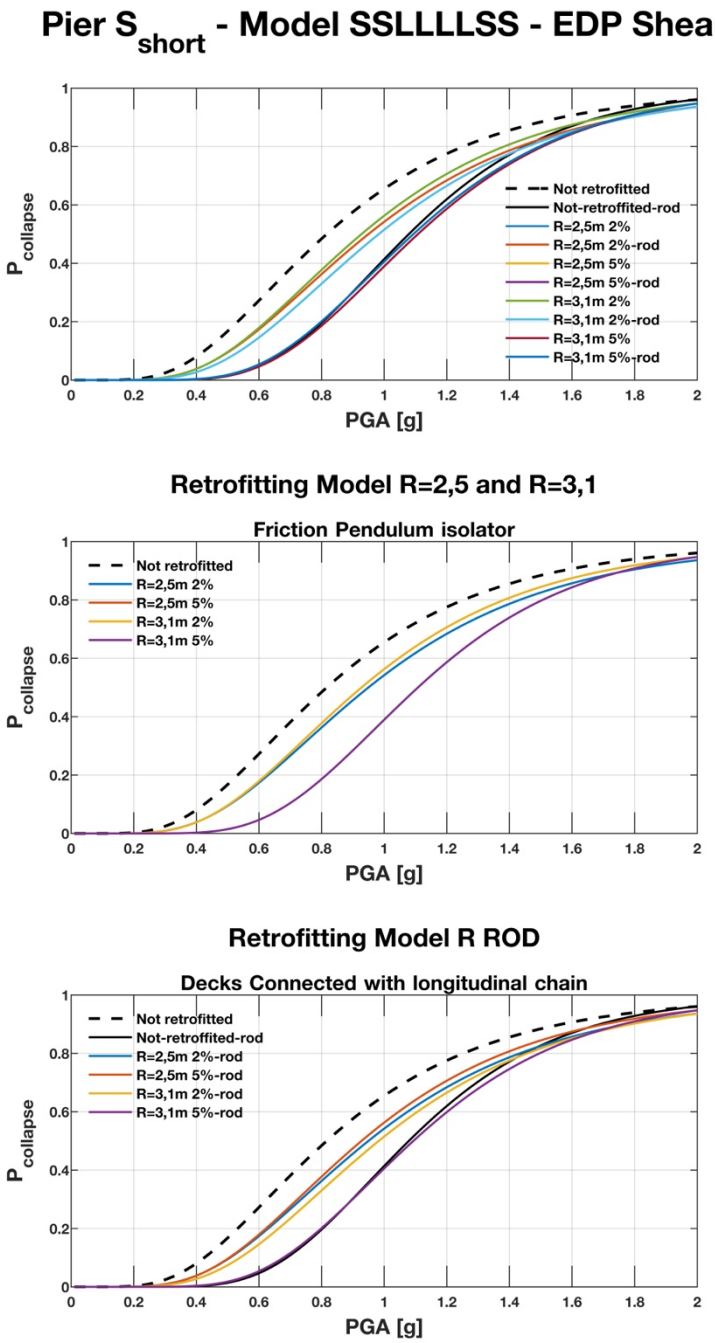

Figure 6.63: Fragility Curves Short Pier – Model SSLLLLSS – EDP Shear.

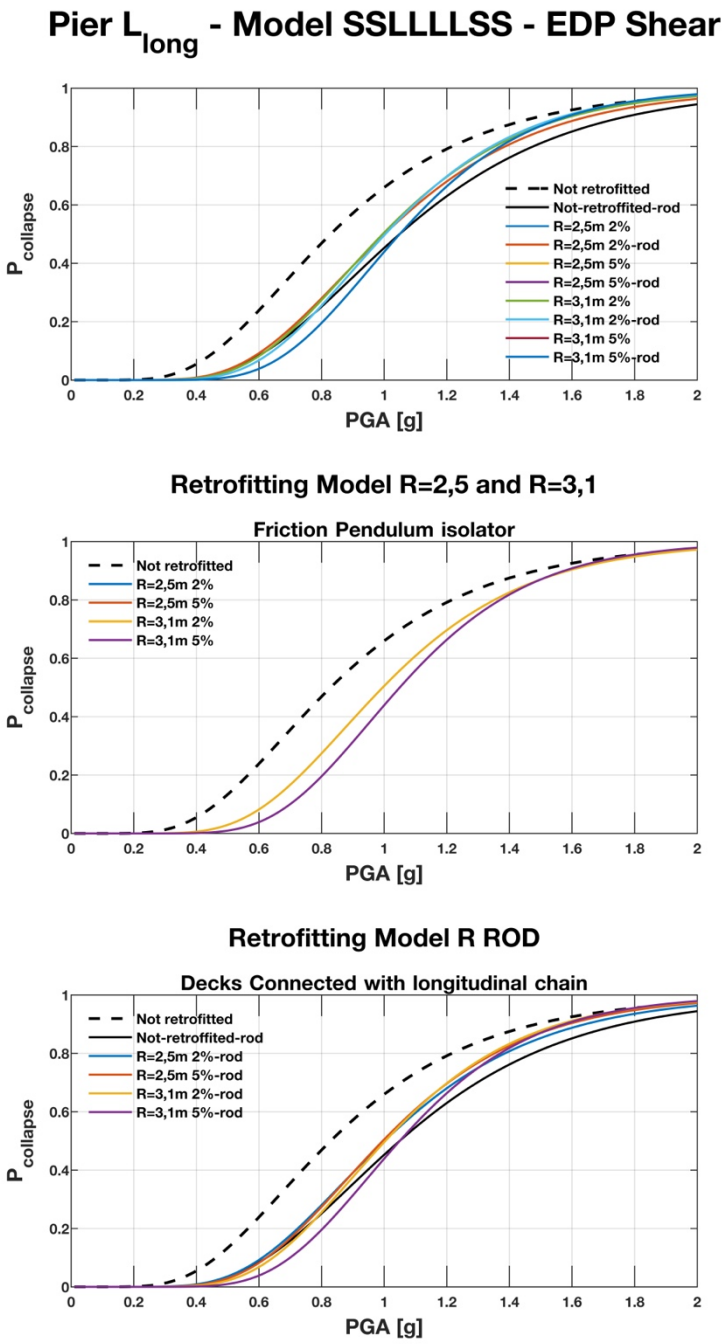

Figure 6.64: Fragility Curves Long Pier – Model SSLLLLSS – EDP Shear.

6.5.5.3 Girder Pounding effect

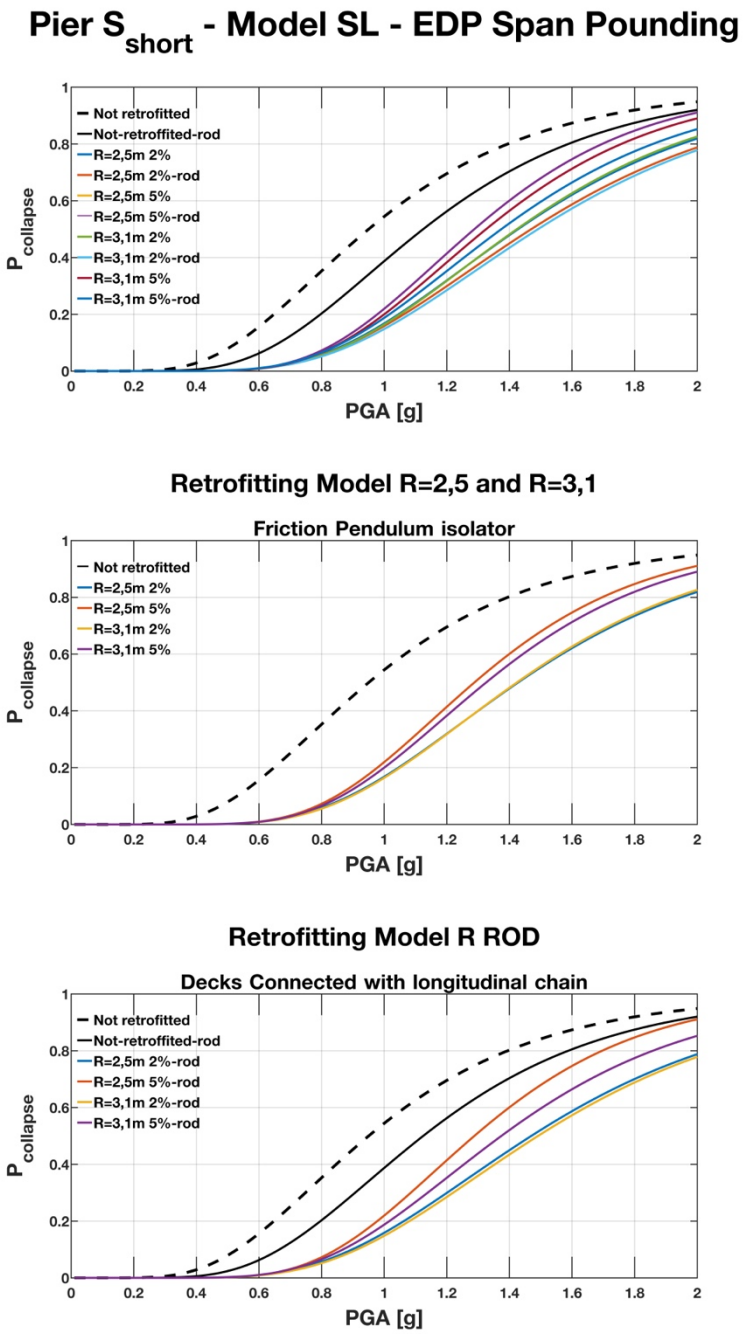

Figure 6.65: Fragility Curves Short Pier – Model SL – EDP Span Pounding.

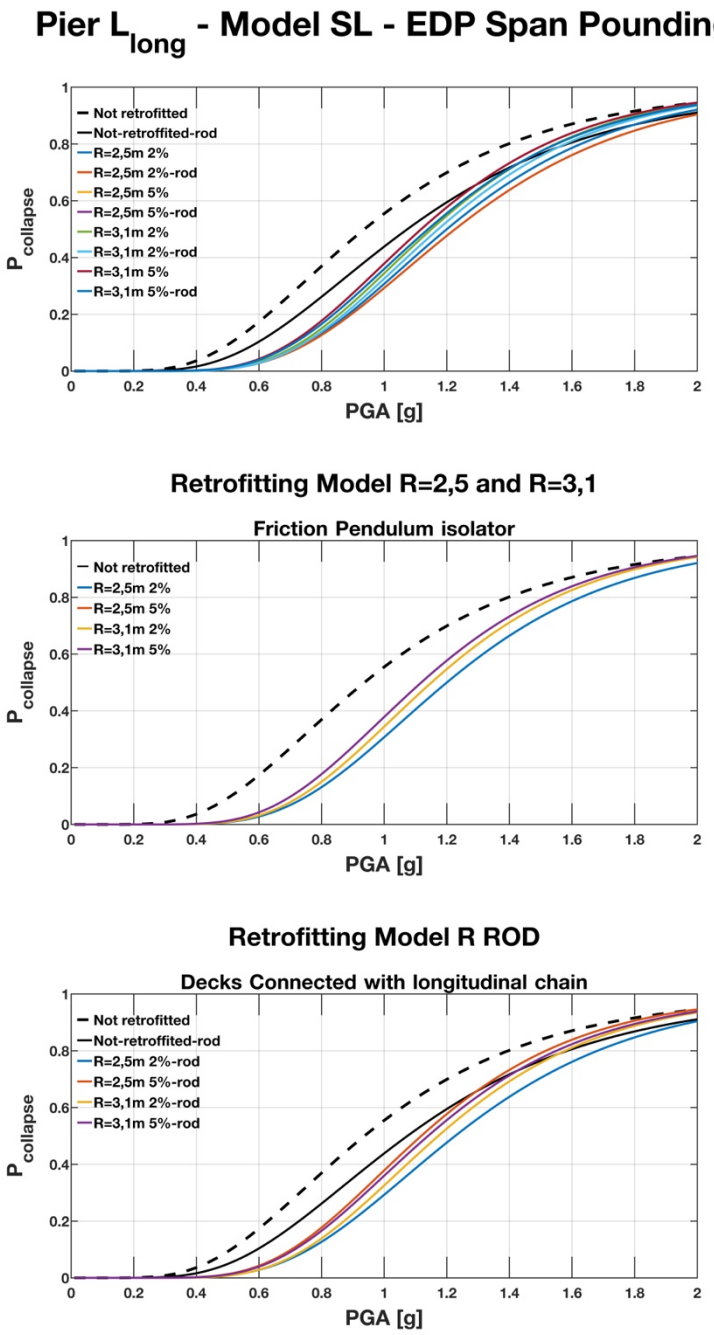

Figure 6.66: Fragility Curves Long Pier – Model SL – EDP Span Pounding

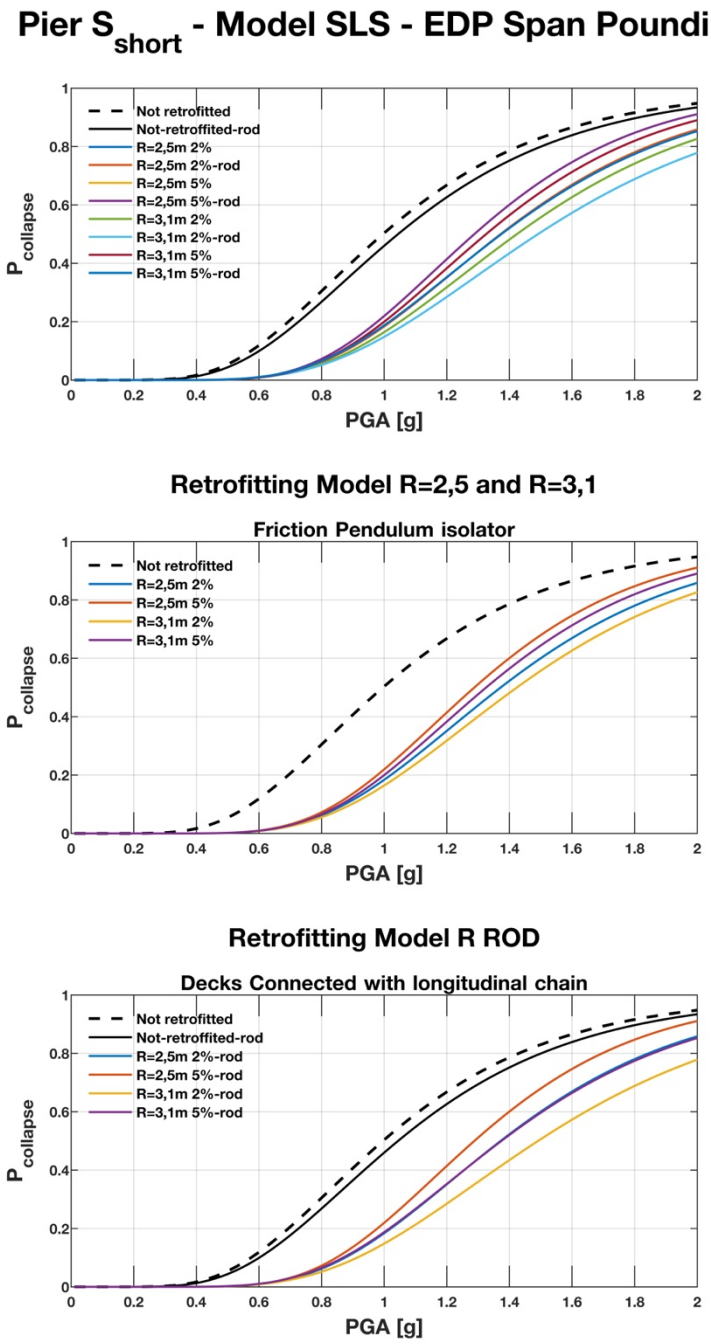

Figure 6.67: Fragility Curves Short Pier – Model SLS – EDP Span Pounding.

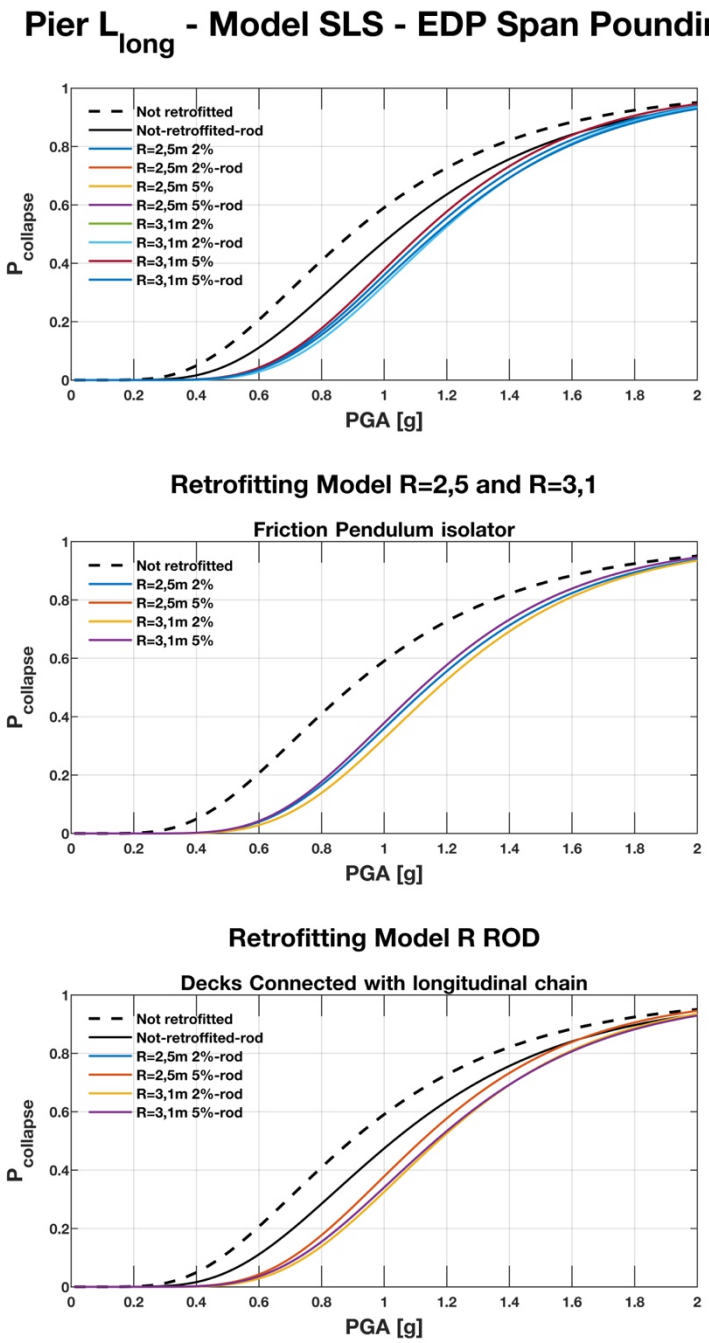

Figure 6.68: Fragility Curves Long Pier – Model SLS – EDP Span Pounding.

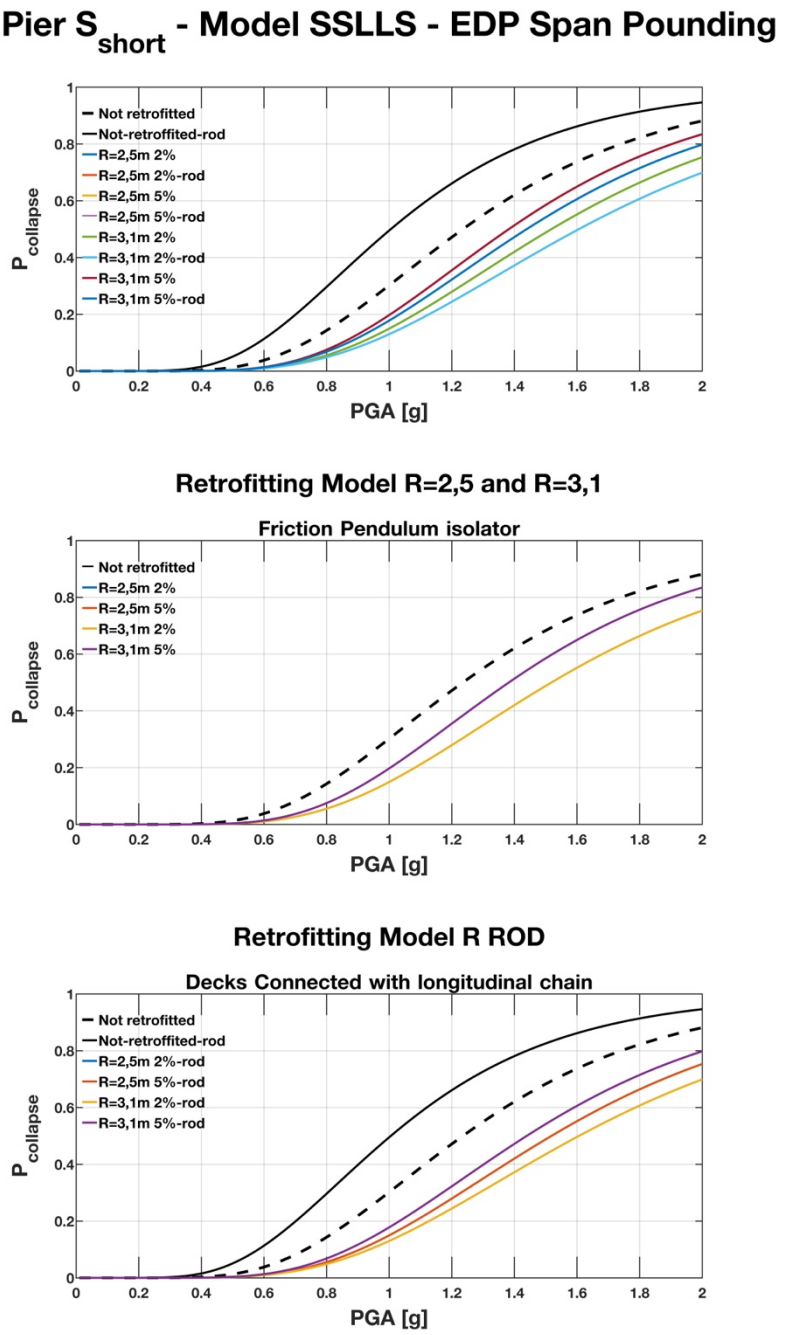

Figure 6.69: Fragility Curves Short Pier – Model SSLLS – EDP Span Pounding.

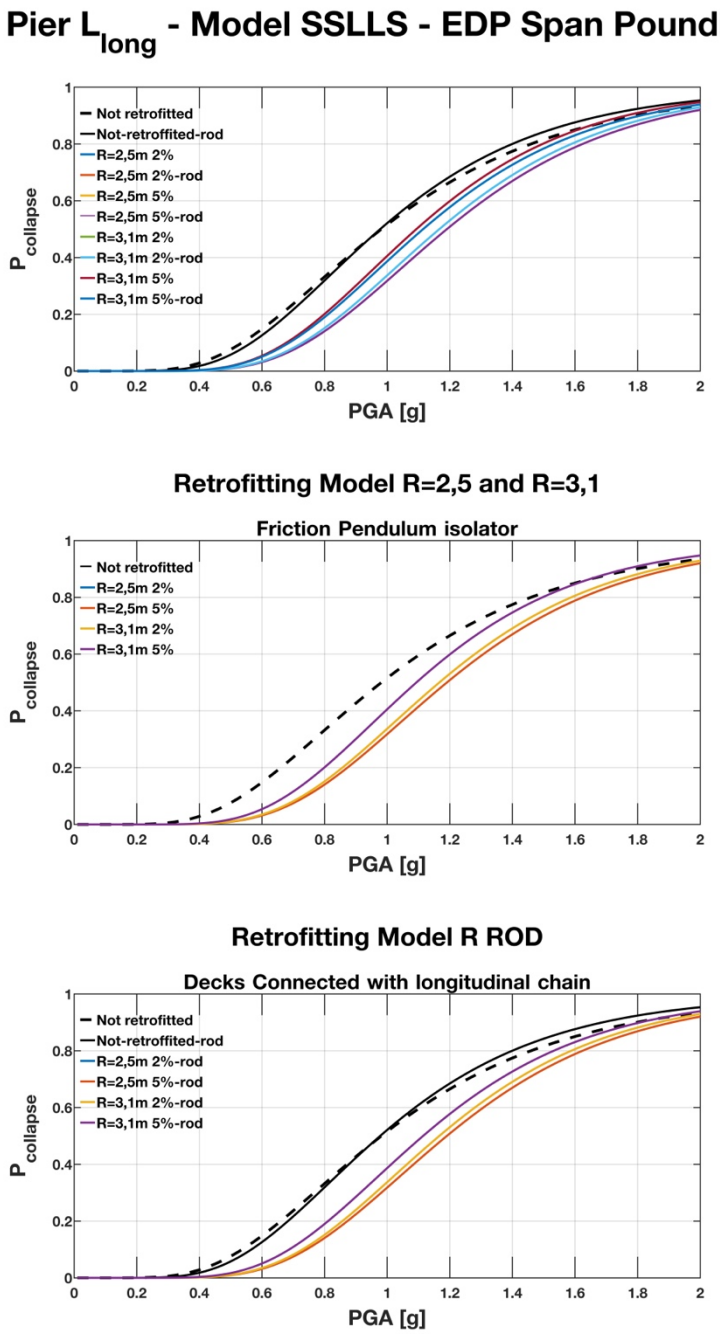

Figure 6.70: Fragility Curves Long Pier – Model SSLLS – EDP Span Pounding.

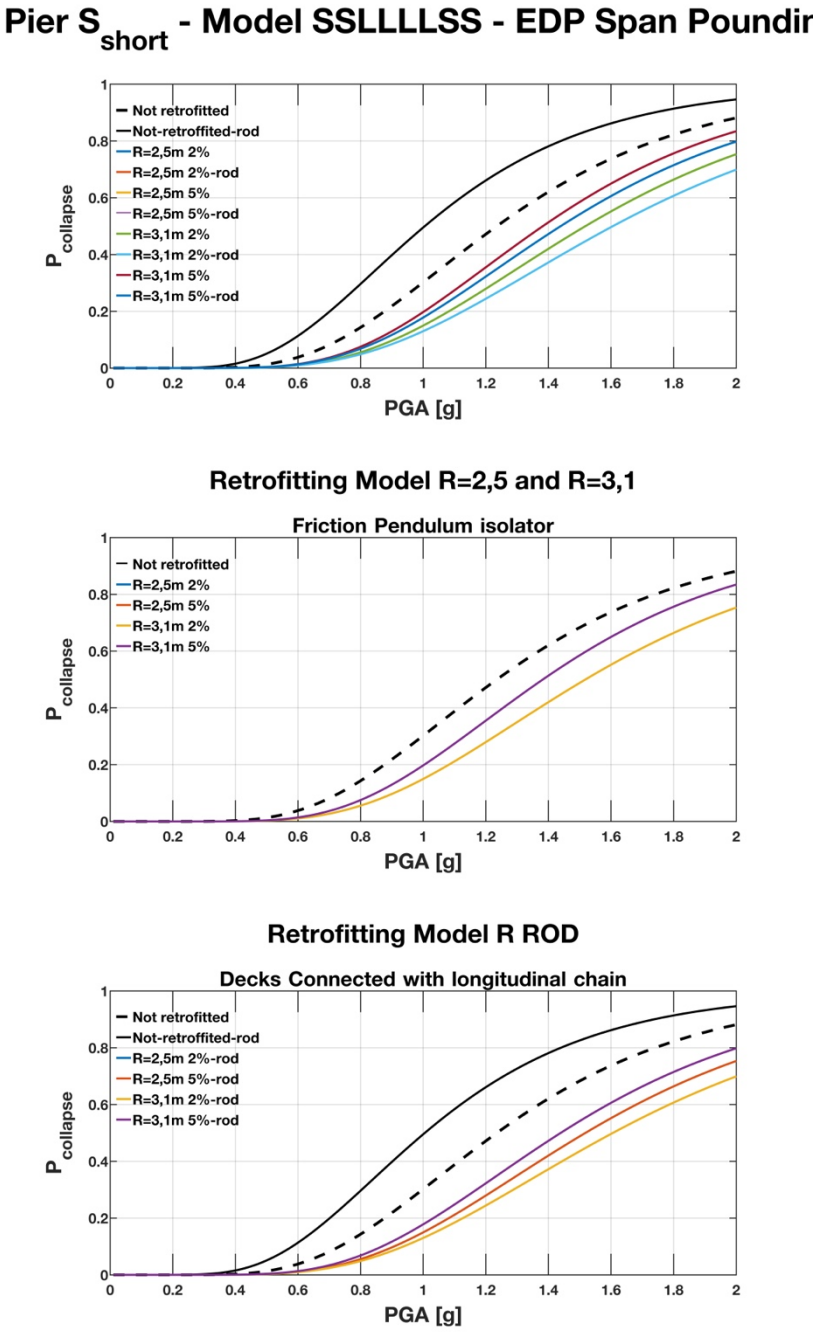

Figure 6.71: Fragility Curves Short Pier – Model SSLLLLSS – EDP Span Pounding.

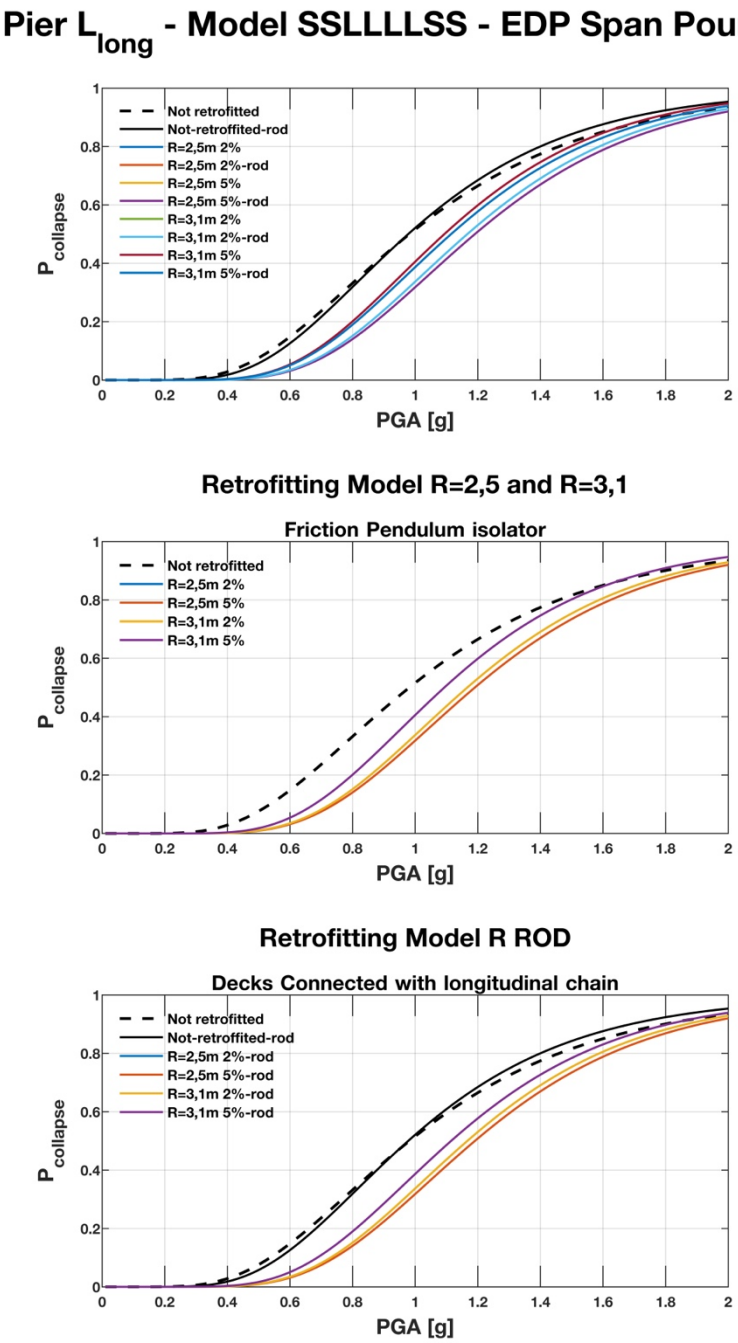

Figure 6.72: Fragility Curves Long Pier – Model SSLLLLSS – EDP Span Pounding.

In the SL model, the ROD retrofit configuration, decks connected with longitudinal chains and elastomeric bearings, does not improve the structure but causes an increase in the probability of collapse for high PGA values. Instead, if combined with the use of FPS both for the piers S and for the piers L involve a slight improvement of rotational behaviour (Figure 6.50 and Figure 6.51) but causes an increase in shear stresses increasing the probability of collapse of the structural element (Figure 6.58 and Figure 6.59). Also, the presence of the FPS provides substantial improvements for the EDP span pounding (Figure 6.65 and Figure 6.61) because with this type of insulators it is possible to govern the relative displacements between the superstructure and the substructure, which is more difficult with the elastomeric bearings.

In the SLS model the effects of the retrofit options proposed for the structure, decks connected with longitudinal chains and use of FPS, make improvements to the structural behaviour in the case of the EDP rotation both for the piers S (Figure 6.51) and for the piers L (Figure 6.52), with the reduction of about 20% of the probability of collapse. Regarding EDP Shear for S piers (Figure 6.59), there is an increase in the probability of collapse and therefore an increase in stresses on the element while substantial improvements are not noticed for the L piers (Figure 6.60). As far as the EDP span pounding (Figure 6.67 and Figure 6.68) is concerned, even in this case, the use of FPS allows the control of movements, limiting the effect.

For the SSLLS model, the effects of the retrofit options with the FPS result in a slight improvement in the overall structure behaviour for both EDP Shear (Figure 6.61 and Figure 6.62) and EDP Rotation (Figure 6.53 and Figure 6.54)for both types of S and L piers. Instead, for the option of retrofit with the connected spans and FPS not in all the models, there are improvements of the structural behaviour. In particular, for the EDP rotation on the piers L we obtain an increase in the probability of collapse, the same thing happens for the EDP shear on the piers L where in the case of the FPS R = 2.5 5% the probability of collapse is higher than the model not retrofitted. The

EDP span pounding (

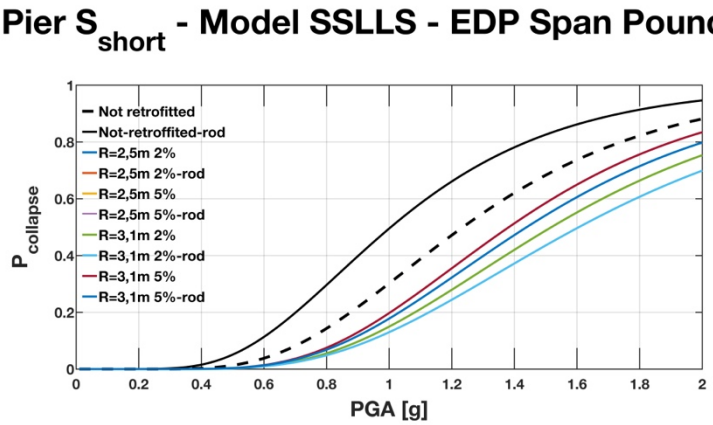

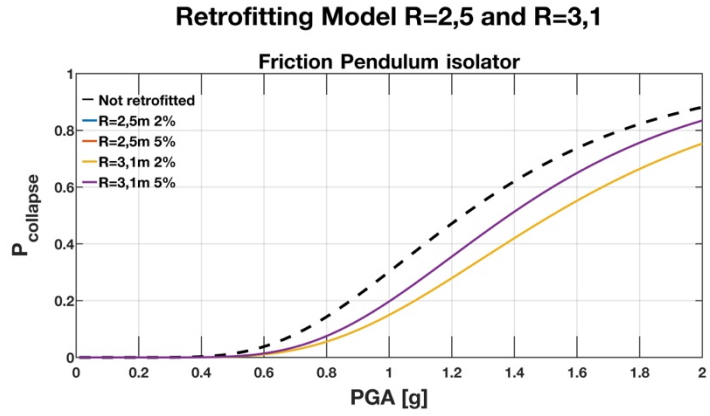

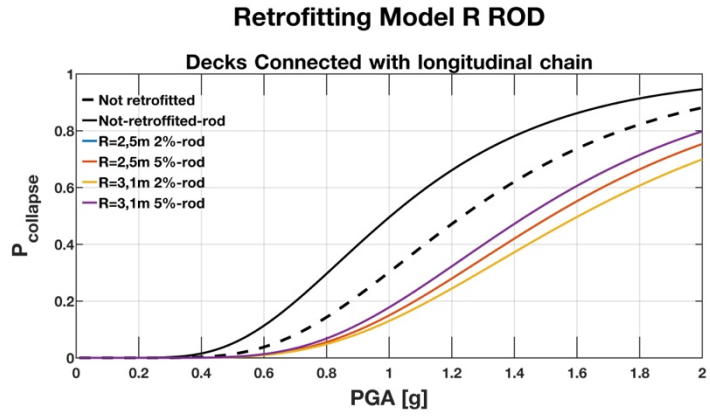

Figure *6.69* and Figure 6.70) also obtains improvements in this case only in the models in which there is the combined use of the two retrofitting solutions, connecting the decks with longitudinal chain and FPS, this can be associated as previously expressed to the possibility to govern the behaviour by the FPS.

The SSLLLLS model achieves an overall improvement in all proposed retrofit configurations. The S piers (Figure 6.63 and Figure 6.55) are positively affected by the presence of FPS both regarding rotation and shear; the same thing happens for the L piers (Figure 6.64 and Figure 6.56). The Pounding EDP is positively affected by the presence of the FPS (Figure 6.71 and Figure 6.72), in fact, the only longitudinal connection of the decks causes negative effects on the structure.

6.6 Combining fragility curves

The variability of single EDPs and the mutual influence of single damage limits leads to a difficult understanding of the overall behaviour of the bridge system. The studies done highlighted the need to understand the global damages, not the local damages of each element. The combination of all the fragility curves hitherto derived would give the possibility of comprehensively comprehending global behaviour. This combination would make it possible to identify the element with the highest probability of collapse, and not only the probability of total collapse, thus giving the possibility to plan retrofitting interventions. For this reason, it will be proposed an innovative method to combine the fragility curves of every single structural element. This method, through the envelope of the fragility curves of each EDPs considered, would give the possibility of intuitively understanding the overall behaviour of the bridge system and in addition, would allow to asses of the probability of collapse of the structural element.

This, however, requires information on the stochastic dependence between bridge components in various damage states. Through the theory of reliability of the first order, one can quickly determine an upper and lower limit of the fragility of the system. The lower limit is the maximum fragility of the individual component while the upper limit is a combination of the fragility of the component. These limits are indicated in Equation 6-2, where the probability of failure of each element is represented by $P(F_i)$ and $P\left(F_{sys}\right)$, is the probability of failure for the whole system.

$$\max_{i=1}[P(F_i)] \leq P\left(F_{sys}\right) \leq 1 - \prod_{i=1}^{m}[1 - P(F_i)] \qquad 6\text{-}2$$

These first order limits are valid for a series-type system, in which a failure of one of the components constitutes a system error (Melchers RE. 1999). When a bridge is modelled in the longitudinal direction as in this study, in fact, it behaves like a series system. The lower limit represents the probability of failure for a system whose components are all entirely dependent on the stochastic point of view. The upper limit assumes that the components are all statistically independent and provide a conservative approach to estimate the overall fragility of the bridge. When the difference between the upper and lower limit decreases, the estimate of the upper limit of the system's fragility becomes more appropriate. The following paragraphs will show the combined fragility curves for the various bridge models used in the research.

6.6.1 Model SL

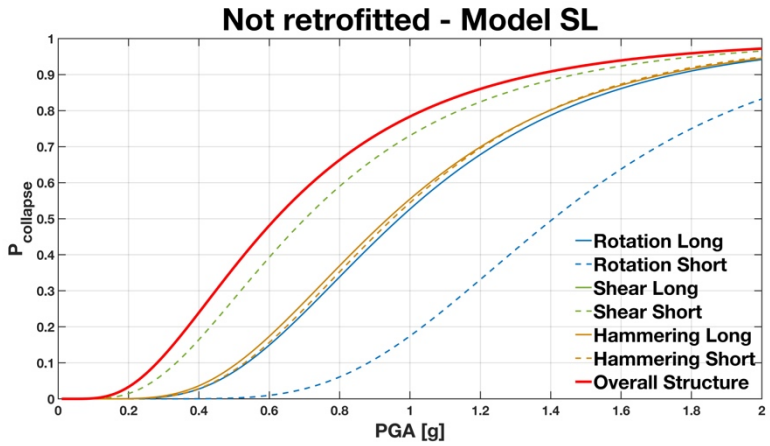

Figure 6.73: Combining Fragility Curves – Model SL Not Retrofitted.

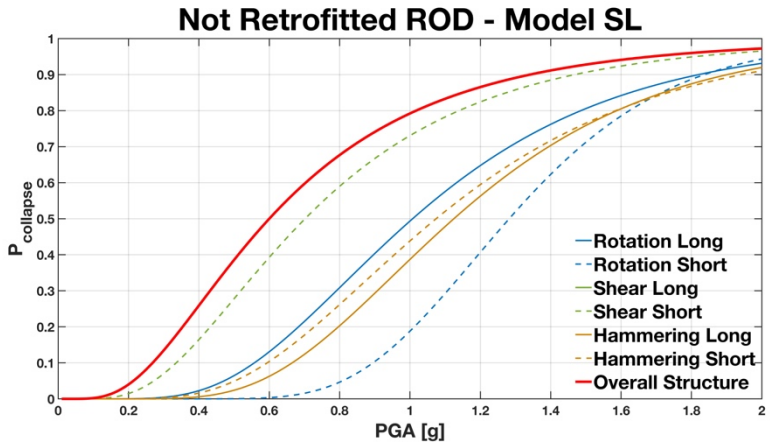

Figure 6.74: Combining Fragility Curves – Model SL Not Retrofitted ROD.

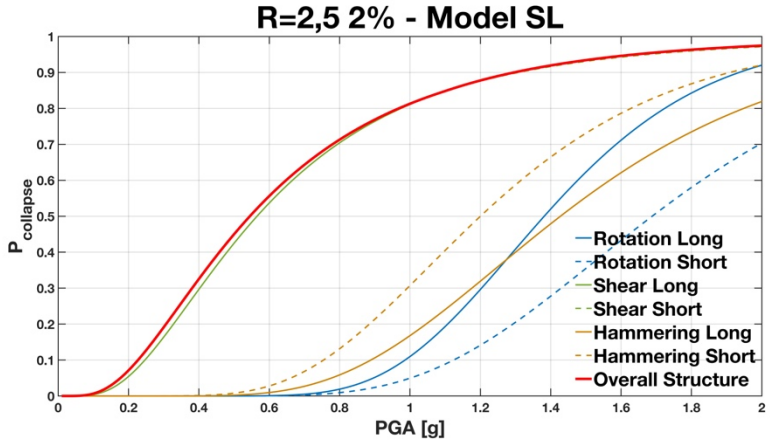

Figure 6.75: Combining Fragility Curves – Model SL R=2.5 2%.

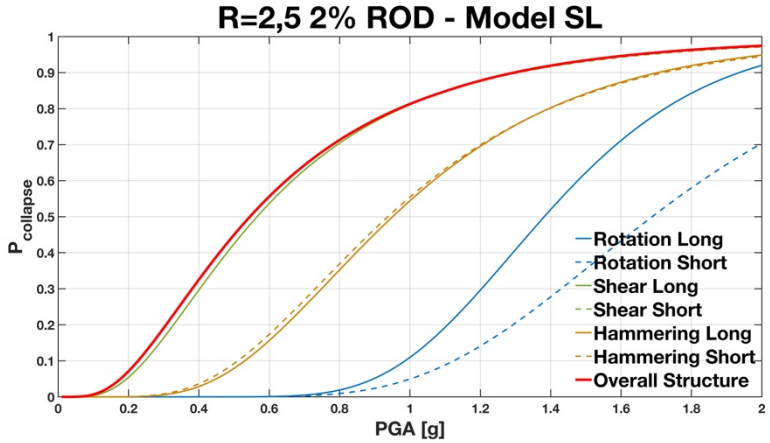

Figure 6.76: Combining Fragility Curves – Model SL R=2.5 2% ROD.

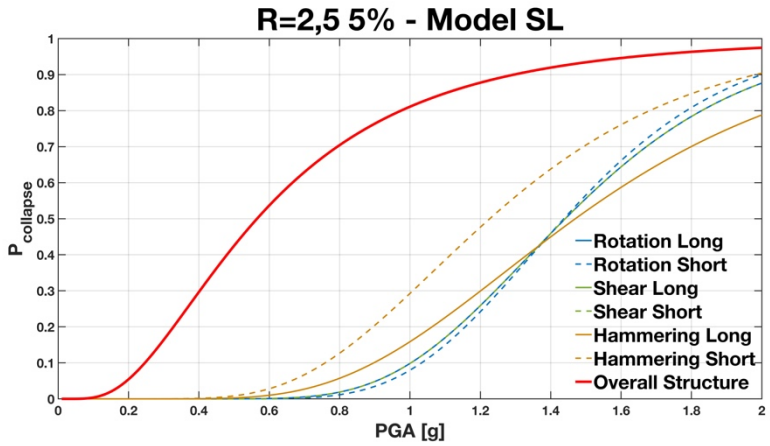

Figure 6.77: Combining Fragility Curves – Model SL R=2.5 5%.

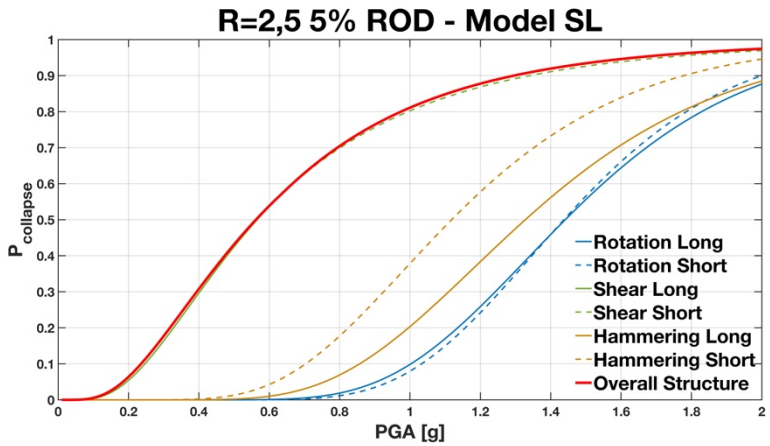

Figure 6.78: Combining Fragility Curves – Model SL R=2.5 5% ROD.

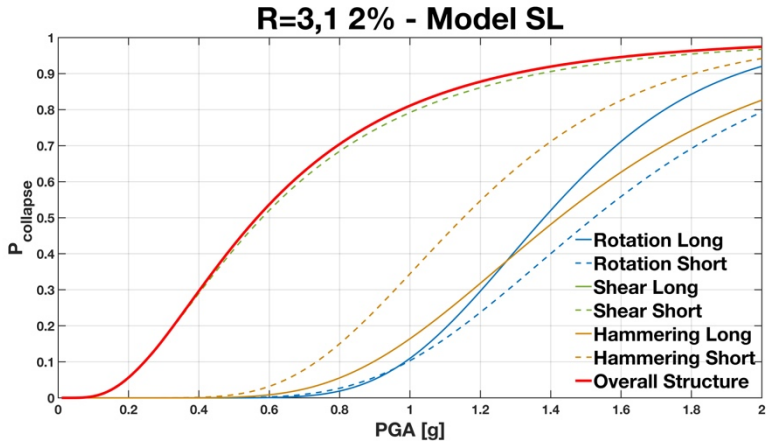

Figure 6.79: Combining Fragility Curves – Model SL R=3.1 2%.

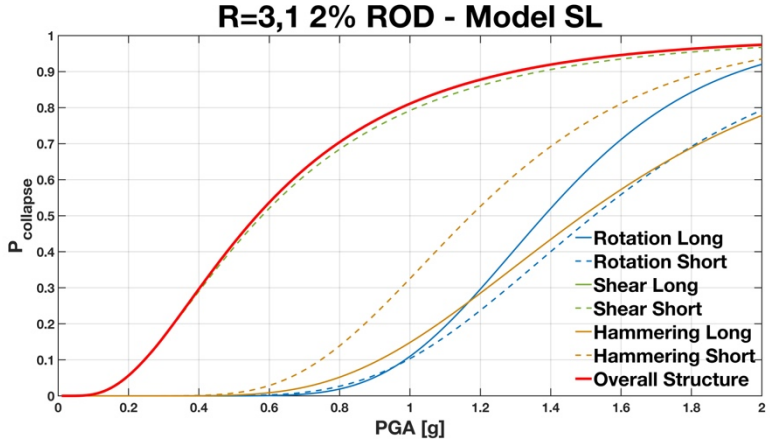

Figure 6.80: Combining Fragility Curves – Model SL R=3.1 2% ROD.

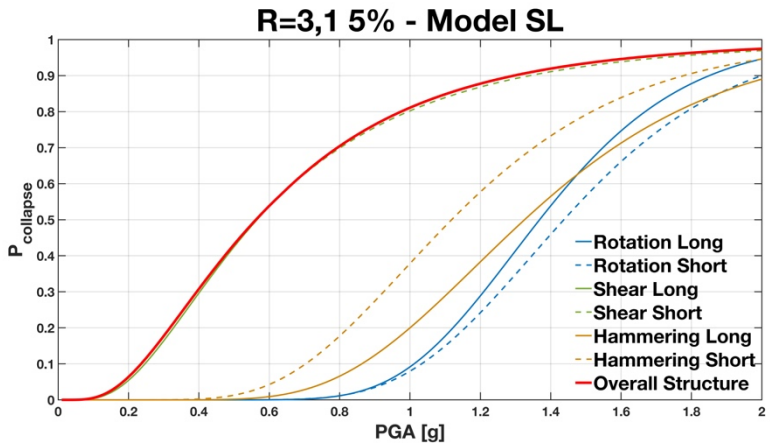

Figure 6.81: Combining Fragility Curves – Model SL R=3.1 5%.

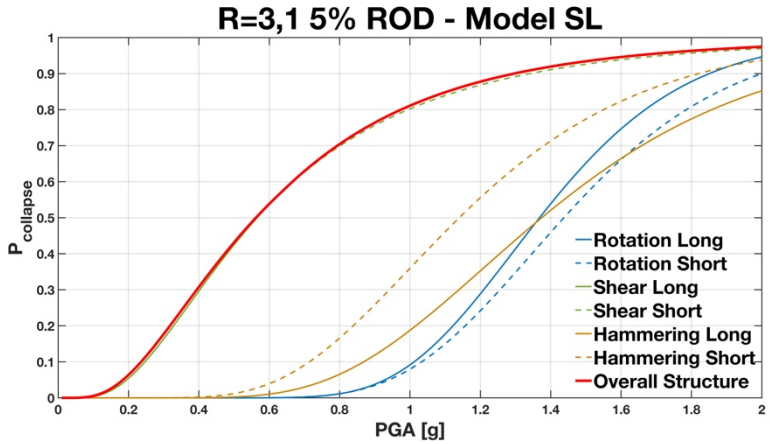

Figure 6.82: Combining Fragility Curves – Model SL R=3.1 5% ROD.

6.6.2 Model SLS

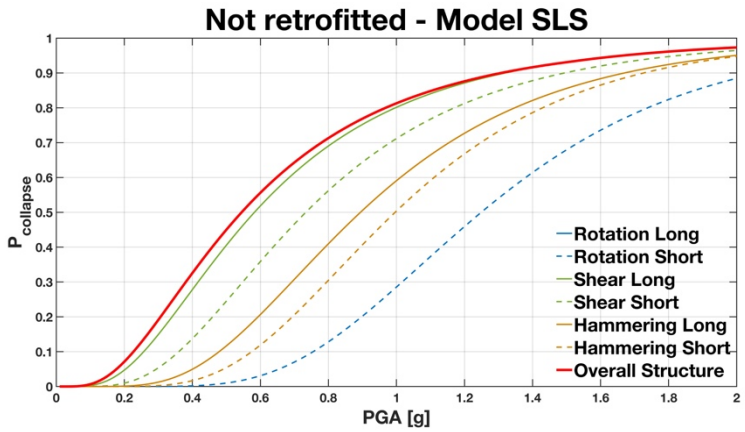

Figure 6.83: Combining Fragility Curves – Model SLS Not Retrofitted.

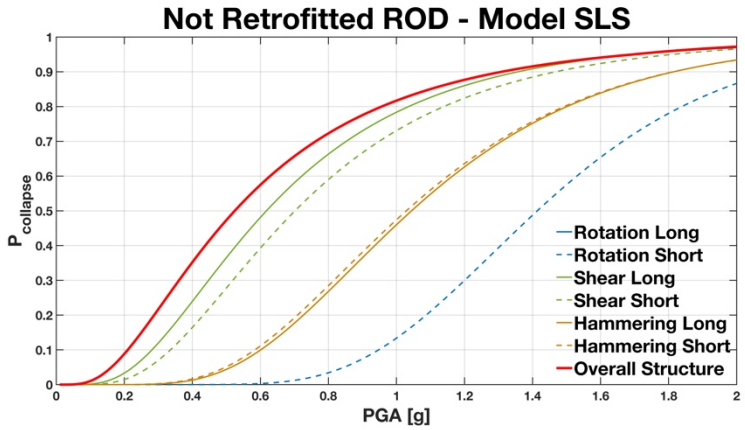

Figure 6.84: Combining Fragility Curves – Model SLS Not Retrofitted ROD.

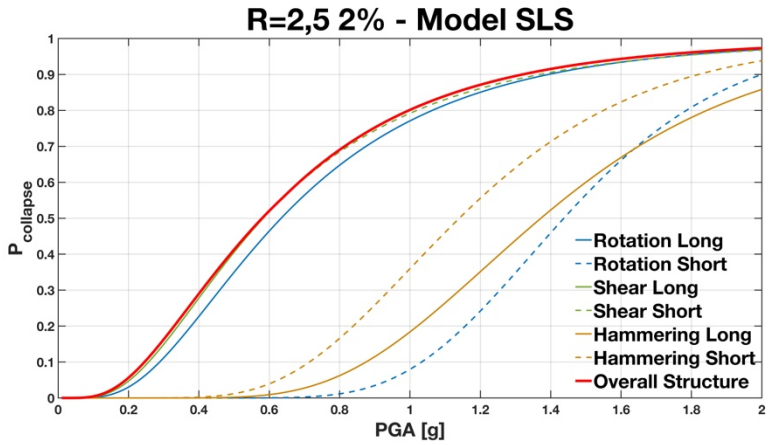

Figure 6.85: Combining Fragility Curves – Model SLS R=2.5 2%.

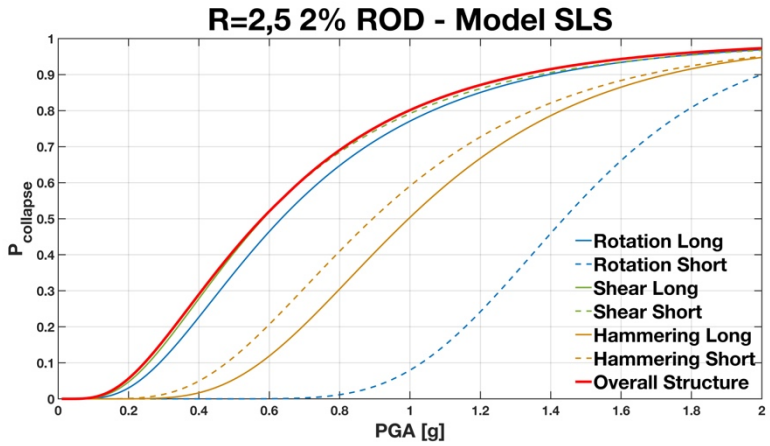

Figure 6.86: Combining Fragility Curves – Model SLS R=2.5 2% ROD.

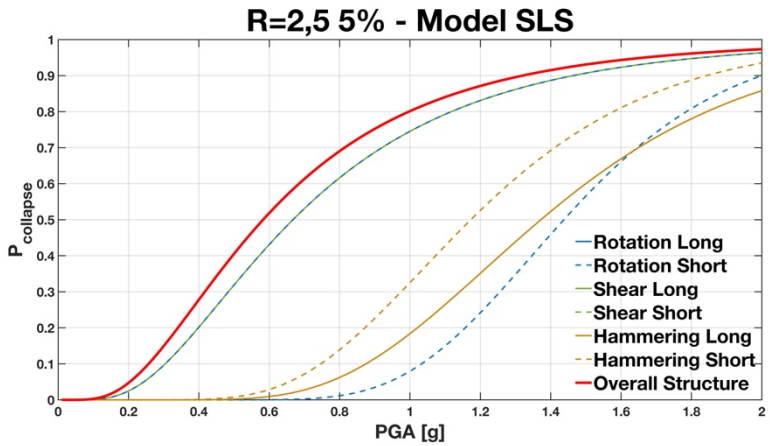

Figure 6.87: Combining Fragility Curves – Model SLS R=2.5 5%.

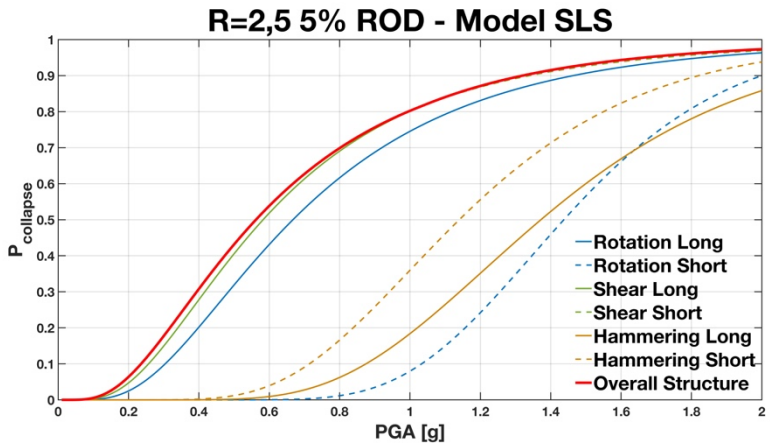

Figure 6.88: Combining Fragility Curves – Model SLS R=2.5 5% ROD.

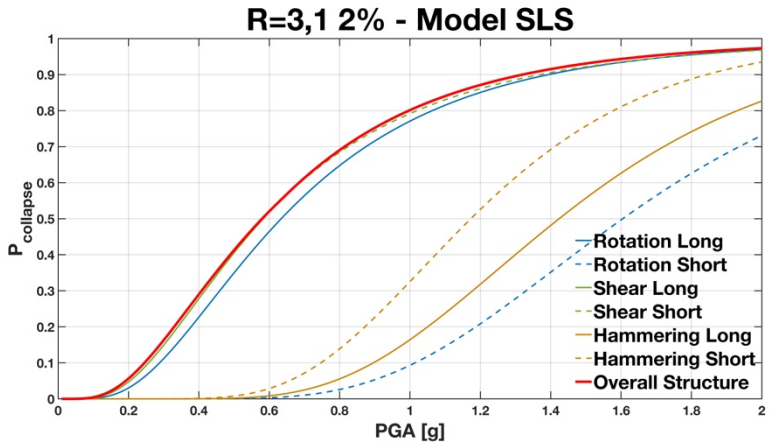

Figure 6.89: Combining Fragility Curves – Model SLS R=3.1 2%.

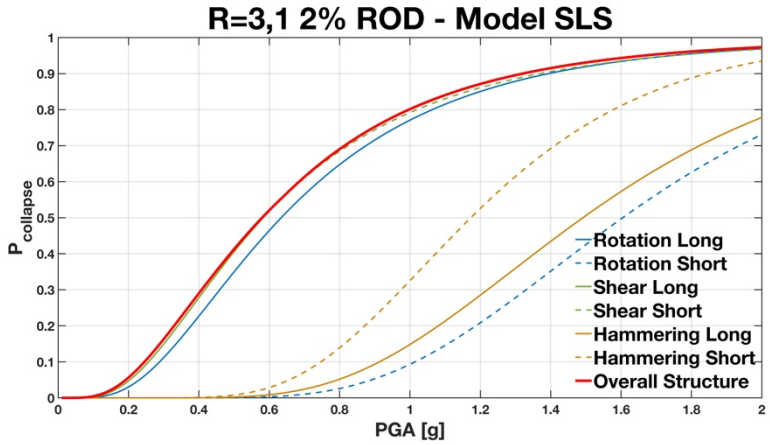

Figure 6.90: Combining Fragility Curves – Model SLS R=3.1 2% ROD.

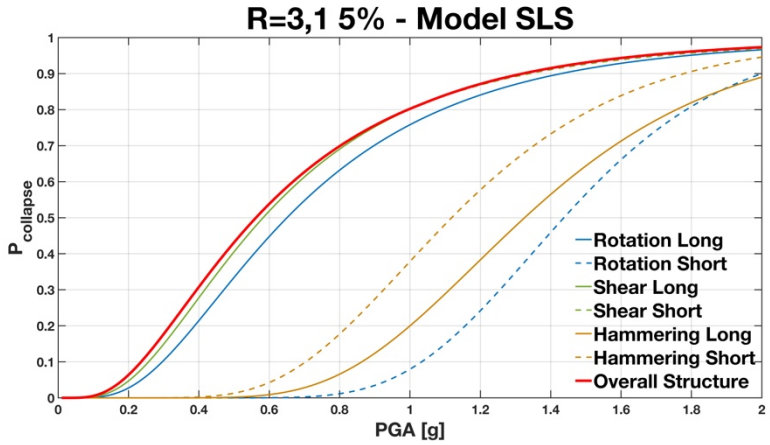

Figure 6.91: Combining Fragility Curves – Model SLS R=3.1 5%.

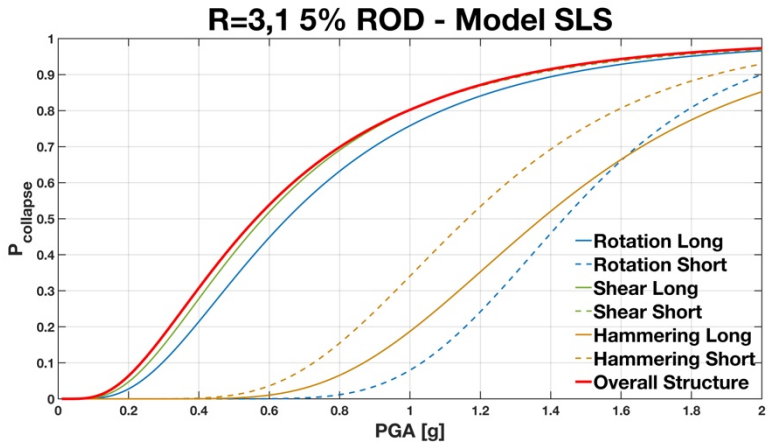

Figure 6.92: Combining Fragility Curves – Model SLS R=3.1 5% ROD.

6.6.3 Model SSLLS

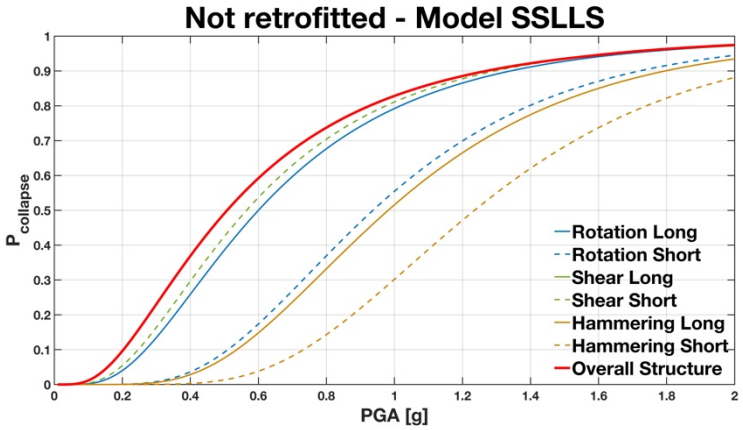

Figure 6.93: Combining Fragility Curves – Model SSLLS Not Retrofitted.

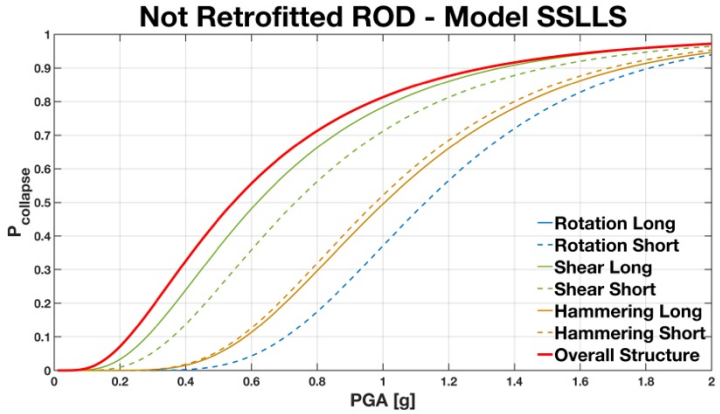

Figure 6.94: Combining Fragility Curves – Model SSLLS Not Retrofitted ROD.

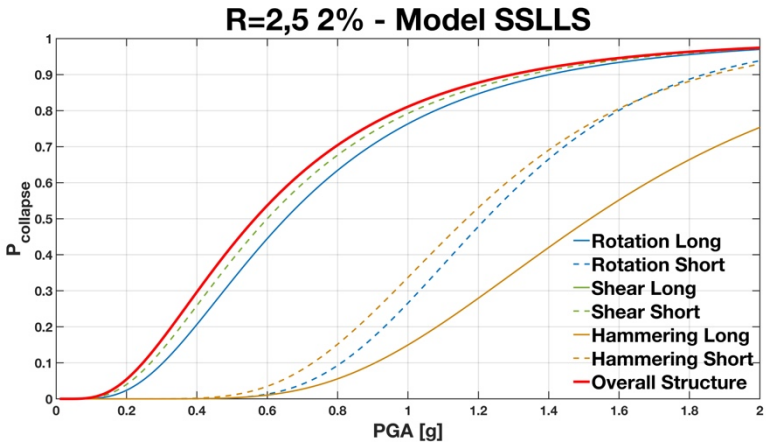

Figure 6.95: Combining Fragility Curves – Model SSLLS R=2.5 2%.

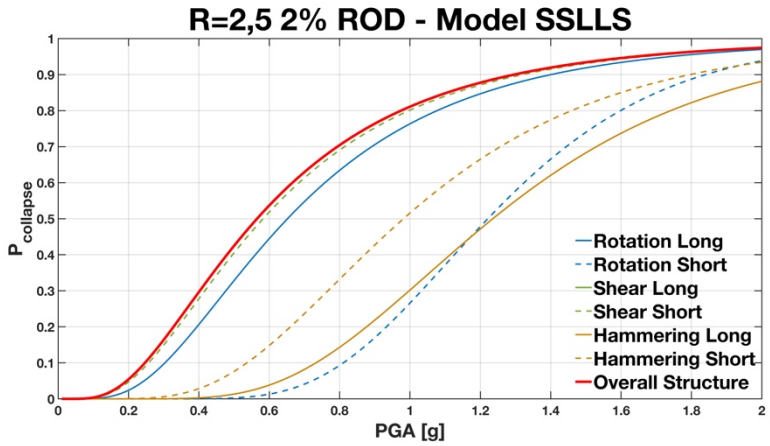

Figure 6.96: Combining Fragility Curves – Model SSLLS R=2.5 2% ROD.

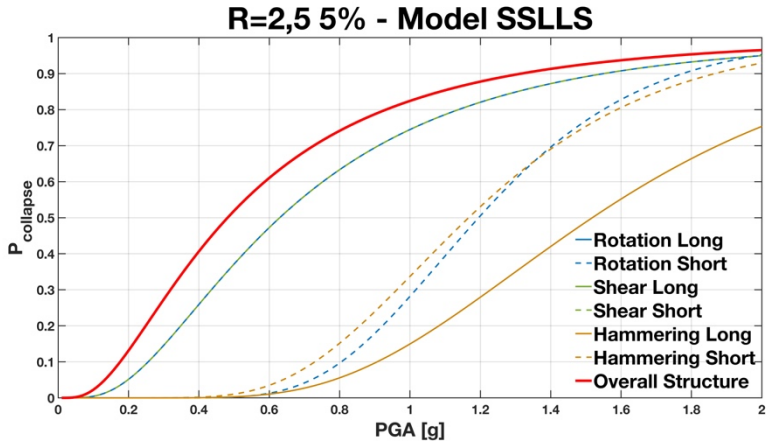

Figure 6.97: Combining Fragility Curves – Model SSLLS R=2.5 5%.

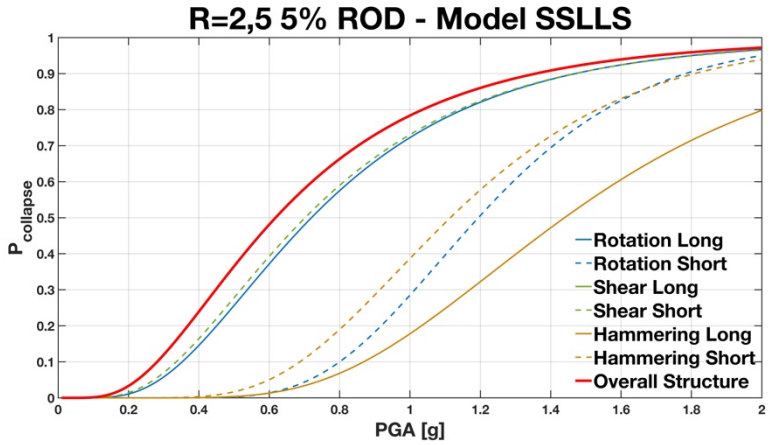

Figure 6.98: Combining Fragility Curves – Model SSLLS R=2.5 5% ROD.

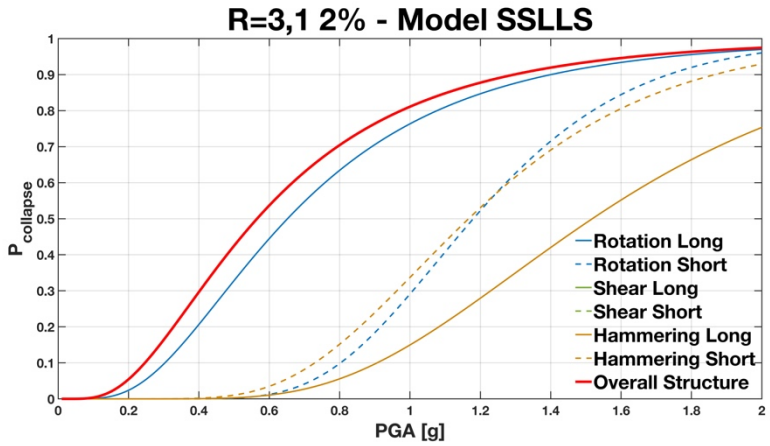

Figure 6.99: Combining Fragility Curves – Model SSLLS R=3.1 2%.

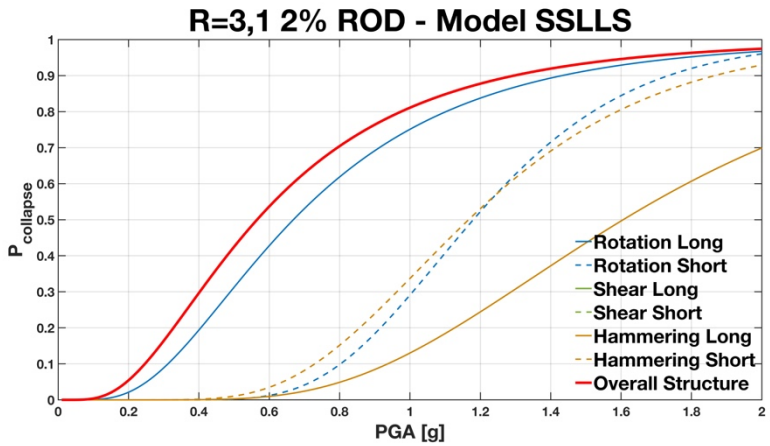

Figure 6.100: Combining Fragility Curves – Model SSLLS R=3.1 2% ROD.

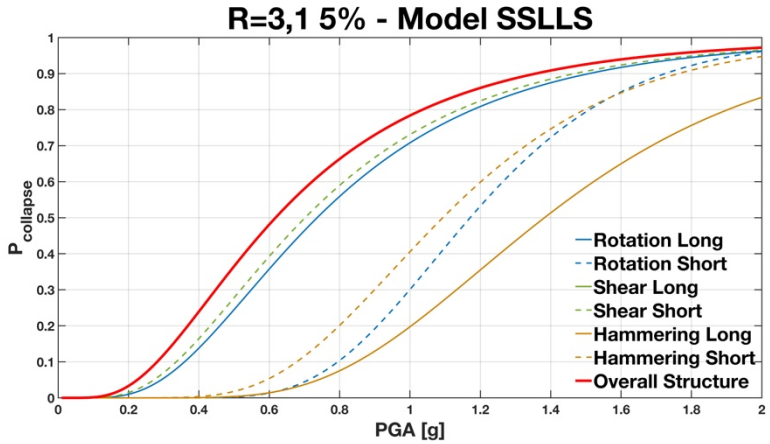

Figure 6.101: Combining Fragility Curves – Model SSLLS R=3.1 5%.

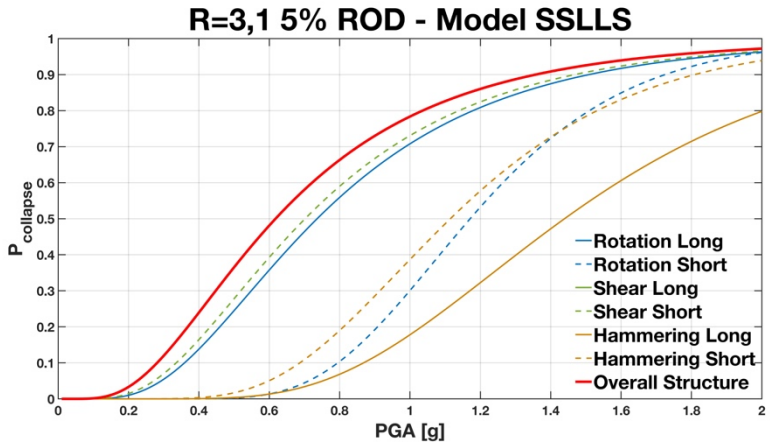

Figure 6.102: Combining Fragility Curves – Model SSLLS R=3.1 5% ROD.

6.6.4 Model SSLLLLSS

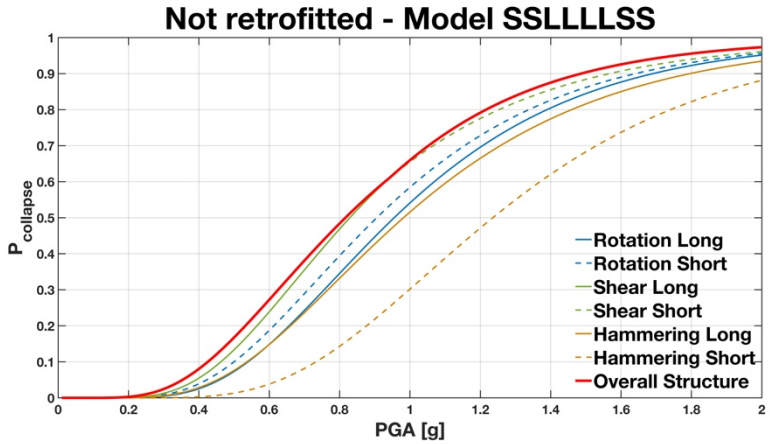

Figure 6.103: Combining Fragility Curves – Model SSLLLLSS Not Retrofitted.

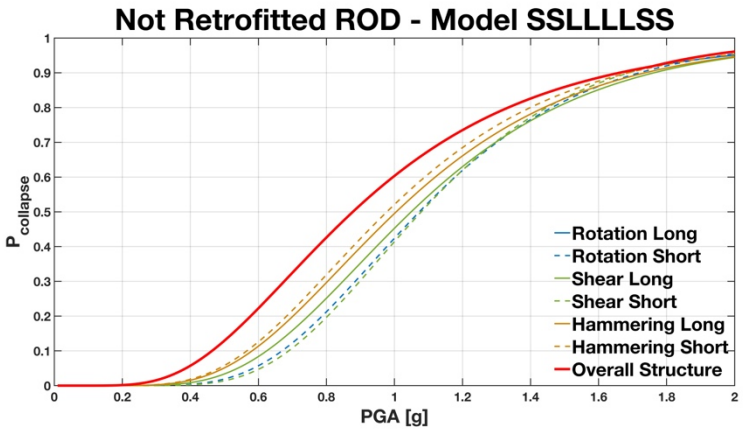

Figure 6.104: Combining Fragility Curves – Model SSLLLLSS Not Retrofitted ROD.

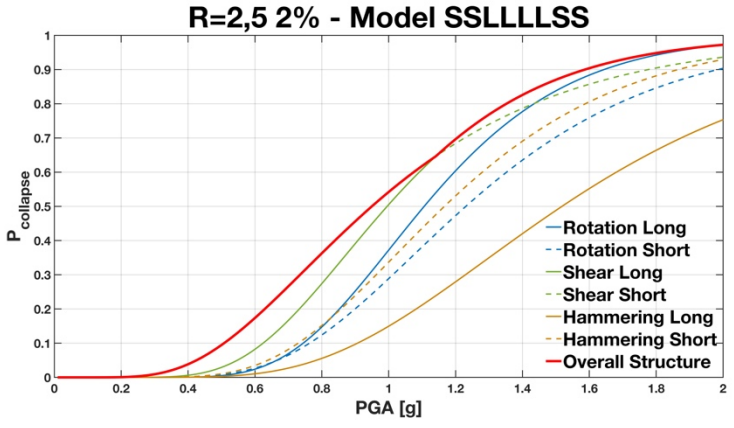

Figure 6.105: Combining Fragility Curves – Model SSLLLLSS R=2.5 2%.

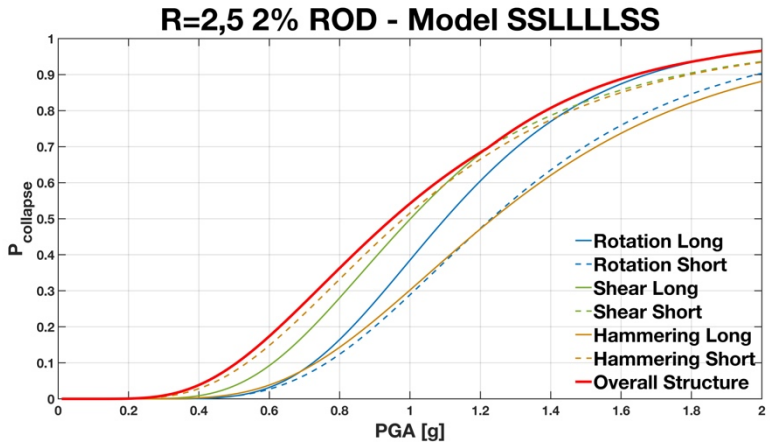

Figure 6.106: Combining Fragility Curves – Model SSLLLLSS R=2.5 2% ROD.

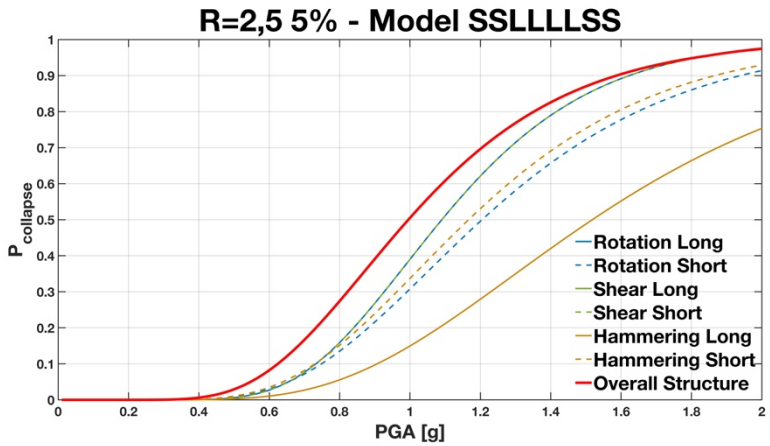

Figure 6.107: Combining Fragility Curves – Model SSLLLLSS R=2.5 5%.

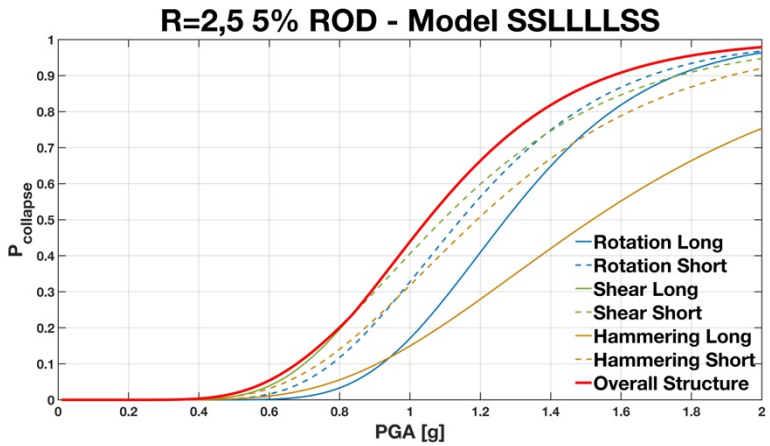

Figure 6.108: Combining Fragility Curves – Model SSLLLLSS R=2.5 5% ROD.

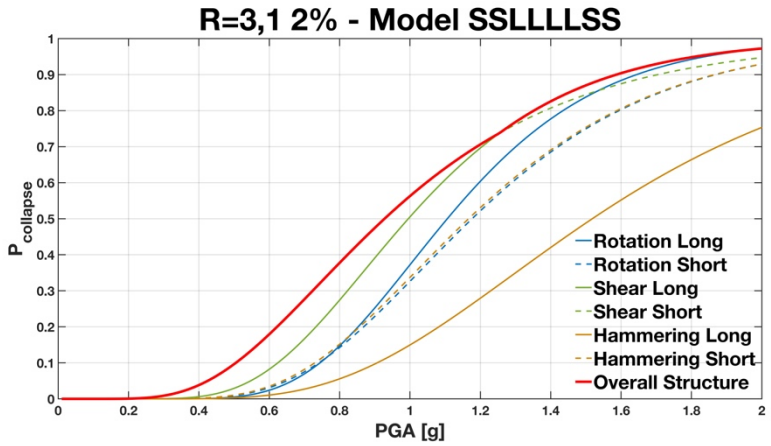

Figure 6.109: Combining Fragility Curves – Model SSLLLLSS R=3.1 2%.

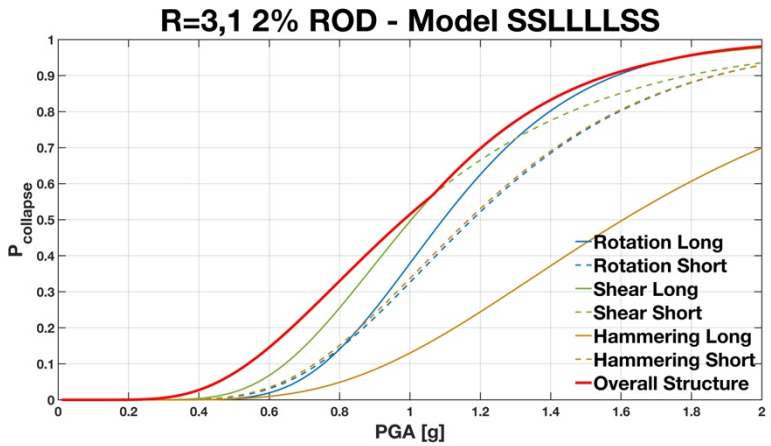

Figure 6.110: Combining Fragility Curves – Model SSLLLLSS R=3.1 2% ROD.

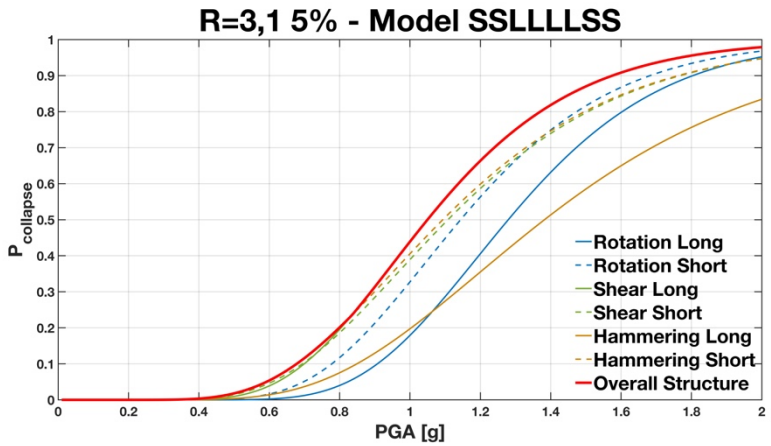

Figure 6.111: Combining Fragility Curves – Model SSLLLLSS R=3.1 5%.

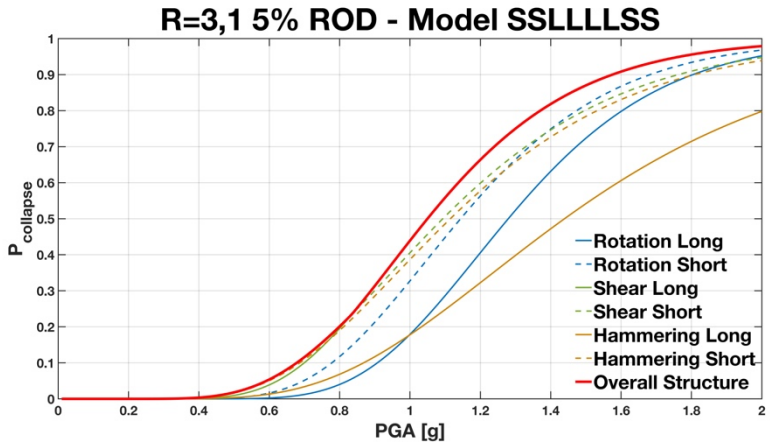

Figure 6.112: Combining Fragility Curves – Model SSLLLLSS R=3.1 5% ROD.

The envelope of the fragility curves of the individual EDPs gives the possibility to understand the mechanism that causes the structural collapse. From the Table 6.18 it is clear that the geometric configuration of the bridge is the first variable that influences the type of collapse mechanism. In fact, in the not retrofitted model, the model adopted as a reference bridge for the various geometric configurations, exhibits various types of collapse mechanisms as a function of the bridges length. This is due to the dynamic interaction between the spans that needs a local analysis in order to better understand the complex behaviour of the structure.

Table 6.18: Typologies of mechanism collapsed.

Model	**Model**			
	SL	**SLS**	**SSLLS**	**SSLLLLSS**
Not Retrofitted	SL	RL	SS-SL	SS-SL
Not Retrofitted -ROD	SL	RL	RL	RL
R=2,5 2%	SS	SL	SS-SL	SL
R=2,5 2%-ROD	SS	SL	SS-SL	SS-SL
R=2,5 5%	SL	SL	RL	SS
R=2,5 5%-ROD	SL	SS	SL	SS
R=3,1 2%	SL	SS-SL	SS-SL	SS
R=3,1 2%-ROD	SL	SS-SL	SS-SL	SS
R=3,1 5%	SL	SS-SL	SS-SL	SL
R=3,1 5%-ROD	SL	SS-SL	SS-SL	SL

SL = Shear Pier Long; SS = Shear Pier Short
RL = Rotation Pier Long; RS = Rotation Pier Short

The collapse mechanisms change according to the retrofit options considered. However, it is noted that the main collapse mechanism for all the models and all the

configurations results is the collapse on the piers. In models with FPS isolators, a reduction in span pounding is always achieved as these devices efficiently manage the maximum displacements.

Table 6.19: Collapse Probability at 0,5 g.

Model	Model			
	SL	**SLS**	**SSLLS**	**SSLLLLSS**
Not Retrofitted	77 %	79 %	77 %	41 %
Not Retrofitted -ROD	78 %	79 %	77 %	41 %
R=2,5 2%	80 %	79 %	80 %	54 %
R=2,5 2%-ROD	80 %	79 %	80 %	49 %
R=2,5 5%	80 %	79 %	77 %	41 %
R=2,5 5%-ROD	80 %	79 %	81 %	48 %
R=3,1 2%	80 %	79 %	80 %	52 %
R=3,1 2%-ROD	80 %	79 %	80 %	52 %
R=3,1 5%	80 %	77 %	80 %	58 %
R=3,1 5%-ROD	80 %	79 %	82 %	64 %

Although improvements have been found for individual EDPs in many cases, as described in paragraph 4, the general behaviour of the bridge system has not undergone a lowering of the probability of collapse as can be seen in Table 6.19 where the probability of collapse is reported to a PGA of 0.5 g.

This highlights the complexity of the bridge structural system, where the improvement of a single element may not lead to the improvement of the overall behaviour. These fragility curves can be used in determining the potential losses resulting from earthquakes and can be used to assign prioritization for retrofitting.

In this case, in fact, the piers are elements endowed with high seismic mass characterized by a relevant dynamic behaviour, moreover, they were designed in the 60s and 70s when the design criteria were noticeably different from the modern ones, and therefore characterized by a fragile behaviour towards shearing actions. For this reason, what has emerged from the results obtained is the difficulty to improve the structural performance of the entire bridge with only the FPS isolators. Therefore, in order to reduce the vulnerability of the piers elements, it might be appropriate to adopt combined retrofit strategies that envisage the use of both retrofitting techniques, aimed at improving flexural and shear strength, as well as seismic isolation.

7. Conclusions

The present work has investigated the problems of girder bridges through the study of a simply supported bridge defined by geometric and mechanical characteristics typical of the Italian bridges of the 60s. Furthermore, more geometric configurations were selected, with the intention of extending the search to a larger number of cases.

To better understand the behaviour of bridges subjected to seismic actions, attention was given to defining, characterising and measuring the safety of existing bridges, in particular, the damage reported to road infrastructures during the recent earthquakes was analysed. Subsequently, the possible retrofitting techniques of bridges and viaducts were analysed, in particular, the replacement of elastomeric bearings with FPS-type devices was chosen as a retrofit technique, because they allow governing the behaviour of the superstructure and they are fast to set up and are economical compared to other types of retrofitting. Moreover, the connecting decks with longitudinal chains have been considered.

The most common methodology for assessing the seismic vulnerability of existing bridges and viaducts is the construction of fragility curves, i.e. the probability of overcoming a predefined level of damage for a given value of seismic intensity. The safety factor has been evaluated in a probabilistic way, that is through the calculation of the probability of failure of the single bridges, whose capacity has an uncertainty duly characterised in front of a specific seismic scenario, also defined statistically. Various numerical procedures have therefore been developed to determine a correlation between the last seismic event and its probable consequences on the damage state. The study of each of the aspects mentioned was systematically carried out using parametric studies, in which the results were submitted to statistical processing, to allow the coverage of a large number of different structural configurations and earthquakes and to obtain generalised results.

The variability of individual EDPs and the mutual influence on individual damage indices leads to a difficult understanding of the general behaviour of the bridge system. The innovative method presented in the work allows to understand both the overall behaviour of the structure and the damages localized on the single elements. The simultaneous view of two indicators such as global damage and local damage

can be an immediate support for the planning of retrofit interventions. Moreover, if empirical data were used, that is coming from real data, the behaviour of the structures could be monitored in real time.

The results show that the application of seismic isolation using FPS systems may not be effective in the improvement or seismic adaptation of particular complex structures such as bridges and viaducts. In cases where the substructure is equipped with high seismic mass, it is necessary to couple the insulation strategy with consolidation operations.

The research can be developed by considering further types of descriptive EDP of the behaviour of the abutments and foundations to more thoroughly investigate the overall response of the structure. Moreover, the choice of the intervention can be related to the costs to define the most effective intervention for the case considered with the lowest cost.

References

A.H.M. Muntasir Billah & M. Shahria Alam, 2015. Seismic fragility assessment of highway bridges: a state-of-the-art review, *Structure and Infrastructure Engineering*, 11:6, 804-832, DOI: 10.1080/15732479.2014.912243

Alam, M.S., Bhuiyan, A.R., & Billah, A.H.M.M. 2012. Seismic fragility assessment of SMA-bar restrained multi-span continuous highway bridge isolated with laminated rubber bearing in medium to strong seismic risk zones. *Bulletin of Earthquake Engineering*, 10, 1885–1909.

ANAS S.p.A. (2010) - Condirezione Generale Tecnica Unità Ricerca e Innovazione, *Relazione Tecnica Esecutiva*, 04.11.10.

ASCE - American Society of Civil Engineers 1995b. "Lifeline Earthquake Engineering - proceedings of the fourth U.S. Conference" - *Technical Council on Lifeline Earthquake Engineering - monograph n°6*.

ASCE - American Society of Civil Engineers, 1990. Recent Lifeline Seismic Risk Studies, Technical Council on Lifeline Earthquake *Engineering-monograph n°1*.

ASCE - American Society of Civil Engineers, 1991. Lifeline Earthquake Engineering - *Technical Council on Lifeline Earthquake Engineering - monograph n°4*.

ASCE - American Society of Civil Engineers, 1992. "Lifeline Earthquake Engineering in the central and eastern U.S." - *Technical Council on Lifeline Earthquake Engineering – monograph n°5*.

ASCE - American Society of Civil Engineers, 1995a. "Critical issues and state-of-the-art in Lifeline Earthquake Engineering" - *Technical Council on Lifeline Earthquake Engineering - monograph n°7*.

ASCE - American Society of Civil Engineers, 1996. "Lifekine Seismic Risk Analysis – case studies" - *Proceedings of the session sponsored by the Technical Council on Lifeline Earthquake Engineering*.

ATC 1985. *Earthquake damage evaluation data for California* (Report No. ATC-13). Redwood City, CA: Applied Technology Council.

ATC 1991. Seismic vulnerability and impact of disruption of lifelines in the Coterminous United States *(Report No. ATC- 25).* Redwood City, CA: Applied Technology Council.

Autostrade per l'Italia S.p.A 1992. *Libro dei Fatti,* Autostrade per l'Italia S.p.A, Rome.

Autostrade per l'Italia S.p.A 2015. *Libro dei Fatti,* Autostrade per l'Italia S.p.A, Rome.

Avsar, O., Yakut, A., & Caner, A. 2011. Analytical fragility curves for ordinary highway bridges in Turkey. *Earthquake Spectra*, 27, 971–996.

Aydan, Ö, Kumsar, H., Toprak, S. and Barla, G. 2009. Characteristics of 2009 L'Aquila earthquake with an emphasis on earthquake prediction and geotechnical damage. *Journal of The School of Marine Science and Technology*, 7(3), pp. 23-51.

B. Borzi, P. Ceresa, P. Franchin, F. Noto, G.M. Calvi, P.E. Pinto, 2014. Seismic Vulnerability of the Italian Roadway Bridge Stock. *Earthquake Spectra*, DOI 10.1193/070413EQS190M.

Baker JW 2015. Efficient analytical fragility function fitting using dynamic structural analysis. *Earthquake Spectra*, 31(1): 579-599.

Baker, J. W., 2008. *An introduction to Probabilistic Seismic Hazard Assessment*. Support of the PSHA lectures, Stanford University, Stanford, USA.

Baker, J. W., Cornell, C. A., 2004. Choice of a vector of ground motion intensity measures for seismic demand hazard analysis. *13th World Conference on Earthquake Engineering*, Vancouver, Canada 2004.

Baker, J. W., Cornell, C. A., 2006a. Which spectral acceleration are you using. *Earthquake Spectra, Volume* 22, No. 2, pages 293–312, May 2006.

Baker, J. W., Cornell, C. A., 2006b. Spectral shape, epsilon and record selection. *Earthquake Engineering and Structural Dynamics*. 2006; 35:1077–1095.

Baker, J., and Cornell, C. A., 2003. Uncertainty specification and propagation for loss estimation using FOSM method*, Pacific Earthquake Engineering Research Center*, University of California, Berkeley, PEER 2003-07.

Baker, J.W., & Cornell, C.A. 2005. A vector-valued ground motion intensity measure consisting of spectral acceleration and epsilon. *Earthquake Engineering and Structural Dynamics*, 34, 1193–1217.

Banerjee, S., & Chi, C. 2013. State-dependent fragility curves of bridges based on vibration measurements. Probabilistic Engineering Mechanics, 33, 116–125.

Banerjee, S., & Shinozuka, M. 2007. Nonlinear static procedure for seismic vulnerability assessment of bridges*. Computer-Aided Civil and Infrastructure Engineering*, 22, 293–305.

Basöz NI, Kiremidjian AS, King SA, Law KH 1999. Statistical analysis of bridge damage data from the 1994 Northridge, CA, earthquake. *Earthquake Spectra*, 15(1): 25-54.

Basoz, N. and Kiremidjian, A. 1998. Evaluation of Bridge Damage Data from the Loma Prieta and Northridge, California Earthquakes. *Technical Report MCEER-98-0004*, Stanford University, Stanford, California.

Basoz, N., & Kiremidjian, A.S. 1997. Evaluation of bridge damage data from the Loma Prieta and Northridge CA earthquakes (Report No. MCEER-98-0004). *Buffalo, NY: MCEER, University at Buffalo*, The State University of New York.

Bazzurro, P., & Cornell, A.C. 2002. *Vector-values probabilistic seismic hazard analysis (VP-SHA)*. Proceedings of the 7th U.S. National Conference on Earthquake Engineering. Boston, MA.

Benjamin, J., Cornell, C. A., 1970. Probability, statistics and decisions for civil engineers*. Mc-Graw Hill Companies*.

Berry, M., & Eberhard, M. 2003. Performance Models for Flexural Damage in Reinforced Concrete Columns, *University of Washington*.

Bhuiyan, A.R., & Alam, M.S. 2012. Seismic vulnerability assessment of a multi-span continuous highway bridge fitted with shape memory alloy bar and laminated rubber bearing. *Earthquake Spectra*, 28, 1379–1404.

Billah, A.H.M.M., & Alam, M.S. 2013. Seismic vulnerability assessment of a typical multi-span continuous concrete highway bridge in British Columbia. *Canadian Journal of Civil Engineering, Manuscript ID: CJCE-2013-0049R2*.

Billah, A.H.M.M., Alam, M.S., & Bhuiyan, A.R. 2013. Fragility analysis of retrofitted multi-column bridge bent subjected to near fault and far field ground motion. *ASCE Journal of Bridge Engineering, 18, 992–1004*.

Bommer, J. J., and Acevedo, A. B., 2004. The Use of Real Earthquake Accelerograms as Input to Dynamic Analysis. *Journal of Earthquake Engineering, 8 (Special Issue 1), 43-9.*

Bradley BA 2010. A generalized conditional intensity measure approach and holistic ground-motion selection. *Earthquake Engineering & Structural Dynamics*, 39(12): 1321-1342.

Buckle IG, Mayes RL 1990. Seismic isolation: History, application and performance a world view. *Earthquake Spectra*, 6(2): 161-201.

California Daprtment of Transportation (Caltrans), 1999. Memo to Deisgners 20-11 Establishing Bridge Seismic Design Criteria, *Caltrans, Sacramento*.

California Daprtment of Transportation (Caltrans), 2010a. Seismic Design Criteria – Version 1.6, *Caltrans, Sacramento.*

California Daprtment of Transportation (Caltrans), 2010b. Memo to Deisgners 20-11 Seismic Design Methodology, *Caltrans, Sacramento*.

Cardone, D., Displacement limits and performance displacement profiles in support of direct displacement-based seismic assessment of bridges. *Earthquake Engineering & Structural Dynamics, 43(8), 1239–1263, 2013*.

Cardone, D., Perrone, G., & Dolce, M., 2007. Seismic risk assessment of highway bridges. *1st US-Italy Seismic Bridge Workshop*. Pavia, Italy.

Casarotti C (2004). Bridge isolation and dissipation devices: state of the art review in bridge isolation, seismic response and modelling of bridge isolation and dissipation devices. MSc dissertation, *ROSE School and University of Pavia*, Italy.

Choi E, DesRoches R, Nielson B 2004. Seismic fragility of typical bridges in moderate seismic zones. *Engineering Structures*, 26(2): 187-199.

Cimellaro, G.P., Reinhorn, A.M., D'Ambrisi, A., De Stefano, M. 2009. Fragility analysis and seismic record selection. *J. Struct. Eng.* 137(3), 379–390.

Comerio, M.C., 2005. PEER tested study on a laboratory building: exercising seismic performance assessment. *PEER Report. PEER 2005/12.*

Computers and Structures, Inc. 2016. CSI Analysis Reference Manual for SAP2000®, ETABS®, SAFE®, and CSiBridge®, Rev. 15, Berkeley, California, USA.

Cooper, J. D., Friedland, I. M., Buckle, I. G., Nimis, R. B. and Bobb, N. M. M. 1994. The Northridge earthquake: progress made, lessons learned in seismic-resistant bridge design. *Public Roads, 58(1), pp. 26-36*.

Cornell C.A., 1968. Engineering seismic risk analysis, B*ulletin of the Seismological Society of America*, 58(5), 1583-1606.

D. Cardone, P. Giuseppe, S. Salvatore 2011. A performance-based adaptive methodology for the seismic evaluation of multi-span simply supported deck bridges. *Bulletin of Earthquake Engineering, 9(5), 1463-1498*.

De Biasio M., 2014. Ground motion intensity measures for seismic probabilistic risk analysis*.* PhD Dissertation, *Civil Engineering. Universit´e Grenoble Alpes.*

Der Kiureghian, A. 2002. Bayesian methods for seismic fragility assessment of lifeline components. In A.D. Kiureghian (Ed.), Acceptable risk processes: Lifelines and natural hazards, Monograph No. 21. *Reston, VA: Technical Council for Lifeline Earthquake Engineering, ASCE*.

DesRoches, R., Padgett, J., Ramanathan, K., & Dukes, J., Feasibility Studies for Improving Caltrans Bridge Fragility Relationships (Vol. 0003). *Georgia Institute of Technology, Atlanta, U.S.A, PhD Thesis, The State University of New York, Buffalo, 2012.*

Di Sarno L., Da Porto F., Guerrini G., Prota A. (2018) *Analysis of the structural response of some bridges during the Central Italy Earthquake*, Progettazione Sismica – Vol. 9, N.1, Anno 2018 DOI 10.7414/PS.9.1.9-23 - http://dx.medra.org/10.7414/PS.9.1.9-23

Dolce, M. 1997. "La valutazione della vulnerabilità per le analisi di rischio e gli scenari di danno", Atti dell'8° Congresso L'Ingegneria sismica in Italia, Settembre 1997, Taormina.

Dutta, A., & Mander, J. B., 1998. Seismic fragility analysis of highway bridges. INCEDE- MCEER Center-to-Center *Workshop on Earthquake Engineering Frontiers in Transportation Systems*. Tokyo, Japan.

Eberhard, M. O., Baldridge, S. , Marshall, J., Mooney, W. and Rix, G. J. (2010) The MW 7.0 Haiti earthquake of January 12, 2010; USGS/EERI Advance Reconnaissance Team Report. U.*S. Geological Survey Open-File Report 2010–1048, USGS, California.*

Ebrahimian H, Jalayer F, Lucchini A, Mollaioli F, Manfredi G (2015). Preliminary ranking of alternative scalar and vector intensity measures of ground shaking. *Bulletin of Earthquake Engineering*, 13(10): 2805-2840.

Ellingwood, B. R. 2008. Structural reliability and performance-based engineering. *Structures and Buildings 161(*SB4):199–207.

Ellingwood, B.R., O.C. Celik, and K. Kinali. 2007. Fragility assessment of building structural systems in mid-America. *Earthquake Engineering and Structural Dynamics 36*:1935–1952.

Elnashai, A., Borzi, B., & Vlachos, S. (2004). Deformation-based vulnerability functions for RC bridges. *Structural Engineering and Mechanics, 17, 215–244*.

Erduran, E., & Yakut, A., Drift based damage functions for reinforced concrete columns. *Computers & Structures*, *82, 121–130, 2004*.

Eurocode, 2008. Eurocode 8.2: Design of Structures for Earthquake Resistance – Part 2. Seismic Design of Bridges, *European Committee for Standardization, Brussels, Belgium.*

Federal Highway Administration (FHWA), Seismic Retrofitting Manual for Highway Structures: Part 1 – Bridges*, FHWA, U.S. Department of Trasportation, McLean, VA., 2006.*

FEMA P695, Federal Emergency Management Agency (ATC-63) *(2009).* Redwood City, CA: *Applied Technology Council (ATC).*

FEMA, 2012. Seismic Performance Assessment of Buildings*,* FEMA P-58. Prepared by the Applied Technology Council for the *Federal Emergency Management Agency, Washington D.C., USA.*

Frankie, T. 2013. Impact of complex system behaviour on seismic assessment of RC bridges, PhD Dissertation*. University of Illinois at Urbana-Champaign, Urbana, Illinois.*

Furlanetto, G., Ferretti Torricelli, L., Marchiondelli, A. 2008 Design Solutions for Widening the A1-A9-A14 Italian Highway. *Structural Engineering in International Vol 4/2008: 356-364.*

Gardoni, P., Der Kiureghian, A., & Mosalam, K.M. 2002. Probabilistic capacity models and fragility estimates for reinforced concrete columns based on experimental observations*. ASCE Journal of Engineering Mechanics, 128, 1024–1038.*

Gardoni, P., Mosalam, K.M., & Der Kiureghian, A. 2003. Probabilistic seismic demand models and fragility estimates for RC bridges. *Journal of Earthquake Engineering, 7, 79–106.*

Ghosh, S., Chakraborty, S. 2017. Seismic performance of reinforced concrete building in Guwahati city, northeast India. *Sci. Iran. Trans. A Civ. Eng. 24(4), 1821–1833*

Giovenale, P., Ciampoli, M., & Jalayer, F. 2003. Comparison of ground motion intensity measures using the incremental dynamic analysis. In A. Der Kiureghian, S. Madanat, & J. Pestana (Eds.), *Proceedings of Applications of Statistics and Probability in Civil Engineering (pp. 1483–1491).*

Groupe de travail G2 AIPCR 1996. "Natural Disaster Reduction for Roads – comprehensive report" - *1996 AIPCR - Association mondiale de la Route - World Road Association.*

Gülerce, Z., and Abrahamson, N. A., 2010. Vector-valued probabilistic seismic hazard assessment for the effects of vertical ground motions on the seismic response of highway bridges, *Earthquake Spectra 26, 999–1016.*

Hamburger, R.O., Foutch, D.A., and Cornell, C.A., 2003. Translating research to practice: FEMA/SAC performance-based design procedures. *Earthquake Spectra, 19 (2), 255 - 267.*

Hansen NM (1965). The Structure and Determinants of Local Public Investment Expenditures. *The Review of Economics and Statistics*, 47(2): 150-162.

HAZUS (1997). Technical Manual. Washington, DC: *Federal Emergency Management Agency.*

HAZUS-MH 2.1 (2012). Multi-Hazard Loss Estimation Methodology: Earthquake Model HAZUS-MH 2.1 Technical Manual. *Washington, DC: Federal Emergency Management Agency.*

HAZUS: Earthquake loss estimation methodology, *2015.* Technical Manual, National *Institute of Building for the Federal Emergency Managment Agency, Whashington, D.C.*

Hwang H, Jernigan JB, Lin Y. Evaluation of seismic damage to memphis bridges and highwaysy stems*. Journal of Bridge Engineering, ASCE 2000;5(4):322–30.*

Hwang, H., Jernigan, J.B., & Lin, Y.W. 2000. Evaluation of seismic damage to Memphis bridges and highway systems*. ASCE Journal of Bridge Engineering, 5, 322–330.*

Hwang, H., Liu, J.B., & Chiu, Y.H. 2001. Seismic fragility analysis of highway bridges*. Mid-America Earthquake Center report: project MAEC RR-4. Urbana: MACE.*

Iervolino I, Galasso C, Cosenza E 2009. Rexel: computer aided record selection for code-based seismic structural analysis. *Bulletin of Earthquake Engineering*, 8(2): 339-362.

Iervolino I, Giorgio M, Galasso C, Manfredi G (2010). Conditional Hazard Maps for Secondary Intensity Measures. *Bulletin of the Seismological Society of America*, 100(6): 3312–3319.

Imbsen RA 2001. Use of isolation for seismic retrofitting bridges. *Journal of Bridge Engineering*, 6(6): 425-438.

Indirli, M., 2010. The 6th April 2009 L'Aquila Earthquake: from ruins to reconstruction, in Seismicity and Earthquake Engineering, *L'Aquila Earthquake of April 2009.*

Jalayer, F. 2003. Direct probabilistic seismic anaysis: implementing non-linear dynamic assessments, *Ph.D. Thesis, Dept. of Civil and Env. Eng., Stanford, CA*

Japan Road Association, Specification for Highway Bridges – Part V, Seismic Design*, Japan Road Association, Tokyo, 1996.*

Kam, W. Y. (2011) Preliminary Report from the Christchurch 22 Feb 2011 6.3Mw Earthquake: Pre-1970s RC and RCM Buildings, and Precast Staircase Damage*. University of Canterbury, Christchurch*.

Kam, W. Y., 2011, *Preliminary Report from the Christchurch 22 Feb 2011 6.3Mw Earthquake: Pre-1970s RC and RCM Buildings, and Precast Staircase Damage*. University of Canterbury, Christchurch

Kaplan, S., H. G. Perla, and D. C. Bley. 1983. A methodology for seismic analysis at nuclear power plants. *Risk Analysis 3(3):169–180.*

Kappos, A. J., & Stefanidou, S. P., Importance of bridge-specific fragility curves in the seismic assessment of road networks. *16th World Conference of Earthquake Engineering. 9-13 January, Santiago, Chile, 2017*

Kappos, A. J., 1991. Analytical Prediction of the Collapse earthquake for R/C buildings: Suggested Methodology. *Earthquake Engineering & Structural Dynamics, 20, 167–176.*

Kappos, A.J. 1997. Discussion of paper: Damage scenarios simulation for seismic risk assessment in urban zones. *Earthquake Spectra, 13, 549–551.*

Kappos, A.J., Panagopoulos, G., Panagiotopoulos, C., & Penelis, G. 2006. A hybrid method for the vulnerability assessment of R/C and URM buildings. *Bulletin of Earthquake Engineering, 4, 391–413.*

Karim, K.R., & Yamazaki, F. 2003. A simplified method of constructing fragility curves for highway bridges. *Earthquake Engineering and Structural Dynamics, 32, 1603–1626.*

Katsanos EI, Sextos AG, Manolis GD 2010. Selection of earthquake ground motion records: a state-of-the-art review from a structural engineering perspective. *Soil Dynamics and Earthquake Engineering 2010;30(4):157–69.*

Kawashima, K. (2007) Seismic Design of Urban Infrastructures. *Lecture Notes, Kawashima Laboratory,* Department of Civil Engineering, Tokyo Institute of Technology, Tokyo.

Kennedy, R.P., et al., 1980. Probabilistic seismic safety of an existing Nuclear power plant. *Nuclear Engineering Design, 59, 315 - 338.*

King, S.A., Kiremidjian, A.S., Basoz, N., Law, K., Vucetic, M., Doroudian, M., Olson, R.A., Eidinger, J.M., Goettel, K.A., & Horner, G. (1997). Methodologies for evaluating the socioeconomic consequences of large earthquakes. *Earthquake Spectra, 13, 565–584.*

Kramer, S. L., 1996. Geotechnical Earthquake Engineering. *Prentice-Hall International series.*

Krawinkler, H., 2005. Van Nuys Hotel building testbed report: exercising seismic performance assessment. *PEER Report. PEER 2005/11.*

Krawinkler, H., and Miranda E., 2004. Performance-based earthquake engineering. In Y. Bozorgnia and V. V. Bertero (Eds.*)*, *Earthquake engineering: from engineering seismology to performance-based engineering. Boca Raton: CRC Press.*

Kwon, O.S., & Elnashai, A.S. 2010. Fragility analysis of a highway over-crossing bridge with consideration of soil–structure interactions. *Structure and Infrastructure Engineering, 6, 159–178.*

L. Petti, A. Lodato, A. Mammone, 2015. Il miglioramento sismico di ponti a travata semplicemente appoggiata mediante isolamento sismico. *XVI Convegno ANIDIS, L'Ingegneria Sismica in Italia, L'Aquila, Italia (in Italian).*

Lallemant, D., Kiremidjian, A., Burton, H. 2015. Statistical procedures for developing earthquake damage fragility curves. *Earthq. Eng. Struct. Dyn. 44(9), 1373–1389.*

Lee, J.-H., Choi, J.-H., Hwang, D.-K., & Kwahk, I.-J., 2014. Seismic performance of circular hollow RC Bridge columns. *KSCE Journal of Civil Engineering,1-12.*

Lee, T. H., and Mosalam, K.M., 2006. Probabilistic seismic evaluation of reinforced concrete structural components and systems. *PEER Report. PEER 2006/04.*

Legg M., Slosson J., Eguchi R. 1982. Seismic hazard for lifelines vulnerability analyses. Proc. 3rd Int. conf. on Microzonation, Seattle, Washington.

Lin Lin, S., Li, J., Elnashai, A.S., & Spencer, B.F. Jr. 2012. NEES integrated seismic risk assessment framework (NISRAF). *Soil Dynamics and Earthquake Engineering, 42, 219–228.*

Lin T, Haselton CB, Baker JW 2013. Conditional spectrum-based ground motion selection. Part I: Hazard consistency for risk-based assessments. *Earthquake Engineering & Structural Dynamics*, 42(12): 1847-1865.

Lomiento, G., Bonessio, N., Benzoni, G. (2013) Friction model for sliding bearings under seismic excitation. *Journal of Earthquake Engineering*, 17(8), 1162-1191

Lomiento, G., Bonessio, N.m Benzoni, G. 2011. Experimental Performance and Modelling of Sliding Anti-Seismic Devices. *7th World Congress on Joints, Bearings, and Seismic Systems for Concrete Structures,* American Concrete Institute.

Lu, Y., Gu, X., & Guan, J., Probabilistic Drift Limits and Performance Evaluation of Reinforced Concrete Columns. *Journal of Structural Engineering, 131(6), 966–978., 2005.*

Luco, N., & Cornell, C.A. 1998. Effects of random connection fractures on the demands and reliability for a three-story pre-Northridge (SMRP) structure. *In Proceedings of the 6th U.S. National Conference on Earthquake Engineering. Oakland, California: Earthquake Engineering Research Institute.*

Luco, N., 2002. Probabilistic seismic demand analysis, SMRF connection fractures, and near-source effects*. Ph.D. Thesis dissertation, Stanford University, California, USA*

Luco, N., and Cornell, C. A., 2007. Structure-Specific Scalar Intensity Measures for Near-Source and Ordinary Earthquake Ground Motions. *Earthquake Spectra: May 2007, Vol. 23, No. 2, pp. 357-392.*

Mackie KR, Stojadinović B 2004. Fragility curves for reinforced concrete highway overpass bridges. *Proceedings of 13th world conference on earthquake engineerin*g, Vancouver, British Columbia, Canada.

Mackie, K. R., & Stojadinović, B., 2007. R-Factor Parameterized Bridge Damage Fragility Curves. *Journal of Bridge Engineering, 12(4), 500–510.*

Mackie, K., & Stojadinovic, B. 2005. Fragility basis for california highway overpass bridge seismic decision making*, PEER Report 2005/02.* Pacific Earthquake Engineering Research Center. Berkeley, CA: University of California.

Mackie, K., and Stojadinovic, B., 2003. Seismic demands for performance-based design of bridges*, Pacific Earthquake Engineering Research Center, University of California, Berkeley, PEER 2003–16*.

Mackie, K.R., & Stojadinovic, B. 2007. Performance-based seismic bridge design for damage and loss limits States. *Earthquake Engineering and Structural Dynamics, 36, 1953–1971.*

Mandal, T.K., Ghosh, S., Pujari, N.N. 2016. Seismic fragility analysis of a typical Indian PHWR containment: comparison of fragility models*. Struct. Saf. 58, 11–19*

Mander JB, Basöz N 1999. Seismic fragility curves theory for highway bridges. *Proceedings of 5th US conference on lifeline earthquake engineering*, Seattle, WA, USA.

Mander, J. B., Priestley, M. J. N., & Park, R., 1988. Theoretical Stress-Strain Model for Confined Concrete. Journal Of Structural Engineering, 114(8), 1804–1826,

Mander, J., & Basöz, N., 1999. Enhanchement of the Highway Transportation Lifeline Module in HAZUS. *Final Pre-Publication Draft (#7) prepared for National Institute of Building Sciences (NIBS*).

Mander, J.B. 1999. Fragility curve development for assessing the seismic vulnerability of highway bridges. *Technical Report, MCEER Highway Project/FHWA.*

Mander, J.B., & Basoz, N. 1999. Seismic fragility curves theory for highway bridges. *In Proceedings of the 5th US Conference on Lifeline Earthquake Engineering (pp. 31–40): ASCE.*

Martin T. Schultz, Ben P. Gouldby, Jonathan D. Simm, and Johannes L. 2010 Wibowo, Beyond the Factor of Safety: Developing Fragility Curves to characterize System Reliability *Engineer Research and Development Center Vicksburg Ms Geotechnical And Structures Lab.*

McGuire, R. K., 2004. Analysis of seismic hazard and risk, *EERI Monograph, Earthquake Engineering Research Center.*

McKeena, F., & Fenves, G. L., Open System for *Earthquake Engineering Simulation. Pacific Earthquake Engineering Research Center, 2015*

Melchers RE. Structural Reliability, 1999. *Analysis and Prediction, 2nd ed. John Wiley& Sons.*

Ministero delle Infrastrutture e dei Trasporti (2008). Norme tecniche per le costruzioni - NTC08 D.M. 14/01/2008, Gazzetta Ufficiale 04/02/2008.

Mitrani-Reiser, J., Haselton, C.B., Goulet C., Porter, K.A., Beck, J., and Deierlein G.G., 2006. Evaluation of the seismic performance of a code-conforming reinforced-concrete frame building - part II: loss estimation. *8th NCEE, San Francisco, California, April 18- 22, 10 pp.*

Miyamoto, K., Yanev, P. and Salvaterra, I. 2009. M6.3 L'Aquila, Italy. Earthquake Field Investigation Report, Global Risk Miyamoto and Miyamoto International.

Moehle, J. P. 1999. Preliminary Observations on the Performance of Concrete Freeway Structures. *National Information Service for Earthquake Engineering*, University of California, Berkeley.

Moehle, J. P. and Eberhard, M. 1999. Earthquake Damage to Bridges. Bridge Engineering Handbook, CRC Press, USA.

Moschonas, I. F., Kappos, A. J., Panetsos, P., Papadopoulos, V., Makarios, T., & Thanopoulos, P., 2008. Seismic fragility curves for greek bridges: methodology and case studies. *Bulletin of Earthquake Engineering, 7(2), 439–468*.

Naeim F, Kelly JM, 1999. Design of seismic isolated structures: From theory to practice, John Wiley & Sons, New York.

Nakata, J.K., Charles E. Meyer, Howard G. Wilshire, John C. Tinsley, William S. Updegrove, D.M. Peterson, Stephen D. Ellen, Ralph A. Haugerud, Robert J.

McLaughlin, G. Reid Fisher, Michael F. Diggles, 1999, *The October 17, 1989, Loma Prieta, California, Earthquake—Selected Photographs,* U.S. Geological Survey Digital Data Series DDS-29.

National Academies of Sciences, Engineering, and Medicine. 2013. Performance-Based Seismic Bridge Design. *Washington, DC: The National Academies Press. https://doi.org/10.17226/22632.*

Nielson, B. G., & DesRoches, R., 2007a. Analytical Seismic Fragility Curves for Typical Bridges in the Central and Southeastern United States. *Earthquake Spectra, 23(3), 615-633,*

Nielson, B. G., & DesRoches, R., 2007b. Seismic fragility methodology for highway bridges using a component level approach. Earthquake *Engineering and Structural Dynamics, 36, 823–839*

Padgett JE 2007. Seismic vulnerability assessment of retrofitted bridges using probabilistic methods, *PhD thesis, Department of Civil and Environmental Engineering, Georgia Institute of Technology, Atlanta, GA.*

Padgett JE, Nielson BG, DesRoches R., 2008. Selection of optimal intensity measures in probabilistic seismic demand models of highway bridge portfolios. *Earthquake Engineering & Structural Dynamics*, 37(5): 711-725.

Wright, T., DesRoches R., Padgett JE, 2010. Bridge Seismic Retrofitting Practices in the Central and Southeastern United States. *Journal of Bridge Engineering*, 16(1): 82-92.

Pan, Y., Agrawal, A.K., Ghosn, M., & Alampalli, S. 2010. Seismic fragility of multi-span simply supported steel highway bridges in New York State. I: Bridge modeling, parametric analysis, and retrofit design. *ASCE Journal of Bridge Engineering, 15, 448–461.*

Papanikolaou, V. K., 2012. Analysis of arbitrary composite sections in biaxial bending and axial load. *Computers and Structures, 98-99, 33–54,*

Park YJ, Ang AH-S. Mechanistic seismic damage model for reinforced concrete. *Journal of Structural Engineering, ASCE 1985;111(4):722–39.*

Park, Y.J., & Ang, A.H.S. (1985). Mechanistic seismic damage model for reinforced concrete. *ASCE Journal of Structural Engineering, 111, 722–739*.

Penelis, G.G., Sarigiannis, D., Stavrakakis, E., & Stylianidis, K.C. 1989. A statistical evaluation of damage to buildings I the Thessaloniki. Greece, earthquake of June, 20, 1978, *Proceedings of 9th World Conference on Earthquake Engineering, August 1989, Tokyo- Kyoto, Maruzen, Japan, VII, 187–192.*

Petti L, Lodato A, Mammone A 2016. Reliability analysis of seismic isolation in retrofitting of simply supported bridges. *Applied Mechanics and Materials,* 847: 391- 400

Petti L, Polichetti F, Lodato A, Palazzo B 2013. Modelling and analysis of base isolated structures with friction pendulum system considering near fault events. *Open Journal of Civil Engineering*, 3: 86-93.

Petti L., Mammone A., 2017. Reliability analysis of seismic isolation in retrofitting of simply supported bridges, *16th World Conference on Earthquake, 16WCEE*.

Petti L., Mammone A., Ansalone A., 2018. Robustness of seismic retrofit isolation strategy of existing multi-span simply supported bridges. *16th European Conference on Earthquake Engineering (16ECEE).*

Porter, K., 2003. An overview of PEER's performance-based earthquake engineering methodology. *Ninth International Conference on Applications of Statistics and Probability in Civil Engineering (ICASP9) July 6-9, 2003, San Francisco, USA.*

Porter, K., Kennedy, R., Bachman, R., 2007. Creating fragility functions for performance-based earthquake engineering. *Earthq. Spectra 23(2), 471–489.*

Priestley M, Seible F, Calvi G 1996. Seismic Design and Retrofit of Bridges, *Wiley Interscience, New York.*

Priestley, M. J. N., & Ranzo, G., 2000. Seismic performance of large rc circular hollow columns. 12th World Conference of Earthquake Engineering Auckland, New Zealand.

Ramanathan, K., DesRoches, R., & Padgett, J.E. 2012. A comparison of pre- and post-seismic design considerations in moderate seismic zones through the fragility assessment of multi-span bridge classes. *Engineering Structures, 45, 559–573.*

Rossetto, T., & Elnashai, A.S. 2003. Derivation of vulnerability functions for European type RC structures based on observational data. *Engineering Structures, 25, 1241–1263. Rotterdam: Millpress.*

Shafieezadeh, A., Ramanathan, K., Padgett, J.E., & DesRoches, R. 2012. Fractional order intensity measures for probabilistic seismic demand modeling applied to highway bridges. *Earthquake Engineering and Structural Dynamics, 41, 391–409.*

Shinozuka M, Feng MQ, Kim HK, Kim SH 2000. Nonlinear static procedure for fragility curve development. *Journal of Engineering Mechanics, 126(12): 1287-1295.*

Shinozuka, M., Chang, S., Eguchi, R.T., Abrams, D.P., Hwang, H., & Rose, A. 1997. Advances in earthquake loss estimation and application to Memphis, Tennessee. Earthquake Spectra, 13, 739–758.

Shinozuka, M., Feng, M. Q., Kim, H., & Kim, S.-H., 2000. Nonlinear Static Procedure for Fragility Curve Development. Journal of Engineering Mechanics, *ASCE, 126(12), 1287– 1295.*

Shinozuka, M., Feng, M. Q., Lee, J., & Naganuma, T. 2000. Statistical Analysis of fragility curves. *Journal of Engineering Mechanics, ASCE, 126(12), 1224–1231.*

Shinozuka, M., Feng, M.Q., Kim, H.-K., & Kim, S.-H. 2000. Nonlinear static procedure for fragility curve development. *ASCE Journal of Engineering Mechanics, 126, 1287–1296.*

Shinozuka, M., Feng, M.Q., Kim, H., Uzawa, T., & Ueda, T. 2001. Statistical analysis of fragility curves, (Report No. MCEER-03-0002). *MCEER, University at Buffalo. Buffalo, NY: The State University of New York.*

Shome, N., & Cornell, A.C. 1999. Probabilistic seismic demand analysis of nonlinear structures. reliability of marine structures (Program Report No. RMS-

35). *Stanford University, CA: Department of Civil and Environmental Engineering.*

Singhal, A., & Kiremidjian, A.S. 1996. Bayesian updating of fragilities with application to RC frames. *ASCE Journal of Structural Engineering, 124, 922–929.*

Siqueira GH, Sanda AS, Paultre P, Padgett JE 2014. Fragility curves for isolated bridges in eastern Canada using experimental results. *Engineering Structures*, 74: 311-324.

Skinner RI, Robinson WH, McVerry GH 1993. An introduction to seismic isolation, *John Wiley & Sons, New York.*

Sommerville P. and Porter. K.A., 2005. Hazard analysis. Chapter 3 in "PEER testbed study on a laboratory building: exercising seismic performance assessment." Comerio *M.C. editor. PEER Report PEER 2005/12.*

Stefanidou, S. P., & Kappos, A. J., Methodology for the development of bridge-specific fragility curves. *Earthquake Engineering & Structural Dynamics, 46, 73–93, 2017.*

Stefanidou, S.P., 2016. Structure-specific Fragility Curves for As- Built and Retrofitted Bridges. PhD Thesis*, Aristotle University of Thessaloniki (in Greek).*

Straub D, Der Kiureghian A 2008. Improved seismic fragility modeling from empirical data. *Structural Safety*, 30(4): 320-336.

Tavares, D.H., Padgett, J.E., & Paultre, P. 2012. Fragility curves of typical as-built highway bridges in eastern Canada. *Engineering Structures, 40, 107–118.*

Todd, D., Carino, N., Chung, M.R., Lew, H.S., Taylor, A.W., Walton, W.D., Cooper, J.D., Nimis, R., 1994, *1994 Northridge Earthquake Performance of Structures, Lifelines, and Fire Protection System*s, NIST Special Publication 862.

Tothong, P., and Cornell, C. A., 2006. Probabilistic seismic demand analysis using advanced ground motion intensity measures, attenuation relationships, and nearfault effects. *Pacific Earthquake Engineering Research Center, University of California, Berkeley, PEER Report 2006–11.*

TRDB (Tohoku Regional Development Bureau), 2011, *Road Department: Damage to Highway Facilities in the 2011 Tohoku-Oki Earthquake*.

Tsai, C.S. 1997. "Finite element formulations for friction pendulum seismic isolation bearings." *International Journal for Numerical Methods In Engineering*, 40(1), 29-49.

Tsionis, G., & Fardis, M. N., 2012. Seismic Fragility of Concrete Bridges with Deck Monolithically Connected to the Piers or Supported on Elastomeric Bearings. 15th World Conference of Earthquake Engineering. Lisbon, Portugal.

Ufficio di Statistica 2014. Conto Nazionale delle Infrastrutture e dei Trasporti 2012-2013. Ministero delle Infrastrutture e dei Trasporti - Dipartimento per le Infrastrutture, i Sistemi Informativi e Statistici - Direzione Generale per i Sistemi *Informativi e Statistici, Istituto Poligrafico e Zecca dello Stato S.p.A., Rome.*

Vamvatsikos, D., & Cornell, A.C. 2002. Incremental dynamic analysis. *Earthquake Engineering & Structural Dynamics, 31, 491–514.*

Veneziano, D., Sussman, J.M., Gupta, U., & Kunnumkal, S.M. 2002. Earthquake loss under limited transportation capacity: assessment, sensitivity and remediation. *In Proceedings of 7th US National Conference on Earthquake Engineering. Boston, Mass: EERI.*

Vosooghi, A., & Saiidi, M.S. 2012. Experimental fragility curves for seismic response of reinforced concrete bridge columns. *ACI Structural Journal, 109, 825–834.*

Wakefield, D., Ravindra, M., Merz, K., and Hardy, G., 2003. Seismic probabilistic risk assessment implementation guide. *Final Report 1002989, EPRI.*

Werner, S.D., Taylor, C., & Moore, J. 1997. Loss estimation due to seismic risks to highway systems. *Earthquake Spectra, 13, 585–604.*

Whitman, R.V., Biggs, J.M., Brennan, J.E., Cornell, A.C., de Neufville, R.L., & Vanmarcke, E.H. 1975. Seismic design decision analysis. *ASCE Journal of Structural Division, 101, 1067–1084.*

Yamazaki, F., Hamada, T., Motoyama, H., & Yamauchi, H. 1999. Earthquake damage assessment of expressway bridges in Japan. *Technical Council on Lifeline Earthquake Engineering Monograph, 16, 361–370.*

Yashinsky, M., 1998a. Cypress Street Viaduct. *US Geological Survey Professional Paper No. 1552-8, pp. 19-26.*

Yashinsky, M., 1998b. Performance of Bridge Seismic Retrofits during Northridge Earthquake. *Journal of Bridge Engineering*, 3(1), pp. 1-14.

Yu, O., Allen, D.L., & Drnevich, V.P. (1991). Seismic vulnerability assessment of bridges on earthquake priority routes in Western Kentucky. *Proceedings of 3rd US National Conference on Lifeline Earthquake Engineering, Los Angeles, CA.*

Yun, S., Hamburger, R.O., Cornell, C.A., & Foutch, D.A. 2012. Seismic performance evaluation for steel moment frames. *ASCE Journal of Structural Engineering, 128, 534–545.*

Zayas, V., Low, S., and Mahin, S. 1987. The FPS earthquake resisting system. Report No. CB/EERC-87/01. *Earthquake Engineering Research Cente*r, University of California, Berkeley, California.

Zhang, J., & Huo, Y. 2009. Evaluating effectiveness and optimum design of isolation devices for highway bridges using the fragility function method. *Engineering Structures, 31, 1648–1660.*

Appendix A

I. Interaction SAP2000 – Matlab

```
%%SAP-Matlab interation
(to make it work both of the program versions must be 32bit)
%% clean-up the workspace & command window
clear;
clc;
%%Output
h1={'1','2','3','4','5','6','7','8','9','10'};
%Acc name
h2={'A','B','C','D','E','F','G'};
%folder name
l_h1=length(h1);
l_h2=length(h2);
for k5=1:l_h2
%Chancing the folder
    % set the installation folder
    ProgramPath='C:\Program Files (x86\Computers and
    Structures\SAP2000 17\sap2000.exe';
    %% pass data to Sap2000 as one-dimensional arrays
    feature('COM_SafeArraySingleDim', 1);
    %% pass non-scalar arrays to Sap2000 API by reference
    feature('COM_PassSafeArrayByRef', 1);
    %% create OAPI helper object
    helper = actxserver('Sap2000v17.helper');
    helper = helper.invoke('cHelper');
    %% create Sap2000 object
    SapObject = helper.CreateObject(ProgramPath);
    %%
    SapModel = SapObject.SapModel;
    %% start Sap2000 application
    SapObject.ApplicationStart;
    %% initialize model
    ret = SapModel.InitializeNewModel;
    %% open file
    ret =
SapModel.File.OpenFile('C:\Users\Angelo\Desktop\Analisi
MSA\Ponte 3Campate\Si\Modello PIANO\Modello piano-3
campate.sdb');
    %%save file
```

```
    save_path=strcat('C:\Users\Angelo\Desktop\Analisi
MSA\Ponte 3Campate\Si\Modello
PIANO\Cu=III\',num2str(h2{k5}),'\Modello piano-3
campate.sdb');
    ret=SapModel.File.Save(save_path);
%%Add Function from txt with equal time and without time
column.
    for k1=1:l_h1
      acc_path=strcat('C:\Users\Angelo\Desktop\Analisi
      MSA\Ponte 3Campate\Si\Modello
      PIANO\Cu=III\',num2str(h2{k5}),'\',num2str(k1),'.txt');
      ret =SapModel.Func.FuncTH.SetFromFile1(h1{k1},
      acc_path,0,0,1,1,true,1,0.005);
    end
      file_path=strcat('C:\Users\Angelo\Desktop\Analisi
      MSA\Ponte 3Campate\Si\Modello
      PIANO\Cu=III\',num2str(h2{k5}));
    filename=fullfile(file_path,'0.txt');
    FID=fopen(filename);
    A=fscanf(FID,'%f');
    ts=length(A);
    ST=fclose(FID);
    for k3=1:l_h1
        %%set case and combo output selections
        caso_di_carico=strcat('NL orizontal-', num2str(k3));
        %set time step data
        ret = SapModel.LoadCases.DirHistNonlinear.
            SetTimeStep(caso_di_carico,ts,0.005);
    end
    %% run analysis
    ret = SapModel.Analyze.RunAnalysis();
    %% close Sap2000
    ret = SapObject.ApplicationExit(false());
    SapModel = 0;
    SapObject = 0;
end
```

II. Interaction SAP2000 – Visual Basic

```
Imports SAP2000v17
Module Module1
    Sub Main()
        For h As Integer = 0 To 10
            For i As Integer = 0 To 6
                Dim ProgramPath As String = "C:\Program Files
(x86)\Computers and Structures\SAP2000 17\sap2000.exe"
                'dimension variables
Dim SapObject As cOAPI
Dim SapModel As cSapModel
```

```
Dim ret As Long
'create Sap2000 object
SapObject = CreateObject("CSI.SAP2000.API.SapObject")
'start Sap2000 application
SapObject.ApplicationStart()
'create SapModel object
SapModel = SapObject.SapModel
'initialize model
ret = SapModel.InitializeNewModel
'open an existing file
Dim indirizzo As String = "C:\Users\Angelo\Desktop\Analisi MSA\Ponte
3Campate\Si\"
Dim indirizzo2 As String = "I:\Il mio Drive\Università\Dati\new\"
Dim modello() As String = {"Modello PIANO", "Modello PIANO - ROD",
"Modello R=2,5 2%", "Modello R=2,5 2% - ROD", "Modello R=2,5 5%",
"Modello R=2,5 5% - ROD", "Modello R=3,1 2%", "Modello R=3,1 2% -
ROD", "Modello R=3,1 5%", "Modello R=3,1 5% - ROD"}
Dim ls As String = "\Cu=III\"
Dim caso() As String = {"A", "B", "C", "D", "E", "F", "G"}
Dim filesap() As String = {"\Modello piano-3 campate.sdb", "\Modello
piano-ROD - 3campate.sdb", "\Modello R2,5 2% - 3campate.sdb",
"\Modello R 2,5 2% ROD - 3campate.sdb", "\Modello R 2,5 5% -
3campate.sdb", "\Modello R 2,5 5% - ROD-3 - campate.sdb", "\Modello
R=3,1 2% - 3campate.sdb", "\Modello R=3,1 2% - ROD - 3 campate.sdb",
"\Modello R=3,1 5% - 3campate.sdb", "\Modello R=3,1 5% - ROD -
3campate.sdb"}

Dim j As Integer = 0
Dim s As String
s = String.Concat(indirizzo, modello(h), ls, caso(i), filesap(h))
ret = SapModel.File.OpenFile(s)
'get results for load patterns 1 through 7
Dim NumberResults As Integer = 0
Dim Obj() As String
Dim ObjSta() As Double
Dim Elm() As String
Dim ElmSta() As Double
Dim LoadCase(0) As String
Dim StepType(0) As String
Dim StepNum(0) As Double
Dim P() As Double
Dim V2(0 To 29) As Double
Dim V3() As Double
Dim T() As Double
Dim M2() As Double
Dim M3() As Double
Dim U1() As Double
Dim U2() As Double
Dim U3() As Double
Dim R1() As Double
```

```
Dim R2() As Double
Dim R3() As Double
Dim SapResult(10, 23) As Double
'set case selected for output 1
ret = SapModel.Results.Setup.DeselectAllCasesAndCombosForOutput
ret = SapModel.Results.Setup.SetCaseSelectedForOutput("NL orizonta-1")
'set output option
ret = SapModel.Results.Setup.SetOptionDirectHist(1)
'get SHEAR frame force for frame object "1"
 ret = SapModel.Results.FrameForce("1", 0, NumberResults, Obj, ObjSta,
Elm, ElmSta, LoadCase, StepType, StepNum, P, V2, V3, T, M2, M3)
SapResult(0, 0) = Math.Max(Math.Abs(V2(0)), Math.Abs(V2(17)))
'get SHEAR frame force for frame object "2"
ret = SapModel.Results.FrameForce("2", 0, NumberResults, Obj, ObjSta,
Elm, ElmSta, LoadCase, StepType, StepNum, P, V2, V3, T, M2, M3)
SapResult(0, 1) = Math.Max(Math.Abs(V2(0)), Math.Abs(V2(29)))
'get LINK LONG PIERS deformations for link object "1"
ret = SapModel.Results.LinkDeformation("9", 0, NumberResults, Obj,
Elm, LoadCase, StepType, StepNum, U1, U2, U3, R1, R2, R3)
SapResult(0, 2) = Math.Max(Math.Abs(R3(0)), Math.Abs(R3(1)))
'get LINK SHORT PIERS deformations for link object "1"
ret = SapModel.Results.LinkDeformation("19", 0, NumberResults, Obj,
Elm, LoadCase, StepType, StepNum, U1, U2, U3, R1, R2, R3)
SapResult(0, 3) = Math.Max(Math.Abs(R3(0)), Math.Abs(R3(1)))
'get DISPLACMENT ABUTMENTS SX for frame object "1"
ret = SapModel.Results.JointDispl("77", 0, NumberResults, Obj, Elm,
LoadCase, StepType, StepNum, U1, U2, U3, R1, R2, R3)
SapResult(0, 4) = Math.Max(Math.Abs(U1.Max), Math.Abs(U1.Min))
'get DISPLACMENT SHORT PILA for frame object "2"
ret = SapModel.Results.JointDispl("35", 0, NumberResults, Obj, Elm,
LoadCase, StepType, StepNum, U1, U2, U3, R1, R2, R3)
SapResult(0, 5) = Math.Max(Math.Abs(U1.Max), Math.Abs(U1.Min))
'get DISPLACMENT SHORT PILA for frame object "3"
ret = SapModel.Results.JointDispl("36", 0, NumberResults, Obj, Elm,
LoadCase, StepType, StepNum, U1, U2, U3, R1, R2, R3)
SapResult(0, 6) = Math.Max(Math.Abs(U1.Max), Math.Abs(U1.Min))
'get DISPLACMENT SHORT PILA for frame object "4"
ret = SapModel.Results.JointDispl("37", 0, NumberResults, Obj, Elm,
LoadCase, StepType, StepNum, U1, U2, U3, R1, R2, R3)
SapResult(0, 7) = Math.Max(Math.Abs(U1.Max), Math.Abs(U1.Min))
'get DISPLACMENT SHORT PILA for frame object "5"
ret = SapModel.Results.JointDispl("38", 0, NumberResults, Obj, Elm,
LoadCase, StepType, StepNum, U1, U2, U3, R1, R2, R3)
SapResult(0, 8) = Math.Max(Math.Abs(U1.Max), Math.Abs(U1.Min))
'get DISPLACMENT SHORT PILA for frame object "6"
ret = SapModel.Results.JointDispl("39", 0, NumberResults, Obj, Elm,
LoadCase, StepType, StepNum, U1, U2, U3, R1, R2, R3)
SapResult(0, 9) = Math.Max(Math.Abs(U1.Max), Math.Abs(U1.Min))
'get DISPLACMENT LONG PILA for frame object "7"
```

```
ret = SapModel.Results.JointDispl("40", 0, NumberResults, Obj, Elm,
LoadCase, StepType, StepNum, U1, U2, U3, R1, R2, R3)
SapResult(0, 10) = Math.Max(Math.Abs(U1.Max), Math.Abs(U1.Min))
'get DISPLACMENT LONG PILA for frame object "8"
ret = SapModel.Results.JointDispl("41", 0, NumberResults, Obj, Elm,
LoadCase, StepType, StepNum, U1, U2, U3, R1, R2, R3)
SapResult(0, 11) = Math.Max(Math.Abs(U1.Max), Math.Abs(U1.Min))
'get DISPLACMENT LONG PILA for frame object "9"
ret = SapModel.Results.JointDispl("42", 0, NumberResults, Obj, Elm,
LoadCase, StepType, StepNum, U1, U2, U3, R1, R2, R3)
SapResult(0, 12) = Math.Max(Math.Abs(U1.Max), Math.Abs(U1.Min))
'get DISPLACMENT LONG PILA for frame object "10"
ret = SapModel.Results.JointDispl("43", 0, NumberResults, Obj, Elm,
LoadCase, StepType, StepNum, U1, U2, U3, R1, R2, R3)
SapResult(0, 13) = Math.Max(Math.Abs(U1.Max), Math.Abs(U1.Min))
'get DISPLACMENT LONG PILA for frame object "11"
ret = SapModel.Results.JointDispl("44", 0, NumberResults, Obj, Elm,
LoadCase, StepType, StepNum, U1, U2, U3, R1, R2, R3)
SapResult(0, 14) = Math.Max(Math.Abs(U1.Max), Math.Abs(U1.Min))
'get DISPLACMENT ABUTMENTS DX for frame object "12"
ret = SapModel.Results.JointDispl("45", 0, NumberResults, Obj, Elm,
LoadCase, StepType, StepNum, U1, U2, U3, R1, R2, R3)
SapResult(0, 15) = Math.Max(Math.Abs(U1.Max), Math.Abs(U1.Min))
'get LINK SHORT PIERS deformations for link object "1"
ret = SapModel.Results.LinkDeformation("2", 0, NumberResults, Obj,
Elm, LoadCase, StepType, StepNum, U1, U2, U3, R1, R2, R3)
SapResult(0, 16) = (U2.Max)
SapResult(0, 17) = (U2.Min)
'get LINK SHORT PIERS deformations for link object "1"
ret = SapModel.Results.LinkDeformation("3", 0, NumberResults, Obj,
Elm, LoadCase, StepType, StepNum, U1, U2, U3, R1, R2, R3)
SapResult(0, 18) = (U2.Max)
SapResult(0, 19) = (U2.Min)
'get LINK LONG PIERS deformations for link object "1"
ret = SapModel.Results.LinkDeformation("4", 0, NumberResults, Obj,
Elm, LoadCase, StepType, StepNum, U1, U2, U3, R1, R2, R3)
SapResult(0, 20) = (U2.Max)
SapResult(0, 21) = (U2.Min)
'get LINK LONG PIERS deformations for link object "1"
ret = SapModel.Results.LinkDeformation("5", 0, NumberResults, Obj,
Elm, LoadCase, StepType, StepNum, U1, U2, U3, R1, R2, R3)
SapResult(0, 22) = (U2.Max)
SapResult(0, 23) = (U2.Min)
'close Sap2000
SapObject.ApplicationExit(False)
SapModel = Nothing
SapObject = Nothing
Dim SSP As String
SSP = String.Concat(indirizzo2, modello(h), "\Shear\", caso(i),
"SS.txt")
```

```
FileOpen(1, SSP, OpenMode.Output)
For j = 0 To 9
WriteLine(1, SapResult(j, 0))
Next
FileClose(1)

Dim SSL As String
SSL = String.Concat(indirizzo2, modello(h), "\Shear\", caso(i),
"SL.txt")
FileOpen(1, SSL, OpenMode.Output)
For j = 0 To 9
WriteLine(1, SapResult(j, 1))
Next
FileClose(1)

Dim RSP As String
RSP = String.Concat(indirizzo2, modello(h), "\Rotation\", caso(i),
"RS.txt")
FileOpen(1, RSP, OpenMode.Output)
For j = 0 To 9
WriteLine(1, SapResult(j, 2))
Next
FileClose(1)

Dim RSL As String
RSL = String.Concat(indirizzo2, modello(h), "\Rotation\", caso(i),
"RL.txt")
FileOpen(1, RSL, OpenMode.Output)
For j = 0 To 9
WriteLine(1, SapResult(j, 3))
Next
FileClose(1)

Dim ABSX As String
ABSX = String.Concat(indirizzo2, modello(h), "\Hammering\", caso(i),
"ABSX.txt")
FileOpen(1, ABSX, OpenMode.Output)
For j = 0 To 9
WriteLine(1, SapResult(j, 4))
Next
FileClose(1)

Dim SP35 As String
SP35 = String.Concat(indirizzo2, modello(h), "\Hammering\", caso(i),
"SP35.txt")
FileOpen(1, SP35, OpenMode.Output)
For j = 0 To 9
WriteLine(1, SapResult(j, 5))
Next
FileClose(1)
```

```
Dim SP36 As String
SP36 = String.Concat(indirizzo2, modello(h), "\Hammering\", caso(i),
"SP36.txt")
FileOpen(1, SP36, OpenMode.Output)
For j = 0 To 9
WriteLine(1, SapResult(j, 6))
Next
FileClose(1)
Dim SP37 As String
SP37 = String.Concat(indirizzo2, modello(h), "\Hammering\", caso(i),
"SP37.txt")
FileOpen(1, SP37, OpenMode.Output)
For j = 0 To 9
WriteLine(1, SapResult(j, 7))
Next
FileClose(1)
Dim SP38 As String
SP38 = String.Concat(indirizzo2, modello(h), "\Hammering\", caso(i),
"SP38.txt")
FileOpen(1, SP38, OpenMode.Output)
For j = 0 To 9
WriteLine(1, SapResult(j, 8))
Next
FileClose(1)
Dim S2MIN As String
S2MIN = String.Concat(indirizzo2, modello(h), "\Link\", caso(i),
"S2MAX.txt")
FileOpen(1, S2MIN, OpenMode.Output)
For j = 0 To 9
WriteLine(1, SapResult(j, 16))
Next
FileClose(1)
Dim S2MAX As String
S2MAX = String.Concat(indirizzo2, modello(h), "\Link\", caso(i),
"S2MIN.txt")
FileOpen(1, S2MAX, OpenMode.Output)
For j = 0 To 9
WriteLine(1, SapResult(j, 17))
Next
FileClose(1)

            Next i
        Next h

    End Sub
End Module
```